STRUCTURE-BASED DESIGN AND SYNTHESIS OF NOVEL INHIBITORS OF BETA-SITE AMYLOID PRECURSOR PROTEIN CLEAVING ENZYME 1

by

Emilio Leal Cárdenas

A Dissertation

Submitted to the Faculty of Purdue University
In Partial Fulfillment of the Requirements for the degree of

Doctor of Philosophy

Department of Chemistry
West Lafayette, Indiana
August 2019

THE PURDUE UNIVERSITY GRADUATE SCHOOL
STATEMENT OF COMMITTEE APPROVAL

Dr. Arun K Ghosh, Chair
    Department of Chemistry
Dr. Jean A. Chmielewski
    Department of Chemistry
Dr. Kavita Shah
    Department of Chemistry
Dr. Elizabeth I. Parkinson
    Department of Chemistry

Approved by:
    Dr. Christine A. Hrycyna
        Head of the Graduate Program

Dedication

To my parents, Leonardo Tamayo Cárdenas and Juanita Leal Cárdenas, for their eternal support, selfless sacrifices and unconditional love

ACKNOWLEDGMENTS

First and foremost, to my family, my parents, Leonardo and Juanita, and my brothers, Adrian, Adam, and Leo. They have provided me with an unmeasurable amount of love and support without the slightest expectation for anything in return. Without their presence the road traveled and the road that remains ahead would be but a barren tundra.

To my lab mates and my chemistry family of the Purdue Chemistry Department. I would like to thank the post-doctoral fellows that have been paramount to my success. To Dr. Bhavanam Sekhara Reddy and Dr. Jean-Rene Ella Menye as they were instrumental in the progress of the Alzheimer's disease and Type-2 Diabetes work that I had the opportunity to expand upon during my graduate studies. To Professor Margherita Brindisi, whom I was extremely fortunate to have as a mentor during my time at Purdue University, as she played a crucial role to the success I was blessed with during my graduate studies. In addition, she was able to instill within me a strong sense of ethics and integrity that was invaluable to me as a young scientist. Additionally, I would like to thank Dr. Satish Kovela, Dr. Kai Lv, and Dr. Venkata Reddy Sheri for their support in regard to chemistry and life itself. I would like to thank my current and former colleagues that I have worked closely with for their friendship and support in and out of the laboratory: Dr. Luke A. Kasserkert, Dr. Anne M. Veitschegger, Dr. Anthony J. Tomaine, Dr. Heather L. Osswald, Dr. Anindya Sarkar, Mr. Joshua R. Born, Mr. Joseph D. Bungard, Ms. Hannah M. Simpson, Ms. Miranda Belcher, Ms. Monika Yadav. I would like to thank Professor Andrew D. Mesecar and Dr. Yu-Chen Yen for their tireless and meticulous work that went towards the biological evaluation of all the compounds that we submitted to their laboratory. They have served as invaluable collaborators throughout the years and I extend to them my deepest of gratitude. To the support staff (business office, main office, procurement center, copy center, PINMRF, Amy Facility, chem

store, chem shop) within the Purdue Chemistry Department for their dedication to the department. I would like to thank our own Operations Manager, Suzy Snoeberger, for her tireless work ethic and unrelenting support during my time at Purdue. Suzy consistently found a way to be keep our laboratory working like a well-oiled machine and I'm forever grateful for her contributions to our group. I would like to thank the members of my committee: Jean A. Chmielewski, Elizabeth I. Parkinson, and Kavita Shah. I am eternally grateful for their support on my committee and will always hold them in high esteem. You all have created a home for me in West Lafayette. The trials and tribulations of the last five years would have been insurmountable without your unrelenting support.

Lastly, to Professor Arun K. Ghosh for his unwavering support and guidance throughout my time at Purdue University. He has provided me with the opportunity to be able to cultivate my love for chemistry. For this opportunity I'm forever grateful.

TABLE OF CONTENTS

LIST OF TABLES 8
LIST OF FIGURES 9
LIST OF SCHEMES 12
ABSTRACT 13
CHAPTER 1. ALZHEIMER'S DISEASE, AD, AND THE STRUCTURE-BASED DRUG DESIGN OF NOVEL BACE1 PROTEASE INHIBITORS 15
  1.1 Alzheimer's Disease 15
    1.1.1 Hallmarks of AD & Their Origins 17
    1.1.2 Processing of Amyloid Precursor Protein (APP) 18
    1.1.3 Mutations of Amyloid Precursor Protein (APP) 20
    1.1.4 Role of α, β, γ-secretase 22
  1.2 BACE1 As A Target and Development of Novel BACE1 Inhibitors 25
    1.2.1 Evolution of BACE1 Inhibitors as A Potential Treatment for AD 27
    1.2.2 Design of Peptidomimetic Inhibitors 31
      1.2.2.1 Statine-based Inhibitors 32
      1.2.2.2 Hydroxyethylene-based Inhibitors 33
      1.2.2.3 Hydroxyethylamine-based Inhibitors 35
      1.2.2.4 Reduced Amide-based Inhibitors 38
      1.2.2.5 Macrocyclic Peptide-based Inhibitors 39
    1.2.3 Nonpeptide Inhibitors 41
      1.2.3.1 Acyl Guanidine-containing Inhibitors 42
      1.2.3.2 2-Aminopyridine-containing Inhibitors 44
      1.2.3.3 Aminoimidazole-containing Inhibitors 45
      1.2.3.4 Aminohydantoin/Iminohydantoin-containing Inhibitors 47
      1.2.3.5 Aminothiazoline and Aminooxazoline-containing Inhibitors 49
      1.2.3.6 Dihydroquinazoline-containing Inhibitors 50
      1.2.3.7 Aminoquinoline-containing Inhibitors 52
      1.2.3.8 Pyrrolidine-containing Inhibitors 53
      1.2.3.9 Macrocyclic-containing Non-peptidic Inhibitors 54

- 1.2.4 Clinical Evaluation of BACE1 Inhibitors ... 56
  - 1.2.4.1 Clinical Evaluation of LY2811376 ... 57
  - 1.2.4.2 Clinical Evaluation of LY2886721 ... 58
  - 1.2.4.3 Clinical Evaluation of AZD3839 ... 59
  - 1.2.4.4 Clinical Evaluation of RG7129 ... 59
  - 1.2.4.5 Clinical Evaulation of MK-8931 ... 60
  - 1.2.4.6 Clinical Evaluation of AZD3293 ... 61
- 1.3 Further Development of Lead Compound, GRL-8234 ... 62
  - 1.3.1 Optimization of Core Scaffold of BACE1 Inhibitors ... 63
    - 1.3.1.1 Alternative Preparation of Core Scaffold: Azo Epoxide ... 73
  - 1.3.2 Optimization of P1’ Ligand: Design & Synthesis of Spirocyclic Amines ... 74
    - 1.3.2.1 Preparation of Spirocyclic Cyclopropyl Benzylamines ... 76
    - 1.3.2.2 Preparation of Racemic Heterospirocyclic Benzylamines ... 78
    - 1.3.2.3 Diastereoselective Approach to Heterospirocyclic Benzylamines ... 81
  - 1.3.3 Preparation of P2-ligand: 7,6,5-Tricyclic Indole ... 88
- 1.4 Preparation of BACE1 Inhibitors ... 91
  - 1.4.1 Biological Evaluation of BACE1 Inhibitors ... 95
  - 1.4.2 Discussion ... 98
- 1.5 Conclusions ... 101
- 1.6 Experimental ... 102

APPENDIX A. NMR SPECTRA ... 145

REFERENCES ... 209

VITA ... 224

PUBLICATIONS ... 225

LIST OF TABLES

Table 1.1 Common Human APP Mutations observed in early-onset familial AD. 21

Table 1.2 Biological evaluation of BACE1 inhibitors **111a-e**. 96

Table 1.3 Biological evaluation of BACE1 inhibitors **112a-e**. 97

LIST OF FIGURES

Figure 1.1 Structure of current FDA approved drugs for Alzheimer's disease and other associated neurodegenerative disease. 16

Figure 1.2 Representation of the amyloid cascade hypothesis (image created with BioRender).[9] 17

Figure 1.3 Processing of Human APP α-, β-, γ-secretase (image adapted from review *Topics of Medicinal Chemistry*; Springer International Publishing: Cham, 2017, 27-85; image created with BioRender).[9] 19

Figure 1.4 Representation of closed (A) Pro-BACE1 and open (B) Pro-BACE1 (image created with BioRender). 23

Figure 1.5 Initial BACE-1 inhibitors that helped advance proof of concept studies. 28

Figure 1.6 Proteolytic cleavage of peptide bond via catalytic aspartyl residues. 29

Figure 1.7 OM99-2-bound within the BACE1 catalytic domain (PDB: 1FKN) (image from review *Topics of Medicinal Chemistry*; Springer International Publishing: Cham, 2017, 27-85.) 30

Figure 1.8 Various transition state isosteres used in peptide-based protease inhibitors. 32

Figure 1.9 Representative examples of statine-based inhibitos **5-6**. 33

Figure 1.10 Representative examples of hyroxyethylene-based inhibitors **7-8**. 34

Figure 1.11 Representation of inhibitor **7** within the catalytic domain of BACE1 (PDB: 2G94) 35

Figure 1.12 Representative examples of hydroxyethylamine-based inhibitors **9-12**. 36

Figure 1.13 Representation of inhibitor **11** within the catalytic domain of BACE1 (PDB:2VKM). 37

Figure 1.14 Representative examples of reduced amide-based inhibitors **13-15**. 38

Figure 1.15 Representation of inhibitor **14** within the catalytic domain of BACE1 (PDB: 4GID). 39

Figure 1.16 Representative examples of macrocyclic-based inhibitors **16-17**. 40

Figure 1.17 Representation of inhibitor **17** within the catalytic domain of BACE1 (PDB: 1XS7). 41

Figure 1.18 Various transition state isosteres used in non-peptidic-based protease inhibitors. 42

Figure 1.19 Representation of inhibitor **18** within the catalytic domain of BACE1. 43

Figure 1.20 Representative examples of acyl guanidine-based inhibitors **18-20**. 43

Figure 1.21 Representative examples of 2-aminopyridine-based inhibitors **21-22**. 44

Figure 1.22 Representation of inhibitor **22** within the catalytic domain of BACE1 45

Figure 1.23 Representative examples of aminoimidazole-based inhibitors **23**-**25**. 46

Figure 1.24 Representation of inhibitor **25**-bound in the catalytic domain of BACE1 (PDB: 4ACX). 47

Figure 1.25 Representative examples of aminohydantoin-based inhibitors **26**-**28**. 48

Figure 1.26 Representation of inhibitor **28**-bound in the catalytic domain of BACE1 (PDB: 4R95). 49

Figure 1.27 Representative examples of aminthiazoline- and aminooxazoline-based inhibitors **29-32**. 50

Figure 1.28 Representation of **32**-bound in the catalytic domain of BACE1 (PDB: 4WTU) 51

Figure 1.29 Representation of **33**-bound in the catalytic domain of BACE1 (PDB: 2Q11) 51

Figure 1.30 Representative examples of dihydroquinazoline inhibitors **33**-**35** 52

Figure 1.31 Representative examples of aminoquinoline-based inhibitors **36-38**. 52

Figure 1.32 Representation of inhibitor **38** within the catalytic domain of BACE1 53

Figure 1.33 Representative examples of pyyrolidine-based inhibitors **39-40**. 53

Figure 1.34 Representation of inhibitor **40** within the catalytic domain of BACE1. 54

Figure 1.35 Representative examples of macrocyclic-based inhibitors **41-42**. 55

Figure 1.36 Representation of inhibitor **41** within the BACE1 active site. 56

Figure 1.37 Representative examples of drug candidates for AD 57

Figure 1.38 Representative examples of BACE1 inhibitors **45** and **46** containing a difluoro isostere. 64

Figure 1.39 Stereoview of GRL-8234-bound BACE1 and its interactions with the flap region of the catalytic active site. (Methylene protons of benzyl amine shown in yellow for clarity) 75

Figure 1.40 Structures of cyclopropyl amines **76a-e**. 77

Figure 1.41 Structures of azo alcohol isosteres **77a-e**. 77

Figure 1.42 Structures of racemic spirocyclic ethers **83a-i**. 80

Figure 1.43 Structures of azo alcohol isosteres **84a-i** 80

Figure 1.44 Explanation of reverse stereoinduction observed for grignard additions to α-benzyloxy and α-silyloxy N-sulfinyl aldimines 82

Figure 1.45 Explanation of a return to expected stereoselectivity for grignard additions to α-benzyloxy and α-silyloxy N-sulfinyl ketimines. 83

Figure 1.46 Structures from the diastereoselective preparation of **93a-c**. 85

Figure 1.47 Inhibitor-bound BACE1 x-ray crystal structure depicting interactions of the 7,6,5-tricyclic indole (shown in blue) in the non-prime subsites of the BACE1 active site. 89

Figure 1.48 Structures of BACE1 inhibitors **111a-e** and **112a-e**. 93

Figure 1.49 Structures of BACE1 inhibitors **113a-i**. 94

Figure 1.50 Structures of BACE1 inhibitors **114a-i**. 94

LIST OF SCHEMES

Scheme 1.1 Reterosynthetic design strategy for preparation of optically active epoxides **46** and **49**………..……………………………………………………………………65

Scheme 1.2 Representative stereochemical model for the syn- and anti-aldol additions involving titanium-mediated (Z)-enolates.……………………………………..………….....66

Scheme 1.3 Preparation of **46** by utilizing a syn aldol as a key step.……………………..…….68

Scheme 1.4 Preparation of **49** by utilizing an anti-aldol addition as a key step…………..…….69

Scheme 1.5 Preparation of **46** by utilizing Evan's diastereoselective syn-aldol addition as a key step…………………………………………………………………………....71

Scheme 1.6 Preparation of BACE1 inhibitor 68 from optically active oxirane **46**……..………72

Scheme 1.7 Preparation of azo epoxide 74 from commercially available butadiene monoxide **69**……………………………………………………………………………..74

Scheme 1.8 Preparation of azo alcohols **77a-e** with a modified Kulinkovich serving as a key step.…………………………..…………………………………………...…..76

Scheme 1.9 Preparation of spirocyclic benzylamines 84a-j from commercially available from oxo-cyclic ethers **78** and **79**……………………………………………………...79

Scheme 1.10 Ellman's and co-workers reterosynthetic design strategy towards optically active 1,2-amino alcohols **85a-d**…………………………………………..……….....81

Scheme 1.11 Preparation of α, α, α-substituted N-sulfinyl amines **(R)-93a-c** and **(S)-93a-c** via a diastereoselective allyl grignard addition to an optically active aryl -silyloxy N-sulfinyl ketimine **92a-c** as a key step…………..………………………………..84

Scheme 1.12 Preparation of highly functionalized spirocylic tetrahydrofuran **(R)-96a** and **(S)-96a** from -trisubstituted N-sulfinyl amine **(R)-93a** and **(S)-93a**…………….……….…86

Scheme 1.13 Preparation of highly functionalized spirocyclic tetrahydropyran **(R)-99a** and **(S)-99a** from N-sulfinyl amine **(R)-93a** and **(S)-93a**…………………..……………....87

Scheme 1.14 Preparation of α, α, α-trimethyl-substituted 7,6,5-tricyclic indole **105**…………….90

Scheme 1.15 Preparation of α, α-cyclopropyl-substituted 7,6,5-tricyclic indole **110**……………91

Scheme 1.16 Preparation of BACE1 inhibitors via coupling of isostere **77a-e** and selected tricyclic indoles **111** and **112**…………………..………………………..………………92

Scheme 1.17 Preparation of BACE1 inhibitors via coupling of isosteres **84a-e** and selected tricyclic indoles **105** and **110**……………..……………………..……...…....92

ABSTRACT

Author: Cárdenas, Emilio, L. PhD
Institution: Purdue University
Degree Received: August 2019
Title: Structure-Based Design and Synthesis of Novel Inhibitors of Beta-Site Amyloid Precursor Protein Cleaving Enzyme 1
Committee Chair: Arun K. Ghosh

Alzheimer's disease (AD) continues to plague the healthcare community as a serious healthcare crisis. Currently there fails to be an effective FDA approved drug that can treat the underlying mechanisms of the disease. Pathologically the disease is characterized by the accumulation of neurotoxic amyloid-β (Aβ) plaques within a diseased patient's brain. These plaques are widely accepted to be generated by the sequential proteolytic cleavage of amyloid precursor protein (APP) by β-secretase (BACE1, memapsin 2) and γ-secretase. Numerous biochemical markers suggest that BACE1 is a viable target for AD drug development. Since the cloning and expression of BACE1 there has been an explosion of drug development efforts that have consisted of peptidomimetic-based and non-peptide-based inhibitors. These efforts have led to 13 BACE1 drug candidates some of which have made it to advanced stages of clinical trials. Unfortunately, an effective and tolerable BACE1 drug candidate continues to be rather elusive to the medicinal chemistry community. GRL-8234 is a potent BACE1 inhibitor that has been extensively shown to be tolerable during several short-term and long-term *in vivo* studies. The scaffold of GRL-8234 provides a suitable template for further lead development. Namely the P1' 3-methoxy-benzylamine is of particular interest due to the advantageous interactions in the flap region of BACE1 that can be achieved by incorporation of substitution at the benzylic position. In the same way, the *meta*-substituent of the benzylamine P1' ligand was investigated to probe the hydrophobic interactions in the S1'-S2' binding pocket. A novel class of BACE1 inhibitors

containing P1’ spirocyclic benzylamine derivatives were designed, synthesized and evaluated for their inhibitory activity against BACE1. In the process of preparing the aforementioned BACE1 inhibitors a method was established to be able to incorporate the desired 3,5-difluorophenyl methyl transition state isostere by utilizing an ester-derived Ti-enolate to access optically pure *syn*- and *anti*-aldol adducts as a key step. Additionally, a novel stereoselective method was established to afford heterospirocyclic benzylamines by utilizing a diastereoselective allyl grignard addition to optically pure α-silyloxy *N*-sulfinyl ketimines as a key step. Biological evaluation of these novel BACE1 inhibitors has been fruitful and continues to be ongoing.

CHAPTER 1. ALZHEIMER’S DISEASE, AD, AND THE STRUCTURE-BASED DRUG DESIGN OF NOVEL BACE1 PROTEASE INHIBITORS

1.1 Alzheimer’s Disease

The treatment of neurodegenerative diseases has emerged as one of the most daunting modern medical challenges. For aging countries, such as the United States, the problems caused by Alzheimer’s disease (AD) and related neurodegenerative diseases continue to swell at alarming rates. Approximately 50 million people worldwide are affected by symptoms of AD and related dementia which include loss of memory and degradation of motor skills.[1,2] Due to the severe cognitive decline that is associated with the progression of many neurodegenerative diseases, patients often need extensive palliative and hospice care. As a result, this unfortunate truth has brought forth a seemingly insurmountable financial burden for countries that have aging populations. Worldwide costs associated with neurodegenerative diseases have been approximated at $605 billion dollars, with costs estimated to rise into the trillions of dollars by 2030.[3]

Currently, there are five FDA-approved drugs that are administered for those afflicted with AD and other related diseases. For instance, acetylcholinesterase inhibitors are designed to inhibit the catabolism of the vital neurotransmitter acetylcholine which is responsible for key signaling between neuronal cells. These class of drugs are summarized in Figure 1.1.[4,5] In an AD diseased brain there is a decrease of acetylcholine levels that result in impaired signaling between neurons and eventual worsening of symptomatic neurodegeneration. Administration of acetylcholinesterase inhibitors disrupt the degradation of acetylcholine levels in the brain to help maintain neural homeostasis. Additionally, memantine (2003), a *N*-methyl D-aspartate (NMDA) receptor antagonist, which helps maintain normal cellular levels of calcium by disrupting glutamate-mediated entry of calcium into the neurons (Figure 1.1).[6,7] In a healthy brain, the interactions of neurotransmitter glutamate with the membrane-bound NMDA receptor is an important cellular event in regard to normal brain function such as memory and the ability to learn. The brains of AD patients tend to be flooded with excess glutamate from damaged cells and lead to an influx of calcium into cells. This prolonged overexposure of calcium leads to excitotoxicity and eventual permanent cellular damage.

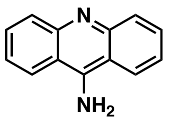

Tacrine (1993)

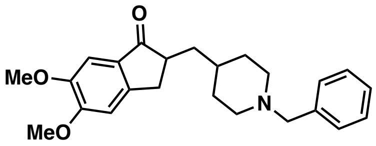

Donepezil (1996)

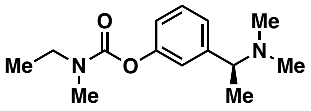

Rivastigmine (1998)

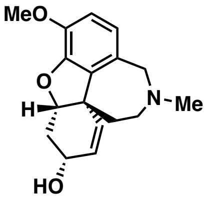

Galantamine (2001)

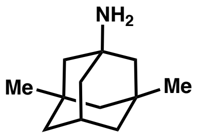

Memantine (2003)

Figure 1.1 Structure of current FDA approved drugs for Alzheimer's disease and other associated neurodegenerative disease.

Although the aforementioned drugs attempt to temper the symptoms associated with neurodegenerative disorders, there is an apparent need for the development of a therapy that can undercut the pathological events that allow the disease to proliferate and cause the neurodegeneration that is observed with AD and related neurodegenerative disorders.

1.1.1 Hallmarks of AD & Their Origins

AD drug development has proven to be an arduous task as current potential therapies have failed to make it through the clinic. Diagnosis of AD can be particularly troublesome due to difficulties monitoring the accumulation of lesions that are present in a diseased brain. The formation of these lesions, neurofibrillary tangles and neuritic plaques, proceed in the following processes (Figure 1.2).[1,8]

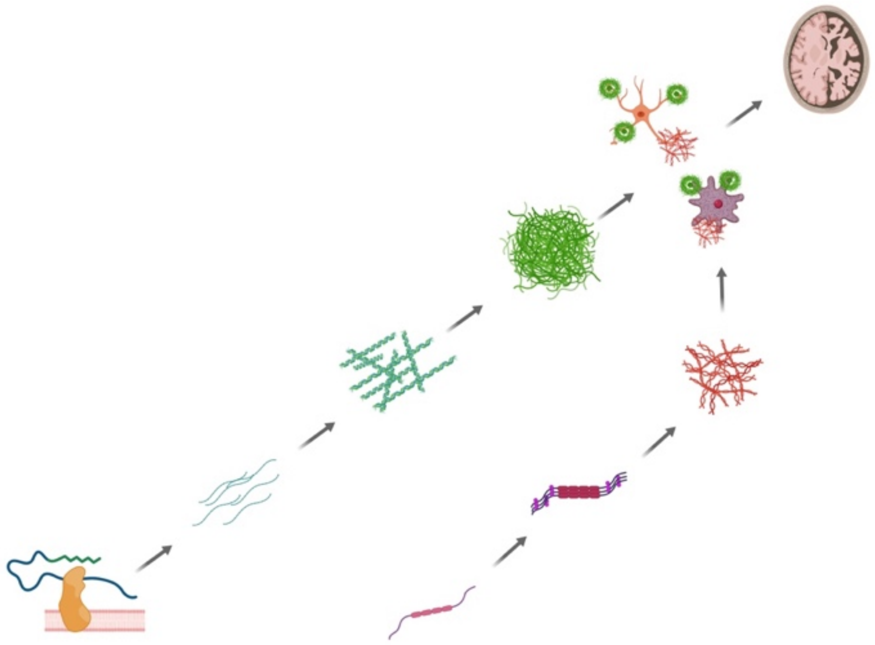

Figure 1.2 Representation of the amyloid cascade hypothesis (image created with BioRender).[9]

Present as insoluble fibers, tangles manifest themselves within the cytoplasm through the aggregation of hyperphosphorylated tau protein. It is known that these tangles are not exclusively associated with AD. However, the lesions that are derived from insoluble neuritic plaques have been identified as the predominant lesion observed in AD. Processing of amyloid precursor protein (APP) furnishes the neurotoxic plaques observed in diseased patients' brains. Further, proteolytic processing of APP by BACE1 and γ-secretase produces the well-known Aβ peptides (Figure 1.3)[9,10]. As a result, peptides of 40- and 42-residues in length are deposited within the brain. Of these two peptides, $A\beta_{42}$ is found to be the more neurotoxic and can lead to increased levels of aggregation.[8,11,12].

Fortunately, not all Aβ plaques are destined to a fate of neurotoxicity. Diffuse Aβ plaques, made almost exclusively of $A\beta_{42}$, do not contain the same degree of amyloidogenic characteristics seen in the neuritic plaques typical of AD. These soluble proteins are not typically found in areas of the brain that undergo neurodegeneration. Additionally, similar plaques are observed in the brains of healthy patients. As a result, insoluble neuritic plaques are thought to play a significant role in AD pathology and are considered the pathological hallmark of AD[13]. In order to uncover the origin of these amyloidogenic and non-amyloidogenic peptides we must delve into the processing of APP.

1.1.2 Processing of Amyloid Precursor Protein (APP)

As a type 1 transmembrane protein, APP serves a wide range of functions. The protein itself is constructed with distinct regions: a N-terminal 17 residue signaling chain, a 23 residue hydrophobic transmembrane domain, a 47 residue cytoplasmic domain, and a fairly large ectodomain.[11,14] The Aβ region is a small 40-42 residue area that exists within the lumenal and transmembrane region. Prior to maturity, APP is translocated to the lumen of endoplasmic reticulum where it is bound through the 23 residue transmembrane region. Posttranslational modification of APP, typically N- and O- glycosylation, sulfation, and phosphorylation, takes place as it chaperoned through the secretory pathway via the Golgi apparatus and endosomes.[11] Only once APP has reached maturity can the proteolytic events that lead to the Aβ plaques take place.[15] APP has varying isoforms generally consisting of 695-770 residues, with the 695th residue variant of the protein being observed in higher concentrations in the brain. Processing of transmembrane APP leads to plaque accumulation in several organs. The proteases involved in this processing are better known as α-secretase, β-secretase (BACE1), and γ-secretase (Figure 1.3).

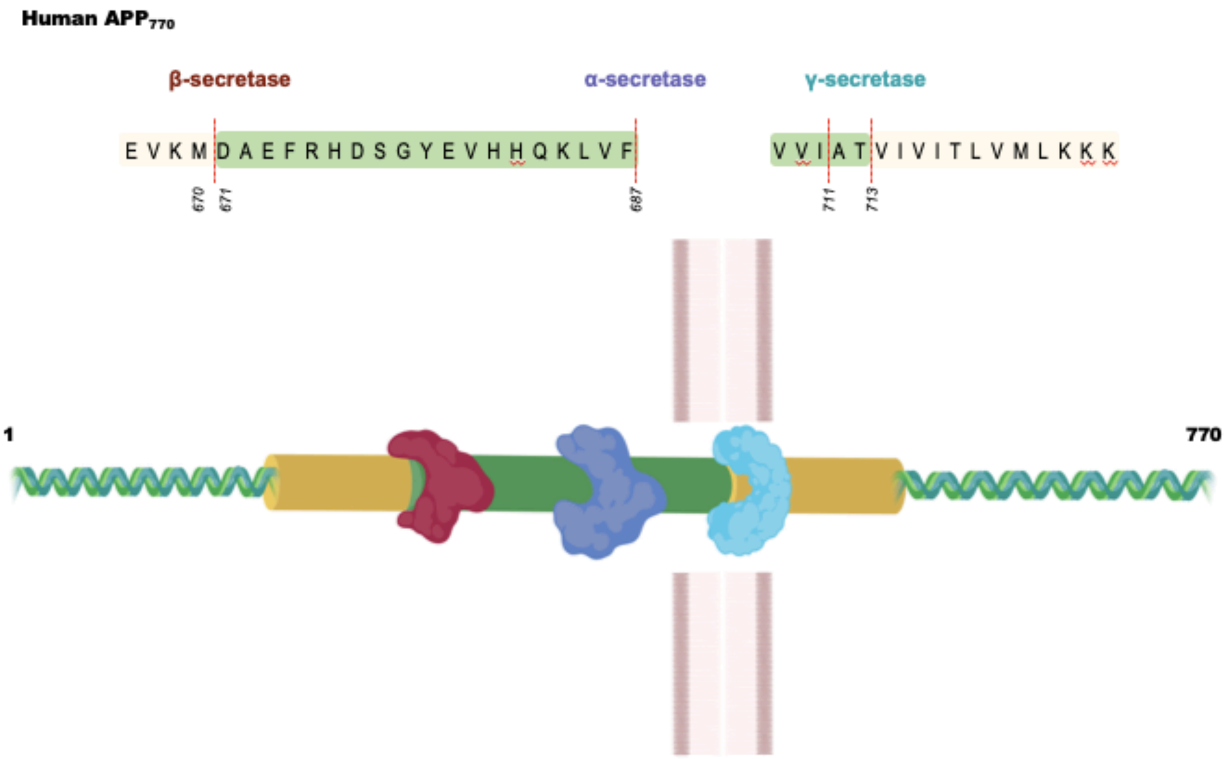
Human APP$_{770}$
β-secretase
α-secretase
γ-secretase
E V K M D A E F R H D S G Y E V H H Q K L V F
V V I A T V I V I T L V M L K K K
670
671
687
711
713
1
770

Figure 1.3 Processing of Human APP α-, β-, γ-secretase (image adapted from review *Topics of Medicinal Chemistry*; Springer International Publishing: Cham, 2017, 27-85; image created with BioRender).[9]

Cleavage of full length APP by α-secretase yields a soluble peptide that gets ejected into extracellular space (sAPPα) and an 83 residue C-terminal membrane bound peptide (C83). It has been found that the cleavage site of α-secretase is located within the Aβ region of APP; thus, the formation of neuritic plaques is circumvented upon proteolytic cleavage by α-secretase.[11,16] As a result, processing by α-secretase is considered to be non-amyloidogenic. The specificity of α-secretase for the scissile bond in APP seems to arise from the proximity of the enzyme to the cell membrane rather than the identity of the residues.[11]

Similarly, to α-secretase, BACE1 acts on full length APP; however, the scissile bond most labile towards BACE1 is located at the N-terminus of the Aβ region.[17] In neuronal cells, this bond is generally located between Met671 and Asp672 of APP. In comparison, this results in the release of a shorter soluble peptide (sAPPβ) and a longer 99 residue C-terminal membrane bound peptide (C99)[1]. C99 shares the same starting residue as Aβ. Further proteolytic processing of C99 via γ-secretase provides two peptides commonly known as Aβ and p3, with the former peptide being associated with the formation of neuritic plaques that are strongly linked to AD pathology.

1.1.3 Mutations of Amyloid Precursor Protein (APP)

The exact cause of sporadic AD has been hypothesized, but is largely unknown; however, it should be noted that patients do not usually have a genetic predisposition for sporadic AD. Alternatively, the onset of some forms of familial AD are fueled by missense mutations in APP and the presenilins enzymes that are known to be involved in regulation of neurotoxic plaque formation (Table 1.1).[1]

Table 1.1 Common Human APP Mutations observed in early-onset familial AD.

Common Human APP Mutation

Mutation	Type	Effect
K670N/M671L	SWEDISH	Increase in β-secretase processing
A692AG	FLEMISH	Increased Aβ aggregation
E693Q	DUTCH	Increased Aβ aggregation
T7141	AUSTRIAN	Increased $A\beta_{42}$ levels
V715M	FRENCH	Increased $A\beta_{42}$ levels
I716V	FLORIDA	Increased $A\beta_{42}$ levels
V717L/V717F	INDIANA/LONDON	Increased $A\beta_{42}$ levels
L723P	AUSTRALIAN	Increased $A\beta_{42}$ levels

For instance, two point mutations near the N-terminal of the Aβ region, known as the Swedish mutation, leads to BACE1 having a better affinity for APP. Therefore, the increased proteolytic activity of BACE1 will form larger amounts of C99 which will inherently lead to overproduction of Aβ[18]. Other mutations found near the γ-secretase cleavage site are found to modulate the processing of APP via γ-secretase. In this instance, the mutations result in an increased production of the more aggregative $A\beta_{42}$.[11,19–23] As a consequence, all of the mutations lead to increased levels of Aβ. The remaining common APP mutations that are observed are found midway in the APP sequence and tend to result in favorable conditions for increased aggregation of Aβ.

In comparison, presenilin mutations are found to be more frequent and are responsible for many cases of early-onset familial AD.[1] Like many of the APP mutations, the presenilin mutations lead to an increase in $A\beta_{42}$ which later leads to a greater concentration of Aβ plaques in a diseased brain. A better understanding of sporadic AD and genetic mutations has led to a clearer picture of the pathological events that lead to AD.

Although the cascade hypothesis is well established, the hypothesis does not necessarily describe all cases of dementia, as the underlying effects that Aβ plaques have on neuronal cells *in* *vivo* is uncertain. However, when studied from a biochemical perspective, it has been shown that the degree of plaque formation is proportional to the degree of cognitive impairment experienced by patients. Although histological studies show mixed support that the degree of plaque deposition is correlated to dementia, the mechanism in which plaques lead to neurotoxicity is not fully understood.[12,24] Taking the preceding into consideration, the amyloid cascade hypothesis is still widely accepted as the pathological vehicle for AD.

1.1.4 Role of α, β, γ-secretase

In an effort to unveil the unknowns that surround the cascade hypothesis, focus shifted upon the identification of the enzymes responsible for the generation of Aβ. Prior to their exact identification, the three enzymes responsible for APP processing are generally referred to as α-, β-, and γ- secretase. In order for AD disease pathology to be fully understood, an exact identity for each enzyme was needed.

It has been found that a wide range of proteins display α-secretase activity. The entirety of these proteins fall under the A disintegrin and metalloprotease (ADAM) families. ADAM10 has been found to be responsible for the majority of α-secretase activity in the brain.[25,26] In contrast, γ-secretase activity is thought to be dependent on a complex of proteins. Presenilins (PSs) have been identified as proteins that are crucial to the modulation of γ-secretase activity.[27] This has been confirmed through crystal structures that show the PS1 aspartic acid residues aligned with transmembrane domain of APP. The importance of PSs in γ-secretase activity has been solidified by observing that mutations of PS1 and PS2 favor the aggregation of Aβ.[17,28,29] In addition, knockout studies with PS1 has led to the decline of Aβ formation. There are other proteins responsible for γ-secretase activity: nicastrin (Nct), anterior pharynx-defective phenotype (APH-

1), and PS-enhancer (PEN-2). The simultaneous expression of all the proteins was able to induce γ-secretase activity in *Saccharomyces cerevisae* where activity is not typically observed. Therefore, it suggests that a complex of all the proteins are needed in order to observe full γ-secretase activity.[28]

A wide array of proteins have been mistaken as the culprit of β-secretase activity: cathepsin D (CatD), cathepsin G, BACE2, metalloendopeptidase MP78, and metalloprotease MP100.[30–33] In the late 1990s, several groups simultaneously uncovered the true identity of the protein responsible for the secretase activity. Presently, the enzyme is referred to by several names in the literature, such as Asp2, β-secretase 1, and memapsin 2.[34–37] Here, it will be referred to exclusively as BACE1. As previously mentioned, BACE 1 makes the first cut in the sequential proteolytic cleavage of APP that leads to neurotoxic Aβ. Therefore, it plays a significant role in the prevailing amyloid cascade hypothesis that has been associated with the pathology of AD and other dementia related diseases. As a result, BACE 1 has been extensively studied as a therapeutic target for AD.

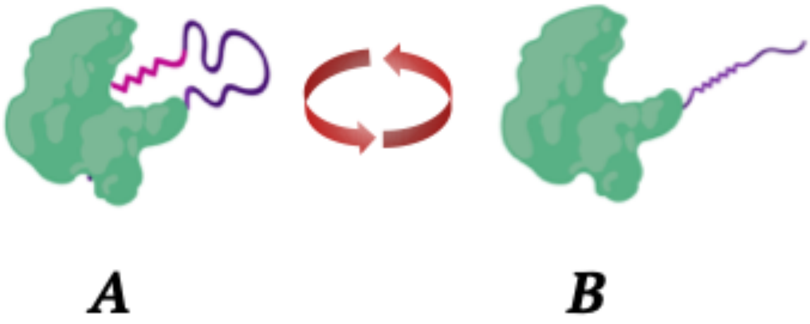

Figure 1.4 Representation of closed (A) Pro-BACE1 and open (B) Pro-BACE1 (image created with BioRender).

The early beginnings of the monomeric BACE1 manifest themselves within the endoplasmic reticulum. Immature glycosylated BACE1, commonly known as pro-BACE1, is processed to yield mature BACE1 in the Golgi apparatus[38,39]. While in the pro-peptide form, pro-BACE1 exists in two distinct conformations, where the open conformation is observed to participate in marginal catalytic activity (Figure 1.4).[39] On the other hand, a decline in catalytic activity of the closed conformation originates from interactions of the pro-domain within the active site. Although the pro-domain exhibits modest inhibitory effects it is ultimately crucial to the folding of the pro-peptide. Following the cleavage of the pro-domain, the active site of the BACE1 is completely accessible to potential substrates.[40] Throughout the maturation process of BACE1, the protein travels between both the endosome and the cell surface.[41] Immature pro-BACE1 has four vacant glycosylation sites as well as six cysteine residues. The disulfide bonds that result from the cysteine residues, particularly Cys330/Cys380, are critical for the folding and stability of the enzyme.[42] As the protein is localized to the endosomal system, three of the four glycosylation sites become glycosylated within the Golgi apparatus and the endoplasmic reticulum. BACE1 finally reaches the endosomes through the help of a dilecuine sequence and can make its way to the cell surface via exocytosis.[41] At this point, the protein can be reinternalized and recycled through the endosomal pathways for further use. Although BACE1 is shuttled between the endosomes and the cell surface, it has been found that the enzyme is most active in environments that are slightly more acidic than physiological pH.[41] This lends to the assumption that the majority of catalytic activity takes place within the endosomes rather than at the cell surface. Much like pro-BACE1, mature BACE1 also has two distinct confirmations. When the catalytic site is not occupied by a substrate the protease resides in an open conformation.[43] The flap closes upon binding with a substrate and leads to a loss of hydrogen bonds within the flap region. Upon binding with a substrate, BACE1 participates in new interactions with Trp76 and Tyr71 to give a stable conformation.[43] These unique forms of conformation provide a flexible cleft that can be used as an advantage for inhibitor design. With that being said, the focus will shift to BACE1 as a therapeutic target and potential complications that arise with targeting BACE1.

1.2 BACE1 As A Target and Development of Novel BACE1 Inhibitors

Studies have shown that dementia-like symptoms can be observed early on in the amyloid cascade, even before widespread neuronal death. Therefore, development of therapeutic agents has focused on the inhibition of enzymes that play a big role in the initial steps of amyloidogenesis. As previously mentioned, α-secretase is not included in these efforts due to it cleaving APP within the Aβ region. This is in stark contrast to the deposition of Aβ that originates from β- and γ-secretase processing of APP.

PS 1 and 2 are widely studied targets for γ-secretase inhibition. Both proteins reside in the ER and Golgi apparatus. Aside from APP processing, they play a significant role in other essential biological events. For instance, they play a crucial role in the Notch signaling pathway that is responsible for embryonic development. PS1 knockout studies have resulted in the premature deaths of test subjects. Several other PSs substrates have been identified, which suggests that inhibition of γ-secretase activity would likely lead to a number of undesired mechanistic side effects.

On the other hand, BACE1 has been suggested to be a viable therapeutic target for curtailing the progression of AD. Knockout studies have suggested that a therapeutic window needs to be established to be able to observe beneficial pharmacological results.[44–46] Transgenic mice studies have shown that inhibiting BACE1 completely can lead to crippling phenotypic responses.[47–52] The quandary of developing therapeutics that are selective for BACE1 is crucial to the development of a viable treatment for AD. BACE1 is one of many aspartic acid proteases found throughout the body: BACE2, pepsin, renin, CatD, cathepsin E, and others. Therefore, off-target toxicity due to non-selective BACE1 inhibition is a huge concern. While the two catalytic aspartic acid residues are conserved throughout the class of proteins, the varying subsites of each provide an opportunity to develop selective inhibitors.[53]

BACE2, also referred to as Asp1 and memapsin 1, belongs to the same family of proteases as BACE1.[37] The two enzymes are 64% homologous.[54] The highest concentrations of BACE2 are found within the colon, kidney, pancreas, and among other systemic organs.[54] It is found in low concentrations in the brain and is actually found to slow the generation of Aβ plaques. This arises from the much more precise proteolytic cleavage of APP that results in a decline of C99 levels.[55] Although BACE2 does not promote amyloidogenesis, the conservation of residues between the enzymes poses a significant threat to the efficacy of potential BACE1 inhibitors.

Another important specificity hurdle resides in selective inhibition over CatD. CatD has roles in a wide range of biological pathways that span from apoptosis regulation to protein degradation. This suggests that inhibition of CatD would likely result in severe side effects. In fact, studies with CatD null mice have led to subjects that suffered from seizures and blindness.

Outside of specificity issues, there are other complications that arise when it comes to the development of BACE1 inhibitors. The large substrate pocket of BACE1 serves as an ideal fit for substrates like APP.[43,56,57] However, the development of large inhibitors that can fill the large cavity of the enzyme generally do not serve as viable therapeutic agents *in vivo*. Efforts to downsize early inhibitors typically led to a decline in potency due to their inability to adequately fill the pocket.

The lipophilicity of BACE1 inhibitors is also a major factor when it comes to developing clinically viable inhibitors. Due to AD being a neurological disorder, viable drug candidates must have the ability to cross the blood brain barrier (BB). The utilization of BBB permeable peptide linkers with inhibitors has been shown to decrease Aβ levels in a diseased brain. Additionally, the incorporation of sterol linkers has led to the assistance of cell permeability.[58] However, P-glycoprotein (Pgp) has been found to eject potential therapeutics out of the brain through a process called drug efflux. Inhibition of Pgp has shown that inhibitors are able to stay within the brain and reduce Aβ peptide levels[59]

While inhibition of BACE1 has been observed to be a potentially viable therapy for AD, knockout mice have been observed to show significant complications. Aβ has been linked to the modulation of synaptic generation. Thus, the inhibition of BACE1 could lead to a disruption in synaptic formation. Furthermore, null mice have endured hippocampal complications which led to memory and learning ailments.[51] Similarly, BACE1 knockout mice were observed to have a greater predisposition for seizures and schizophrenic behavior.[4748] A successful drug candidate must be able to inhibit BACE1 within a thereapeutic window.

Presently, a large number of academic and industrial laboratories have strived to produce clinically relevant inhibitors. Progress has been made in this endeavor, but there fails to be an FDA approved drug. These efforts have resulted in many classes of preclinical inhibitors which have been evaluated *in vitro* and in preclinical animal models. any inhibitors have impressive potency and selectivity profiles and have been tested in a myriad of biological assays.

1.2.1 Evolution of BACE1 Inhibitors as A Potential Treatment for AD

Following the isolation and cloning of BACE1 in 1999, there have been numerous BACE1 inhibitor design campaigns that have sought out to develop a viable therapy for AD[37,60]. Initial studies provided valuable insight of the point mutations of BACE1 that are often seen in patients that are diagnosed with familial AD. These mutations include the Swedish APP (SEVNL/DAEFR) which is observed to be proteolytically cleaved by BACE1 at rates as much as 40 times more efficiently than its wild-type counterpart. Additionally, it was discovered that the S1' subsite of the catalytic domain of BACE1 prefers the presence of a Leu-Ala dipeptide at the scissile region.[61] Equipped with the preceding information the design, synthesis, and biological evaluation of the first substrate-based BACE1 inhibitors were carried out,

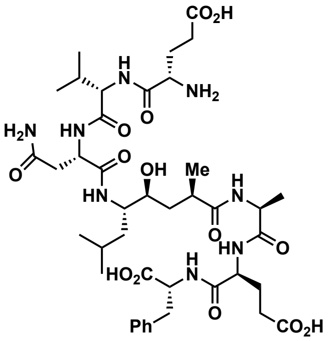

1 (OM99-2)
Ki = 1.6 nM (MW 893 Da)

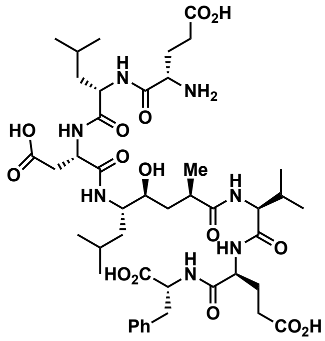

2 (OM00-3)
Ki = 0.3 nM (MW 921 Da)

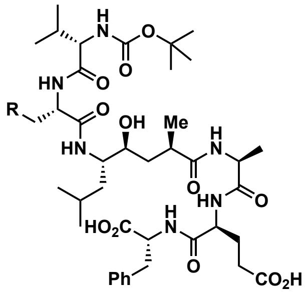

3 R = $CONH_2$
Ki = 5.9 nM (MW 704 Da)
4 R = CH_2SMe
Ki = 2.5 nM (MW 722 Da)

Figure 1.5 Initial BACE-1 inhibitors that helped advance proof of concept studies.

Initial inhibitor OM99-2 (**1**) was developed concurrently with the elucidation of BACE1 (Figure 1.5).[36] Engineering of this first inhibitor was carried out through the use of a transition-state mimetic concept. The hallmark of this design hinges on the presence of a non-hydrolyzable dipeptide isostere at the scissile bond (Figure 1.6). As discussed previously, the proteolytic cleavage is favored when an alanine residue is present within the S1' subsite. This suggests that an inhibitor with a Leu-Ala transition state mimic would provide a serviceable inhibitor. OM99-2, an inhibitor containing a Leu-Ala dipeptide hydroxyethylene transition state mimic, proved to be a very potent BACE1 inhibitor with a K_i of 1.6 nM.

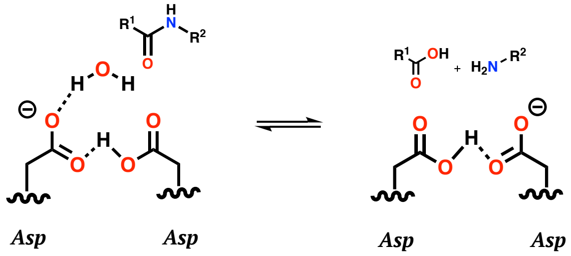

Figure 1.6 Proteolytic cleavage of peptide bond via catalytic aspartyl residues.

A crystal structure of OM99-2 in the BACE1 active site has been prepared to study interactions within the catalytic domain(Figure 1.7).[43] The active site is made up of an extensive network of hydrogen bonds and the hallmark of the protease is the catalytic dyad, Asp228 and Asp32. Inhibitor-bound OM99-2 is found to have four hydrogen bonds between the hydroxyethylene isostere and the catalytic aspartate residues. There are an additional ten hydrogen bonds that get formed between the active site and the flap region. As mentioned previously, the newly formed hydrogen bonds within the flap region causes a conformational change that results in the flap being draped over the cleft of the enzyme. Further, the elucidation of the chemical makeup of the subsites has proven to be a valuable asset in the design of potential inhibitors. The S2 and S4 subsites have been found to be mostly hydrophilic in nature, while the S1 and S3 subsites are typically made up of hydrophobic residues. As a result, the P1 leucine and P3 valine of OM99-2 are able to adequately fill the S1 and S3 sites with an abundance of hydrophobic interactions. The P2 asparagine is also found to form hydrogen bonds with the P4 glutamate and Asp235.

Although OM99-2 is found to be very potent, interactions with the active site are limited due to a unique kink at the P2' ligand that causes the P3' and P4' ligands to be situated away from the active site.[62]

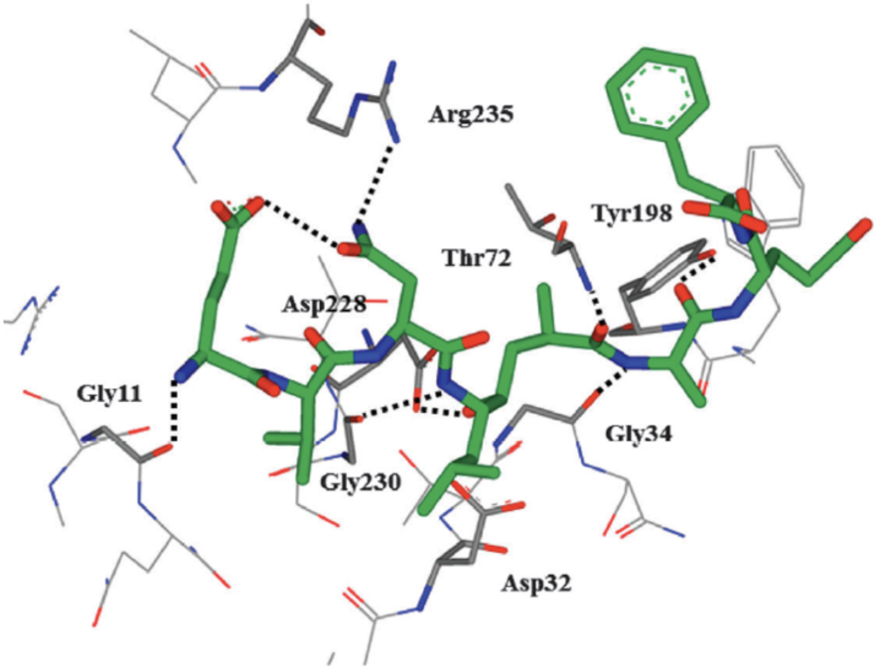

Figure 1.7 OM99-2-bound within the BACE1 catalytic domain (PDB: 1FKN) (image from review *Topics of Medicinal Chemistry*; Springer International Publishing: Cham, 2017, 27-85.).

With an inhibitor-bound crystal structure in hand, there could be a logical progression of inhibitor design that explores the many interactions within the BACE1 active site. Taking the preceding knowledge into consideration, the structure-based design of OM00-3 (**2**) led to a five-fold enhancement of inhibitory activity with a K_i of 0.3 nM (Figure 1.10).[43,57] This increase of potency was achieved through a better understanding of substrate specificity of the active site. It was found that BACE1 can accommodate up to eight side chains. The nonprime subsites were determined to be less tolerable to a variety of substrate side chains. This provided the opportunity to modulate the potency of inhibitors by varying the side chains of potential inhibitors. In result, OM00-3 has displayed an augmented affinity for glutamine at P4, isoleucine at P3, aspartate or asparagine at P2 and leucine, phenylalanine, or methionine at P1, with P1 being the most intolerant of different side chains.[55] Similar to OM99-2, OM00-3 adopts the same conformation of its predecessor between the P3 and P2' subsites. However, stabilization of an extended confirmation is conserved past P2' due to interactions between the backbone carbonyl of P3' to Asp235 and the P4' backbone to Tyr198.

Moreover, the conserved interactions observed along the S3'-S4' subsites for OM99-2 and OM00-3 suggests that the P3' and P4' ligands can be truncated or optimized in future generations of BACE1 inhibitors. Utilizing the same hydroxyethylene transition state mimic, inhibitor **3** was designed through truncation of the P3', P4' and P4 ligands that exist in proof-of-concept inhibitors, OM99-2 and OM00-3. As a result, inhibitor **3** was found to maintain potency against BACE1 with a K_i of 5.9 nM. Further, replacement of P2 amide with a methylcysteine moiety led to inhibitor **4** which displayed greater than 2-fold enhancement of enzymatic inhibitory activity (K_i = 2.5 nM) but did not display selectivity for BACE1.[62]

1.2.2 Design of Peptidomimetic Inhibitors

These initial inhibitors helped establish BACE1 as a viable target in the fight against AD. With the aid of sensible structure-based design, facilitated by X-ray structural studies, a number of structurally diverse peptidomimetic inhibitors (Figure 1.8) with improved pharmacological properties have come to fruition. The following outlines a discussion the details the progress of BACE1 inhibitor design.[63,64]

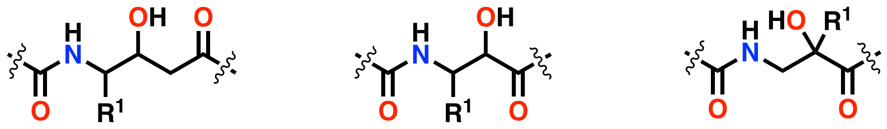

Statine **Norstatine** ***Tert*-hydroxyl**

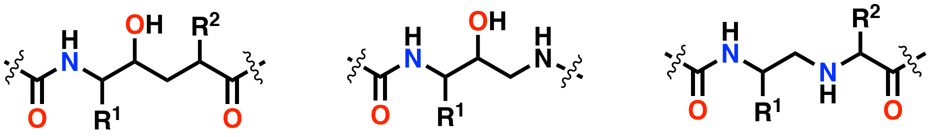

Hydroxyethylene **Hydroxyethylamine** **Reduced Amide**

Figure 1.8 Various transition state isosteres used in peptide-based protease inhibitors.

1.2.2.1 Statine-based Inhibitors

Statines are often identified by the presence of a leucine side chain at the P1 subsite. Their relevance lies in the fact that they resemble Swedish mutant APP which exhibits a greater affinity for BACE1 compared to wild type APP. Exploration of the utility of statine has provided a large library of inhibitors. Initial statine-based inhibitors established subsite specificity within the S2 and S3 subsites. Through significant subsite structure-activity relationship (SAR) studies, inhibitor **5** was found to be potent against BACE1 (IC_{50} = 110 nM) with optimized P3, P2, and P2' ligands (Figure 1.12).

The emergence of phenylstatine based inhibitors was a result of exploring the size of the hydrophobic S1 pocket. The installation of a larger benzyl substituent at P1 led to a more than 20-fold increase inhibitory activities over smaller substitutents such as a leucine or methionine side chain. For instance, compound **6** displayed an improvement in potency against BACE1 with an enzymatic IC_{50} of 21 nM (Figure 1.9). Molecular docking studies confirmed that the secondary alcohol from the phenylstatine moiety occupied the scissile site and was in proximity to participate in hydrogen bonding interactions with the two catalytic aspartic acid residues, Asp32 and Asp228. The benzyl P1 side chain filled the large S1 hydrophobic pocket. The S2 pocket is more promiscuous and accommodates both large and small moieties well. The C-terminal benzoic acid benefited from an interaction with Lys224. Furthermore, the *N*-acetyl-leucine participated in extensive hydrogen bonding in the S3 site which included a crucial hydrogen bond with Gln73.

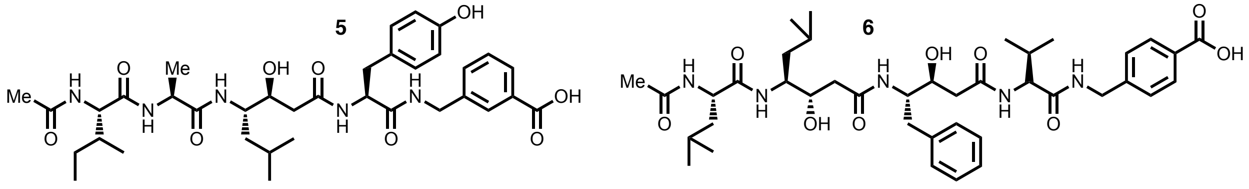
5

6

BACE1 IC$_{50}$ = 110 nM

BACE1 IC$_{50}$ = 21 nM

Figure 1.9 Representative examples of statine-based inhibitors **5**-**6**.

1.2.2.2 Hydroxyethylene-based Inhibitors

The early beginnings of hydroxyethylene-based inhibitors originate from the discovery of previously mentioned OM99-2 and OM00-3. In these initial studies, OM99-2 pleasantly displayed 5-fold selectivity for BACE1 over CatD. Further, the establishment of the crucial specificity within the S1, S2, S1', and S2' binding pockets of aspartic acid proteases provided invaluable insight in the future design of BACE1inhibitors. Hydroxyethylene-based mimics that are designed from the initial leucine-alanine scaffold make these inhibitors amongst the earliest studied isostere. Compound **7** (Figure 1.10) exhibited an enzymatic inhibitory activity of 0.3 nM.[65] It also displayed a good selectivity profile. An x-ray crystal structure of **7** led to further substrate-based design strategies (Figure 1.11). A hydrogen beyond between the pyrazole nitrogen and Thr232 were observed. Additionally, alkyl moieties from the pyrazole ring seemed to accommodate the S3 subsite. [65] Arg235 and Thr232 were found to make beneficial interactions with the sulfone P2 ligand. Inhibitor **7** lost activity when tested within a cell assay, with inhibitory values of 1.4 μM and 1.7 μM.[65]

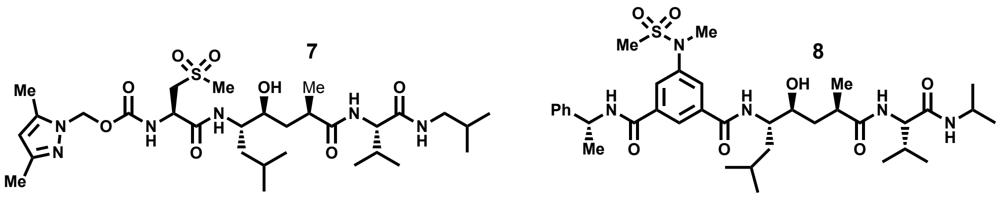

7

BACE$_1$ Ki = 0.3 nM
Ab cell IC$_{50}$ = 1400 nM
BACE$_2$ IC$_{50}$ = 356 nM
CatD IC$_{50}$ = 131 nM

8

BACE1 IC$_{50}$ = 1.1 nM
Ab cell IC$_{50}$ = 39 nM
BACE2 IC$_{50}$ = 31 nM
CatD IC$_{50}$ = 41 nM

Figure 1.10 Representative examples of hyroxyethylene-based inhibitors **7**-**8**.

Compound **8** (Figure 1.10) was designed in order to explore the utility of the lipophilic isophthalamide derivatives within the Non-prime subsites. Inhibitor **8** was observed to have enzymatic and cellular inhibitory activities of 1.1 nM and 39 nM.[66] The incorporation of a *N*-methylsulfonamide on the P2-isophthalamide was shown to be amenable in the S2 site. Computational and modeling studies also revealed a P3 (*R*)-α-methylbenzylamide accommodates the S3 pocket due to a unique conformational change that is observed upon inhibitor binding.[66] In the span of 8 hours, the administration of a dose of 8 mg/kg of the inhibitor lowered $A\beta_{40}$ in the plasma by 30% in a transgenic mouse model. Unfortunately, the inhibitors displayed poor selectivity against BACE1 when compared to similar inhibitors with varying heterocycles at the P4 site [66]

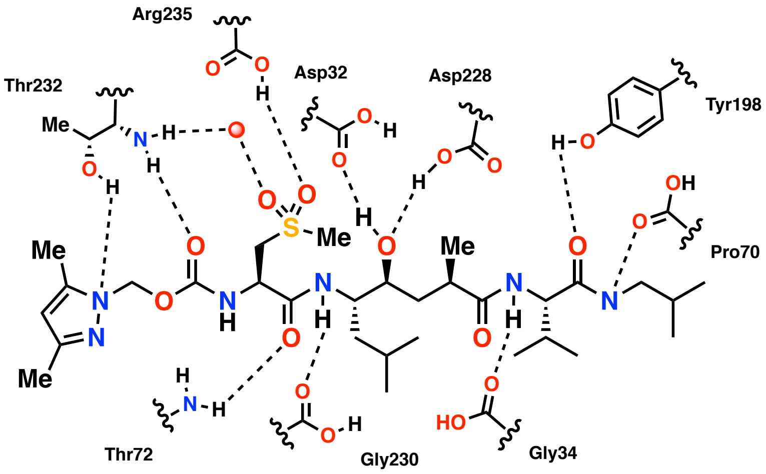

Figure 1.11 Representation of inhibitor **7** within the catalytic domain of BACE1 (PDB: 2G94)

1.2.2.3 Hydroxyethylamine-based Inhibitors

The presence of hydroxyethylamine transition state mimics have been widely known to be pertinent to the utility of many FDA-approved HIV-1 protease inhibitors.[53] Their therapeutic potential has also been extensively investigated for BACE1 inhibition. Much like other pseudopeptidic inhibitors, initial inhibitors incorporated a P1 leucine ligand as well as a (*S*)-hydroxyl of the transition-state isostere, inhibitor **9**. Additionally, the inhibitor design studies provided that a phenylalanine moiety was better than a leucine moiety at the P1 site.[67]

Equipped with the structural insight provided by hydroxyethylene inhibitors, the development of inhibitor **10** (Figure 1.12) led to an enzymatic and cellular inhibitory activity of 15 nM an 29 nM, respectively.[65] Crystal structure studies showed the isophthalic sulfonamide ligand at the P2 site and α-methylbenzylamine at the P3 site participated in a network of hydrogen bonding interactions with Asn233 and Arg235.

9

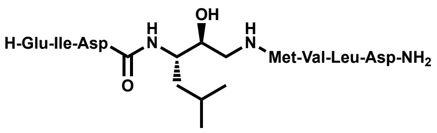

BACE1 IC$_{50}$ = 49 nM

10

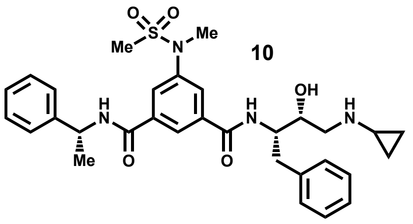

BACE1 IC$_{50}$ = 15 nM
Ab cell IC$_{50}$ = 29 nM
BACE2 IC$_{50}$ = 230 nM
CatD IC$_{50}$ = 7500 nM

11

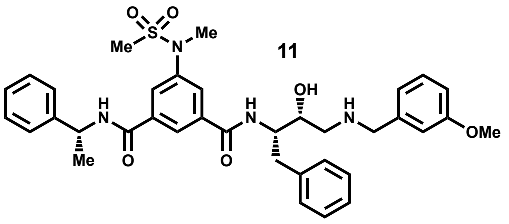

BACE1 K$_i$ = 1.8 nM
Ab cell IC$_{50}$ = 1 nM
BACE2 IC$_{50}$ = 70.2 nM
CatD IC$_{50}$ = 41.4 nM

12

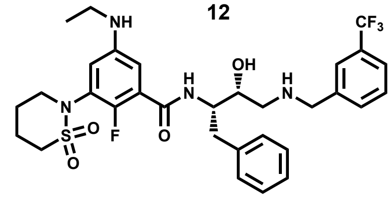

BACE1 IC$_{50}$ = 4 nM
Ab cell IC$_{50}$ = 5 nM
BACE2 IC$_{50}$ = 177 nM
CatD IC$_{50}$ = 2653 nM

Figure 1.12 Representative examples of hydroxyethylamine-based inhibitors **9-12**.

Extensive biological evaluation of potent and selective inhibitor **11** (Figure 1.12) uncovered a great deal about the clinical viability of this class of compounds. Compound **11** shows excellent enzymatic *K*i of 1.8 nM.[68,69] With a resolution of 2.05 Å, the crystal structure of **11** was solved (Figure 1.13). The incorporation of the lipophilic methoxybenzylamine allowed it to take advantage of a favorable pocket consisting of a slew of hydrophobic substituents. The catalytic dyad, Asp228 and Asp32, had strong interactions with the transition state isostere.

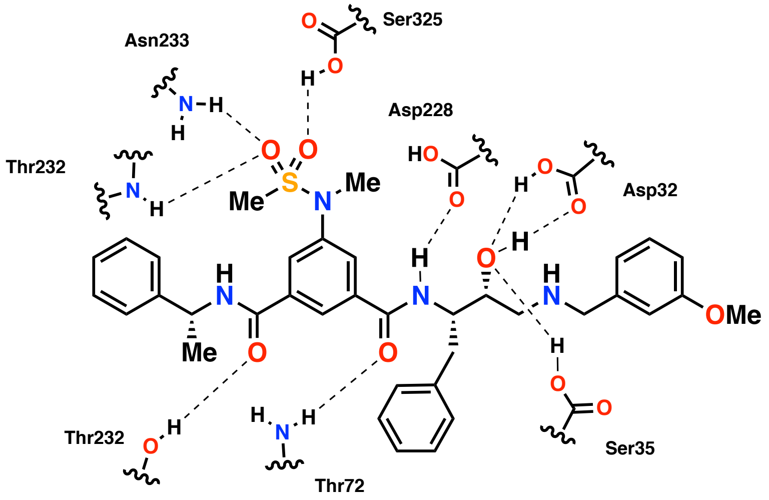

Figure 1.13 Representation of inhibitor **11** within the catalytic domain of BACE1 (PDB:2VKM).

The sulfonamide substituent made a myriad of hydrogen bonding interactions with Ser325, Asn233, and Thr232.[69] Additional investigations resulted in compound **12** (Figure 1.12) with an exceedingly potent cell-based IC_{50} of 5 nM.[70] The P2-sulfonamide was maintained as a six-membered sultam that resulted in the favored constrained conformation of the corresponding ligand. An SAR study revealed that the *meta*-ethylamine that occupied the S3 site displayed promising selectivity against BACE1. More importantly, **12** was observed to have modest oral bioavailability in TASTPM transgenic mouse studies. A 23% decline of $A\beta_{42}$ was observed with orally administered twice daily doses of 250 mg/kg. When inhibitor **12** was administered in conjunction with a Pgp inhibitor, $A\beta_{42}$ reduction was observed to be 55%. Furthermore, a tricyclic sultam indole as a non-prime ligand was found to be an amenable replacement. Which displayed a BACE1 IC_{50} of 2 nM as well as fair selectivity against other off-site targets such as BACE2 and CatD.[71]

13

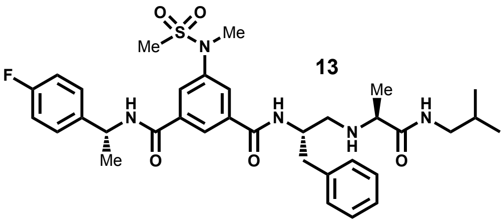

BACE1 IC_{50} = 8 nM
Ab cell IC_{50} = 22 nM

14

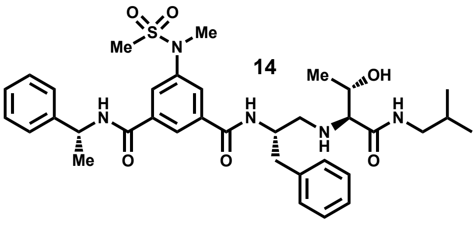

BACE1 IC_{50} = 0.017 nM
Ab cell IC_{50} = 1 nM
BACE2 IC_{50} = >7000 nM
CatD IC_{50} = >250 000 nM

15

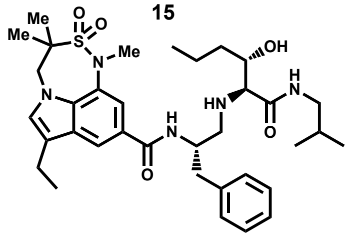

BACE1 K_i = 36 pM
cell IC_{50} = 15 nM
BACE2 K_i = 11 nM
CatD K_i = 530 nM

Figure 1.14 Representative examples of reduced amide-based inhibitors **13**-**15**.

1.2.2.4 Reduced Amide-based Inhibitors

SAR studies of the P1' ligand have led to the design of some of the most potent and selective BACE1 inhibitors to date. Initial design involved the installation of small alkyl substituents, such as methyl and ethyl, at the P1' site which in turn furnished inhibitors with great enzymatic and cellular potency.[72] Although inhibitor **13** showed moderate selectivity of 55-fold and 300-fold selectivity over BACE2 and CatD, molecular modeling of the compound led to enhanced subsite specificity for BACE1 (Figure 1.14).[73] The non-prime side sulfonamide and α-methylbenzylamide of the following inhibitors were optimized for BACE1 potency and selectivity in previous studies with varying transition state mimics. Installation of an allothreonine moiety in compound **14** revealed that the orientation of the P1' hydroxyl group was inherent to the superb selectivity. The opposite configuration of the P1' hydroxyl was found to lose a key interaction with Tyr198 within the S1' subsite, thus resulting in a decline of potency and selectivity (Figure

1.15). Additionally, inhibitor **14** was found to exhibit remarkable enzymatic potency of 17 pM. As previously mentioned, the 7,6,5-tricyclic indole of inhibitor **15** with the optimized allothreonine moiety provided an inhibitor of excellent potency (K_i = 36 pM) and selectivity (>300-fold against BACE2 and >14, 722-fold against CatD).

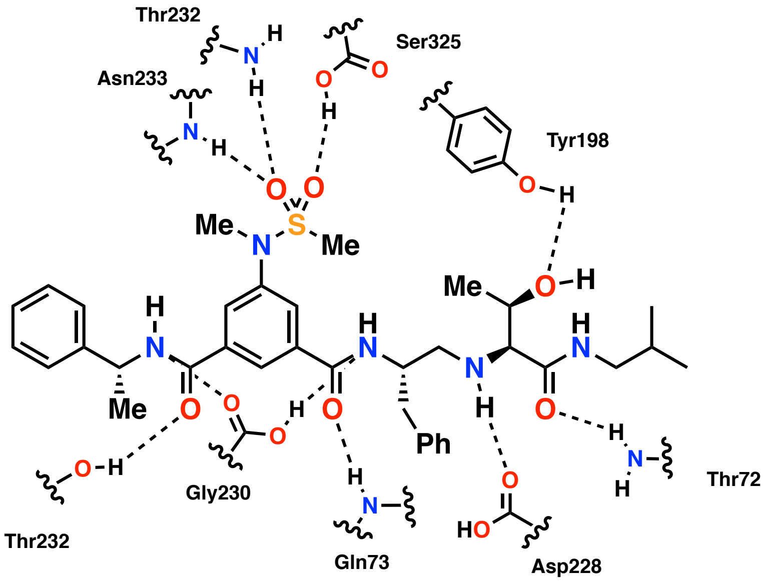

Figure 1.15 Representation of inhibitor **14** within the catalytic domain of BACE1 (PDB: 4GID).

1.2.2.5 Macrocyclic Peptide-based Inhibitors

Macrocyclic inhibitors allow for inhibitors to be restricted in their bioactive confirmation. From previous X-ray crystal structural analysis, it is known that the S1-S3 subsites are part of a vast binding pocket that can be filled with a variety of suitable ligands. Taking this into consideration, design of macrocyclic inhibitors typically involved the installation of the macrocycle through the P1 ligand and an appropriate P2 amide.

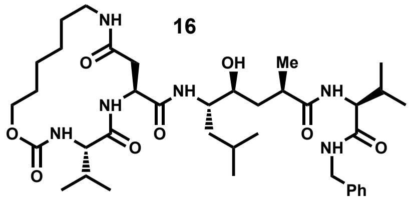

16

BACE1 K$_i$ = 25.1 nM
cell IC$_{50}$ = 3900 nM
BACE2 K$_I$ = 4.5 nM

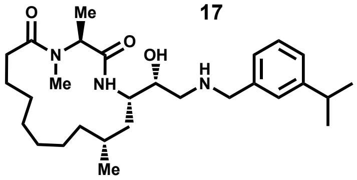

17

BACE1 IC$_{50}$ = 25 nM
cell IC$_{50}$ = 45 nM
CatD IC$_{50}$ = 1400 nM

Figure 1.16 Representative examples of macrocyclic-based inhibitors **16**-**17**.

The same Leu-Ala hydroxylethylene isostere found in OM99-2, Swedish mutant APP mimic, has been incorporated in order to fill the hydrophobic sites found within the S1 and S1’ pockets. Further derivatization at other subsites was carried out through SAR studies. For instance, the design of inhibitor **16** involved a P2-cycloamide-urethane with a valine side chain that was able to accommodate the corresponding hydrophobic pocket rather nicely.[63] It was also revealed that a 16-membered ring was optimal due to the P2-asparigine located in the backbone of the ring being able to effectively interact with Arg235 of the active site. Compound **16** exhibited good enzymatic potency (K_i = 25.1 nM), but a meager cellular potency (IC_{50} =3.9 μM) (Figure 1.19). There was no observed selectivity as the inhibitor was found to be fairly potent against BACE2 as well (0.45 nM K_i).

Introduction of a hydroxyethylamine transistion state isostere with a lipophlic benzylamine prime ligand led to an improved cellular inhibitory activity (IC_{50} = 45 nM) (Figure 1.17).[74] A return to a modest selectivity profile was also observed for inhibitor **17** with a 63-fold selectivity against CatD (Figure 1.16). In an effort to enhance the pharmacological properties of macrocyclic inhibitors, the reduced amide isostere was incorporated in several inhibitors. Inhibitor **17** with a 14-membered macrocycle, was found to have promising enzymatic and cellular inhibitory activity.[74] Additionally, animal studies with transgenic mice showed that **17** was able to remove 25% of $A\beta_{40}$ levels in the brain at a dose of 100 mg/kg.

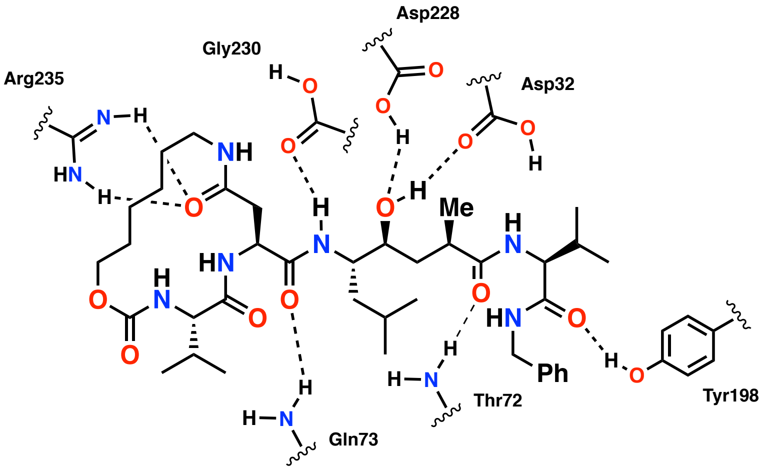

Figure 1.17 Representation of inhibitor **17** within the catalytic domain of BACE1 (PDB: 1XS7).

1.2.3 Nonpeptide Inhibitors

As seen with peptidomimetic inhibitors, size and metabolic liable substituents can place severe limitations on a BACE1 inhibitor design campaign. Extensive structural activity relationship studies have shown that the vast BACE1 active site and necessity to cross the blood-brain barrier creates an arduous inhibitor design challenge. Along with high-throughput screening and structural optimization, the development of nonpeptide inhibitors has helped address the pharmacokinetic issues seen in previous BACE1 inhibitors (Figure 1.18). More specifically, the smaller molecular size of nonpeptide inhibitors are thought to enhance BBB penetration through the reduction of drug efflux by Pgp.[53,63]

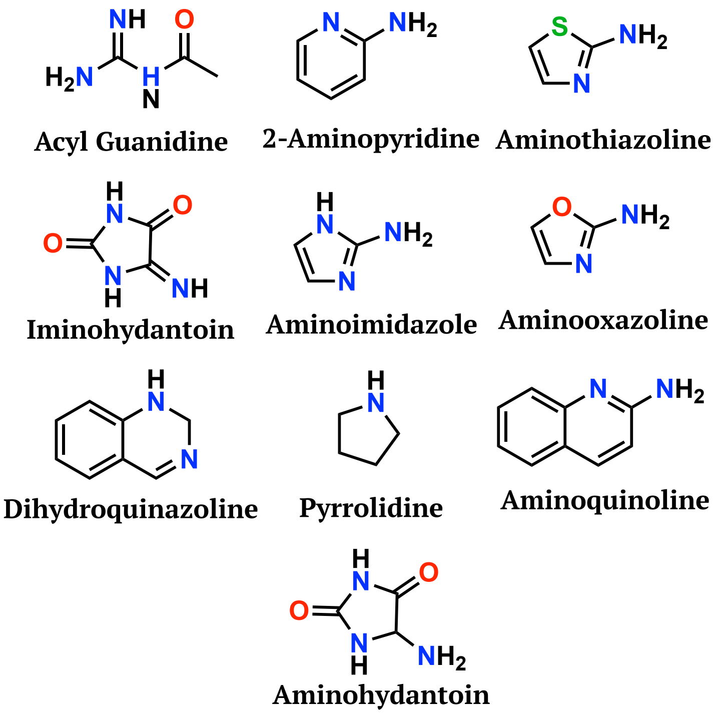
Acyl Guanidine
2-Aminopyridine
Aminothiazoline
Iminohydantoin
Aminoimidazole
Aminooxazoline
Dihydroquinazoline
Pyrrolidine
Aminoquinoline
Aminohydantoin

Figure 1.18 Various transition state isosteres used in non-peptidic-based protease inhibitors.

1.2.3.1 Acyl Guanidine-containing Inhibitors

The hallmark of these inhibitors is the presence of the acyl guanidine core that is observed to make interactions with the aspartyl dyad of memapsin 2 (Figure 1.19).[75] High-throughput screening yielded inhibitor **18** which featured an acyl guanidine-based inhibitor with an enzymatic inhibitory activity of 3.7 μM (Figure 1.20).[75] A *p*-propyloxyphenyl was installed on the P1-phenyl ligand. Moreover, one of the guanidinium nitrogen was substituted with a propyl alcohol moiety which led to an inhibitor with good potency (IC_{50} 110 nM) (Figure 1.20).[75] It was found that the series of biphenyl acyl guanidine inhibitors are not selective against common aspartyl protease off-site targets.

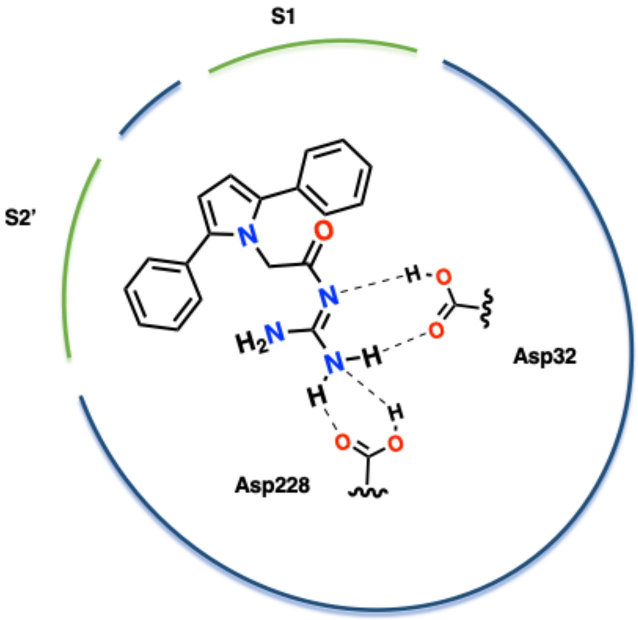
S1
S2'
Asp32
Asp228
O
N
H_2N
N-H
H
H
O
O
O
O

Figure 1.19 Representation of inhibitor **18** within the catalytic domain of BACE1.

A number of chromane-based inhibitors featuring an acyl guanidine warhead as BACE1 inhibitors have been investigated. Inhibitor **20** was found to have excellent potency (9.5 nM IC_{50}) and was able to clear as much as 63% CSF $A\beta_{40}$ levels (Figure 1.20).[76]

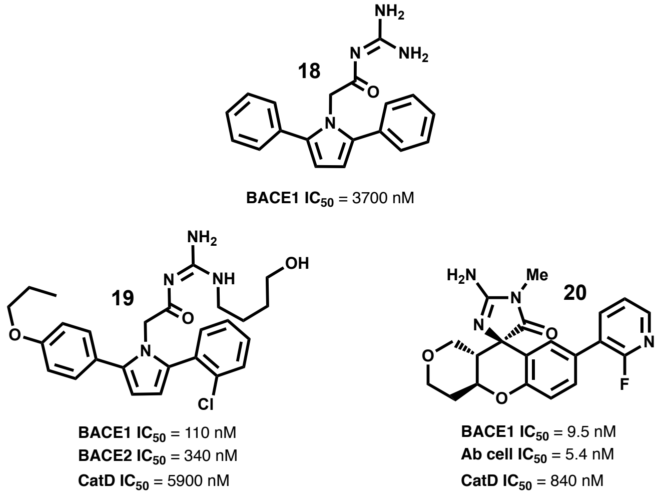
18
BACE1 IC_{50} = 3700 nM
19
BACE1 IC_{50} = 110 nM
BACE2 IC_{50} = 340 nM
CatD IC_{50} = 5900 nM
20
BACE1 IC_{50} = 9.5 nM
Ab cell IC_{50} = 5.4 nM
CatD IC_{50} = 840 nM

Figure 1.20 Representative examples of acyl guanidine-based inhibitors **18-20**.

1.2.3.2 2-Aminopyridine-containing Inhibitors

2-aminopyridine-based inhibitors bound to BACE1 adopt a flap-open conformation which lead to Tyr71 being positioned above the pyridine of the transition state isostere. In silico screening and structure-based design of the scaffold provided initial hits including inhibitor **21** (Figure 1.21).[77]

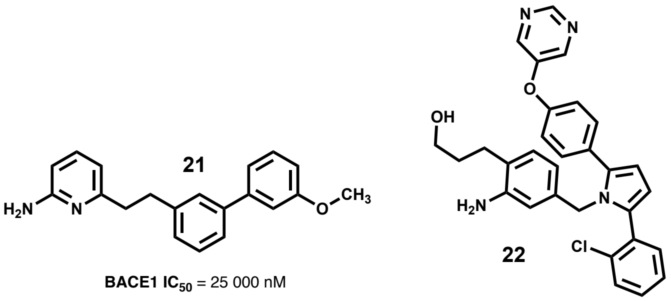

21

BACE1 IC$_{50}$ = 25 000 nM

22

BACE1 IC$_{50}$ = 40 nM
Ab cell IC$_{50}$ = 440 nM
BACE2 = 5.43% @ 12 500 nM
CatD = 23% @ 12 5000 nM

Figure 1.21 Representative examples of 2-aminopyridine-based inhibitors **21-22**.

A 2,3,6-trisubstitued aminopyridine with an ancillary disubstituted pyrrole moiety that took advantage of hydrophobic interactions along the S1-S3 subsites which provided inhibitor **22** with promising cellular inhibitory activity of 440 nM (Figure 1.21).[78] Moreover, inhibitor **22** displayed a good selectivity profile. A closer look into the binding mode of inhibitor **22** reveals that the 2-aminopyridine in fact participates in hydrogen bonding interactions with the catalytic dyad of BACE1 as well as the pyrimidine group making an interaction with Ser229 (Figure 1.22).

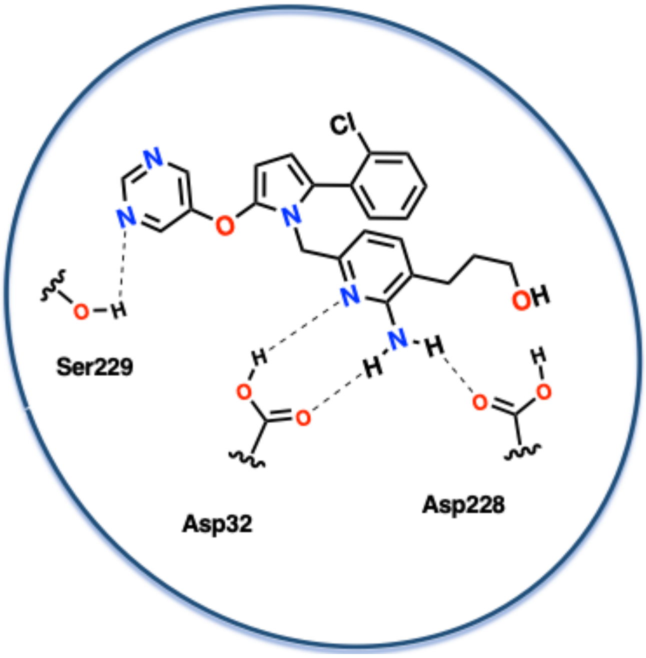

Figure 1.22 Representation of inhibitor **22** within the catalytic domain of BACE1.

1.2.3.3 Aminoimidazole-containing Inhibitors

As seen with previous nonpeptide scaffolds, HTS provided an initial hit of a BACE1 inhibitor with a dibenzyl-substituted imidazole core, inhibitor **23**. Computational studies revealed that the aminoimidazole scaffold indeed interacted with the catalytic aspartyl residues of BACE1. Development of BACE1 inhibitors with conformationally constrained aminoimidazoles has led to inhibitor **24** with good potency (63 nM IC_{50}) (Figure 1.23).[79]

Additional, structural studies found inhibitors with a fused aminoimidazole core that weakly inhibited BACE1. Optimization of these inhibitors led to the replacement of functionalized aryl rings in the favor of the biphenyl moiety observed in initial studies. For instance, inhibitor **25** with a *para*-difluoromethyl on one aryl ring and a *meta*-alkynylether on the adjacent aryl ring exhibited great enzymatic and cellular potency (7.11 and 7.46 pIC_{50} respectively).[80] X-ray structural studies resulted in a **25**-bound BACE1 crystal structure at 2.0 angstroms resolution that revealed the binding mode of the inhibitor (Figure 1.24).[80] As expected, the aminoimidazole isostere was found to make strong hydrogen bond interactions with the catalytic dyad (Asp32 and Asp228).

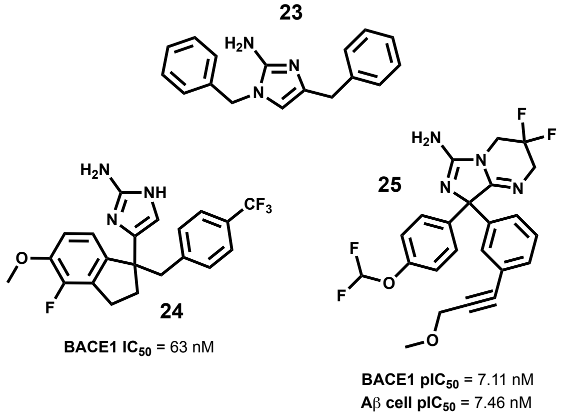

23

24

BACE1 IC$_{50}$ = 63 nM

25

BACE1 pIC$_{50}$ = 7.11 nM
Aβ cell pIC$_{50}$ = 7.46 nM

Figure 1.23 Representative examples of aminoimidazole-based inhibitors **23-25**.

Upon binding BACE1 was found to be in an open-flap conformation that allowed for interactions with Trp76 and the *p*-difluoromethyl ether. The alkynyl ether substituent was found to extend into the S3 binding pocket.

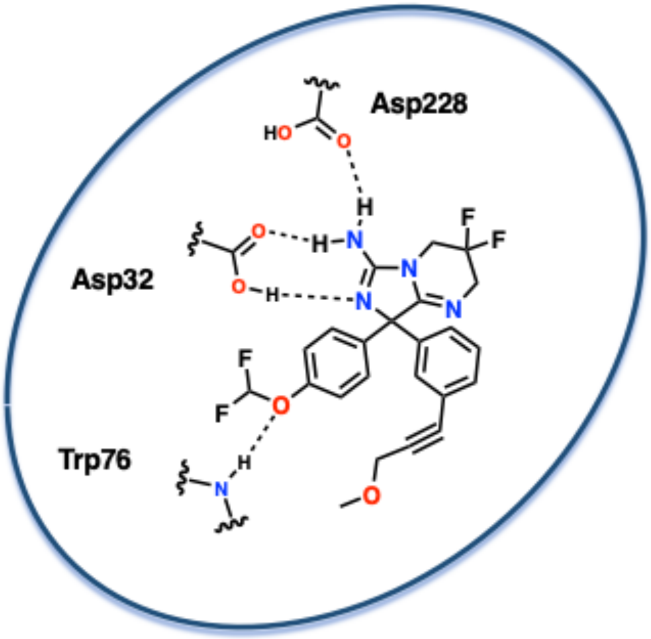

Figure 1.24 Representation of inhibitor **25**-bound in the catalytic domain of BACE1 (PDB: 4ACX).

1.2.3.4 Aminohydantoin/Iminohydantoin-containing Inhibitors

Modification of the bicyclic aminoimidazole core scaffold led to the initial hit, inhibitor **26** (Figure 1.25). Optimization of the aminohydantoin scaffold with *tri*-substituted aryl rings led to a vast improvement in potency (10 nM IC_{50}) and moderate selectivity (~80-fold against BACE2 and CatD).[81] It was observed the aminohydantoin moiety makes several interactions with Asp228 and Asp32 (Figure 1.26). Further analysis divulged that the phenylpyridine moiety made a water mediated hydrogen bond with Ser229. The corresponding aryl ring extends into the S2' binding pocket where the *p*-methoxy substituent makes a hydrogen bonding interaction with Trp76.[81] A Transgenic mouse model studies found that oral administration of inhibitor **27** at a dose of 100 mg/Kg resulted in the clearance of 69% of plasma $A\beta_{40}$ levels.[81]

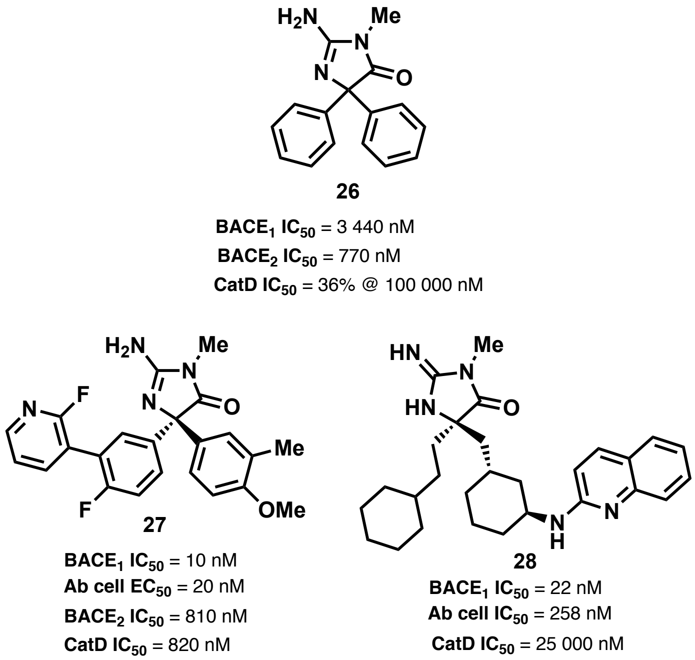

26

BACE$_1$ IC$_{50}$ = 3 440 nM
BACE$_2$ IC$_{50}$ = 770 nM
CatD IC$_{50}$ = 36% @ 100 000 nM

27

BACE$_1$ IC$_{50}$ = 10 nM
Ab cell EC$_{50}$ = 20 nM
BACE$_2$ IC$_{50}$ = 810 nM
CatD IC$_{50}$ = 820 nM

28

BACE$_1$ IC$_{50}$ = 22 nM
Ab cell IC$_{50}$ = 258 nM
CatD IC$_{50}$ = 25 000 nM

Figure 1.25 Representative examples of aminohydantoin-based inhibitors **26**-**28**.

Incorporation of an optimized aminocyclohexyl moiety was able to adequately accommodate the S1 pocket. The inhibitor **28** resulted in an exceedingly potent BACE1 inhibitor with a cellular inhibitory activity of 22 nM and >1136-fold selectivity against CatD.[82] Inhibitor **28** was found to participate in Van der Waals interactions with Ile110 and Lys107 while being situated in a solvent exposed pocket of the BACE1active site (Figure 1.26). In addition, the inhibitor **28** was administered *via* subcutaneous injection and orally in an *in vivo* study with rats and resulted in only the clearance of Aβ_{40} plasma levels by 55% and 65%, respectively.[82]

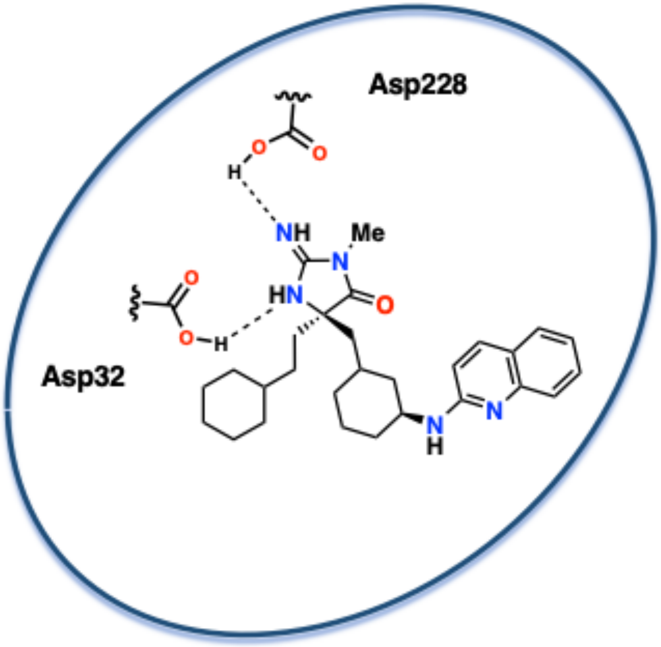

Figure 1.26 Representation of inhibitor **28**-bound in the catalytic domain of BACE1 (PDB: 4R95).

1.2.3.5 Aminothiazoline and Aminooxazoline-containing Inhibitors

Much like other non-peptide inhibitor campaigns discussed, the initial aminothiazoline core scaffold was discovered with HTS strategies (Figure 1.27).[83] Although inhibitor **29** exhibited moderate activity against BACE1, structural studies revealed that potential *meta*-substituents on the aryl ring could optimize interactions with the catalytic domain (Figure 1.28). Inhibitor **30** was a result of extensive optimization in which the fused bicyclic aminothiazoline was found to have excellent enzymatic and cellular potency against BACE1.[83] Moreover, oral administration (30 mg/Kg) of **30** was found to clear 10% of $A\beta_{40}$ levels which suggests that the compound has good affinity for PgP.

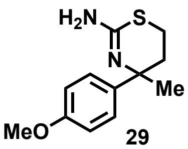

29

BACE1 IC$_{50}$ = 41 200 nM

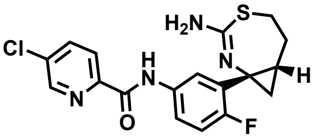

30

BACE1 IC$_{50}$ = 27 nM

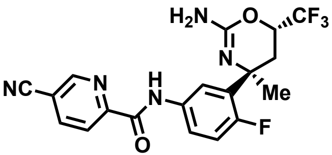

31

BACE1 IC$_{50}$ = 12 nM
Cell IC$_{50}$ = 2 nM
BACE2 IC$_{50}$ = >200 000 nM
CatD IC$_{50}$ = >200 000 nM

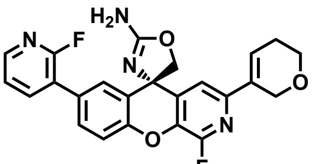

32

BACE1 IC$_{50}$ = 0.3 nM
Cell IC$_{50}$ = 4.0 nM

Figure 1.27 Representative examples of aminthiazoline- and aminooxazoline-based inhibitors **29**-**32**.

1.2.3.6 Dihydroquinazoline-containing Inhibitors

The unique hairpin-conformation observed for initial hit **33** is characteristic of the dihydroquinazoline isostere (Figure 1.29).[84] Structure activity relationships studies were conducted to explore ligands that could accommodate the largely vacant S1' subsite. Introduction of the (*S*)-cyclohexyl moiety was found to vastly improve potency (11 nM K_i) presumably from advantageous hydrophobic interactions in the S1' binding pocket (Figure 1.30). *In vivo* studies in rats resulted in clearance of up to 70% Aβ_{40} plasma levels but it's high affinity for PgP (efflux ratio 12.2) implies poor penetration of the BBB.[85] Replacement of the *N*-methyl amide for a substituted methyl thiazole furnished a BACE1 inhibitor **35** with promising inhibitory activity (Enzyme IC$_{50}$ = 13 nM and Cell IC$_{50}$ = 21 nM) (Figure 1.30).

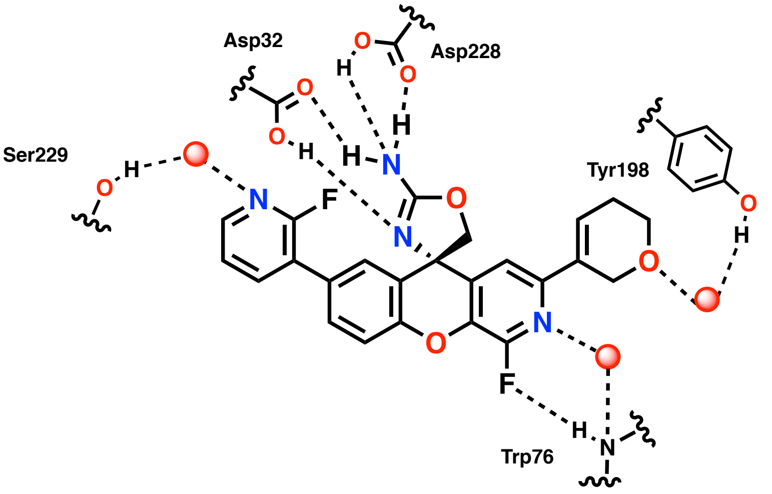
Asp32
Asp228
Ser229
Tyr198
Trp76

Figure 1.28 Representation of **32**-bound in the catalytic domain of BACE1 (PDB: 4WTU).

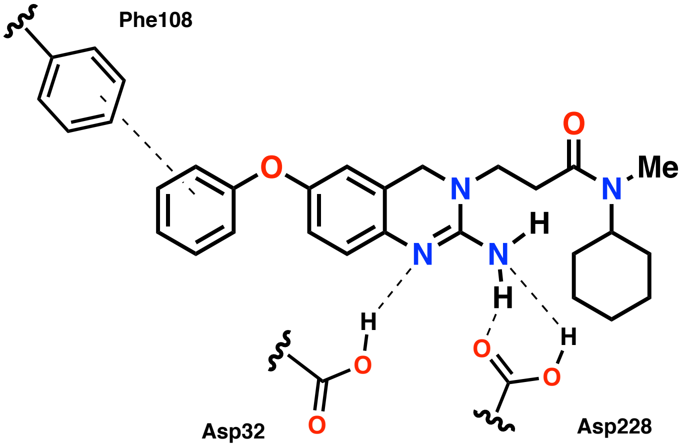
Phe108
Asp32
Asp228

Figure 1.29 Representation of **33**-bound in the catalytic domain of BACE1 (PDB: 2Q11).

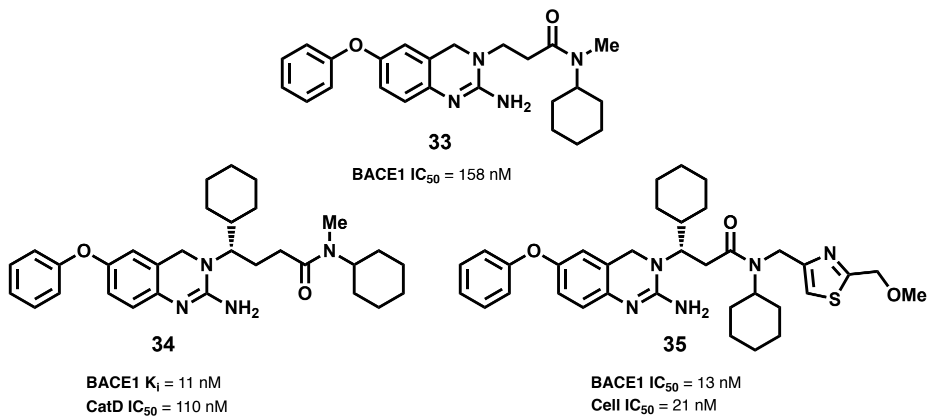
O
N
Me
N
NH2
33
BACE1 IC50 = 158 nM
Me
34
BACE1 Ki = 11 nM
CatD IC50 = 110 nM
S
OMe
35
BACE1 IC50 = 13 nM
Cell IC50 = 21 nM

Figure 1.30 Representative examples of dihydroquinazoline inhibitors **33**-**35**

1.2.3.7 Aminoquinoline-containing Inhibitors

A fragment-based approach was utilized to uncover the aminoquinoline scaffold (K_D = 900 μM) as a building block for BACE1 inhibitor design (Figure 1.31).[86] Further SAR studies revealed that

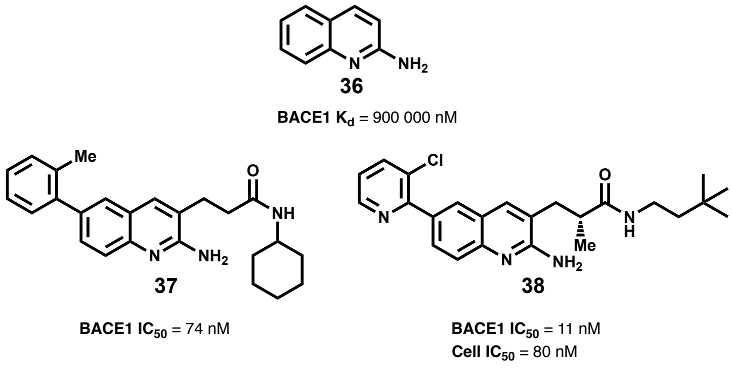
N
NH2
36
BACE1 Kd = 900 000 nM
Me
O
NH
37
BACE1 IC50 = 74 nM
Cl
N
Me
H
38
BACE1 IC50 = 11 nM
Cell IC50 = 80 nM

Figure 1.31 Representative examples of aminoquinoline-based inhibitors **36**-**38**.

C6 substitution of the aminoquinoline core as well as installation of a C3 *N*-substituted propionamide led to a number of potent inhibitors.[86] Inhibitor **37** with a C3 *N*-cyclohexyl amide moiety off the quinoline scaffold exhibited good inhibitory activity (74 nM IC_{50}) Incorporation of a (*R*)-α-methyl and a bulkier neohexyl propionamide, inhibitor **38**, showed to have improved enzymatic (11 nM IC_{50}) and cellular (80 nM IC_{50}) activity against BACE1 (Figure 1.32).[86]

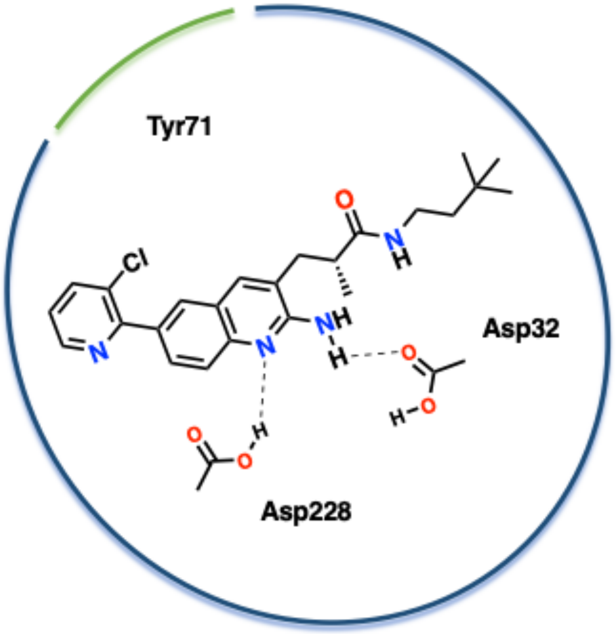

Figure 1.32 Representation of inhibitor **38** within the catalytic domain of BACE1 .

1.2.3.8 Pyrrolidine-containing Inhibitors

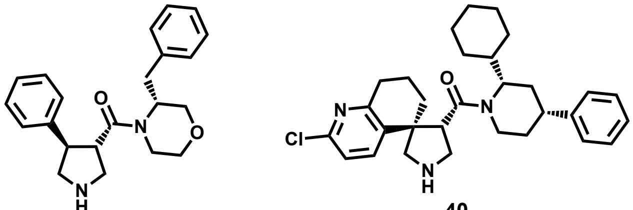

39

BACE1 IC_{50} = 240 000 nM

40

BACE1 IC_{50} = 29 nM
Cell IC_{50} = 570 nM
BACE2 IC_{50} = 29 nM
CatD IC_{50} = 6212 nM

Figure 1.33 Representative examples of pyyrolidine-based inhibitors **39-40**.

The initial hit, inhibitor **39**, of this series of compounds was discovered through the aid of HTS and was found to have poor infinity for BACE1 (240 μM) (Figure 1.33).[87] Through extensive SAR studies it was found that the 2,3-substituion of the pyrrolidine core was amenable to further inhibitor design. Moreover, the *cis*-2,4-substituded piperidine moiety of inhibitor **40** was shown to adequately fill a hydrophobic binding pocket located underneath the flap region of the BACE1 active site (Figure 1.34). As a result, the inhibitor **40** exhibited an improved enzymatic activity (29 nM IC_{50}) but a dramatic drop in potency in cell-based studies (570 nM IC_{50}). In addition, compound **40** was more potent against BACE2 while it was >200-fold selectivity against CatD.[87]

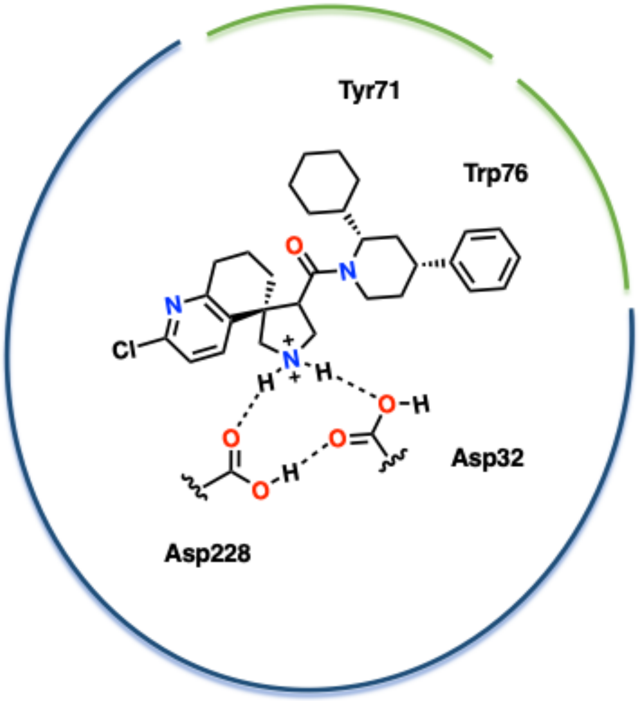

Figure 1.34 Representation of inhibitor **40** within the catalytic domain of BACE1.

1.2.3.9 Macrocyclic-containing Non-peptidic Inhibitors

As discussed earlier, macrocycles provide the opportunity to be able to restrict inhibitors in their bioactive conformation. The rare hairpin conformation observed in the class of inhibitors containing a dihydroquinazoline scaffold provides the opportunity for a macrocyclic inhibitor design strategy.[84] Inhibitor **41** with a dihydroquinazoline core was found to be exceedingly potent in enzymatic (5.0 nM, K_i) and cellular (7.0 nM IC_{50}) studies (Figure 1.35). Structural analysis of the binding mode of **41** revealed that the cyclohexyl functionality was situated within the S1 and S1' subsites (Figure 1.36).[88] Further, biological evaluation of inhibitor **41** found that the compound was a substrate of PgP and did not exhibit a propensity to clear Aβ levels. Additionally, macrocycles with an acyl guanidine core have been explored in detail. Inhibitor **42**, containing a 26-membered ring, proved to be a potent BACE1 inhibitor (32 nM IC_{50}) (Figure 1.35).[89] In a mouse model, inhibitor **42** was subcutaneously administered and found to clear 74% of Aβ levels found within the serum. In contrast, Aβ levels in the brain were maintained upon dosing with inhibitor **42**.[89]

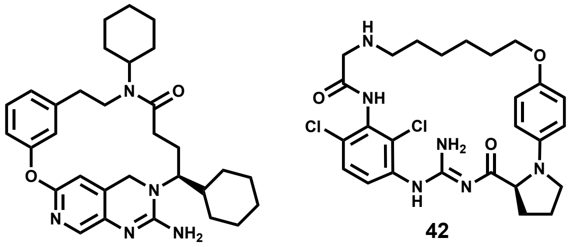

41

BACE1 IC_{50} = 5.0 nM
Cell IC_{50} = 7.0 nM

42

BACE1 IC_{50} = 32 nM
Cell EC_{50} = 140 nM
CatD IC_{50} = 22 400 nM

Figure 1.35 Representative examples of macrocyclic-based inhibitors **41**-**42**.

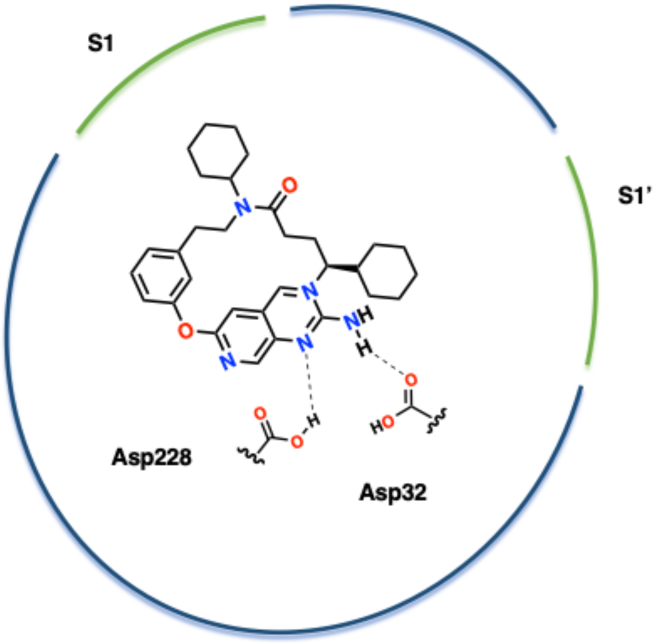

Figure 1.36 Representation of inhibitor **41** within the BACE1 active site.

1.2.4 Clinical Evaluation of BACE1 Inhibitors

Although there have been several fruitful endeavors in regard to BACE1 inhibitor design, the discovery of a successful BACE1 inhibitor in the clinic has proven to be an arduous task. Drug design campaigns that involve neurodegenerative diseases provide unique hurdles when compared to other drug design efforts. In the United States, thirteen potential AD therapies have entered clinical trials. Herein, six compounds, which have reached as far as phase II and III in clinical trials, will be briefly discussed in the following section (Figure 1.37).

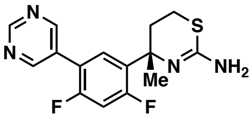

LY2811376
IC_{50} = 240 nM
EC_{50} = 303 nM

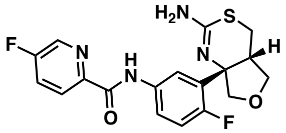

LY2886721
IC_{50} = 20.3 nM
EC_{50} = 10.7 nM

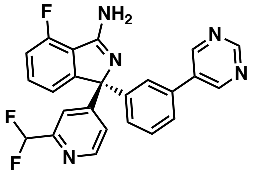

AZD3839
K_I = 26 nM
Caco-2 P_{app} = 23 X 10^{-6}
efflux ratio = 3.5
BACE2 K_i = 372.4 nM
catD K_i > 25 000 nM

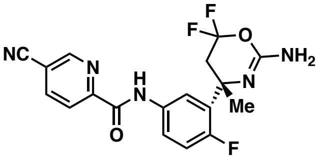

RG7129
BACE1 IC_{50} = 30 nM
HEK293 APP cell IC_{50} = 18 nM
BACE 2 IC_{50} = 40 nM

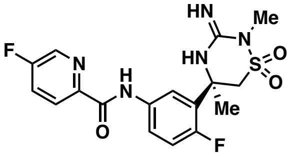

MK-8931

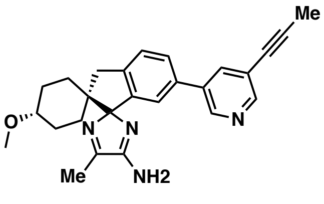

AZD3293

Figure 1.37 Representative examples of drug candidates for AD.

1.2.4.1 Clinical Evaluation of LY2811376

In 2009, Eli Lily initiated phase I of a clinical study for LY2811376. As previously discussed, the inhibitor belongs to the aminothiazoline-based inhibitors. In order to gauge the safety and tolerability of the inhibitor, 61 healthy women and men were entered into a dose dependent study (5 to 500 mg doses) where the inhibitor was administered orally to the patients.[90] It was found that maximal plasma and CSF levels were reached after 2h and 5h post-dose, respectively. Additionally, a dose of 90 mg resulted in an 80% clearance of CSF Aβ over 7 h after dosing with LY2811376. More importantly, the inhibitor was found to be tolerable with doses up to 500 mg.[91]

Further, a long term rat toxicology study was initiated in parallel with the phase I clinical trial. When doses of 30 mg/kg were administered over a 3 month period it was observed that the rats were developing a retinal toxicity. In result, the inhibitor was pulled from clinical trials prior to the initiation of phase II. A follow up study uncovered that there was no significant retinal toxicity found in participants of the human clinical trials that were conducted in phase 1.[91]

1.2.4.2 Clinical Evaluation of LY2886721

The next drug candidate with an aminothiazoline core from Eli Lily, LY2886721, was able to reach phase II of clinical trials. The inhibitor was put through an extensive phase I clinical study that encompassed over 150 patients.[92] Several dose-dependent studies in which LY2886721 was administered orally were done to evaluate the safety and tolerability of the compound in healthy subjects. In addition, concentrations of the inhibitor as well of the clearance of $A\beta_{40}$ in the plasma and CSF were measured throughout the study.

Additionally, in 2010 a single-dose dependent study was conducted on healthy adult males and females with the spectrum of dosing being 1 to 200 mg or the administration of a placebo. A multiple-dose dependent study which involved the oral administration of doses in the range of 5-35 mg to 42 healthy adults. Participants of the clinical trial were screened for any clinical benefits of the treatment and clearance of the inhibitor as well as $A\beta_{40}$ within the plasma and CSF.[93]

Further, LY2886721 was administered to 128 patients that were showing mild symptoms of Alzheimer's disease. Over 26 weeks LY2886721 or a placebo was orally administered in a range of doses (15 mg, 35 mg, 70 mg).[94] Several cognitive tests as well as monitoring the clearance of $A\beta_{40/42}$ in the plasma and CSF were conducted during the study.[95] Due to abnormal biochemistry observed in the liver the phase II clinical trial was immediately terminated by Eli Lily. Currently, Eli Lily has not published the clinical results from the previous studies.[94]

1.2.4.3 Clinical Evaluation of AZD3839

Preclinical studies found that AZD3839 had good enzymatic inhibitory activity as well as a moderate selectivity profile against common aspartic acid proteases.[96] Several animal studies exhibited that the inhibitor was able to reduce brain and plasma $A\beta_{40/42}$ levels at varying doses. As a result, in 2001 AstraZeneca moved AZD3839, containing an aminopyrimidinone core scaffold, into phase I clinical trials.[96] 72 healthy patients were given oral capsules as part of a single-dose dependent study (1 to 300 mg dose or placebo). The inhibitor was proven to be tolerable as less patients taking AZD3839 reported adverse effects, 31%, when compared to the cohort taking a placebo, 39%. AZD3839 was able to clear $A\beta_{40/42}$ plasma levels up to 56% and 39% in a dose-dependent fashion.[97] Upon completion of the phase I clinical trial in 2011, Astrazeneca terminated any future plans for clinical studies of AZD3839.

1.2.4.4 Clinical Evaluation of RG7129

In September 2011, Hoffman-La Roche's RG7129, also known as RO5508887, entered clinical trials as a BACE1 inhibitor for the treatment of AD. The inhibitor exhibited great cellular potency, 18 nM cell IC_{50}, but it failed to have any selectivity against common off-site target, BACE2.[98] Initial clinical studies featured a cohort made up of 49 healthy males. A single-dose dependent study was conducted and plasma levels of the inhibitor and $A\beta_{42}$ were measured for up to 142.5 h post-administration. Dietary effects on the pharmacological properties of RG7129 and the appearance of adverse effects were studied.[99] A cohort of 42 healthy patients were recruited to investigate the biomarker levels found in the plasma and CSF.[100] Another phase I trial study was carried out to gather information about the safety profile of RG7129 after prolonged administration of the inhibitor.[101] In the fall of 2013, Hoffman-La Roche terminated the clinical development of RG7129 without disclosing the results of their clinical studies.

1.2.4.5 Clinical Evaulation of MK-8931

Merck brought their BACE1 drug candidate, MK-8931 (verubecestat), into the clinic in December 2011. Subjects that made up the initial clinical studies were provided with single- and multiple-increasing daily doses over the course of 14 days.[102] In all of these initial studies, MK-8931 was found to be tolerable in all subjects. A dose-dependent reduction of $A\beta_{40}$ levels in the CSF in both the single-dose and multiple-dose studies were 25-61% and 32 to 94%, respectively.[102] Safety and pharmacokinetic properties of MK-8931 were investigated in 32 patients with mild-to-moderate AD. Volunteers of the study received a once daily oral dose of MK-8931 at varying doses (12 mg, 40 mg, 60 mg) as well as a placebo over 7 days. The $A\beta_{40}$ and *s*APPβ levels in the CSF of the diseased patients were evaluated during the trial.[103] Moreover, MK-8931 was administered to patients that were inflicted with varying degrees of renal impairment. A one-time oral dose of MK-8931 was given to patients and its pharmacokinetic properties were measured over 120 h: plasma concentration, degree of renal clearance, and excretion through the urinary tract.[104]

400 mild-to-moderate AD patients were recruited for an extended safety study that was part of a phase II/III clinical trial. Diseased patients were treated once daily with an oral dose of MK-8931 over the course of 78 weeks and efficacy was evaluated with a myriad of cognitive and pharmacokinetic tests. The second part of the clinical study consisted of a similar dosing regimen but lasted up to 260 weeks.

In late 2013, the Data Monitoring Committee suggested that MK-8931 should proceed to phase II/III clinical trials. At the same time, Merck decided to begin a 104 week phase III trial that consisted of oral administration of 12 or 40 mg once daily in early-onset AD patients. The trial was supposed to be completed in March of 2021.[105] However, Merck decided to abruptly end its phase 3 clinical trial in early 2018. The company cited that there was a small chance for a positive benefit from continuation of treatment with MK-8931.

1.2.4.6 Clinical Evaluation of AZD3293

Belonging to the nonpeptide aminoimidazole-based inhibitors, AZD3293 (lanabecestat) was brought forward into clinical trials after the termination of drug candidate AZD3893. Initiation of a phase I clinical trial involved the oral administration of a single dose-dependent regime in healthy patients.[106] In order to investigate potential adverse effects, an oral dose of AZD3293 was provided in the range of 1 to 1000 mg or placebo over the course of 10 days.[107] An additional phase I two-part clinical trial was carried out with 47 patients. During part one of the study healthy elderly patients were exposed to an oral solution of 5 mg or greater of AZD3293.[108] The second part of the study consisted of patients that were exhibiting mild-to-moderate AD symptoms. Patients from part one and two were evaluated for adverse effects, plasma and CSF clearance, biomarkers, and clearance of AZD3293.

In order to study possible drug-drug interactions, the drug candidate was co-administered with common FDA approved drugs: itraconazole (anti-fungal), diltiazem (anti-hypertensive), and midazolam (sedative).[109] A cohort of healthy Japanese patients were given single and multiple doses of varying concentrations. The pharmacokinetic profile of AZD3293 and reduction of $A\beta_{40/42}$ concentrations were investigated for the cohort. Additional studies investigated the potential modulation that AZD3293 could have on patients' QT interval.[110] Bioavailability studies were conducted in order to observe the difference in uptake of an oral solution versus tablet formulations.

In September of 2014, AstraZeneca partnered with Eli Lilly to further develop AZD3292 as a drug candidate for AD. This culminated in a phase II/III clinical trial that aimed to recruit over

2,000 patients with mild AD symptoms.[111] The diseased patients were orally administered AZD3293 (LY3312814) once daily at a dose of 20 or 50 mg for 104 weeks. However, in June 2018 the clinical trial was terminated due to lack of efficacy observed in patients.

With as many as 13 drug candidates having gone through extensive clinical trials, the two recent late phase terminations of the clinical trials of MK-8931 and AZD3293 provides a sobering reminder of the difficulties that come along with drug development of neurodegenerative diseases such as AD. However, the wealth of knowledge that has been gathered in regard to BACE1 drug design continues to suggest that BACE1 is a viable target for AD. Current advancements in BACE1 drug development provide hope that a successful clinical outcome is on the horizon.

1.3 Further Development of Lead Compound, GRL-8234

With the absence of a successful BACE1 inhibitor within the clinic, Alzheimer's disease drug development continues to be a significant hurdle in the realm of drug discovery. Our laboratory has been a pioneer and leader in the search of a clinically viable BACE1 inhibitor. One of the promising inhibitors that has been a product of these endeavors is GRL-8234, **11** (Figure 1.12). As previously discussed, **11** is an exceedingly potent (1.0 nM K_i) and moderately selective inhibitor (BACE2 K_i = 137 nM & CatD K_i = 81 nM) against BACE1.[69]

Further, GRL-8234 was subjected to a myriad of proof-of-concept studies. Initial studies involved the administration of **11** *via* intraperitoneal injection which exhibited a clearance of interstitial $A\beta_{40}$ levels by as much as 65% over a duration of 12 h.[69] An additional long term transgenic (Tg2576) mouse model study was carried out with the administration of a solution of GRL-8234 *via* implanted osmotic pumps over 220 days; this resulted in 65% clearance of $A\beta_{40/42}$ levels when compared to the control cohort.[68] Treatment of **11** in a mouse model over approximately 7 months showed better results when compared to a control group that participated in cognitive tests such as the Morris water maze.[68]

Recent animal studies with 5XFAD transgenic mice were completed with mice at different stages of disease progression. Younger 5XFAD mice (4 months), which were observed to have moderate Aβ plaque deposition, exhibited a return in cognitive function after daily doses (33.4 mg/kg) over 2 months. In contrast, older 5XFAD mice (10 months) with a severe amount of plaque deposition remained cognitively impaired when treated with the same regimen of GRL-8234.[112] In addition, AD biomarkers in the older mice suggested that GRL-8234 failed to deter the harmful mechanisms that are responsible for the increased accumulation of Aβ plaque in a diseased brain. Nonetheless, GRL-8234 proves to be well tolerated and safe in animal models during short- and long-term studies.[112] Therefore, it continues to be considered a viable lead compound that is a prime candidate for further drug development in hopes to furnish a successful outcome within the clinic. Herein, the design strategy, synthesis, and biological evaluation of a novel class of BACE1 inhibitors that are inspired by GRL-8234 will be discussed in detail

1.3.1 Optimization of Core Scaffold of BACE1 Inhibitors

A successful drug candidate must have the ability to be able to cross the BBB, neuronal, and other cell membranes.[113] Previous studies have installed fluorines within traditional transition-state mimics to be able to optimize the pharmacological properties of BACE1 inhibitors.[53,63,114] For instance, peptidomimetic inhibitors **43** and **44** installed a 3,5-difluorophenylmethyl moiety as a P1 ligand with both hydroxyethylamine and hydroxyethylene transition-state isosteres (Figure 1.38).[115,116]

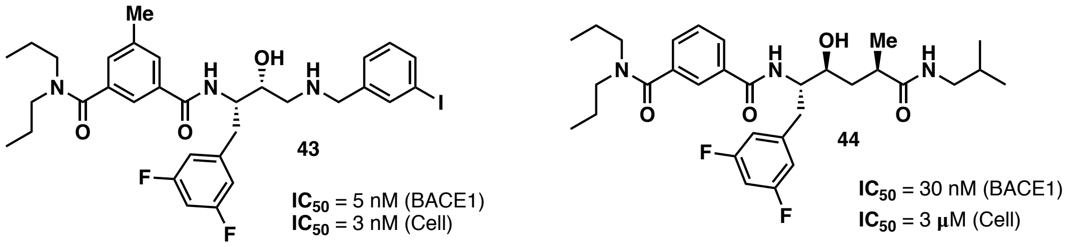

43

IC_{50} = 5 nM (BACE1)
IC_{50} = 3 nM (Cell)

44

IC_{50} = 30 nM (BACE1)
IC_{50} = 3 μM (Cell)

Figure 1.38 Representative examples of BACE1 inhibitors **45** and **46** containing a difluoro isostere.

BACE1 inhibitors that utilize a non-hydrolyzable dipeptide isostere containing a phenylalanine P1 ligand are prevalent in numerous potent, selective, and cell permeable inhibitors. The core scaffold of inhibitor **45** is typically prepared through the nucleophilic addition of an appropriate amine with an optically active phenylmethyl epoxide **46** (Scheme 1.1).[63,117] Stereoselective synthesis of the desired phenylmethyl epoxides are usually furnished by utilizing optically pure 3,5-difluorophenyl alanine **47**.[118] A novel approach to furnish the 3,5-difluorophenyl alanine containing core scaffold can be realized from *tert-butyl*-((*S*)-1-(*S)*-oxiran-2yl)-2-phenylethyl carbamate **46**.

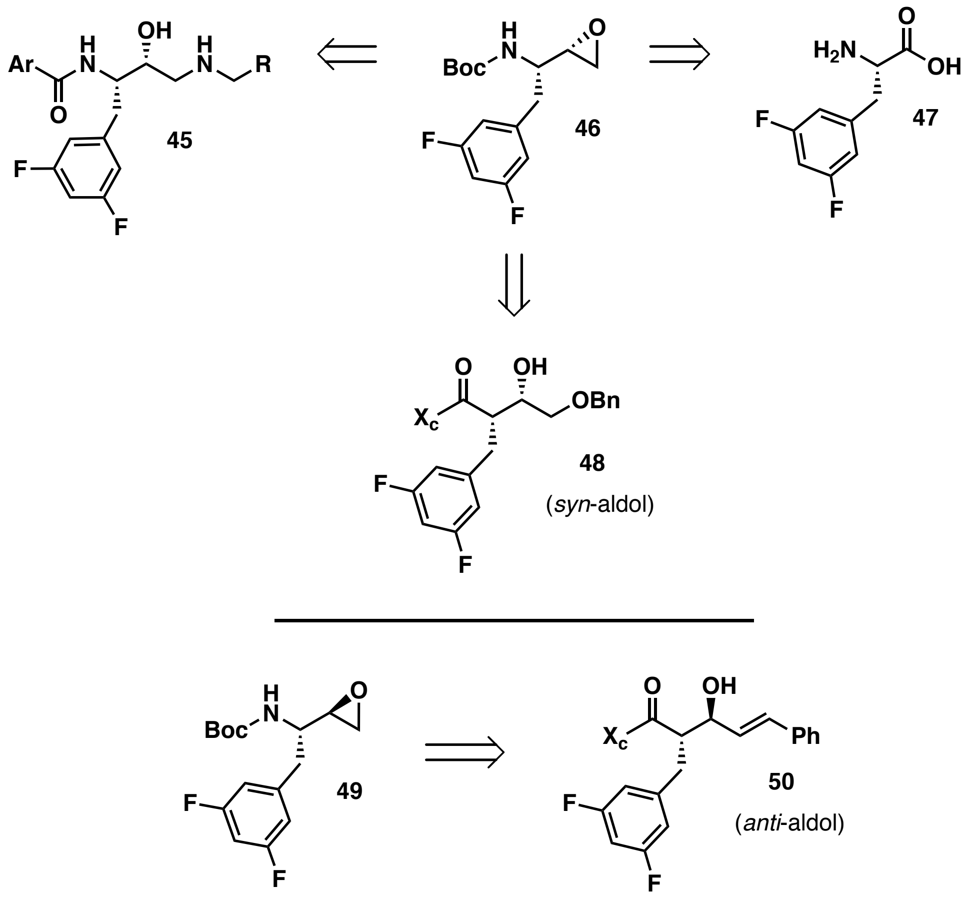

Scheme 1.1 Reterosynthetic design strategy for preparation of optically active epoxides **46** and **49**.

Our laboratory envisaged that an asymmetric *syn*-aldol can be used as a key step in route to the valuable building block, difluoroepoxide **46**.[119,120] The *syn*-aldol adduct **48** establishes a route to **46** by cleavage of the chiral auxiliary (Xc) and subsequent Curtius rearrangement of the resulting acid to afford the crucial amine functionality (Scheme 1.1). The diastereocontrol of the aldol additions can be explained by the stereochemical model shown in scheme 1.2. Utilizing a monodentate and bidentate aldehyde will lead to stereo-defined aldol adducts, *anti*- and *syn*-adducts

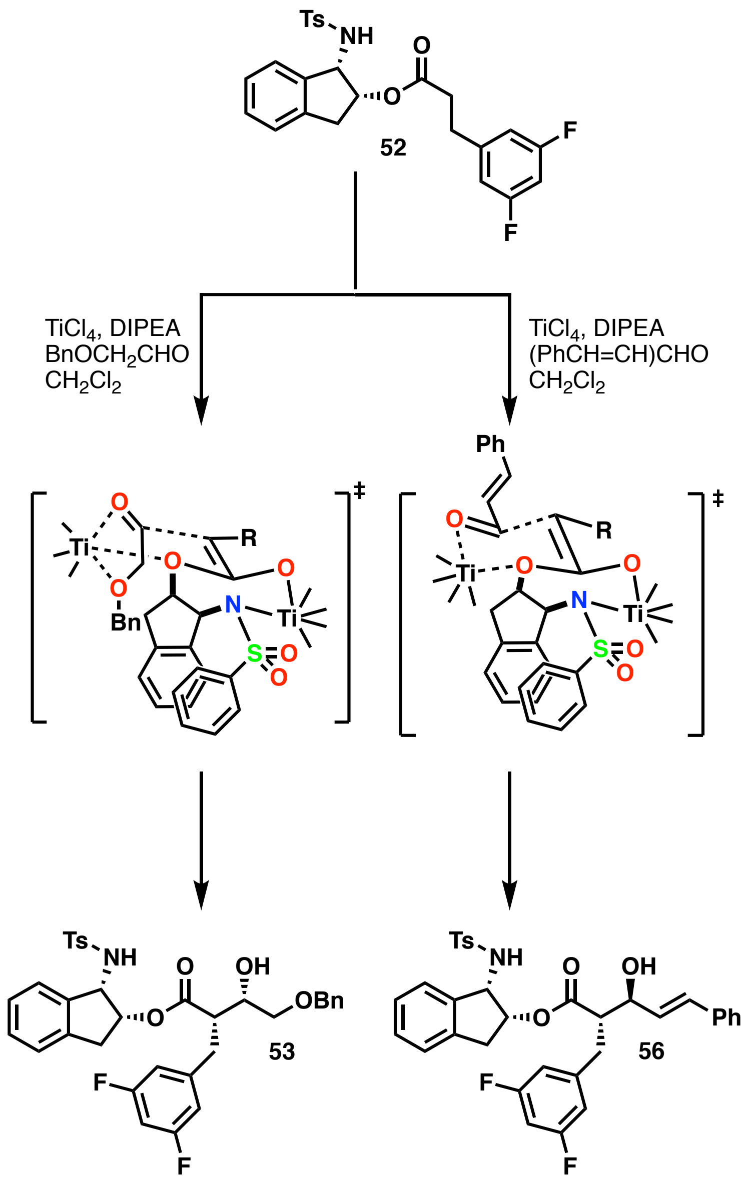
Ts
NH
O
O
52
F
F
TiCl4, DIPEA
BnOCH2CHO
CH2Cl2
TiCl4, DIPEA
(PhCH=CH)CHO
CH2Cl2
Ph
O
Ti
R
O
O
O
Bn
N
Ti
S
O
O
‡
53
OH
OBn
56
Ph

Scheme 1.2 Representative stereochemical model for the syn- and anti-aldol additions involving titanium-mediated (Z)-enolates.

respectively.[119–121] Analysis of the transition state in previous work has revealed that the ether oxygen of a bidentate aldehyde, such as (benzyloxy)acetaldehyde, can coordinate with $TiCl_4$ which results in the benzyloxy substituent to be positioned in a pseudo axial orientation. As a result, the reaction of a (*Z*)-titanium enolate with a precomplexed bidentate aldehyde would provide the *syn*-aldol addition product with excellent diastereocontrol. Conversely, identical aldol addition conditions with a monodentate aldehyde, *trans*-cinnamaldehyde, proceed through an expected Zimmerman-Traxler transition state to provide the *anti*-aldol product **50** almost exclusively. The following provides a protocol for diastereoselective preparation of (2*R*,3*S*)-1,2-epoxy-3-(Boc-amino)-4-(3,5-difluorophenylmethyl)-butane **46** and its corresponding diastereomer **49**.

Initially, we explored an ester-derived titanium enolate based asymmetric aldol to yield *syn*- and *anti*-aldol adducts for the preparation of optically active oxiranes, **46** and **49**.[119] Scheme 1.3, depicts the protocol used to prepare oxirane **46** where easily accessible 3,5-difluorohydrocinnamic acid, prepared in multi-gram quantities as outlined in the literature, is used as a starting point. Treatment of acid **50** with commercially available auxiliary, *N*-tosyl-1-aminoindan-2-ol, **51** with DCC along with catalytic DMAP in CH_2Cl_2 at 23 °C at 18 h provides ester **52** in 76% yield.[120] Exposure of ester **52** to a solution of $TiCl_4$ followed by treatment with Hünig's base in CH_2Cl_2 at 0 °C and warmed to 23 °C which was stirred for 2 h at the same temperature. Precomplexing (benzyloxy)acetaldehyde with $TiCl_4$ at -78 °C and slow addition of the titanium enolate over 5 minutes provided the *syn*-aldol adduct **53** in 60% yield as a single diastereomer by ^1H NMR.[119] Hydrolysis of the chiral auxiliary of **53** with an aqueous solution of lithium hydroperoxide at 0 °C which was allowed to stir overnight at 23 °C to furnish the desired acid. In refluxing benzene, the acid was treated with diphenylphophorazidate and triethylamine for 12 h to afford the oxazolidinone **54** in 70% yield. Diol **55** was prepared in a two-step sequence: base mediated hydrolysis of **54** in the presence of KOH, exposure to di-*tert*-butyl dicarbonate in aqueous CH_2Cl_2 at 23 °C for 4 h. Palladium catalyzed reductive cleavage of the benzyl ether in the presence of a hydrogen atmosphere in ethyl acetate at 23 °C provided diol **55** in 77% yield. Regioselective monotosylation of **55** was done by treatment with dibutyltin oxide (25 mol%) in the presence of *para*-toluenesulfonylchloride and triethylamine at 23 °C for 4 h.[122]

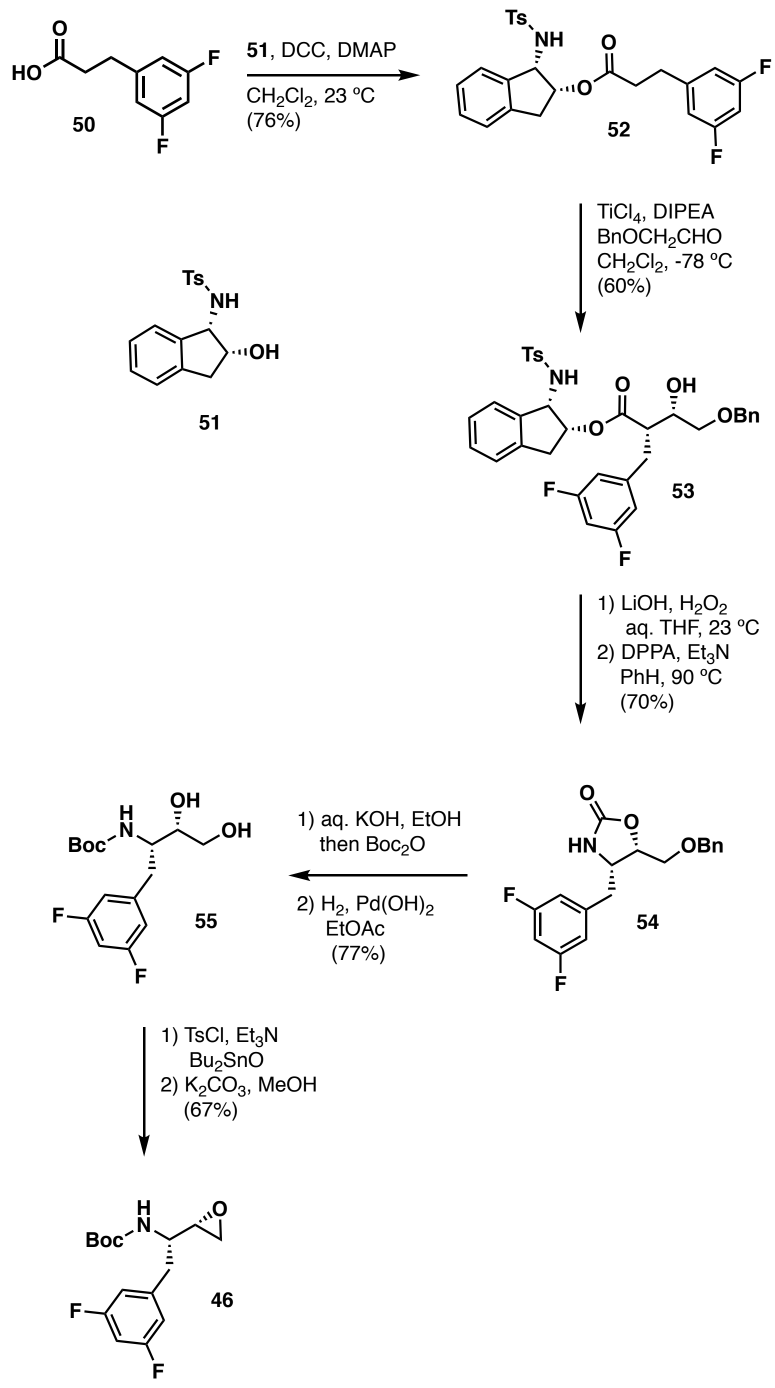
50
51, DCC, DMAP
CH2Cl2, 23 °C
(76%)
52
51
TiCl4, DIPEA
BnOCH2CHO
CH2Cl2, -78 °C
(60%)
53
1) LiOH, H2O2
aq. THF, 23 °C
2) DPPA, Et3N
PhH, 90 °C
(70%)
54
1) aq. KOH, EtOH
then Boc2O
2) H2, Pd(OH)2
EtOAc
(77%)
55
1) TsCl, Et3N
Bu2SnO
2) K2CO3, MeOH
(67%)
46

Scheme 1.3 Preparation of **46** by utilizing a syn aldol as a key step.

Immediate exposure of the tosylate with potassium carbonate at 0 °C followed by 1 h at 23 °C provided the (*S*)-2-(3,5-difluorophenyl)-(*S*)-oxiranyl ethyl carbamate **46** in 67% in two-steps.[122]

The route provided the 3,5-difluoroepoxide in good yields and was shown to be amenable to multi-gram scale up for the preparation of BACE1 inhibitors.

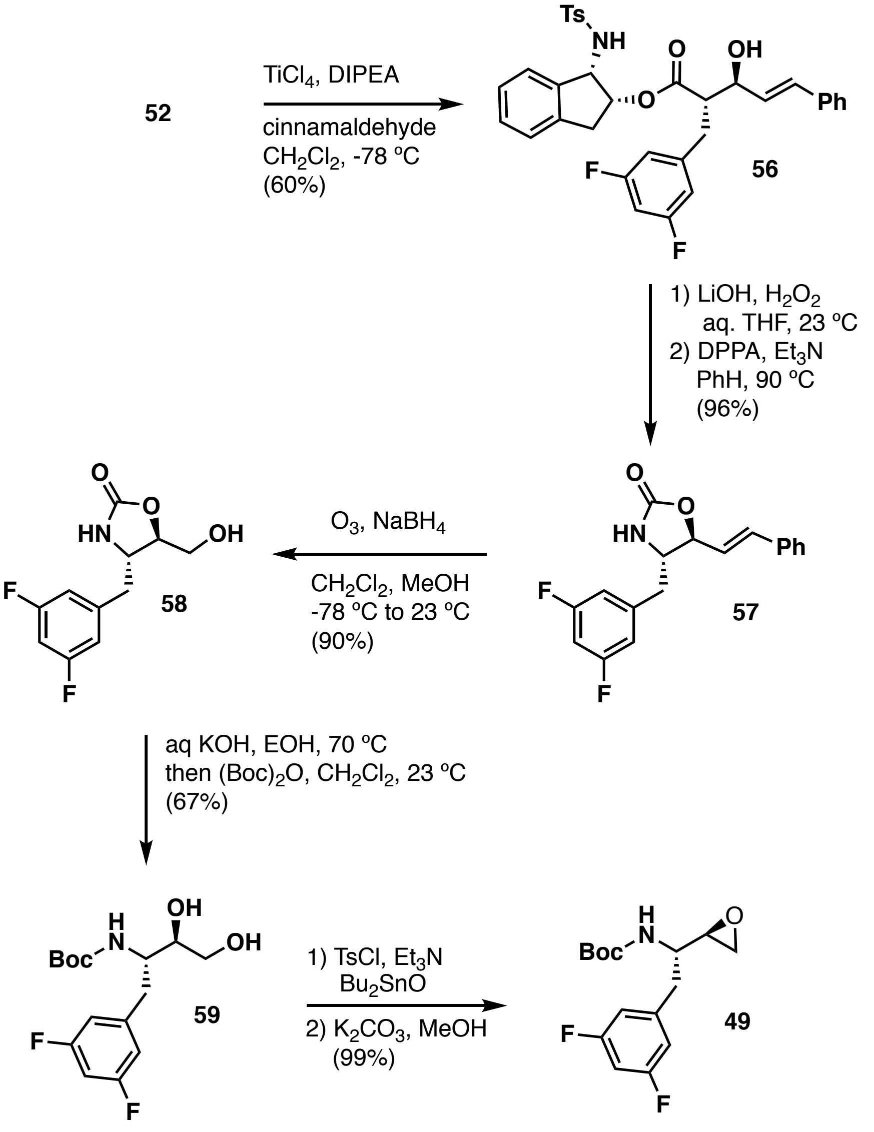
52
TiCl4, DIPEA
cinnamaldehyde
CH2Cl2, -78 °C
(60%)
Ts
NH
O
OH
O
Ph
F
F
56
1) LiOH, H2O2
aq. THF, 23 °C
2) DPPA, Et3N
PhH, 90 °C
(96%)
O
O
HN
Ph
F
F
57
O3, NaBH4
CH2Cl2, MeOH
-78 °C to 23 °C
(90%)
O
O
HN
OH
F
F
58
aq KOH, EOH, 70 °C
then (Boc)2O, CH2Cl2, 23 °C
(67%)
H
N
Boc
OH
OH
F
F
59
1) TsCl, Et3N
Bu2SnO
2) K2CO3, MeOH
(99%)
H
N
Boc
O
F
F
49

Scheme 1.4 Preparation of **49** by utilizing an anti-aldol addition as a key step.

Preparation of oxirane **49** was furnished by utilizing a diastereoselective *anti*-aldol with (*E*)-cinnamaldehyde as a key step (Scheme 1.4).[121] In the same way, the corresponding titanium enolate was generated by treating **52** with a 1M solution of $TiCl_4$ in CH_2Cl_2 in the presence of

Hünig's base. Upon treatment with precomplexed (*E*)-cinnamaldehyde at -78 °C for 3 h furnished *anti*-aldol adduct **56** as one diastereomer (confirmed by ^{1}H and ^{13}C NMR). Further, saponification of **56** with lithium hydroperoxide in aqueous tetrahydrofuran and a subsequent Curtius Rearrangement yielded oxazolidinone **57** in 96% over a two-step sequence. Ozonolytic cleavage of the styrenyl moiety in a (4:1) mixture of CH_2Cl_2 and MeOH at -78 °C was subjected to sodium borohydride mediated reduction to provide **58** in 90% yield. The two-step protocol discussed earlier was used, base-mediated hydrolysis and *N*-Boc protection, to yield the desired diol **59** in 67% yield over two steps. Selective monotosylation followed by ring closure in the presence of potassium carbonate in MeOH at 23 °C furnished (*S*,*R*)-3,5-difluorophenylmethyl oxirane **49** in 99% yield.[122]

As shown in scheme 1.5, the utilization of Evans' diastereoselective *syn*-aldol as a key step to provide oxirane **46** was also explored as an alternative route. Preparation of the optically active carboxamide **61** was done by the corresponding mixed anhydride, formed *in situ* with pivaloyl chloride, being treated with lithiated oxazolidinone **60**.[123] The *syn*-aldol product **62** was prepared through an Evan's diastereoselective aldol addition to (benzyloxy)acetaldehyde in the presence of *N,N*-diisopropylethylamine and dibutylboron trifluoromethanesulfonate (Bu_2BOTf) in CH_2Cl_2 at -78°C as exclusively one diastereomer.[123] The isolated *syn*-aldol product **62** was converted to the chiral oxazolidinone **63** over three chemical steps: hydrolysis of the chiral auxiliary with lithium hydroperoxide in aqueous tetrahydrofuran and a Curtius Rearrangement in the presence of DPPA and triethylamine at 90 °C, and palladium catalyzed reductive cleavage of the benzyl ether. Utilizing conditions described previously, epoxide **46** can be accessed in three additional chemical steps. In addition, we explored an alternative route to **46** in order to expand the utility of the methodology (Scheme 1.5). In this revised route, *trans*-cinnamaldehyde was used in our Evan's diastereoselective aldol addition.

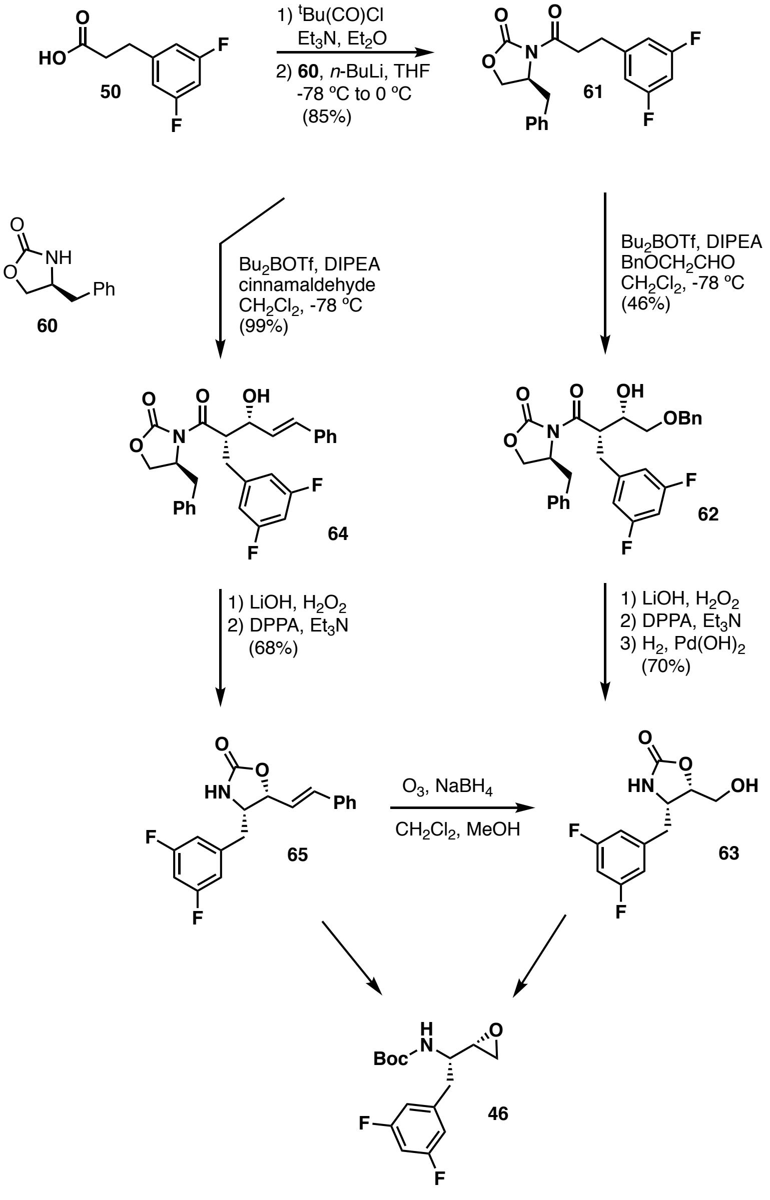
1) ^{t}Bu(CO)Cl
Et$_3$N, Et$_2$O
2) 60, n-BuLi, THF
-78 °C to 0 °C
(85%)
50
61
60
Bu$_2$BOTf, DIPEA
cinnamaldehyde
CH$_2$Cl$_2$, -78 °C
(99%)
Bu$_2$BOTf, DIPEA
BnOCH$_2$CHO
CH$_2$Cl$_2$, -78 °C
(46%)
64
62
1) LiOH, H$_2$O$_2$
2) DPPA, Et$_3$N
(68%)
1) LiOH, H$_2$O$_2$
2) DPPA, Et$_3$N
3) H$_2$, Pd(OH)$_2$
(70%)
65
O$_3$, NaBH$_4$
CH$_2$Cl$_2$, MeOH
63
46

Scheme 1.5 Preparation of **46** by utilizing Evan's diastereoselective syn-aldol addition as a key step.

The diastereoselective aldol addition went smoothly with the previously discussed 3,5-difluorohydrocinnamic acid derivative and *trans*-cinnamaldehyde to give the *syn*-aldol product **64** in 99% yield. This provides a significant improvement from our aldol addition with (benzyloxy)aldehyde in our previous strategy. In addition, trans-cinnamaldehyde (25 g/$20.80) is markedly less expensive than (benzyloxy)acetaldehyde (5 g/$159.00). The styrenyl oxazolidinone **65** was prepared by base-mediated hydrolysis and concomitant Curtius rearrangement over 2 steps in 68% yield. Ozonolytic cleavage of **65** provided alcohol **63** that can be converted to epoxide **46** over three steps.

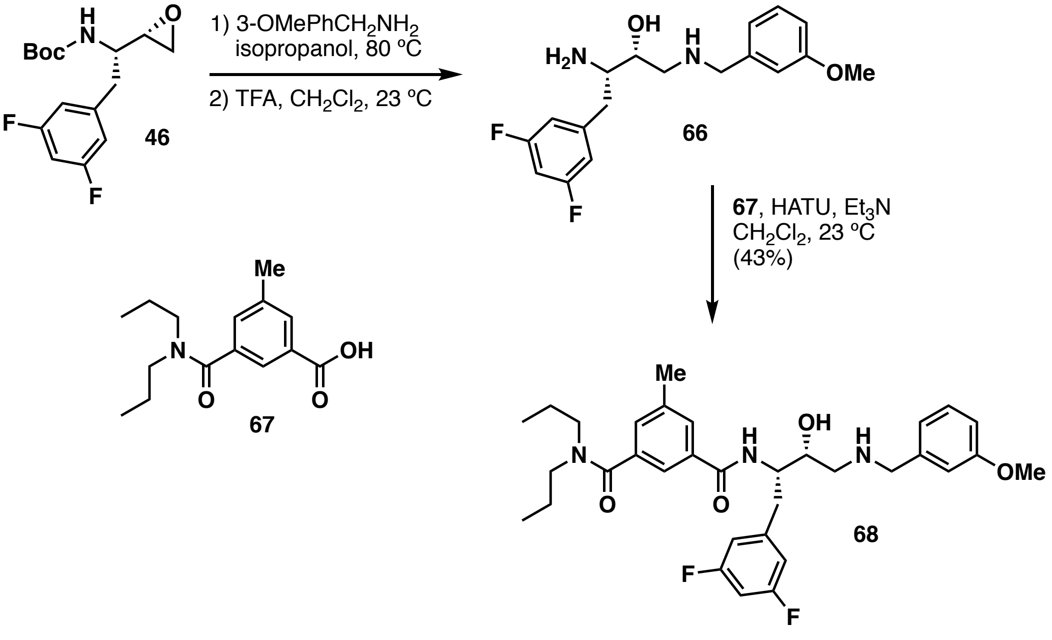

Scheme 1.6 Preparation of BACE1 inhibitor **68** from optically active oxirane **46**.

We employed *tert*-butyl((*S*)-2-(3,5-difluorophenyl)-1-((*S*)-oxrian-2-yl)ethyl)carbamate for the preparation of known inhibitor **68** (Scheme 1.6). Optically active oxirane **46** was submitted to nucleophilic epoxide opening in the presence of 3-methoxybenzylamine in refluxing isopropanol followed by deprotection with trifluoroacetic acid provided amino alcohol **66**. Acid **67** was coupled to amino alcohol **66** in the presence of HATU and triethylamine to provide inhibitor **68** in 43% yield over three steps.[120]

The following methodology establishes an amenable route towards the preparation of aminoalkyl epoxides **46** and **49** with a 3,5-difluorophenylmethyl substituent using an asymmetric aldol addition reaction as the key step.[120] In order to install the desired amine functionality a Curtius Rearrangement was carried out in refluxing benzene. The synthetic strategy establishes a modular, scalable and efficient route towards valuable building blocks that can be used to prepare a wide array of inhibitors.

1.3.1.1 Alternative Preparation of Core Scaffold: Azo Epoxide

Additionally, we have prepared the core scaffold of BACE1 inhibitors in an alternative method. Desired alkyl azo epoxides have been prepared previously in the literature to prepare hydroxyethylamine isosteres for inhibition of aspartic acid proteases, such as HIV-1 protease.[124] In accord with previous literature, allyl alcohol can **71** can prepared by 1,4-addition of butadiene monoxide **69**.[124] This provides the allyl alcohol **71** that can be subjected to asymmetric Sharpless epoxidation to provide the optically active oxirane **72**. Further, regioselective azidation of **72** in presence of trimethylsilyl azide and titanium(IV) isopropoxide furnishes 1,2-diol **73**.[125] Lastly, a two step ring closure process is carried out to yield the optically pure 3,5-difluorophenylmethyl azo epoxide **74** which can be used to prepare a wide variety of isosteres for protease inhibitor design campaigns.

Commercially available butadiene monoxide **69** was treated with 3,5-difluorophenylmagnesium bromide **70** in the presence of catalytic copper cyanide in tetrahydrofuran at -78 °C for 1.5 h in a 79% yield (Scheme 1.7). The resulting allylic alcohol **71** was subjected to asymmetric Sharpless epoxidation conditions with (-)-diethyl-*D*-tartrate, *tert*-butylhydroperoxide, and titanium(IV) isopropoxide at -20 °C to provide epoxide **72** in excellent yields and enantioselectivity. A regioselective epoxide opening was carried out with diazidodiisopropoxytitanium, which was prepared *in situ* by treatment of trimethylsilyl azide with titanium(IV) isopropoxide, in refluxing benzene to provide diol **73** in a moderate yield.[125] Optically active azido epoxide **74** was prepared over two chemical steps in good yields: regioselective tosylation in the presence of catalytic dibutyltin oxide, 4-dimethylaminopyridine, tosyl chloride and triethylamine in CH_2Cl_2 at 23 °C for 12 h and K_2CO_3 mediated ring closure in methanol at 0 °C for 3 h. The isolated azido epoxide **74** was used in the preparation of the BACE1 inhibitors discussed in the following discussion.[122]

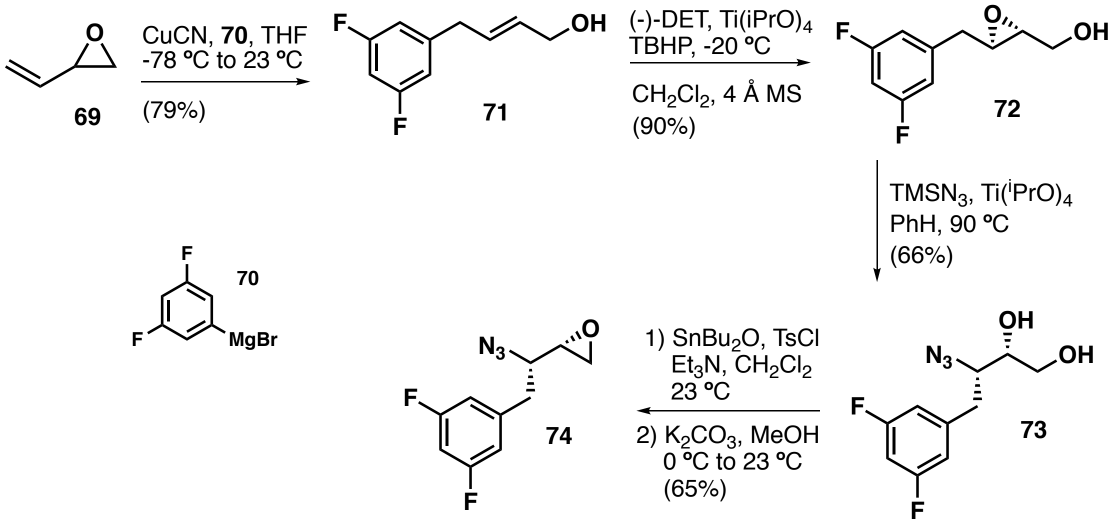
69
CuCN, 70, THF
-78 °C to 23 °C
(79%)
71
(-)-DET, Ti(iPrO)4
TBHP, -20 °C
CH2Cl2, 4 Å MS
(90%)
72
TMSN3, Ti(iPrO)4
PhH, 90 °C
(66%)
70
MgBr
F
N3
OH
O
73
1) SnBu2O, TsCl
Et3N, CH2Cl2
23 °C
2) K2CO3, MeOH
0 °C to 23 °C
(65%)
74

Scheme 1.7 Preparation of azo epoxide **74** from commercially available butadiene monoxide **69**.

1.3.2 Optimization of P1’ Ligand: Design & Synthesis of Spirocyclic Amines

As previously discussed, one of the hallmark challenges in AD drug development is that AD is a chronic disease and a drug must be administered throughout the life of a patient. As a result, a successful BACE1 inhibitor must be selective against other common off-site targets, namely BACE2 and CatD.[63,94] Several laboratories, including our laboratory, have targeted opportune interactions within the flap region of the catalytic domain in a pursuit to prepare potent and selective BACE1 inhibitors. The P1’ 3-methoxybenzylamine of GRL-8234 is situated conveniently to take advantage of a slew of hydrophobic and hydrogen bonding interactions. Taking a closer look at a GRL-8234-bound BACE1 X-ray crystal structure, it appears that a P1’α- and α,α-substituted benzyl amine can potentially access additional interactions in the BACE1 active site (Figure 1.39).[69] It possible that small- and medium-sized spirocyclic rings can accommodate the binding pocket. Moreover, the 3-methoxy substituent of the benzylamine does not participate in any additional interactions with the active site so a survey of substituents with various electronic and steric profiles can lead to further optimization. In the following section, the synthetic design and preparation of the proposed α,α-spirocyclic benzylamines as P1’ ligands will be discussed in length.

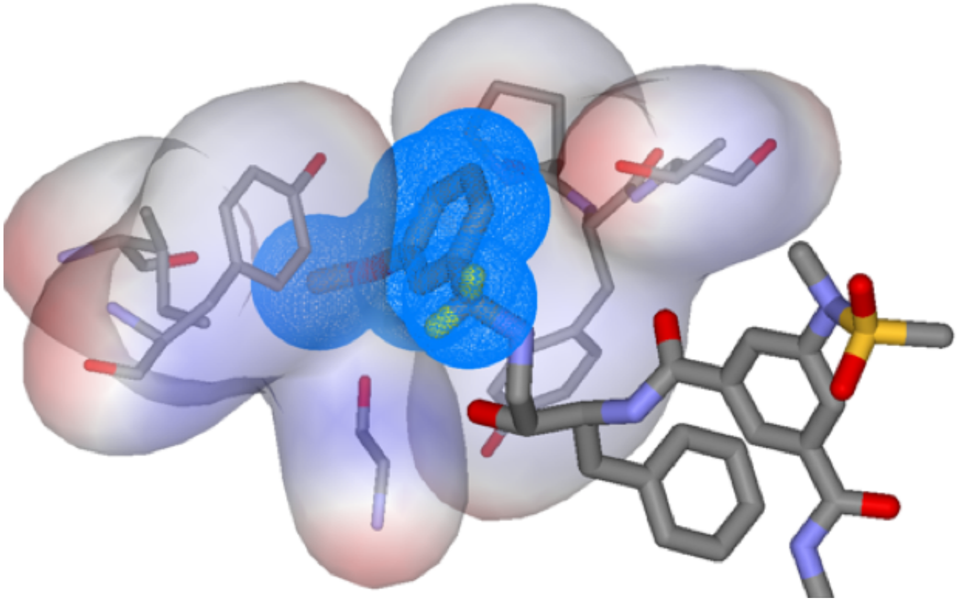

Figure 1.39 Stereoview of GRL-8234-bound BACE1 and its interactions with the flap region of the catalytic active site. (Methylene protons of benzyl amine shown in yellow for clarity)

1.3.2.1 Preparation of Spirocyclic Cyclopropyl Benzylamines

Initially, installation of spirocyclic cyclopropanes were investigated at the benzylic position of the 3-methoxybenzylamine. Simmons-Smith cyclopropanation conditions are often the most commonly used method to efficiently furnish cyclopropanes.[126–128] In order to furnish the desired spirocyclic benzyl amines, α,β-unsaturated esters can be used to provide the spirocyclic cyclopropyl esters through a Simmons-Smith or Corey-Chaykovsky protocol[129–131]. Upon saponification of the ester followed by Curtius Rearrangement conditions could furnish the cyclopropyl amine. However, the deactivation of the olefin caused by an electron withdrawing moiety, such as an ester, can lend to sluggish reactions and poor yields when traditional conditions are used to prepare the cyclopropane. An alternative approach involves the use of a modified Kulinkovich reaction where treatment of nitriles with alkyl grignard and stoichiometric titanium(IV) isopropoxide has been extensively shown in the synthesis of cyclopropyl

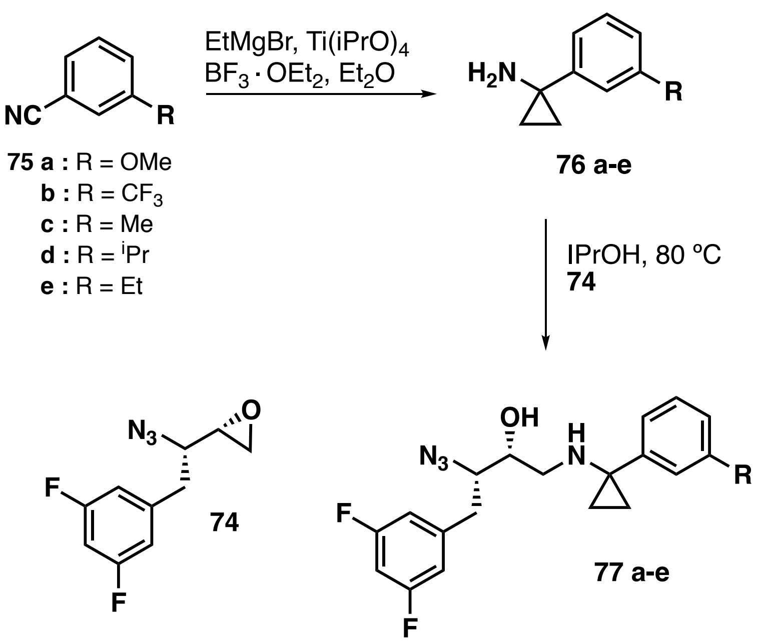

Scheme 1.8 Preparation of azo alcohols **77a-e** with a modified Kulinkovich serving as a key step.

amines.[132,133] Moreover, it has been shown that the cyclopropyl amines (Figure 1.40) can be prepared over a broad scope of substrates which makes it ideal for the preparation of several amines in a structure activity relationship (SAR) study (Figure 1.41).

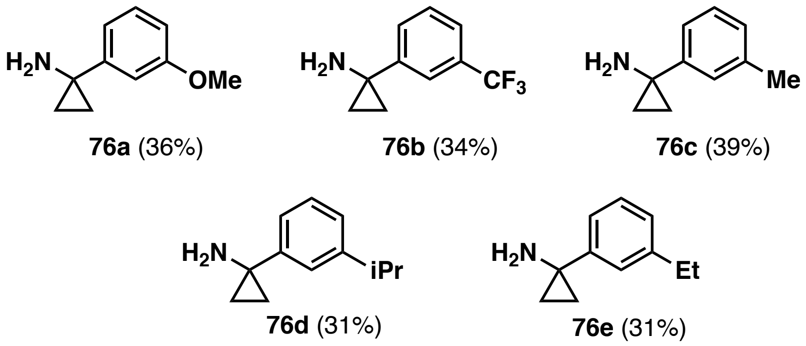
76a (36%)
76b (34%)
76c (39%)
76d (31%)
76e (31%)

Figure 1.40 Structures of cyclopropyl amines **76a-e**.

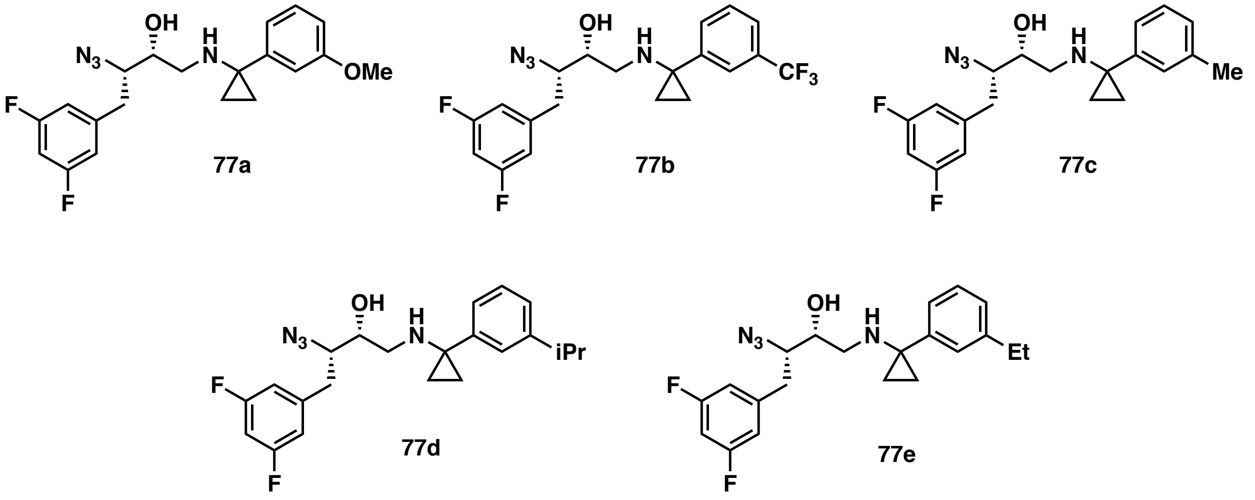
77a
77b
77c
77d
77e

Figure 1.41 Structures of azo alcohol isosteres **77a-e**.

Our laboratory utilized the modified Kulinkovich conditions to produce a number of cyclopropyl benzylamines as P1' ligands. Treatment of the commercially available nitrilearenes **75a-e** with titanium(IV) isopropoxide with ethylmagnesium bromide in ether at -78 °C provides a reactive titanacyclopropane that can react with nitriles to provide an azatitanacycle which can be quenched with boron trifluoride diethyl etherate to provide cyclopropyl amines **76a-e** in modest yields (Scheme 1.8).[133] Epoxide opening of **74** with selected amines **76a-e** in refluxing isopropanol for 12 h provided the azido alcohols **77a-e** in good yields over two steps in moderate to excellent yields.[124]

1.3.2.2 Preparation of Racemic Heterospirocyclic Benzylamines

In addition to cyclopropylamines, it was envisaged that small- to medium-sized heterocyclic rings can take advantage of not only hydrophobic interactions within the flap region but also pick up additional hydrogen bonding interactions. Our laboratory has explored a racemic preparation of both spirocyclic tetrahydrofurans and tetrahydropyrans.

A common approach to preparation of the proposed heterospirocycles is the addition of an appropriate organometallic reagent, often generated *in situ*, to widely commercially available oxo-cyclic ethers. Previously in the literature, it has been shown that the desired spirocyclic amines can be made in three steps: nucleophilic addition to an appropriate ketone, acid-mediated substitution with sodium azide, and reduction over catalytic Pd/C in a hydrogen atmosphere.[134] As a result, we elected to use dihydrofuran-3-one **78** and dihydropyran-3-one **79** to be able to furnish oxo-spirocyclic benzylamines in a racemic protocol. The synthetic strategy for the preparation of the aforementioned amines is discussed in detail below (Scheme 1.9).

The appropriate oxo-cyclic ethers **78** and **79** were treated with *in situ* prepared *meta*-substituted arylmagnesium bromides **80a-e** in refluxing tetrahydrofuran for 1 h to furnish tertiary alcohols **81a-j** (Scheme 1.10). The resulting alcohols **81a-j** were subjected to trifluoroacetic acid in the presence of sodium azide at 0 °C and was allowed to stir for 24-48 h at 23 °C to yield azides **82a-j**. It should be noted that depending on the substituent of the aryl ring and size of the cyclic ether the β-elimination product was observed as a minor product. Reductions of the azides **82a-j** were carried out in the presence of catalytic Pd/C in a hydrogen atmosphere for 12 h to provide the desired oxo-spirocyclic benzylamines **83a-j** (Figure 1.42). As discussed above, the epoxide **74** was subjected to ring opening conditions by treatment with appropriate amines **83a-j** in refluxing isopropanol to furnish isosteres **84a-j** in good yields over four chemical steps (Figure 1.43).[124]

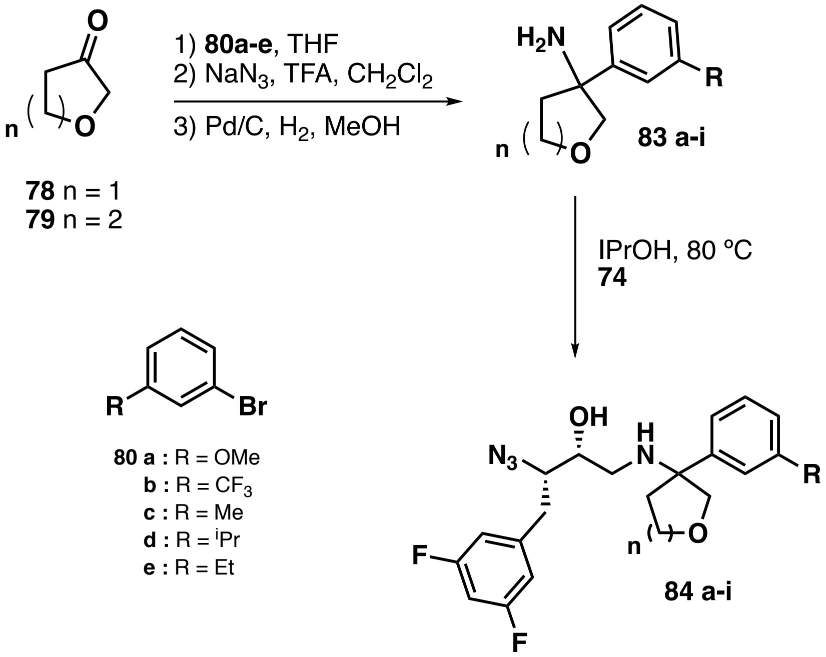

O
n
O
78 n = 1
79 n = 2
1) 80a-e, THF
2) NaN$_3$, TFA, CH$_2$Cl$_2$
3) Pd/C, H$_2$, MeOH
H$_2$N
R
n
O
83 a-i
IPrOH, 80 °C
74
R
Br
80 a : R = OMe
b : R = CF$_3$
c : R = Me
d : R = ^{i}Pr
e : R = Et
OH
N$_3$
H
N
R
n
O
F
F
84 a-i

Scheme 1.9 Preparation of spirocyclic benzylamines 84a-j from commercially available from oxo-cyclic ethers **78** and **79**.

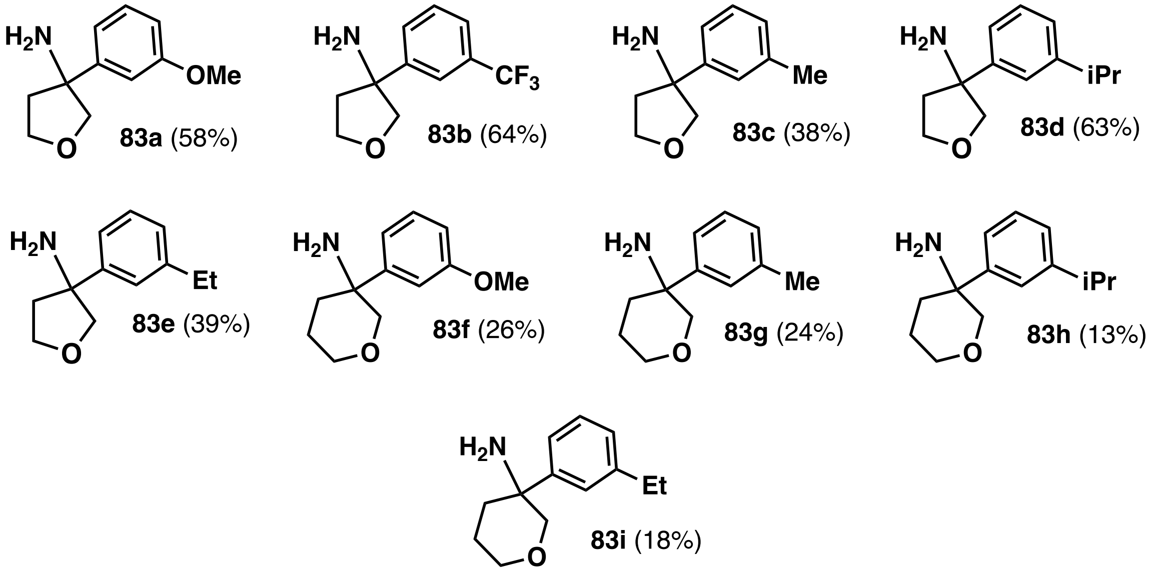

83a (58%)
83b (64%)
83c (38%)
83d (63%)
83e (39%)
83f (26%)
83g (24%)
83h (13%)
83i (18%)

Figure 1.42 Structures of racemic spirocyclic ethers **83a-i**.

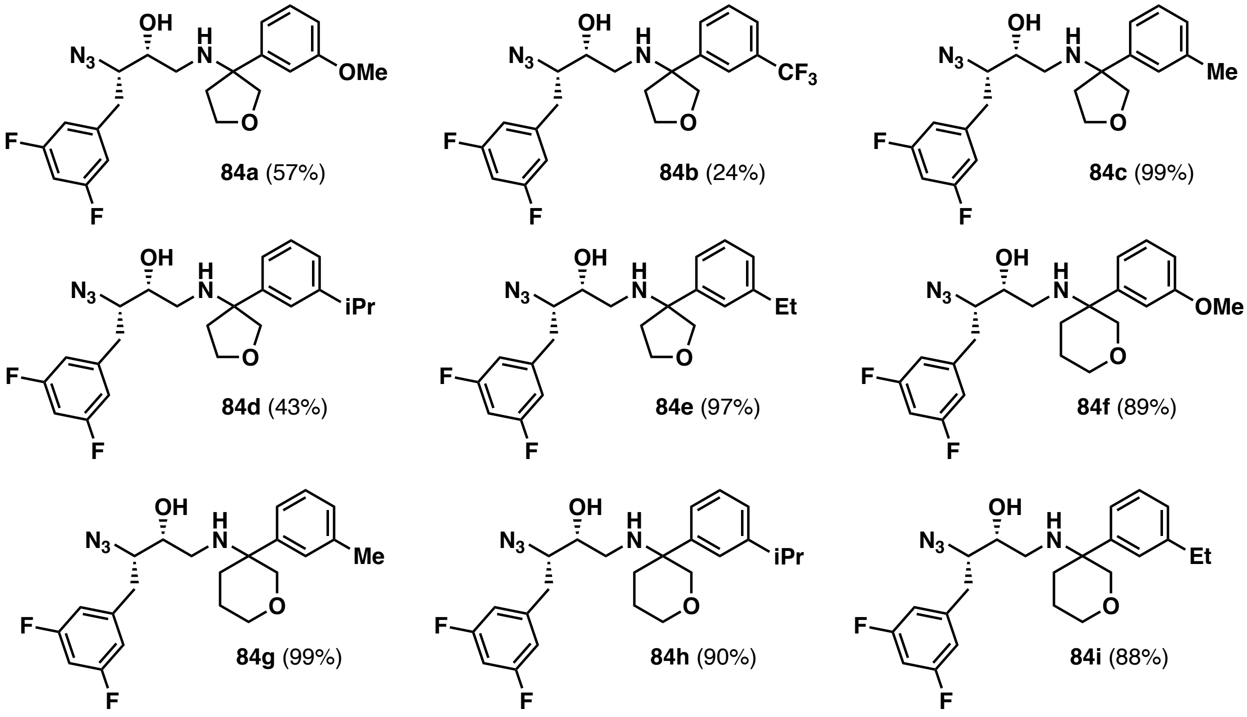

84a (57%)
84b (24%)
84c (99%)
84d (43%)
84e (97%)
84f (89%)
84g (99%)
84h (90%)
84i (88%)

Figure 1.43 Structures of azo alcohol isosteres **84a-i**

1.3.2.3 Diastereoselective Approach to Heterospirocyclic Benzylamines

Ellman's auxillary has been used extensively in the literature to be able to prepare optically active amines for various applications.[135] More specifically, Ellman and co-workers have prepared optically active 1,2-amino alcohols **85a-d** and precursors **86a-d** in good yields and stereoselectivity from the addition of various organometallic reagents to *tert*-butylsulfinyl aldimines **87a-b** and ketimines **87c-d** which contain α-benzyloxy and α-silyloxy-substituents (Scheme 1.10).[136,137]

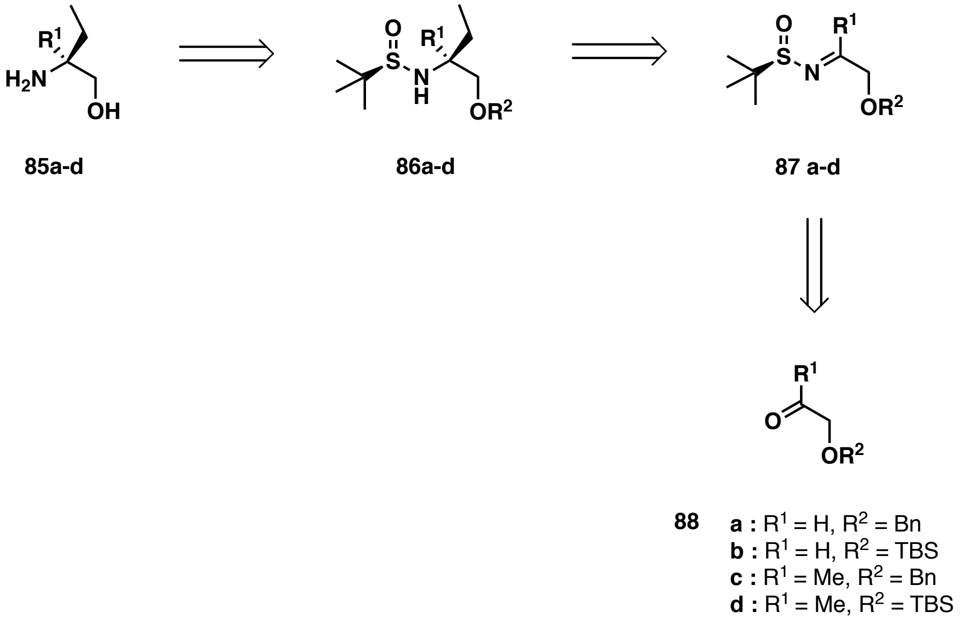
85a-d
86a-d
87 a-d
88
a : R^1 = H, R^2 = Bn
b : R^1 = H, R^2 = TBS
c : R^1 = Me, R^2 = Bn
d : R^1 = Me, R^2 = TBS

Scheme 1.10 Ellman's and co-workers reterosynthetic design strategy towards optically active 1,2-amino alcohols **85a-d**.

Where the imines were prepared through condensation of α-benzyloxy or α-silyloxy methyl ketone **88a-d** with an optically active *tert*-butylsulfonamide.[137] Interestingly, it was found that inverse stereoinduction, addition from *Re* face, from what has been previously reported in the literature was observed for grignard additions to alkyl or aryl-substituted α-benzyloxy and α-silyloxy *N*-sulfinyl aldimines. This inverse stereoinduction can be explained by the transition state analysis shown in figure 1.44.[136,137] Moreover, it was found that analogous *N*-sulfinyl ketimines that were subjected to grignard additions did not experience the same inverse stereoinduction, addition from the *Si* face, as the proceeding *N*-sulfinyl aldimines (Figure 1.45).[137–139] As a result, the grignard additions proceeded through the expected six-membered transition state, shown in figure 1.45, observed with alkyl and aryl *N*-sulfinyl imines in the literature. In an effort to prepare the desired oxo-spirocyclic benzylamines in an enantioselective manner, our laboratory has explored a route that utilizes a diastereoselective allylation of aryl *N*-sulfinyl ketimines **92a-c** as a key step.

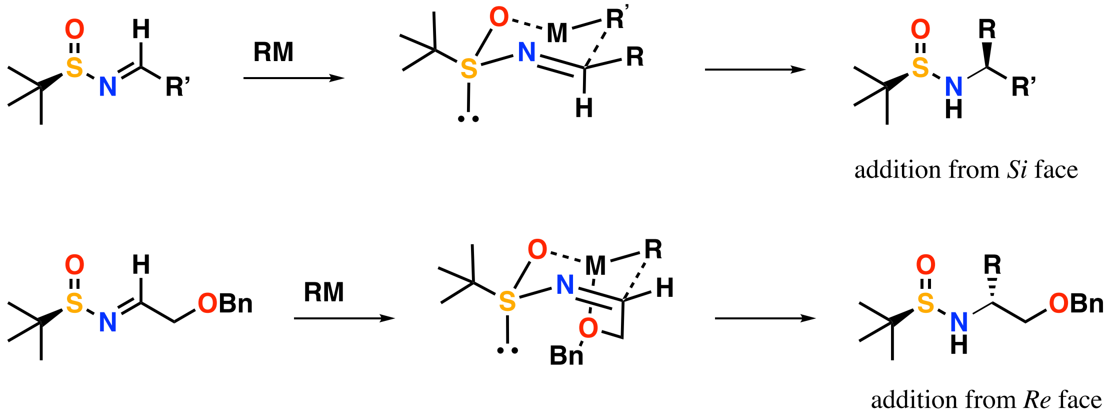

addition from *Si* face

addition from *Re* face

Figure 1.44 Explanation of reverse stereoinduction observed for grignard additions to α-benzyloxy and α-silyloxy N-sulfinyl aldimines

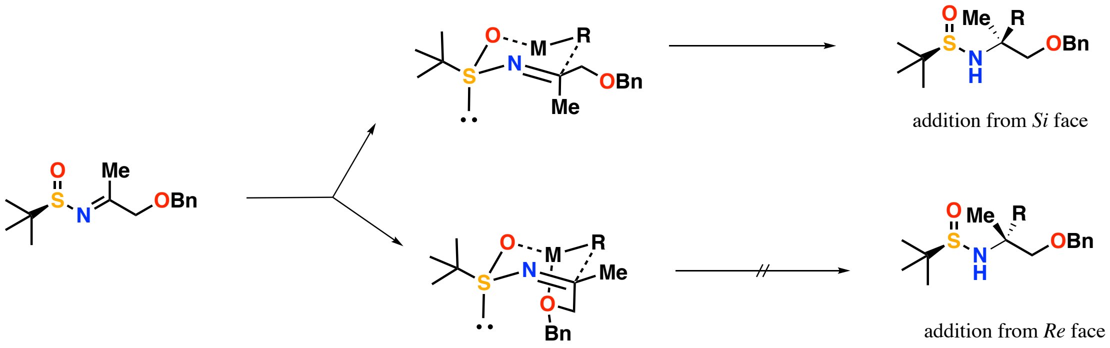

Figure 1.45 Explanation of a return to expected stereoselectivity for grignard additions to α-benzyloxy and α-silyloxy N-sulfinyl ketimines.

Initial studies involved the diastereoselective allylation of aryl-substituted α-silyloxy *N*-sulfinyl ketimine **92a-c** prepared at a gram scale from the appropriate aryl-substituted α-(silyloxy)ketone **91a-c** (Scheme 1.11). The resulting α,α-substituted *N*-sulfinyl amine **(*R*)-93a-c** is proposed to be a common intermediate that can be utilized to furnish both THF- and THP-based spirocyclic benzylamines, **(*R*)-96a** and **(*R*)-99a** respectively. In order to furnish the THF-based spirocycle, ozonolytic cleavage of **(*R*)-93a** followed by a reductive workup would provide the alcohol **(*R*)-94a** (Scheme 1.12). Deprotection of the silylether upon treatment with *tert*-butylammonium fluoride provided diol **(*R*)-95a** followed by a ring closure protocol would furnish the corresponding spirocyclic ether **(*R*)-96a**. Additionally, the THP-based derivatives could be accessed through hydroboration-oxidation of the **(*R*)-93a** to afford the desired alcohol **(*R*)-97a** (Scheme 1.13). Following the same protocol discussed above, it was proposed that the desired spirocycle **(*R*)-99a** could be obtained. The proposed synthetic strategy to prepare the desired spirocyclic amines will be discussed in detail.

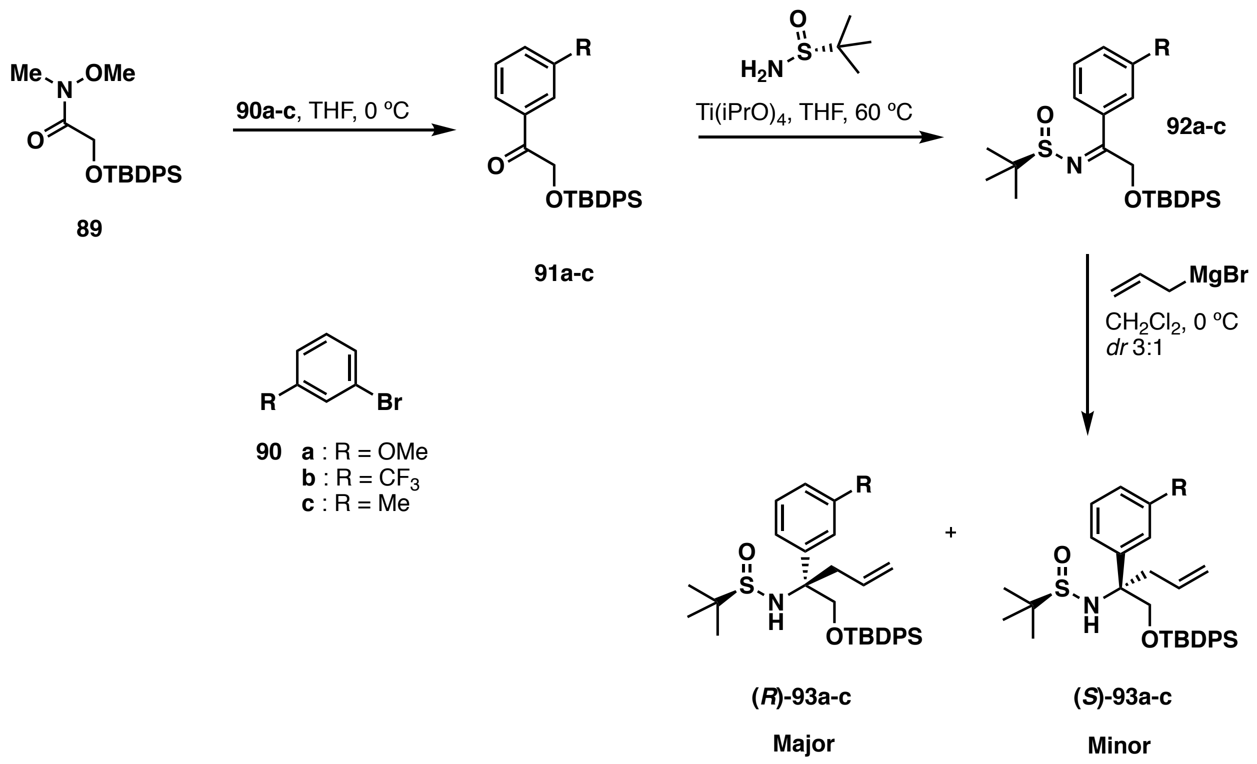

Scheme 1.11 Preparation of α, α, α-substituted N-sulfinyl amines **(R)-93a-c** and **(S)-93a-c** via a diastereoselective allyl grignard addition to an optically active aryl α-silyloxy N-sulfinyl ketimine **92a-c** as a key step.

The aryl ketones **91a-c** can be prepared by addition of arylmagnesium bromide **90** in tetrahydrofuran at 0 °C to the corresponding weinreb amide **89** to provide the desired product **91a-c** in excellent yields (Scheme 1.11). Condensation of the aryl α-silyloxy ketone **91a-c** in the presence of titanium(IV) isopropoxide and (*R*)-*tert*-butyl-sulfonamide in toluene at 80 °C for 12 h furnished the product in moderate yields. Addition of allylmagnesium bromide to the aryl *N*-sulfinyl ketimine **92a-c** in CH_2Cl_2 at 0 °C for 1 h gave the corresponding sulfinyl amines **(*R*)-93a-c** and **(*S*)-93a-c** as an inseparable diastereomeric mixture of 3:1 (determined by ^{1}HNMR) and in excellent yields (Figure 1.46). In an effort to assign configuration, we envisaged that the grignard addition follows the mnemonic discussed previously in the work of Ellman and co-workers (Figure 1.45).[137]

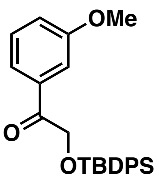
91a (91%)

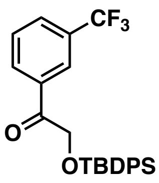
91b (90%)

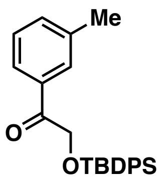
91c (94%)

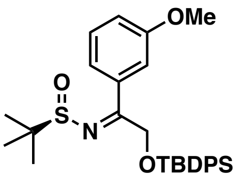
(***R***)**-92a** (60%)

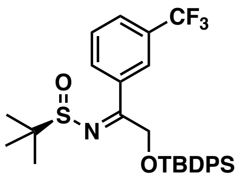
(***R***)**-92b** (72%)

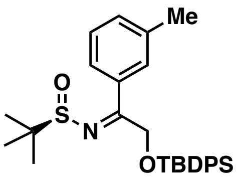
(***R***)**-92c** (50%)

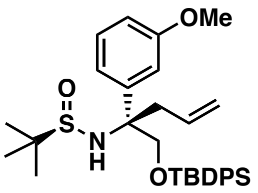
(***R***)**-93a** (96%)

+

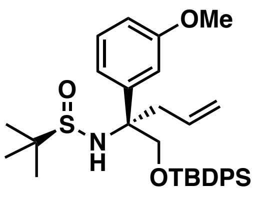
(***S***)**-93a**

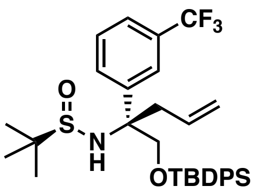
(***R***)**-93b** (89%)

+

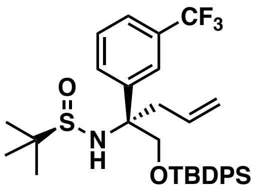
(***S***)**-93b**

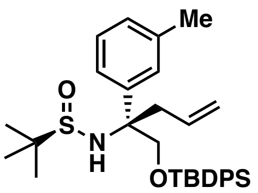
(***R***)**-93c** (91%)

+

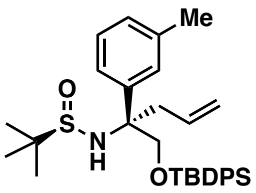
(***S***)**-93c**

Figure 1.46 Structures from the diastereoselective preparation of **93a-c**.

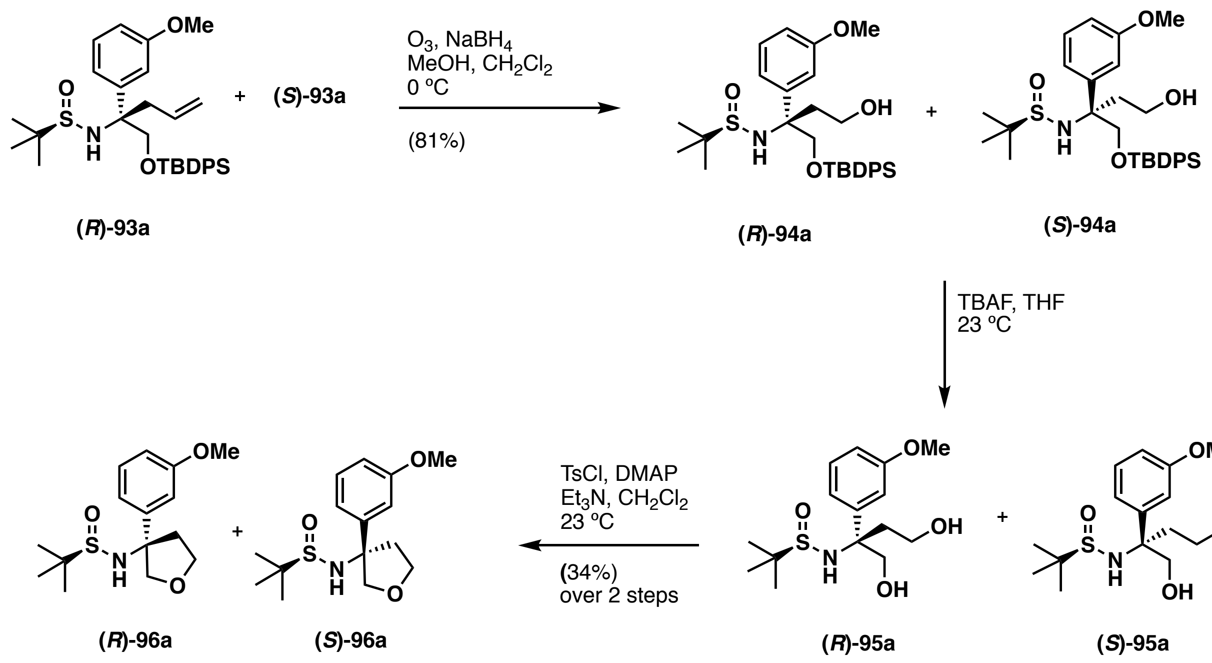
(R)-93a
+ (S)-93a
O3, NaBH4
MeOH, CH2Cl2
0 °C
(81%)
(R)-94a
+
(S)-94a
TBAF, THF
23 °C
(R)-95a
+
(S)-95a
TsCl, DMAP
Et3N, CH2Cl2
23 °C
(34%)
over 2 steps
(R)-96a
+
(S)-96a

Scheme 1.12 Preparation of highly functionalized spirocylic tetrahydrofuran **(R)-96a** and **(S)-96a** from -trisubstituted N-sulfinyl amine **(R)-93a** and **(S)-93a**.

At this point of the methodology the *meta*-methoxy-substituted derivative as a mixture of diastereomers, **(*R*)-93a** and **(*S*)-93a**, was carried forward for optimization of the ring closure strategy. Ozonolytic cleavage of **(*R*)-93a** and **(*S*)-93a** in a 4:1 mixture of CH_2Cl_2 and MeOH at -78 °C followed by treatment with sodium borohydride at 0 °C in MeOH for 1 h provided alcohol **(*R*)-94a** and **(*S*)-94a** in good yields (Scheme 1.12). Deprotection of the *tert*-butyldiphenylsilyl ether was carried in the presence of *tert*-butylammonium fluoride in tetrahydrofuran at 23 °C for 3 h provided diol **(*R*)-95a** and **(*S*)-95a**. The subsequent cyclization was done in the presence of tosyl chloride, 4-dimethylaminopyridine, and triethylamine in CH_2Cl_2 at 23 °C for 12 h afforded the spirocyclic tetrahydrofuran **(*R*)-96a** and **(*S*)-96a** as a mixture of diastereomers in moderate yields.

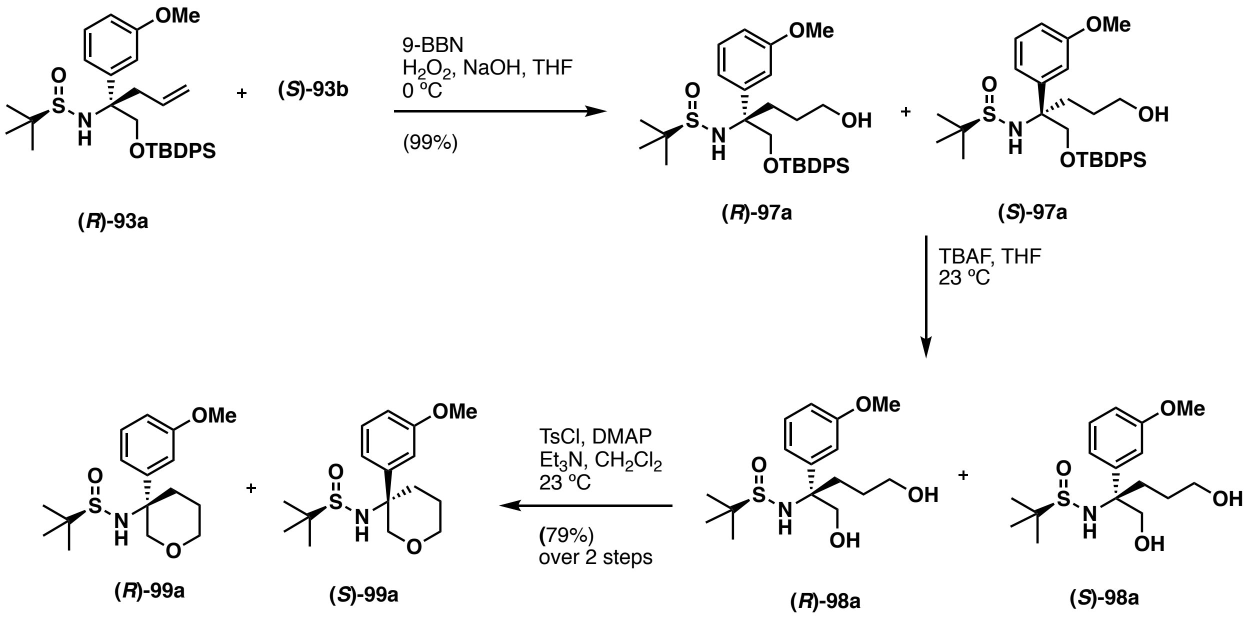

Scheme 1.13 Preparation of highly functionalized spirocyclic tetrahydropyran **(R)-99a** and **(S)-99a** from N-sulfinyl amine **(R)-93a** and **(S)-93a**.

To access the spirocyclic tetrahydropyran, common intermediates **(*R*)-93a** and **(*S*)-93a** were treated with 9-borabicyclo(3.3.1)nonane in tetrahydrofuran at 0 °C followed by hydrogen peroxide (30% w/w in H_2O) and aqueous sodium hydroxide for 15 h at 0 °C provided alcohols **(*R*)-97a** and **(*S*)-97a** in moderate yields (Scheme 1.13). Following the same, deprotection-cyclization protocol outlined above led to good yields of **(*R*)-99a** and **(*S*)-99a**. Further studies with additional derivatives, with the exception of the 3-methoxy derivative **97a**, revealed that the *N*-*tert*-butylsulfinyl amine was a liability for the favorable cyclization of diols **(*R*)-98a** and **(*R*)-98a**. We later divulged that replacing the *N*-*tert*-butylsulfinyl amine with a *N*-protected carbamate, such as benzylcarbamate or *tert*-butyl-carbamate, would lead to improved yields of the desired spirocyclic THP. Development of this methodology is ongoing, our laboratory is working towards a more selective diastereoselective allylmagnesium bromide addition and assignment of configuration of the quaternary center of the spirocycles. To the best of our knowledge, the methodology serves as the first reported route for the stereoselective preparation of heterospirocyclic benzylamines. Moreover, it provides a method that is amenable for multigram preparation of valuable building blocks, such as 1,2-amino alcohols and α,α-substituted amino acids.

1.3.3 Preparation of P2-ligand: 7,6,5-Tricyclic Indole

The highly peptidic nature of the P2 isophthalamide containing an *N*-methylsulfonamide substituent can be vulnerable to hydrolysis *via* amidases. In previous studies, our laboratory has succeeded in replacing this P2 isophthalamide with a non-peptidic 7,6,5-tricyclic indole which has been shown to retain crucial hydrogen bonding interactions within the non-prime binding pockets (Figure 1.47).[73,140]

Indole **101**, can be prepared from 4-amino-3-nitro-benzoic acid **100** over 7 chemical steps as described by Charrier and co-workers (Scheme 1.15).[141] Preparation of α,β-unsaturated sulfonamide **103** was done by addition of 2-chloroethanesulfonyl chloride **102** in the presence of 4-dimethylaminopyridine and pyridine in CH_2Cl_2 for 48 h to provide the product which was taken to the next step without further purification. Trimethyl-substituted 7,6,5-tricyclic indole can be prepared by treatment of **103** with sodium hydride followed by a large excess of methyl iodide at 23 °C for 3 h furnished **104** in a 16% yield over two steps. Saponification of **104** with sodium hydroxide in a mixture of ethanol and tetrahydrofuran at 50 °C for 12 h provided the desired acid **105** in an 81% yield (Scheme 1.14).[142]

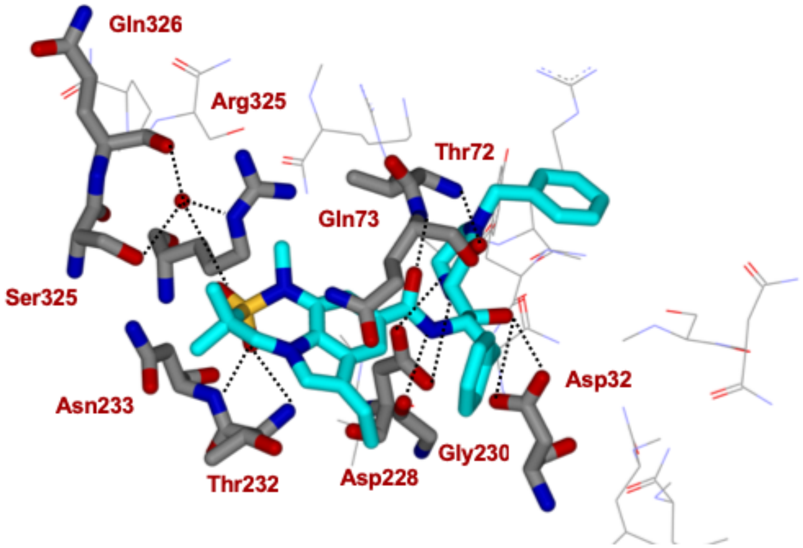

Figure 1.47 Inhibitor-bound BACE1 x-ray crystal structure depicting interactions of the 7,6,5-tricyclic indole (shown in blue) in the non-prime subsites of the BACE1 active site.

Preparation of α,α-cyclopropyl-substituted 7,6,5-tricyclic indole was carried out utilizing the previously established method. Initially, 7-amino indole **101** was treated with sulfonyl chloride **106** along with 4-dimethylaminopyridine and pyridine in CH_2Cl_2 for 48 h which furnished sulfonamide **107** in 84% yield. Deprotection of the benzyl ether is accomplished by dropwise addition of a solution of boron tribromide in CH_2Cl_2 at -78 °C and stirred for 1 h to yield the primary alcohol **108**. The *N*-methyl-tricyclic sultam **109** can be prepared in one pot: mesylation of the alcohol, sodium hydride-mediated ring closure, followed by *N*-methylation with methyl iodide.

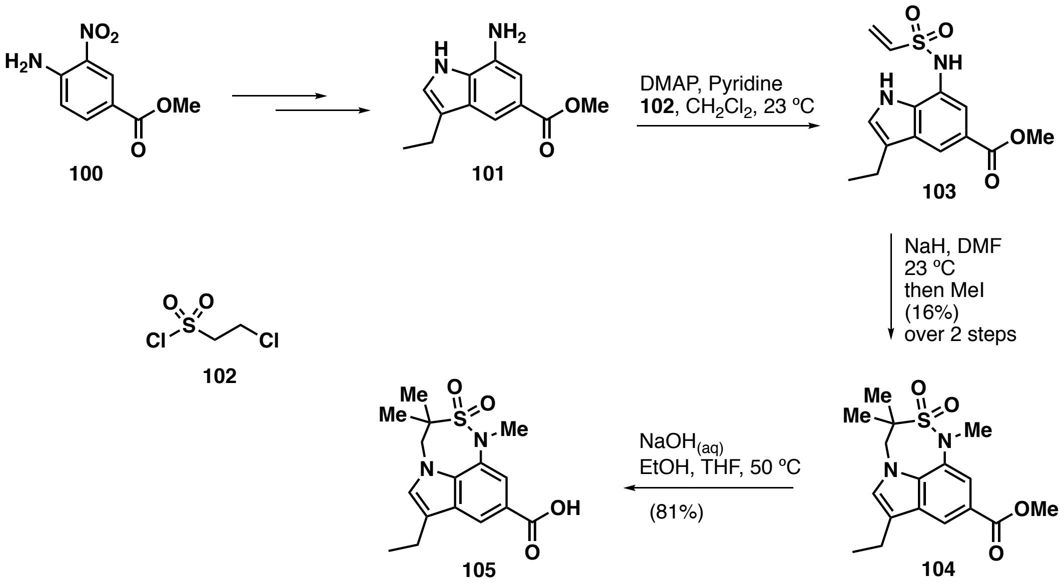
NO₂
H₂N
OMe
100
NH₂
H
N
OMe
101
DMAP, Pyridine
102, CH₂Cl₂, 23 °C
O
S
O
NH
H
N
OMe
103
NaH, DMF
23 °C
then MeI
(16%)
over 2 steps
O O
Cl S Cl
102
Me
Me
O
S
O
N
Me
N
OH
105
NaOH(aq)
EtOH, THF, 50 °C
(81%)
Me
Me
O
S
O
N
Me
N
OMe
104

Scheme 1.14 Preparation of α, α, α-trimethyl-substituted 7,6,5-tricyclic indole **105**.

Hydrolysis of **109** in the presence of sodium hydroxide in mixture of ethanol and tetrahydrofuran at 50 °C for 12 h furnished the α,α-cyclopropyl-substituted acid **110** in 60% yield over three steps (Scheme 1.15).[142] The preceding acids **105** and **110** were used in the preparation of the proposed novel class of BACE1 inhibitors.

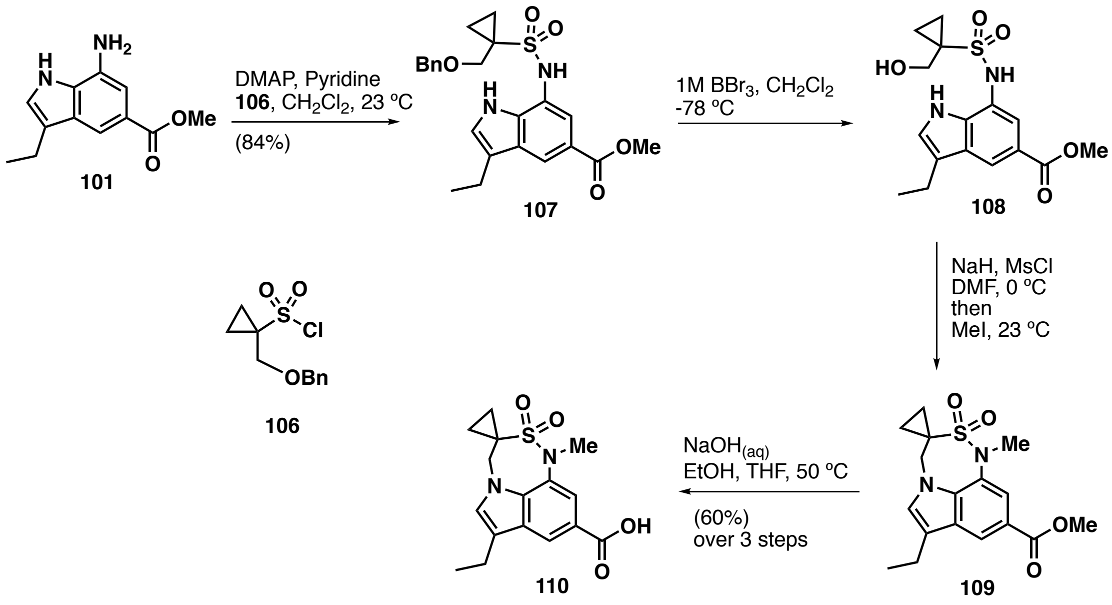
DMAP, Pyridine
106, CH2Cl2, 23 °C
(84%)
1M BBr3, CH2Cl2
-78 °C
NaH, MsCl
DMF, 0 °C
then
MeI, 23 °C
NaOH(aq)
EtOH, THF, 50 °C
(60%)
over 3 steps
101
107
108
106
110
109

Scheme 1.15 Preparation of α, α-cyclopropyl-substituted 7,6,5-tricyclic indole **110**.

1.4 Preparation of BACE1 Inhibitors

The SAR was carried forward by preparation of a novel inhibitor class containing a hydroxyethyl amine transition state isostere. Preparation of BACE1 inhibitors was done in a two step process. Reduction of azido alcohols **77a-e** or **84a-i** over catalytic Pd/C in ethyl acetate followed by amide coupling with acids **105** or **110** in the presence of triethylamine and HATU in CH_2Cl_2 at 23 °C for 36 h provided BACE1 inhibitors **111a-e**, **112a-e** (Scheme 1.16), **113a-i**, and **114a-i** (Scheme 1.17).[120,124] The inhibitors **113a-i (**Figure 1.49) and **114a-i (**Figure 1.50) were subjected to reverse phase HPLC separation to isolate the optically active diastereomers prior to submission for biological evaluation. Following purification by flash chromatography, the remaining inhibitors **111a-e** and **112a-e** (Figure 1.48) were submitted for biological evaluation.

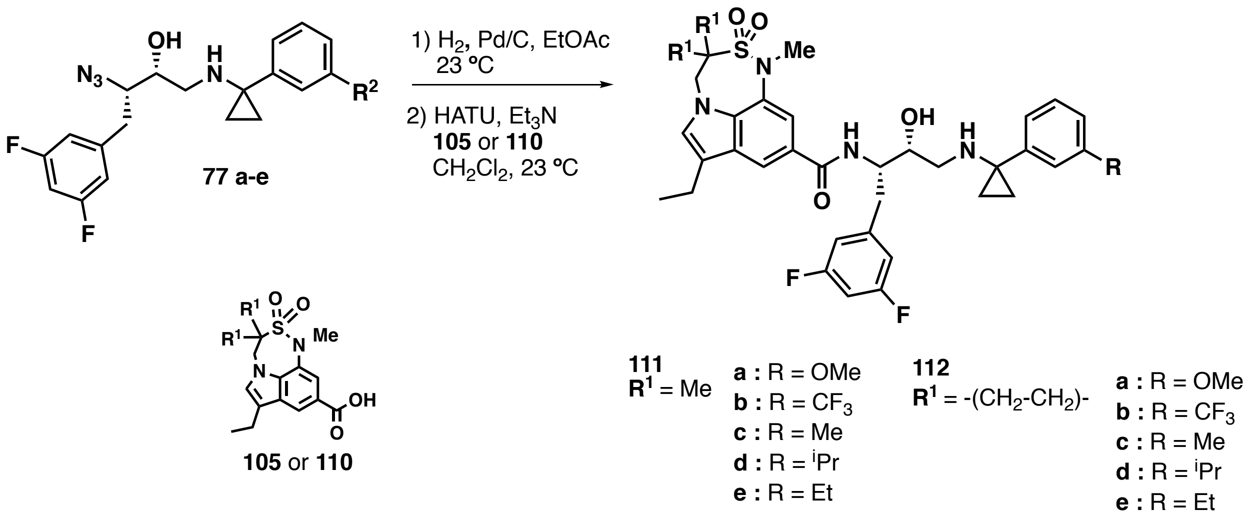
77 a-e
1) H2, Pd/C, EtOAc 23 °C
2) HATU, Et3N 105 or 110 CH2Cl2, 23 °C
105 or 110
111
R1 = Me
a : R = OMe
b : R = CF3
c : R = Me
d : R = iPr
e : R = Et
112
R1 = -(CH2-CH2)-
a : R = OMe
b : R = CF3
c : R = Me
d : R = iPr
e : R = Et

Scheme 1.16 Preparation of BACE1 inhibitors via coupling of isostere **77a-e** and selected tricyclic indoles **111** and **112**.

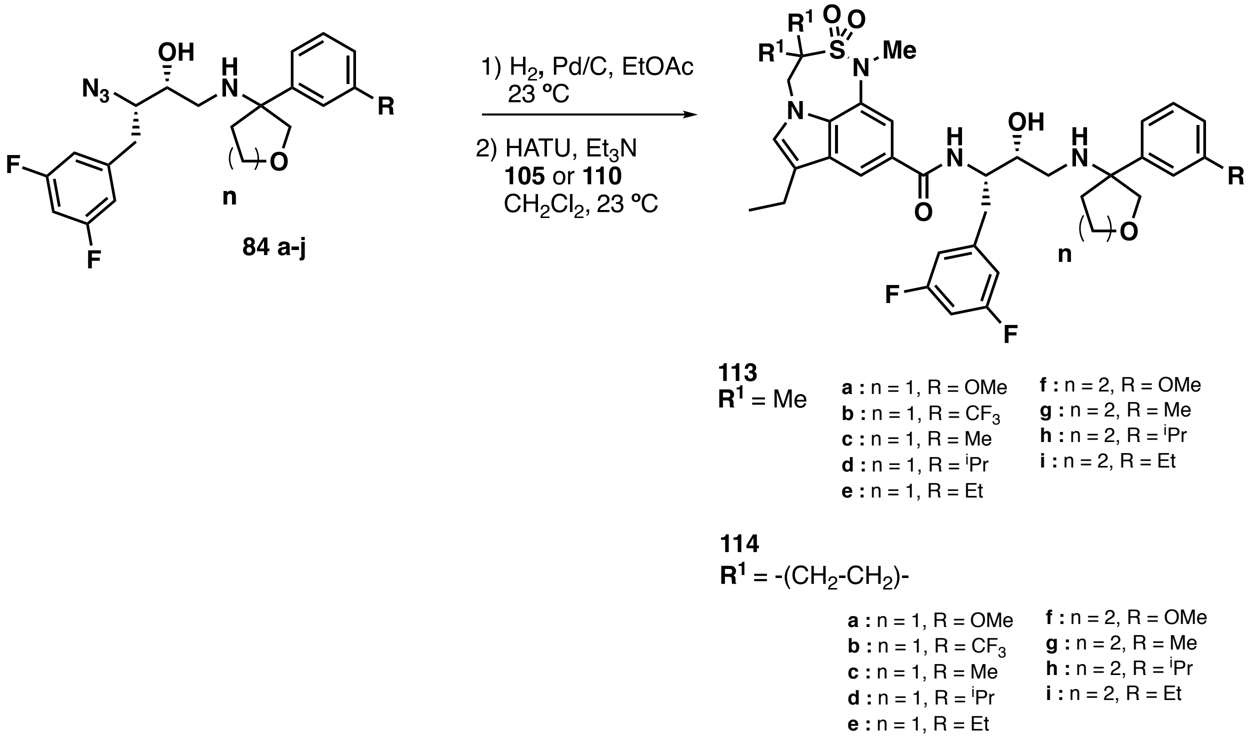
84 a-j
1) H2, Pd/C, EtOAc 23 °C
2) HATU, Et3N 105 or 110 CH2Cl2, 23 °C
113
R1 = Me
a : n = 1, R = OMe
b : n = 1, R = CF3
c : n = 1, R = Me
d : n = 1, R = iPr
e : n = 1, R = Et
f : n = 2, R = OMe
g : n = 2, R = Me
h : n = 2, R = iPr
i : n = 2, R = Et
114
R1 = -(CH2-CH2)-
a : n = 1, R = OMe
b : n = 1, R = CF3
c : n = 1, R = Me
d : n = 1, R = iPr
e : n = 1, R = Et
f : n = 2, R = OMe
g : n = 2, R = Me
h : n = 2, R = iPr
i : n = 2, R = Et

Scheme 1.17 Preparation of BACE1 inhibitors via coupling of isosteres **84a-i** and selected tricyclic indoles **105** and **110**.

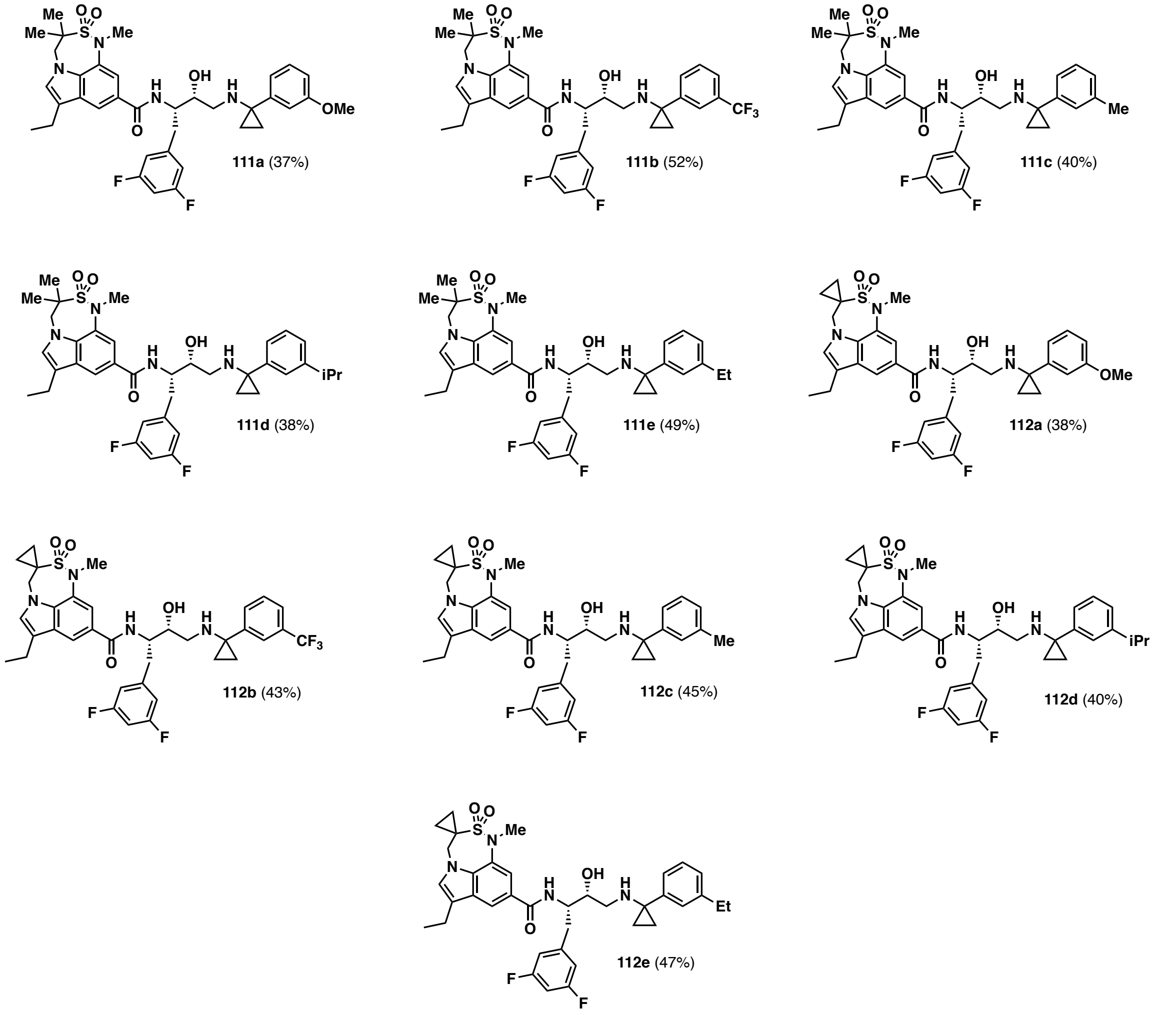

111a (37%)

111b (52%)

111c (40%)

111d (38%)

111e (49%)

112a (38%)

112b (43%)

112c (45%)

112d (40%)

112e (47%)

Figure 1.48 Structures of BACE1 inhibitors **111a-e** and **112a-e**.

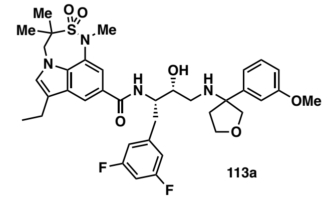
113a

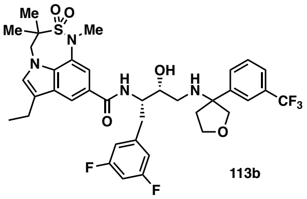
113b

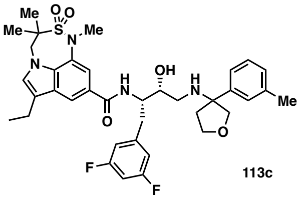
113c

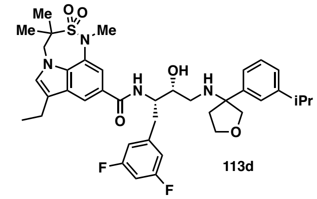
113d

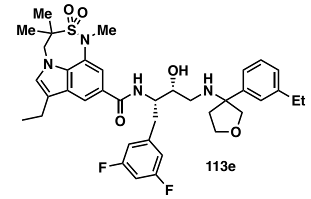
113e

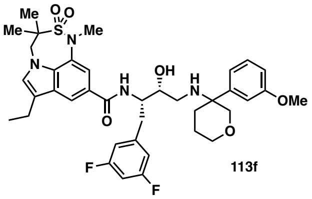
113f

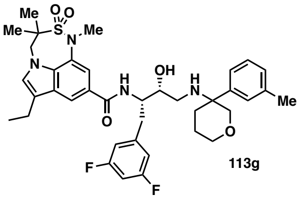
113g

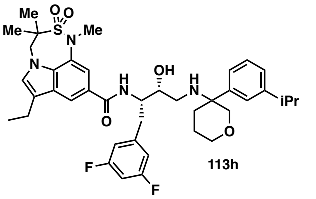
113h

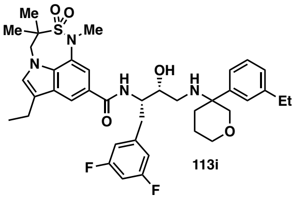
113i

Figure 1.49 Structures of BACE1 inhibitors **113a-i**.

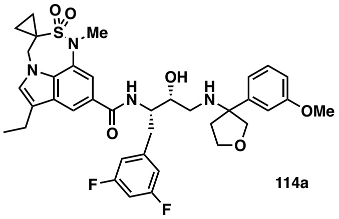
114a

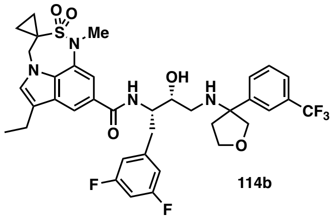
114b

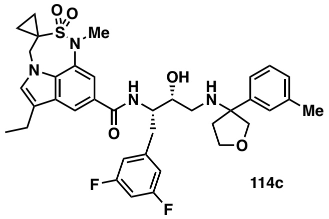
114c

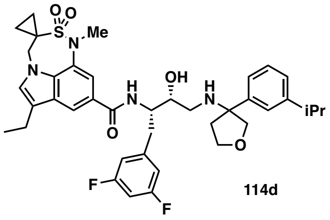
114d

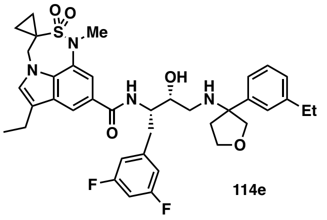
114e

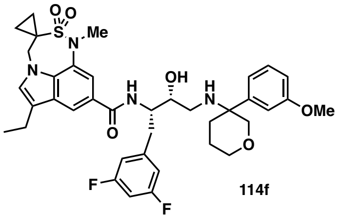
114f

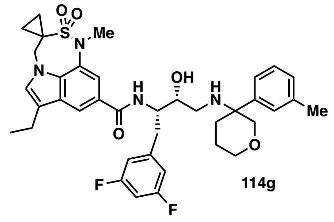
114g

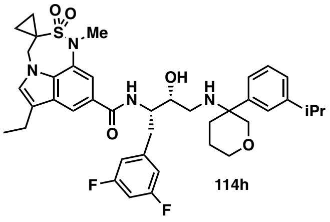
114h

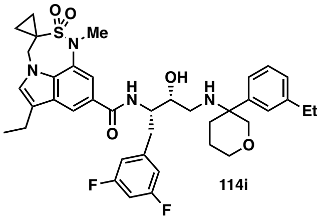
114i

Figure 1.50 Structures of BACE1 inhibitors **114a-i**.

1.4.1 Biological Evaluation of BACE1 Inhibitors

A FRET-based (Fluorescence resonance energy transfer) assay was used to monitor the enzymatic activity of BACE1[40] and BACE2[143]. The assay was performed with a fluorogenic, 8-mer peptide substrate (Mca-S-E-V-N-L-D-A-E-F-K-Dnp). Assays (100 µL final volume) were conducted in black, half-area 96-well plates (Corning Glass). Each assay contained a final concentration of 100 nM for BACE1 or BACE2, and the inhibitor concentrations were varied in the reaction buffer (0.1 M acetic acid, pH 4). The inhibitors were first incubated in the assay buffer for 5 minutes at 37°C. The BACE enzyme was then added to the above solution and further incubated for an additional 10 minutes at 37°C. The enzymatic reactions were then initiated by the addition of peptide substrates to a final concentration 1 µM. The increase in the fluorescence of the reaction at 393 nm (excitation wavelength = 328 nm) was measured using a BioTek Synergy plate reader. Biological evaluation of BACE1 inhibitors **111a-e** and **112a-e** are depicted in table 1.2 and 1.3.

Table 1.2 Biological evaluation of BACE1 inhibitors **111a-e**.

Inhibitor	**Ki [nM]**	
	BACE1	**BACE2**
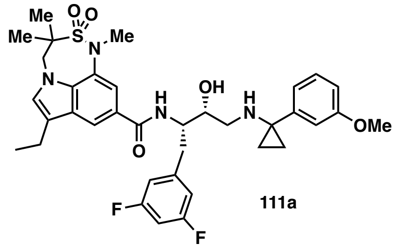 **111a**	22.45	45.8 ± 7.2
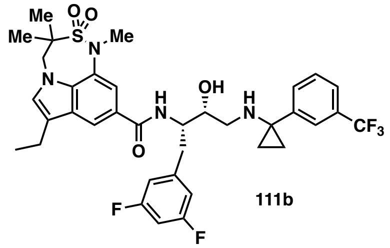 **111b**	6.003	23.1 ± 5.0
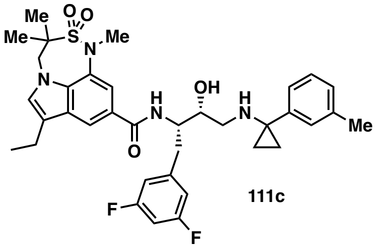 **111c**	54.71	108.8 ± 24.3
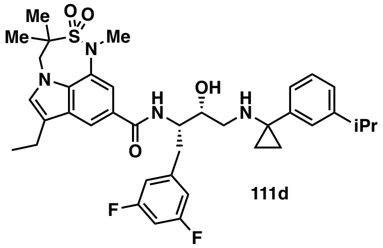 **111d**		33.8 ± 5.7
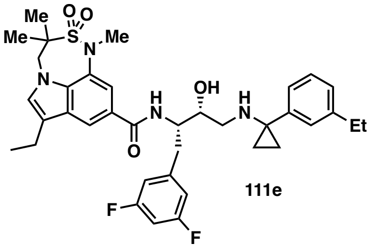 **111e**	372.6 ± 56.8	190.6 ± 75.5

Table 1.3 Biological evaluation of BACE1 inhibitors **112a-e**.

	Ki [nM]	
Inhibitor	**BACE1**	**BACE2**
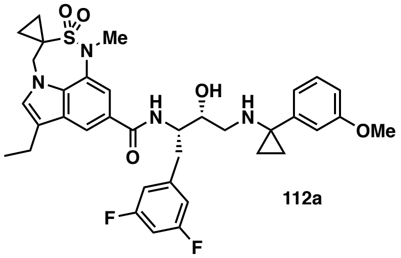 **112a**	33.53	68.3 ± 7.9
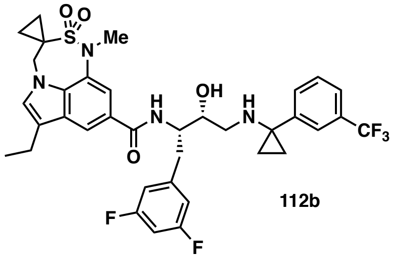 **112b**	178.3	169.7 ± 52.0
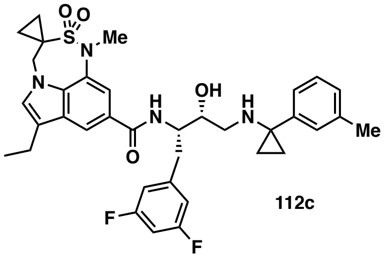 **112c**	6.417	28.12 ± 4.4
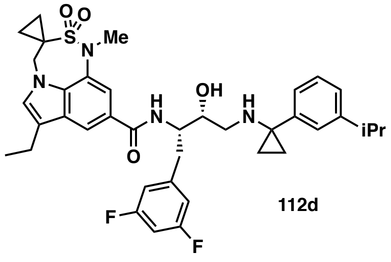 **112d**		43.5 ± 7.1
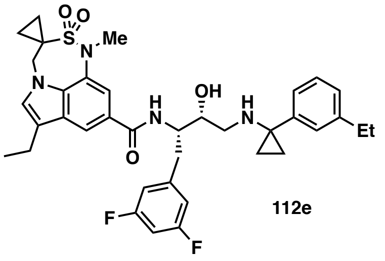 **112e**	65.6 ± 13.6	43.92 ± 7.6

1.4.2 Discussion

In the preceding sections it has been shown that valuable building blocks for aspartyl protease inhibition can be prepared in an efficient and scalable manner. Utilizing an ester-derived Ti-enolate and a precomplexed monodentate or bidentate aldehyde the stereoinduction of an aldol can be tuned to be able to provide *syn*- and *anti*-aldol adducts as nearly one diastereomer. Transition state analysis provides insight to the source of the stereoinduction of the preceding aldol. Upon treatment of the ester-derived Ti-enolate with a monodentate aldehyde the aldol proceeds through an expected Zimmerman-Traxler transition state to provide *anti*-aldol adduct **56**. Furthermore, treatment of the Ti-enolate with a precomplexed bidentate aldehyde, (benzyloxy)acetaldehyde, leads to secondary coordination of the benzyl ether oxygen which orientates it in a pseudo-axial orientation which leads to the *syn*-aldol adduct **53** (scheme 1.2). Through further chemical manipulation both **53** and **56** can be elaborated to furnish optically pure oxiranes **46** and **49**. In addition, with aid from previous literature azo epoxide **74** was furnished in 5 chemical steps as an alternative to oxirane **46**. The advantage of azo epoxide **74** is the thermal stability in the crucial epoxide opening step with selected amines which is commonly used to prepare isosteres in protease inhibitor design strategies. At high temperatures, above 80 °C, oxirane **46** is known to form an oxazolidinone byproduct that is not conducive to good yields. Preparation of azo epoxide **74** involve an asymmetric sharpless epoxidation and a regioselective ring opening with $TMSN_3$ as key steps. In result, azo epoxide **74** was utilized to prepare all the transition state isosteres in this study.

In order to explore interactions within the flap region of the BACE1 active site, the P1’ 3-methoxy benzyl amine of GRL-8234 was modified by incorporating spirocycles at the benzyl position of the P1’ ligand. Initially, smaller carbocycle rings were incorporated at the benzylic position. Utilizing the Kulinkovich reaction, benzonitrile **75a-e** were treated with Ti(IV) isopropoxide and ethyl magnesium bromide to afford cyclopropyl benzylamine **76a-e**. Moreover, epoxide opening of azo epoxide **74** upon treatment with amine **76a-e** provided the isosteres utilized in preparation of BACE1 inhibitors. Heterocycles were also incorporated at the benzylic position of the P1' ligand. Ketone **78** and **79** were subjected to a three step process: grignard addition with selected aryl magnesium bromide, substitution with sodium azide, and reduction over Pd/C in a hydrogen atmosphere. The resulting racemic benzylamine derivatives **83a-i** were further subjected to epoxide opening conditions to afford isosteres **84a-i**.

In addition, a novel diastereoselective preparation of the aforementioned heterospirocyclic amines was established in an effort to establish absolute configuration of the quaternary center. Utilizing insight proposed by Ellman and co-workers, it was determined that a diastereoselective allyl grignard addtion to an α-silyloxy *N*-sulfinyl ketimine can be used as a key step (figure 1.45 and 1.46). In result, allyl addition to ketmines **92a-c** provided the highly substituted *N*-sulfinyl amine **93a-c** as a mixture of diastereomers (*dr* ~3:1 *via* ^{1}H NMR) in excellent yields. Elaboration of **93a-c** provided the desired *N*-sulfinyl amino heterocycles **95a** and **97a** from three chemical steps: ozonolysis/hydroboration-oxidation, *tert*-butyl-ammonium fluoride mediated deprotection, and tosyl chloride mediated cyclization.

Upon standard amide coupling conditions with HATU and triethylamine BACE1 inhibitors **111a-e** and **112a-e** were prepared in moderate yields. Biological evaluation of **111a-e** and **112a-e** showed that inhibitors containing a spirocyclic cyclopropyl benzylamine as a P1' ligand were potent inhibitors of BACE1. Additionally, it was shown that the size of the *meta*-substituent of the P1' benzylamine plays a significant role in the potency and selectivity of the inhibitor. For instance, inhibitors with smaller *meta*-substituents, such as methoxy, methyl, and trifluoromethyl, exhibited good to excellent inhibitory activity against BACE1. Inhibitors **111a** and **112a** both exhibited moderate potency against BACE1, K_i = 22.45 nM and K_i = 33.53 nM respectively. Additionally, inhibitors **111b** (K_i = 6.003 nM BACE1) and **112c** (K_i = 6.417 nM BACE1) showed excellent inhibitory activity against BACE1. Inhibitor **111c** was observed to have a K_i of 54.71 nM against BACE1. Interestingly, it was shown that they P2 cyclopropyl containing tricyclic indole seemed to have a large effect on the potency of the inhibitors **112a-e** against BACE1. This effect in potency was observed between both *meta*-trifluoromethyl derivatives where **112b** was found to have a K_i of 178.3 nM (29-fold less potent than **111b**). Conversely, **112c** (K_i = 6.417 nM BACE1) was found to be nearly 9-fold more potent than its trimethylated counterpart **112c** (K_i = 54.71 nM BACE1). In the same way, inhibitor **112e** was observed to be approximately 6-fold more potent than **111e** (K_i = 65.5 nM BACE1 vs. K_i 372.6 nM BACE1) The larger *meta*-ethyl substituent was found to have a large effect on the selectivity of inhibitors **111e** and **112e**. It was shown that **111e** and **112e** was approximately 2-fold more potent against BACE2, K_i = 190.6 nM BACE2 and K_i = 43.92 nM BACE2 respectively. This may suggest that larger *meta*-substituents allow for enhanced hydrophobic interactions in the prime side binding pockets of BACE2. The larger isopropyl substituent of inhibitor **111d** and **112d** both show good activity against BACE2 but further biological evaluation is needed for BACE1 to conclude that the larger *meta*-substituent is in fact playing a role in selectivity of the preceding inhibitors. Lastly, inhibitors **111b** and **112c** both displayed the best selectivity against BACE1 with approximately a 4-fold difference in potency against BACE2. Identical conditions were utilized to furnish BACE1 inhibitors **113a-i** and **114a-i** in moderate yields. Currently these inhibitors are undergoing further characterization and biological evaluation.

1.5 Conclusions

A series of BACE1 inhibitors, **111a-e** and **112a-e**, have been design, synthesized, and evaluated for their inhibitory activity against BACE1. Inhibitor **112c** was found to be exceedingly potent against BACE1 (K_i = 6.417 nM) as well as a moderate selectivity against BACE1 with being over 4-fold more potent. Interestingly, we found that inhibitors **111e** and **112e** with larger P1' *meta*-substituents, such as ethyl, can possibly lead to inhibitors being more selective against BACE2. Currently, there is ongoing preparation of inhibitors to be able to investigate both BACE1 and BACE2 inhibitory activity. Further, inhibitors **113a-i** and **114a-i** are under biological evaluation for their inhibitor activity against BACE1 and BACE2.

In addition, the preparation of valuable building blocks for aspartic acid protease inhibitors has been established. Utilizing a *syn*- and *anti*-aldol protocol mediated by an ester-derived Ti-enolate as a key step, the facile and scalable preparation of optically pure oxiranes **46** and **49**. In order to make the route more cost effective Evan's diastereoselective *syn*-aldol was used mediated by a boron-enolate to be able to furnish oxirane **46** as a single diastereomer. Oxirane **46** was then used to be able to furnish a known BACE1 inhibitor that contained a P1 3,5-difluorophenyl methyl ligand. A novel stereoselective preparation of medium sized heterospirocyclic benzylamines as P1' ligands for BACE1 inhibitors was accomplished. This method took advantage of a diastereoselective allyl grignard addition to α-silyloxy *N*-sulfinyl ketimine to furnish a highly substituted α-silyloxy *N*-sulfinyl amine which was extrapolated to prepare the aforementioned spirocycles. Ongoing investigations are underway to optimize this route and establish absolute configuration of the spirocycles.

1.6 Experimental

All chemicals and reagents were purchased from commercial suppliers and used without further purification unless otherwise noted. The following reaction solvents were distilled prior to use: dichloromethane from calcium hydride, diethyl ether and tetrahydrofuran from Na/benzophenone, methanol and ethanol from activated magnesium under argon. All reactions were carried out under an argon atmosphere in either flame or oven-dried (120 ^{o}C) glassware. TLC analysis was conducted using glass-backed Thin-Layer Silica Gel Chromatography Plates (60 Å, 250 μm thickness, F-254 indicator). Column chromatography was performed using 230-400 mesh, 60 Å pore diameter silica gel. ^{1}H and ^{13}C NMR spectra were recorded at room temperature on a Varian Inova 300, Bruker Avance ARX-400 or Bruker DRX-500 spectrometers. Chemical shifts (δ values) are reported in parts per million, and are referenced to the deuterated residual solvent peak. NMR data is reported as: δ value (chemical shift, J-value (Hz), integration, where s = singlet, d = doublet, t = triplet, q = quartet, brs = broad singlet). Optical rotations were recorded on a Perkin Elmer 341 polarimeter. HRMS spectra were recorded at the Purdue University Department of Chemistry Mass Spectrometry Center.

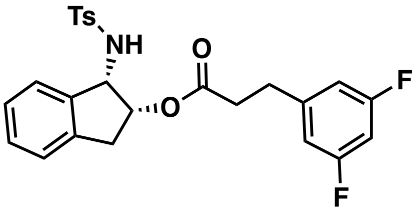

(1*S*,2*R*)-1-((4-Methylphenyl)sulfonamido)-2,3-dihydro-1*H*-inden-2-yl 3-(3,5-difluoro phenyl) propanoate 52: *N*-tosyl-1-aminoindan-2-ol **51** (514 mg, 2.00 mmol), DMAP (122 mg, 1.00 mmol) and dihydrocinnamic acid **50** (372 mg, 2.00 mmol) were dissolved in dichloromethane (15 mL) at 23 °C. To the resulting mixture, *N*,*N*'-dicyclohexylcarbodiimide (413 mg, 3 mmol) in 5 mL of dichloromethane was added dropwise. The white slurry reaction mixture was stirred at 23 °C for 18 h. The reaction mixture was diluted with dichloromethane and filtered through a cotton plug. The filtrate was concentrated and the white residue was purified via silica gel chromatography (20% ethyl acetate/hexanes) to yield the desired ester **52** as a white solid (717 mg, 76%).^{1}H NMR (400 MHz, $CDCl_3$, 298 K) δ 7.79 (m, 2H), 7.25 (m, 6H), 7.16 (m, 1H), 6.67 (m, 3H), 5.41 (d, *J* = 10.1 Hz, 1H), 5.16 (td, *J* = 5.1, 1.6 Hz, 1H), 4.94 (dd, *J* = 10.1, 5.2 Hz, 1H), 2.81 (m, 3H), 2.49 (td, *J* = 7.8, 7.4, 5.1 Hz, 2H), 2.43 (s, 3H); ^{13}C NMR (101 MHz, $CDCl_3$, 298 K) δ 171.2, 164.0, 143.8, 139.4, 138.4, 137.7, 129.8, 128.6, 127.3, 126.9, 124.9, 124.1, 111.1, 101.7, 77.3, 76.9, 76.6, 75.1, 59.4, 37.2, 34.6, 30.1, 21.5; $[\alpha]^{20}_D$ -54.0, (*c* 1.45, $CHCl_3$); HRMS-ESI (*m/z*): $[M+Na]^+$ calcd for $C_{25}H_{23}F_2NO_4S$ 494.1214; found 494.1208.

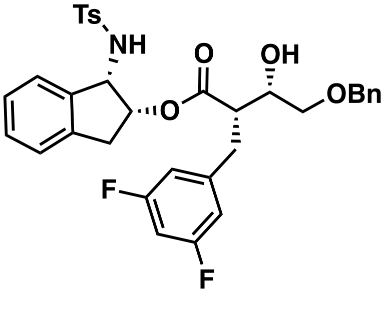

(1*S*,2*R*)-1-((4-Methylphenyl)sulfonamido)-2,3-dihydro-1*H*-inden-2-yl-(2*S*,3*S*)-4-(benzyloxy) -2-(3,5-difluorobenzyl)-3-hydroxybutanoate 53: Ester **52** (150 mg, 0.35 mmol) was dissolved in dichloromethane (10 mL) and the solution was cooled to 0 °C. To this mixture a solution of $TiCl_4$ (1M in CH_2Cl_2, 0.53 mmol, 0.53 mL) was added dropwise and the resulting yellow clear mixture was warmed to 23°C. After 15 minutes of stirring at 23 °C, *N,N*-diisopropylethylamine (1.4 mmol, 0.30 mL) was added dropwise and the resulting enolate was allowed to stir for an additional 2 h. In a separate flask, benzyloxyacetaldehyde (0.70 mmol, 105 mg) was dissolved in dichloromethane (10 mL) and pre-complexed with $TiCl_4$ (1M in CH_2Cl_2, 1.1 mmol, 1.1 mL) at -78 °C and stirred for 30 minutes. The enolate was added to the pre-complexed aldehyde *via* cannula at -78 °C over five minutes and stirred for an additional 2 h. The reaction was quenched with saturated NH_4Cl and warmed to 23 °C. The crude mixture was extracted with chloroform thoroughly and dried with sodium sulfate, filtered and concentrated. The crude residue was purified by silica gel chromatography (25% ethyl Acetate/hexanes) to provide the title aldol adduct **53** (127.2 mg, 60% yield) as a single diastereoisomer by NMR.^{1}H NMR (400 MHz, $CDCl_3$, 298K) δ 7.77 (m, 2H), 7.28 (m, 12H), 7.16 (d, *J* = 7.0 Hz, 1H), 6.62 (ddd, *J* = 9.0, 6.7, 2.3 Hz, 1H), 6.42 (m, 2H), 6.03 (d, *J* = 9.9 Hz, 1H), 5.28 (m, 1H), 4.84 (dd, *J* = 9.9, 4.8 Hz, 1H), 4.50 (d, *J* = 4.8 Hz, 2H), 3.47 (m, 2H), 3.05 (d, *J* = 3.9 Hz, 1H), 2.95 (ddd, *J* = 17.0, 4.6, 1.1 Hz, 1H), 2.87 (m, 1H), 2.73 (m, 1H), 2.55 (d, *J* = 17.1 Hz, 1H), 2.43 (s, 3H); ^{13}C NMR (101 MHz, $CDCl_3$, 298 K) δ 171.1, 164.0, 143.6, 142.7, 139.8, 138.2, 137.6, 137.2, 129.7, 128.5, 128.0, 127.8, 127.3, 127.0, 125.0, 124.1, 111.6, 111.4, 101.9, 76.2, 73.4, 71.2, 70.5, 59.6, 49.9, 36.9, 31.0, 21.5; $[\alpha]^{20}_D$ -15.2, (*c* 0.243, $CHCl_3$); HRMS-ESI (*m/z*): $[M+Na]^+$ calcd for $C_{34}H_{33}F_2NO_6S$ 644.1895; found 644.1889.

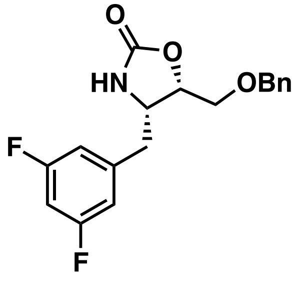

(4*S*,5*S*)-5-((Benzyloxy)methyl)-4-(3,5-difluorobenzyl)oxazolidin-2-one 54: Aldol adduct **53** (0.16 mmol, 100 mg) was dissolved in a mixture of tetrahydrofuran and water (3:1) and treated with lithium hydroxide (0.15 mmol) and hydrogen peroxide (30% in H_2O, 0.3 mmol) and the resulting mixture was stirred at 25 °C for 12 h. The reaction was quenched with a saturated solution of sodium thiosulfate. The crude mixture was extracted with chloroform and the aqueous layer was acidified (pH ~1). The aqueous layer was extracted with chloroform and the resulting organic layer was dried with sodium sulfate. The organic layer was concentrated under reduced pressure and the resulting crude acid was used without further purification.

The crude β-hydroxyacid was dissolved in dry benzene (10 mL) along with triethylamine (0.39 mmol, 54 μL), and DPPA (0.39 mmol, 84 μL). The resulting mixture was warmed to 90 °C and stirred for 12 h. Upon completion of the reaction, the mixture was cooled to 23 °C and diluted with ethyl acetate. The crude mixture was washed with saturated $NaHCO_3$ and brine. Drying of the organic layer with sodium sulfate followed by filtration and removal of volatiles provided the crude residue which was purified *via* silica gel chromatography (15% ethyl acetate/hexanes) to yield the desired optically active oxazolidinone **54** as a yellow oil (30 mg, 70% yield over 2 steps). ^{1}H NMR (400 MHz, $CDCl_3$, 298 K) δ 7.35 (m, 5H), 6.72 (m, 3H), 5.19 (bs, 1H), 4.81 (dt, *J* = 7.7, 5.9 Hz, 1H), 4.60 (s, 2H), 4.07 (ddd, *J* = 11.2, 7.8, 3.6 Hz, 1H), 3.76 (d, *J* = 5.9 Hz, 2H), 2.97 (dd, *J* = 13.5, 3.6 Hz, 1H), 2.71 (dd, *J* = 13.5, 10.9 Hz, 1H); ^{13}C NMR (101 MHz, $CDCl_3$, 298 K) δ 164.5, 162.0, 157.8, 140.6, 137.0, 128.5, 127.8, 111.9, 111.6, 102.7, 73.8, 66.89, 55.4, 35.8; $[\alpha]^{20}_D$ -66.8, (*c* 0.19, $CHCl_3$); HRMS-ESI (*m/z*): $[M+H]^+$ calcd for $C_{18}H_{17}F_2NO_3$ 334.1255; found 334.1251.

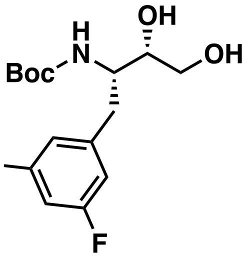

***tert*-Butyl ((2*S*,3*S*)-1-(3,5-difluorophenyl)-3,4-dihydroxybutan-2-yl)carbamate 55**: In a 1:1 mixture of water and ethanol the (4*S*,5*S*)-5-((benzyloxy)methyl)-4-(3,5-difluorobenzyl)oxazolidin-2-one **54** (650 mg, 1.95 mmol) was treated with anhydrous potassium hydroxide (460 mg, 8.19 mmol). The suspension was warmed to 70 °C and stirred for 4 h. The resulting clear yellow solution was cooled to 23 °C and neutralized to pH 7.0 with 1N HCl. A solution of $(Boc)_2O$ (851 mg, 3.90 mmol) in dichloromethane (4 mL) was added dropwise to the reaction mixture. This mixture was allowed to stir for 4 h at 23 °C and quenched with saturated NH_4Cl. The crude product was extracted with ethyl acetate and the resulting organic layer was washed with brine. After drying over Na_2SO_4 and filtration, volatiles were removed under reduced pressure and the crude product was carried on without further purification.

A suspension of $Pd(OH)_2$ (65 mg, 10% w/w) in ethyl acetate (10 mL) was treated with the crude *N*-Boc-amino alcohol. The mixture was stirred under hydrogen atmosphere for 24 h at 23 °C. The catalyst was filtered off over a pad of celite and washed with methanol. The volatiles were removed under reduced pressure to yield pure *tert*-butyl ((2*S*,3*S*)-1-(3,5-difluorophenyl)-3,4-dihydroxybutan-2-yl)carbamate **55** as a clear colorless oil (476 mg, 77%). ^{1}H NMR (300 MHz, $CDCl_3$, 298 K) δ 6.77 (m, 2H), 6.69 (tt, *J* = 9.0, 2.3 Hz, 1H), 4.50 (d, *J* = 8.9 Hz, 3.81 (qd, *J* = 8.8, 4.0 Hz, 1H), 3.68 (s, 3H), 3.35 (s, 1H), 3.14 (dd, *J* = 14.5, 4.0 Hz, 1H), 2.82 (dd, *J* = 14.4, 8.6 Hz, 1H); 1.40 (s, 9H); ^{13}C NMR (75 MHz, $CDCl_3$, 298 K) δ 171.0, 156.6, 146.6, 112.2, 111.9, 105.4, 85.1, 80.4, 73.3, 63.0, 60.4, 52.7, 36.5, 27.4; $[\alpha]^{20}_{D}$ –8.20 (*c* 0.15, MeOH); MS-ESI (*m/z*): $[M+Na]^+$ calcd for $C_{15}H_{21}NaF_2NO_4$, 340.1; found 340.1.

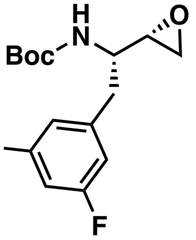

***tert*-Butyl ((*S*)-2-(3,5-difluorophenyl)-1-((*S*)-oxiran-2-yl)ethyl)carbamate 46**: Tosyl chloride (702 mg, 3.68 mmol), triethylamine (0.51 mL, 3.68 mmol), and dibutyltin oxide (229 mg, 0.92 mmol) were suspended in dichloromethane (25 mL). *tert*-Butyl ((2*S*,3*S*)-1-(3,5-difluorophenyl)-3,4-dihydroxybutan-2-yl)carbamate **45** (476 mg, 3.07 mmol) was added to the suspension and the resulting mixture was allowed to stir for 4 h at 23 °C. Upon completion the mixture was diluted with dichloromethane and washed with water and brine. The organic layer was separated, dried over sodium sulfate, filtered and concentrated. The crude residue was used in the next step without further purification.

The crude tosylate was dissolved in methanol (5 mL) and cooled to 0 °C. At the same temperature, K_2CO_3 (116 mg, 0.84 mmol) was added and the reaction was allowed to slowly warm to 23 °C. The resulting mixture was allowed to stir for 1 h and then concentrated under reduced pressure. The crude residue was diluted in ethyl acetate and washed with water and brine. The organic layer was dried over sodium sulfate. The crude product was purified *via* column chromatography (20% acetone/hexanes) to give *tert*-butyl ((*S*)-2-(3,5-difluorophenyl)-1-((*S*)-oxiran-2-yl)ethyl) carbamate **46** as a white solid (300 mg, 67%). ^{1}H NMR (300 MHz, $CDCl_3$, 298 K) δ 7.36 (m, 3H), 6.71 (m, 3H), 4.90 (bs, 1H), 4.83 (dt, J = 7.1, 5.8 Hz, 1H), 4.61 (s, 2H), 4.08 (ddd, J = 11.2, 7.8, 3.5 Hz, 1H), 3.77 (m, 2H), 2.98 (dd, J = 13.5, 3.5 Hz, 1H), 2.71 (dd, 13.5, 11.1 Hz, 1H), 1.40 (s, 9H); ^{13}C NMR (100 MHz, $CDCl_3$, 298 K) δ 160.1, 128.4, 128.3, 126.0, 111.8, 101.8, 60.3, 58.4, 50.7, 35.3, 32.2, 28.1, 18.3; $[\alpha]^{20}_{D}$ -8.13 (*c* 0.086, $CHCl_3$); MS-ESI (*m/z*): $[M+H]^+$ calcd for $C_{15}H_{19}F_2NO_3$, 299.1; found 300.1.

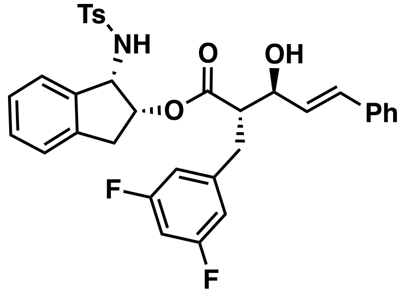

(1*S*,2*R*)-1-((4-Methylphenyl)sulfonamido)-2,3-dihydro-1*H*-inden-2-yl (2*S*,3*S*,*E*)-2-(3,5-difluorobenzyl)-3-hydroxy-5-phenylpent-4-enoate 56: Ester **52** (0.55 mmol, 260 mg) was dissolved in dichloromethane (5 mL) and the resulting solution was cooled to 0 °C and treated with a freshly made solution of $TiCl_4$ (1 M in CH_2Cl_2, 0.66 mmol, 0.66 mL). The resulting clear yellow solution was warmed to 23 °C and stirred for 15 min. Treatment with *N,N*-diisopropylethylamine (1.8 mmol, 0.33 mL) followed by an additional 2 h of stirring at 23 °C provided the desired enolate. In a separate flask, *trans*-cinnamaldehyde (1.1 mmol, 145 mg) was dissolved in dichloromethane (5 mL) and treated with $TiCl_4$ (1 M in CH_2Cl_2, 1.4 mmol, 1.4 mL) at -78 °C. The pre-complexed aldehyde was allowed to stir for 30 minutes and the enolate was added dropwise *via* cannula over 5 minutes. After stirring for 2.5 h at -78 °C, the reaction was quenched with saturated NH_4Cl and allowed to reach room temperature. The resulting mixture was thoroughly extracted with chloroform and dried with sodium sulfate. The volatiles were removed and the crude residue was purified *via* silica gel chromatography (20% ethyl acetate/ hexanes) to yield the aldol adduct **56** as a single diastereomer (199 mg, 60% yield) by NMR. ^{1}H NMR (400 MHz, $CDCl_3$, 298 K) δ 7.77 (d, J = 8.3 Hz, 2H), 7.34 (s, 2H), 7.29 (m, 4H), 7.23 (m, 3H), 7.11 (m, 2H), 6.65 (m, 3H), 6.30 (d,

J = 9.5 Hz, 1H), 6.13 (dd, J = 15.8, 7.2 Hz, 1H), 5.33 (t, J = 4.8 Hz, 1H), 4.80 (dd, J = 9.5, 4.9 Hz, 1H), 4.37 (t, J = 6.5 Hz, 1H), 3.00 (m, 2H), 2.89 (m, 1H), 2.81 (d, J = 6.6 Hz, 2H), 2.69 (d, J = 17.2 Hz, 1H), 2.46 (s, 1H), 2.39 (s, 3H); ^{13}C NMR (101 MHz, $CDCl_3$, 298 K) δ 170.5, 164.1, 161.7, 143.5, 139.9, 138.1, 137.4, 135.7, 133.2, 129.7, 128.5, 128.4, 128.2, 128.1, 127.3, 127.1, 126.7, 124.9, 124.4, 111.8, 111.5, 102.2, 75.7, 73.3, 59.6, 53.4, 37.1, 34.6, 21.4; $[\alpha]^{20}_{D}$ -21.1, (*c* 0.62, $CHCl_3$); HRMS-ESI (*m/z*): $[M+Na]^+$ calcd for $C_{34}H_{31}F_2NO_5S$ 626.1789; found 626.1784.

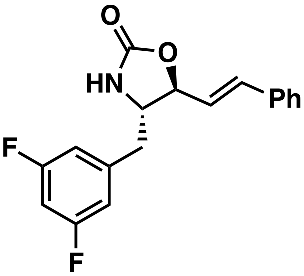

4*S*,5*S*)-4-(3,5-Difluorobenzyl)-5-((*E*)-styryl)oxazolidin-2-one 57: Aldol adduct **56** (0.33 mmol, 199 mg) was dissolved in a mixture of tetrahydrofuran and water (3:1) and treated with lithium hydroxide (0.99 mmol, 42 mg) and H_2O_2 (30% in H_2O, 1.98 mmol, 0.2 mL). The reaction was quenched with a saturated solution of sodium thiosulfate and extracted with chloroform. The aqueous layer was acidified (pH ~1) and extracted with chloroform. The resulting organic layer was dried with sodium sulfate and concentrated to provide the desired styrenyl oxazolidinone **57** as a yellow oil (100 mg, 96% yield).^{1}H NMR (400 MHz, $CDCl_3$, 298 K) δ 7.35 (m, 5H), 6.74 (m, 3H), 6.68 (s, 1H), 6.15 (dd, J = 15.8, 7.5 Hz, 1H), 5.48 (s, 1H), 4.83 (t, J = 6.9 Hz, 1H), 3.85 (dt, J = 8.6, 5.8 Hz, 1H), 2.97 (dd, J = 13.7, 5.1 Hz, 1H), 2.86 (dd, J = 13.7, 8.4 Hz, 1H); ^{13}C NMR (101 MHz, $CDCl_3$, 298 K) δ 158.0, 134.9, 128.7, 126.8, 123.8, 112.0, 102.9, 82.2, 59.3, 40.4; $[\alpha]^{20}_{D}$ -22.4, (*c* 0.085, $CHCl_3$) HRMS-ESI (*m/z*): $[M+Na]^+$ calcd for $C_{18}H_{15}F_2NO_2$, 338.0969; found 338.0966.

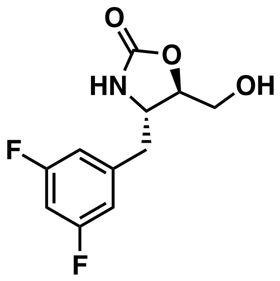

(4S,5*R*)-4-(3,5-Difluorobenzyl)-5-(hydroxymethyl)oxazolidin-2-one 58: The styrenyl oxazolidinone **57** (0.32 mmol, 100 mg) was dissolved in a mixture of dichloromethane and methanol (2:1) at -78 °C and treated with ozone until the reaction mixture was saturated with a blue color. Oxygen gas was passed through the reaction mixture until the color was clear and colorless. The resulting crude ozonide was quenched with $NaBH_4$ (0.48 mmol, 27 mg) and was allowed to warm to room temperature. The reaction mixture was treated with a 20% aqueous solution of Na_2CO_3 (8 mL) and was extracted with ethyl acetate. The resulting organic layer was washed with water and a saturated brine solution. After drying with sodium sulfate and concentrating under reduced pressure the title compound was isolated as a white amorphous solid (90% yield). This crude solid was used without further purification.

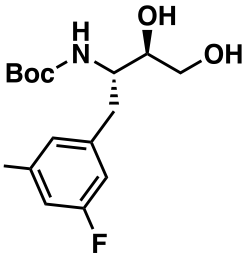

***tert*-Butyl ((2*S*,3*R*)-1-(3,5-difluorophenyl)-3,4-dihydroxybutan-2-yl)carbamate 59**: The crude oxazolidinone **58** was dissolved in a mixture of ethanol and water (1:1) and treated with KOH (1.34 mmol, 75 mg). The resulting mixture stirred at 70 °C for 4 h. Reaction mixture was then concentrated to yield the crude amino diol which was subjected to protection conditions by treating with a solution of $(Boc)_2O$ (0.48 mmol, 105 mg) in 3 mL of CH_2Cl_2 and stirred for 8 h at 23 °C. The reaction mixture was extracted with ethyl acetate and washed with water and brine. The organic layer was dried with sodium sulfate and concentrated to yield title *N*-Boc-amino diol as a white amorphous solid (68 mg, 67% yield).^{1}H NMR (400 MHz, CD_3OD) δ 6.84 (m, 2H), 6.75 (m,

1H), 6.57 (d, *J* = 9.6 Hz, 1H), 3.77 (m, 1H), 3.63 (t, *J* = 5.4 Hz, 1H), 3.51 (m, 2H), 3.29 (bs, 1H) 3.11 (dd, *J* = 13.9, 3.5 Hz, 1H), 2.92 (t, *J* = 7.5 Hz, 1H), 2.60 (m, 1H), 1.32 (s, 9H); ^{13}C NMR (101 MHz, CD_3OD) δ 164.1, 156.6, 146.9, 111.9, 111.7, 110.6, 100.6, 78.6, 73.8, 63.2, 53.5, 35.9, 27.1, 26.1; $[\alpha]^{20}_{D}$ +9.32, (*c* 0.072, $CHCl_3$); HRMS-ESI (*m/z*): $[M+Na]^+$ calcd for $C_{15}H_{21}F_2NO_4$, 340.1337; found 340.1325.

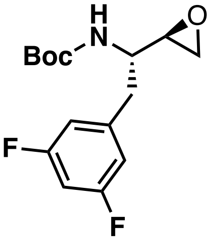

***tert*-Butyl ((*S*)-2-(3,5-difluorophenyl)-1-((*R*)-oxiran-2-yl)ethyl)carbamate 49**: *N*-Boc-amino-diol **49** (0.21 mmol, 68 mg) was subjected to identical conditions as **46**. The title *N*-Boc-amino-epoxyarylbutane **7** was isolated as white amorphous solid (64 mg, 99% yield). ^{1}H NMR (400 MHz, $CDCl_3$) δ 6.76 (ddt, *J* = 10.4, 6.6, 1.7 Hz, 2H), 6.68 (m, 1H), 4.46 (s, 1H), 4.12 (m, 1H) 2.91 (m, 2H), 2.82 (dd, *J* = 4.8, 3.9 Hz, 1H), 2.73 (dt, *J* = 4.7, 3.5 Hz, 1H), 2.45 (m, 1H), 1.39 (s, 9H); ^{13}C NMR (101 MHz, $CDCl_3$) δ 161.7, 155.0, 140.8, 112.2, 112.0, 102.1, 79.9, 53.0, 52.4, 46.7, 28.1. $[\alpha]^{20}_{D}$ +1.29; (*c* 0.31, $CHCl_3$) MS-ESI (*m/z*): $[M+H]^+$ calcd for $C_{15}H_{19}F_2NO_3$, 300.1; found 300.2

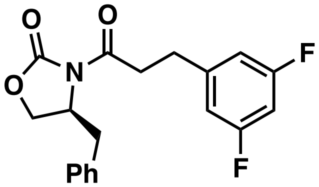

(*S*)-4-Benzyl-3-(3-(3,5-difluorophenyl)propanoyl)oxazolidin-2-one 61: A mixture of 3-(3,5-difluorophenyl)propanoic acid **50** (14.6 g, 65.4 mmol) and triethylamine (10 mL, 71.94 mmol) was dissolved in diethyl ether (600 mL). The resulting solution was cooled to -78 °C and pivaloyl chloride (8.85 mL, 71.94 mmol) was added dropwise over five minutes. The mixture was warmed to 0 °C and the white slurry was stirred for 1 h. Meanwhile in a separate flask the chiral (*S*)-oxazolidinone **60** (11.58 g, 65.4 mmol) was dissolved in tetrahydrofuran (300 mL) and cooled to

-78 °C. To this mixture *n*-BuLi (1.6 M in Hex., 45 mL, 71.94 mmol) was added dropwise over 10 min. The metallated solution was stirred at -78 °C for 30 minutes. The original reaction mixture was cooled to -78 °C and the metallated solution was added dropwise *via* cannula. This mixture was warmed to 0 °C and stirred for an additional hour. At this time, the reaction was quenched with a saturated NH_4Cl solution and extracted with ethyl acetate. The organic layer was washed with water and brine, dried with Na_2SO_4, filtered and concentrated. The crude product was purified *via* column chromatography (10% ethyl acetate/hexanes). The (*S*)-4-benzyl-3-(3-(3,5-difluorophenyl)propanoyl)oxazolidin-2-one **61** was isolated as a white solid (19.29 g, 85 %). ^{1}H NMR (300 MHz, $CDCl_3$, 298 K) δ 7.31 (m, 5H), 6.97 (m, 1H), 6.84 (m, 1H), 6.65 (m, 1H), 6.29 (ddt, *J* = 16.0, 6.8, 1.9 Hz, 1H), 4.63 (m, 2H), 4.04 (m, 2H), 3.08 (m, 2H), 2.48 (m, 2H); ^{13}C NMR (100 MHz, $CDCl_3$, 298 K) δ 173.2, 153.3, 134.7, 135.3, 129.2, 128.6, 128.8, 128.0, 111.9, 73.9, 65.9, 55.2, 49.8, 37.6, 33.7; MS-ESI (*m/z*): calcd for $C_{20}H_{17}F_2NO_3$ $[M+H]^+$ 345.1, found 346.5.

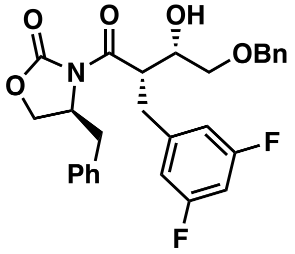

(*S*)-4-Benzyl-3-((2*S*,3*S*)-4-(benzyloxy)-2-(3,5-difluorobenzyl)-3-hydroxybutanoyl) oxazolidin-2-one 62: A solution of dibutylboron trifluoromethanesulfonate (1 M in CH_2Cl_2, 60.72 mmol, 60.72 mL) was added to a solution of (*S*)-4-benzyl-3-(3-(3,5-difluorophenyl)propanoyl)oxazolidin-2-one **61** (17.5 g, 50.6 mmol) and *N,N*-diisopropylethylamine (11.5 mL, 65.78 mmol) in 780 mL of dichloromethane at 0 °C. The resulting solution was warmed to 23 °C and stirred for 1 h. The reaction mixture was cooled to -78 °C and a solution of 2-(benzyloxy)acetaldehyde (8.36 g, 55.66 mmol) in 30 mL of dichloromethane was added dropwise. After stirring 30 minutes at -78 °C the reaction was warmed to room temperature and stirred for an additional 2 h. The reaction mixture was then cooled and quenched with 10 mL of pH 7.0 phosphate buffer. At the same temperature, a 2:1 solution of MeOH (125 mL) and H_2O_2 (68 mL) was added dropwise. The mixture was concentrated under reduced pressure. The remaining residue was extracted with ethyl acetate. The organic layer was washed with a saturated $NaHCO_3$ solution and brine, dried with Na_2SO_4, filtered and concentrated. The crude product was dried over Na_2SO_4 and purified *via* column chromatography (25% ethyl acetate/hexanes).(*S*)-4-benzyl-3-((2*S*,3*S*)-4-(benzyloxy)-2-(3,5-difluorobenzyl)-3 hydroxybutanoyl)oxazolidin-2-one **62** was isolated as single diastereomer as a clear colorless oil (11.5 g, 46%). ^{1}H NMR (300 MHz, $CDCl_3$, 298 K) δ 7.29 (m, 6H), 6.99 (m, 1H), 6.98 (s, 1H), 6.82 (m, 2H), 6.65 (ddt, *J* = 9.0, 6.2, 3.5 Hz, 1H), 4.53 (m, 3H), 4.17 (dd, *J* = 6.0, 2.8 Hz, 1H), 3.92 (dq, *J* = 8.8, 4.7, 3.1 Hz, 1H), 3.78 (m, 1H), 3.58 (dd, *J* = 5.8, 2.2 Hz, 2H), 3.13 (m, 2H), 2.98 (dq, *J* = 12.3, 3.4 Hz, 1H), 2.33 (ddt, *J* = 13.2, 9.4, 5.4 Hz, 1H); ^{13}C NMR (100 MHz, $CDCl_3$, 298 K) δ 173.4, 164.0, 161.5, 153.1, 142.6, 137.6, 134.9, 129.1, 128.4, 127.8, 127.7, 127.2, 112.3, 102.2, 101.9, 77.3, 77.0, 76.7, 73.3, 72.1, 70.9, 65.6, 55.5, 47.0, 37.4, 34.1; $[\alpha]^{20}_D$ +34.04 (*c* 0.20, $CHCl_3$); HRMS-ESI (*m/z*): $[M+H]^+$ calcd for $C_{29}H_{27}F_2NO_5$, 496.1936; found 496.1932.

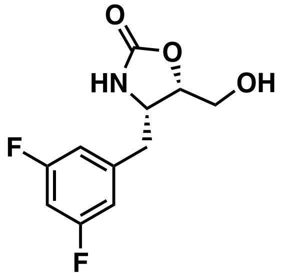

(4*S*,5*S*)-4-(3,5-Difluorobenzyl)-5-(hydroxymethyl)oxazolidin-2-one 63: To a 1:1 mixture of THF (25 mL) and H_2O (25 mL) was added (*S*)-4-benzyl-3-((2*S*,3*S*)-4-(benzyloxy)-2-(3,5-difluorobenzyl)-3-hydroxybutanoyl)oxazolidin-2-one **62** (1.18 g, 2.38 mmol). The mixture was cooled to 0 °C and a 30% solution of H_2O_2 (15 mL) was added dropwise. The resulting mixture was treated with $LiOH{\cdot}H_2O$ (200 mg, 4.76 mmol) at 0 °C and was allowed to slowly reach 23 °C. The resulting suspension was allowed to stir for 10 h and was quenched with saturated solution of NaS_2O_3 at 0 °C. The mixture was diluted with CH_2Cl_2 and washed with brine. The crude product was dried over Na_2SO_4 and concentrated. The crude product was carried on without further purification.

To a solution of the crude residue in toluene (80 mL) was added triethylamine (0.66 mL, 4.75 mmol) and DPPA (0.96 mL, 4.45 mmol). This mixture was warmed to 90 °C and stirred for 16 h. The resulting clear orange mixture was cooled to 23 °C and diluted with ethyl acetate. The resulting organic layer was washed with a saturated solution of $NaHCO_3$, water, brine, dried over Na_2SO_4, filtered and concentrated. The volatiles were removed and the crude residue was purified by column chromatography over silica gel (30% ethyl acetate/hexanes). (4*S*,5*S*)-5-((benzyloxy)methyl)-4-(3,5-difluorobenzyl)oxazolidin-2-one **54** was isolated as a clear yellow oil (650 mg).^{1}H NMR (300 MHz, $CDCl_3$, 298 K) δ 7.36 (m, 3H), 6.71 (m, 3H), 4.90 (bs, 1H), 4.83 (dt, *J* = 7.1, 5.8 Hz, 1H), 4.61 (s, 2H), 4.08 (ddd, *J* = 11.2, 7.8, 3.5 Hz, 1H), 3.77 (m, 2H), 2.98 (dd, *J* = 13.5, 3.5 Hz, 1H), 2.71 (dd, 13.5, 11.1 Hz, 1H); ^{13}C NMR (75 MHz, $CDCl_3$, 298 K) δ 160.1, 128.4, 128.3, 126.0, 111.8, 101.8, 60.3, 58.4, 50.7, 35.3, 32.2, 28.1, 18.3; $[\alpha]^{20}_D$ -70.22 (*c* 0.046, $CHCl_3$); HRMS-ESI (*m/z*): $[M+H]^+$ calcd for $C_{18}H_{18}F_2NO_3$, 334.1255; found 334.1249.

A suspension of $Pd(OH)_2$ (65 mg, 10% w/w) in ethyl acetate (10 mL) was treated with **54**. A hydrogen balloon was attached to a three-way adapter and the mixture was stirred for 24 hours at 23 °C. The catalyst was filtered over a pad of celite and washed with methanol. The volatiles were removed under reduced pressure to give pure **63** in 82% yield over three steps.

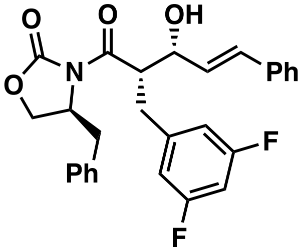

(*S*)-4-Benzyl-3-((2*S*,3*R*,*E*)-2-(3,5-difluorobenzyl)-3-hydroxy-5-phenylpent-4-enoyl) oxazolidin-2-one 64: The same general procedure for (*S*)-4-benzyl-3-((2*S*,3*S*)-4-(benzyloxy)-2-(3,5-difluorobenzyl)-3-hydroxybutanoyl)oxazolidin-2-one **61** was carried out with *trans*-cinnamaldehyde. The aldol product, (*S*)-4-benzyl-3-((2*S*,3*R*,*E*)-2-(3,5-difluorobenzyl)-3-hydroxy-5-phenylpent-4-enoyl)oxazolidin-2-one **64** was isolated as a clear oil (6.25 g, 99 %).^{1}H NMR (300 MHz, $CDCl_3$, 298 K) δ 7.32 (m, 1H), 7.18 (m, 1H), 6.80 (m, 1H), 6.66 (m, 1H), 4.67 (m, 1H), 4.20 (m, 1H), 3.26 (m, 2H), 3.01 (t, *J* = 7.4 Hz, 1H), 2.77 (dd, *J* = 13.4, 9.6 Hz, 1H); ^{13}C NMR (75 MHz, $CDCl_3$, 298 K) δ 160.1, 128.4, 128.3, 126.0, 111.8, 101.8, 60.3, 58.4, 50.7, 35.3, 32.2, 28.1, 18.3; $[\alpha]^{20}_D$ +78.79 (*c* 0.25, $CHCl_3$); HRMS-ESI (*m/z*): $[M+Na]^+$ calcd for $C_{28}H_{25}NaF_2NO_4$, 500.1650; found 500.1643

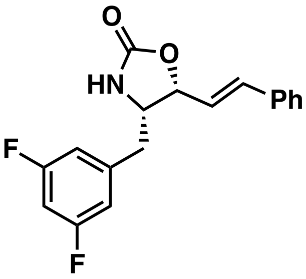

(4*S*,5*R*)-4-(3,5-Difluorobenzyl)-5-((*E*)-styryl)oxazolidin-2-one 65: The same general procedure used to provide (4*S*,5*S*)-5-((benzyloxy)methyl)-4-(3,5-difluorobenzyl)oxazolidin-2-one **63** was used to prepare (4*S*,5*R*)-4-(3,5-difluorobenzyl)-5-((*E*)-styryl)oxazolidin-2-one **65** (6.0 g, 12.56 mmol). The product was isolated as a pale yellow solid (2.67 g, 68%). ^{1}H NMR (300 MHz, CDCl$_3$, 298 K) δ 7.37 (m, 4H), 6.76 (m, 1H), 6.70 (ddd, *J* = 7.3, 3.6, 2.1Hz, 2H), 6.23 (dd, *J* = 15.9, 7.4 Hz, 3H), 5.95 (s, 1H), 5.30 (m, 1H), 4.15 (m, 1H), 2.85 (dd, *J* = 13.7, 4.6 Hz, 1H), 2.72 (dd, *J* = 13.7, 10.0 Hz, 1H); ^{13}C NMR (101 MHz, CDCl$_3$, 298 K) δ 171.6, 153.3, 144.3, 135.0, 129.3, 128.9, 127.3, 111.4, 111.2, 102.0, 101.7, 66.2, 55.0, 37.7, 36.5, 29.7; $[\alpha]^{20}_D$ -48.27 (*c* 0.25, CHCl$_3$); HRMS-ESI (*m/z*): [M+H]$^+$ calcd for $C_{19}H_{15}F_2NO_2$, 316.1144; found 316.1144.

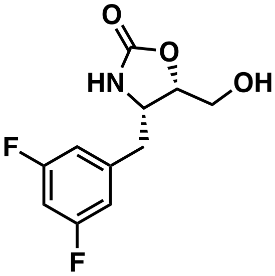

(4*S*,5*S*)-4-(3,5-Difluorobenzyl)-5-(hydroxymethyl)oxazolidin-2-one 63: In a (2:1) mixture of dichloromethane (25 mL) and methanol (12.5 mL) the (4*S*,5*R*)-4-(3,5-difluorobenzyl)-5-((*E*)-styryl)oxazolidin-2-one **65** was dissolved and cooled to -78 °C. Ozone was bubbled into the reaction mixture until the mixture was saturated with ozone. At this time, oxygen was bubbled into the mixture until it was made clear. At the same temperature, sodium borohydride (432 mg, 11.4 mmol) was added and the reaction mixture was allowed to slowly warm to 23 °C. The resulting mixture was allowed to stir for 2 h and the reaction was quenched with ethyl acetate. The mixture was diluted with water and the product was extracted with ethyl acetate. The organic layer was washed with water and brine and dried over sodium sulfate. The volatiles were removed under reduced pressure and the crude alcohol **63** was used without further purification.^{1}H NMR (400 MHz, $CDCl_3$, 298 K) δ 6.75 (m, 3H), 4.99 (s, 1H), 4.77 (dt, *J* = 8.0, 4.9 Hz, 1H), 4.16 (ddd, *J* = 11.3, 5.4, 2.9 Hz, 1H), 3.96 (t, *J* = 5.1 Hz, 2H), 3.00 (dd, *J* = 13.5, 3.8 Hz, 1H), 2.88 (dd, *J* = 13.6, 10.7 Hz, 1H); ^{13}C NMR (101 MHz, $CDCl_3$, 298 K) δ 165.6, 153.46, 137.3, 111.4, 102.9, 128.9, 78.4, 60.4, 55.3, 38.4; MS-ESI (*m/z*): $[M+H]^+$ calcd for $C_{15}H_{11}F_2NO_3$, 243.1; found 244.0.

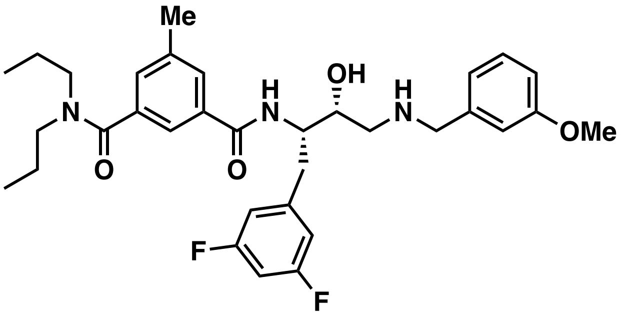

N^1-((2*S*,3*R*)-1-(3,5-Difluorophenyl)-3-hydroxy-4-((3-methoxybenzyl)amino)butan-2-yl)-5-methyl-N^3,N^3-dipropylisophthalamide 68: To a solution of **46** (15 mg, 0.0501 mmol) in *i*PrOH (2 mL) 3-methoxybenzylamine (20 μL, 0.150 mmol) was added and the reaction mixture was refluxed for 20 h. Solvent was evaporated under reduced pressure and the residue was purified *via* column chromatography (CH_2Cl_2 / MeOH 99:1 to 96:4) providing *tert-butyl ((2S,3R)-1-(3,5-difluorophenyl)-3-hydroxy-4-((3-methoxybenzyl)amino)butan-2-yl)carbamate* (15 mg, 69%) as a glossy white solid. This latter was dissolved in CH_2Cl_2 (200 mL) and treated with trifluoroacetic acid. The reaction mixture was allowed to slowly warm to 23 °C. The resulting solution was stirred for 1.5 hours. The volatiles were removed under reduced pressure. The residue was taken up with CH_2Cl_2 (10 mL) and treated with aqueous saturated $NaHCO_3$ (2 mL). The organic layer was dried over Na_2SO_4, filtered and concentrated providing *(2R,3S)-3-amino-4-(3,5-difluorophenyl)-1-((3-methoxybenzyl)amino) butan-2-ol* which was submitted to the next step without further purification. Acid **26** (13 mg, 0.0474 mmol) was dissolved in dry CH_2Cl_2 (2 mL). Triethylamine (44 μL, 0.316 mmol) and HATU (26 mg, 0.0685 mmol) were sequentially added and the mixture was stirred for 30 min at 25 °C. The resulting mixture was added to a solution of *(*2*R,*3*S)-3-*amino-4-(3,5-difluorophenyl)-1-((3-methoxybenzyl)amino) butan-2-ol (18 mg, 0.0527 mmol) in dry CH_2Cl_2 (2 mL). The reaction mixture was stirred at 23 °C for 16 h and then poured in saturated aqueous $NaHCO_3$ and extracted twice with CH_2Cl_2. The organic layer was dried over sodium sulfate, filtered and concentrated. The residue was purified via column chromatography (CH_2Cl_2 / MeOH 99:1 to 95:5). Compound **68** was obtained as a white amorphous solid (12 mg, 43% over 3 steps). ^1H NMR (500 MHz, $CDCl_3$, 298 K) δ 7.50 (bs, 1H), 7.52 (s, 1H), 7.29 (s, 1H), 7.24 (m, 2H), 7.18 (s, 1H), 6.99-6.94 (m, 2H), 6.86-6.81 (m, 2H), 6.59 (m, 1H), 4.26 (m, 1H), 3.99-3.88 (m, 2H), 3.79 (s, 3H), 3.72 (m, 1H), 3.49 (s, 1H), 3.44-3.35 (m, 2H), 3.10-3.05 (m, 3H), 2.96-2.91 (m, 1H), 2,80-2.73 (m, 2H), 2.34 (s, 3H)), 1.69 (m, 2H), 1.49 (m, 2H), 0.98 (m, 3H), 0.71 (m, 3H); ^{13}C NMR (200 MHz, $CDCl_3$, 298 K) δ 171.2, 167.6, 163.5, 162.3, 160.0, 142.2, 139.0, 137.4, 134.1, 129.9, 129.1, 121.9, 121.3, 114.5, 114.1, 112.2, 112.1, 102.0, 70.4, 55.3, 53.7, 52.8, 50.8, 50.1, 46.5, 36.0, 29.7, 21.8, 21.2, 20.7, 11.5, 11.0. MS-ESI (*m/z*): $[M+H]^+$ 582.3.

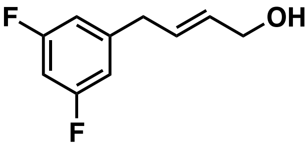

(*E*)-4-(3,5-difluorophenyl)but-2-en-1-ol 71: To a solution of butadiene monoxide **69** (24.82 mmol, 2 mL) in THF (30 mL) was added CuCN (10 mol%, 222 mg) at -78 °C. A solution of 3,5-difluoromagnesium bromide (0.25 M in THF, 4.57 mL) was added dropwise to the reaction mixture at -78 °C. The resulting reaction mixture was stirred for 1.5 h at -78 °C and then warmed to 23 °C. The reaction was quenched with saturated aqueous NH_4Cl and extracted with EtOAc. The organic layer was dried with Na_2SO_4 and concentrated under reduced pressure. The crude was purified *via* flash chromatography (10% EtOAc/Hexanes). Compound **71** was obtained as a clear yellow oil (3.26 g, 79%); ^1H NMR (400 MHz, $CDCl_3$) δ 6.71 – 6.65 (m, 2H), 6.65 – 6.56 (m, 1H), 5.82 – 5.62 (m, 2H), 4.09 (s, 2H), 3.32 (d, J = 6.3 Hz, 2H), 2.56 (s, 1H); ^{13}C NMR (101 MHz, $CDCl_3$) δ 164.21, 164.08, 161.75, 161.62, 144.04, 143.95, 143.87, 131.50, 129.14, 111.29, 111.23, 111.11, 111.05, 101.68, 101.43, 101.18, 77.31, 77.00, 76.68, 62.84, 38.06.

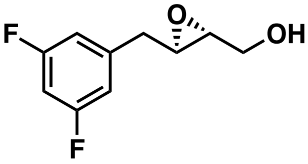

((2*R*,3*R*)-3-(3,5-difluorobenzyl)oxiran-2-yl)methanol 72: In a dry 2-neck round bottom flask with CH_2Cl_2 (158 mL) Ti(^{i}PrO)$_4$ (1.38 mmol, 0.42 mL), (-)-DET (1.04 mmol, 0.17 mL), and 4 Å MS (20 mg of MS/0.1 mmol of SM) were added. The resulting mixture was cooled to -20 °C and a solution of TBHP (5-6 M in decane, 38.2 mmol, 7.6 mL) was added dropwise and stirred for 30 minutes at the same temperature. The allylic alcohol **71** was added as a solution in CH_2Cl_2 (100 mL) and stirred for 12 h. The reaction mixture was filtered through a pad of celite and concentrated. The resulting epoxide **72** was isolated and used without further purification (3.12 g, 90%); ^{1}H NMR (400 MHz, $CDCl_3$) δ 6.81 – 6.72 (m, 2H), 6.72 – 6.63 (m, 1H), 3.89 (dq, *J* = 12.7, 2.6 Hz, 1H), 3.67 – 3.58 (m, 1H), 3.17 (ddd, *J* = 6.6, 4.5, 2.3 Hz, 1H), 2.99 – 2.93 (m, 1H), 2.93 – 2.86 (m, 1H), 2.80 (dd, *J* = 14.8, 6.4 Hz, 1H), 2.33 (s, 1H); ^{13}C NMR (101 MHz, $CDCl_3$) δ 164.21, 164.08, 161.74, 161.61, 140.73, 111.83, 111.77, 111.65, 111.58, 102.39, 102.14, 101.89, 77.28, 76.96, 76.64, 61.11, 58.10, 54.96, 37.35.

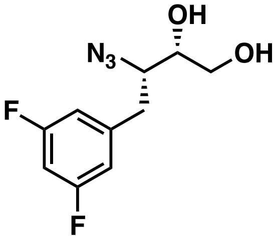

(2*S*,3*S*)-3-azido-4-(3,5-difluorophenyl)butane-1,2-diol 73: In a clean and dry 2-neck Ti(^{i}PrO)$_4$ (23.98 mmol, 7.27 mL) and $TMSN_3$ (47.96 mmol, 6.36 mL) was added to benzene (80 mL) The resulting mixture was refluxed for 5 h. Optically pure oxirane **72** (14.99 mmol, 3.0 g) was dissolved in benzene (80 mL) and added dropwise to the refluxing reaction mixture. The resulting mixture was refluxed for an additional 20 minutes and cooled to 23 °C. An aqueous 5% H_2SO_4 solution was added over 1 h. The reaction mixture was extracted with EtOAc and dried with $MgSO_4$ prior to being concentrated under reduced pressure. The residue was purified *via* flash chromatography (50% EtOAc/Hexanes). The resulting diol **74** was isolated as a white semi-solid (2.38 g, 66%); ^{1}H

NMR (500 MHz, $CDCl_3$) δ 6.82 (dt, *J* = 6.4, 2.1 Hz, 2H), 6.72 (tt, *J* = 9.0, 2.3 Hz, 1H), 3.87 – 3.73 (m, 2H), 3.73 – 3.62 (m, 2H), 3.08 (dd, *J* = 14.2, 3.5 Hz, 1H), 2.77 (dd, *J* = 14.2, 9.0 Hz, 1H), 2.58 (d, *J* = 5.3 Hz, 1H), 1.88 (d, *J* = 5.1 Hz, 1H); ^{13}C NMR (101 MHz, $CDCl_3$) δ 161.91, 112.44, 112.19, 102.51, 72.79, 64.77, 63.20, 36.75.

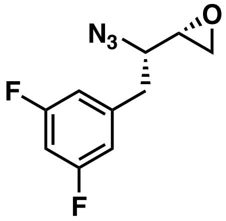

(*S*)-2-((*S*)-1-azido-2-(3,5-difluorophenyl)ethyl)oxirane 74: To a solution of diol **73** (9.46 mmol, 2.3 g) in CH_2Cl_2 (30 mL) was added triethylamine (18.92 mmol, 2.64 mL), catalytic dibutyltin(IV) oxide (2 mol%, 47 mg), and 4-dimethylamino pyridine (10 mol%, 116 mg). To the resulting mixture TsCl (10.41 mmol, 1.98 g) in a CH_2Cl_2 (5 mL) at 0 °C was added dropwise. The slurry was slowly warmed to 23 °C and stirred for an additional 2 h. Water was added and the organic layer was extracted with CH_2Cl_2. The organic layer was washed with brine and dried with Na_2SO_4. The crude mono-tosylate was isolated and carried forward to the next step without further purification. The tosylate was dissolved in MeOH (30 mL) and cooled to 0 °C. Potassium carbonate was added in one portion to the reaction mixture at 0 °C. The resulting white slurry was warmed to 23 °C and stirred for an additional 2 h. The reaction mixture was concentrated and extracted with Et_2O. The organic layer was dried with Na_2SO_4 and concentrated. The crude was purified *via* flash column chromatography (5% EtOAC/Hexanes). The optically pure epoxide **74** was isolated (1.38 g, 65% over 2 steps); ^1H NMR (400 MHz, $CDCl_3$) δ 6.82 – 6.67 (m, 3H), 3.54 (ddd, *J* = 8.9, 5.6, 4.1 Hz, 1H), 3.05 (ddd, *J* = 5.6, 3.8, 2.5 Hz, 1H), 2.97 (dd, *J* = 14.1, 4.1 Hz, 1H), 2.86 (dd, *J* = 4.9, 3.8 Hz, 1H), 2.84 – 2.71 (m, 2H); ^{13}C NMR (101 MHz, $CDCl_3$) δ 164.20, 161.60, 140.31, 112.33, 112.08, 102.50, 77.23, 76.91, 76.60, 63.16, 52.70, 45.26, 37.79.

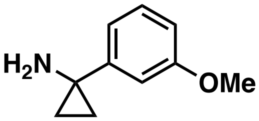

Preparation of 1-(3-methoxyphenyl)cyclopropan-1-amine 76a: In a dry and clean 2-neck flask, benzonitrile **75a** (880 mg, 17.5 mmol) was dissolved in Et_2O (90 mL) and cooled to -78 °C. $Ti(^iPrO)_4$ (19.25 mmol, 5.7 mL) is added dropwise followed by the dropwise addition of EtMgBr (1.0 M in Et_2O, 38.5 mmol, 38.5 mL) at the same temperature. The resulting mixture was allowed to stir at -78 °C for 15 minutes and warmed to 23 °C. Boron trifluoride etherate (25 mmol, 4.3 mL) was added slowly over 5 minutes at 23 °C and stirred for an additional 4 h at the same temperature. The reaction was quenched with aqueous 1M HCl (45 mL) and basified with aqueous 4N NaOH. The reaction mixture was extracted with Et_2O and dried with Na_2SO_4 followed by removal of the volatiles under reduced pressure. The crude product was purified *via* column chromatography (1% $MeOH/CH_2Cl_2$). Amine **76a** was isolated as a clear yellow oil (880 mg, 36%); ^1H NMR (400 MHz, $CDCl_3$) δ 7.23 (t, *J* = 8.2 Hz, 1H), 6.90 – 6.83 (m, 2H), 6.74 (ddd, *J* = 8.2, 2.4, 1.0 Hz, 1H), 3.80 (s, 3H), 2.11 (s, 2H), 1.06 (d, *J* = 2.3 Hz, 2H), 0.98 (d, *J* = 2.2 Hz, 2H); ^{13}C NMR (101 MHz, $CDCl_3$) δ 159.63, 148.68, 129.32, 117.61, 111.51, 110.88, 77.35, 77.04, 76.72, 55.11, 36.63, 17.90; LRMS-ESI (*m/z*) $[M+H]^+$ = 164.1.

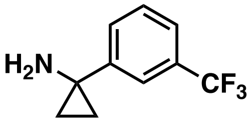

1-(3-(trifluoromethyl)phenyl)cyclopropan-1-amine 76b: Amine **76b** was prepared from nitrile **75b** (5.12 g, 29.9 mmol) to provide **76b** as a clear yellow oil (2.04 g, 34%); ^1H NMR (400 MHz, $CDCl_3$) δ 7.58 (s, 3H), 7.42 (s, 6H), 1.90 (s, 7H), 1.12 (d, *J* = 2.4 Hz, 5H), 1.04 – 0.98 (m, 5H); ^{13}C NMR (101 MHz, $CDCl_3$) δ 148.01, 128.70, 128.45, 122.56, 122.06, 122.02, 77.28, 76.96, 76.64, 36.36, 18.41; LRMS-ESI (*m/z*) $[M+H]^+$ = 202.0.

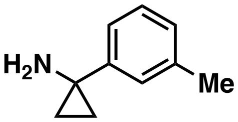

1-(*m*-tolyl)cyclopropan-1-amine 76c: Amine **76c** was prepared from nitrile **75c** (2.13 g, 18.2 mmol) to afford amine **76c** a clear yellow oil (1.0 g, 39%); ^1H NMR (300 MHz, $CDCl_3$) δ 7.30 – 7.06 (m, 3H), 7.03 (d, *J* = 7.5 Hz, 1H), 2.38 (s, 3H), 1.94 (s, 2H), 1.08 (q, *J* = 3.3 Hz, 2H), 1.00 (t,

J = 2.8 Hz, 2H). ^{13}C NMR (75 MHz, CDCl$_3$) δ 146.87, 137.75, 128.26, 126.64, 126.14, 122.38, 36.77, 36.16, 21.69, 17.98, 8.35; LRMS-ESI (*m/z*) [M+H]$^+$ = 148.1.

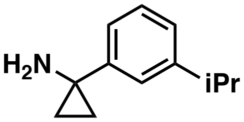

1-(3-isopropylphenyl)cyclopropan-1-amine 76d: Amine **76d** was prepared from nitrile **75d** (1.8 g, 12.4 mmol) to afford amine **76d** as an orange oil (670 mg, 31%); ^{1}H NMR (400 MHz, CDCl$_3$) δ 7.31 – 7.18 (m, 2H), 7.16 – 7.06 (m, 2H), 1.92 (s, 1H), 1.29 (dd, J = 7.0, 1.4 Hz, 6H), 1.08 (qd, J = 4.1, 3.5, 1.3 Hz, 2H), 1.04 – 0.96 (m, 2H); ^{13}C NMR (101 MHz, CDCl$_3$) δ 148.95, 146.83, 128.32, 123.93, 123.64, 122.86, 36.78, 35.87, 34.20, 24.07, 24.01, 17.65; LRMS-ESI (*m/z*) [M+H]$^+$ = 176.1.

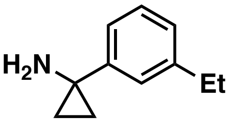

1-(3-ethylphenyl)cyclopropan-1-amine 76e: Amine **76e** was prepared from nitrile **75e** (2.3 g, 17.5 mmol) to afford amine **76e** as a clear yellow oil (881 mg, 31%); ^{1}H NMR (400 MHz, CDCl$_3$) δ 7.28 – 7.18 (m, 1H), 7.18 – 6.92 (m, 3H), 2.70 – 2.56 (m, 2H), 1.30 – 1.17 (m, 4H), 1.13 – 1.02 (m, 2H), 0.98 (q, J = 3.0, 2.3 Hz, 1H); ^{13}C NMR (101 MHz, CDCl$_3$) δ 146.83, 144.28, 128.30, 125.43, 125.00, 122.65, 35.88, 28.88, 17.61, 15.60, 8.04.

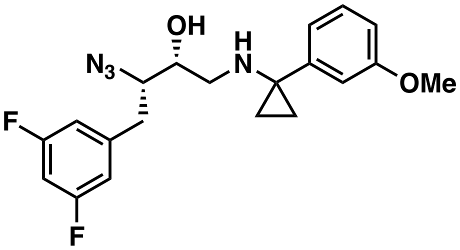

Preparation of (2*R*,3*S*)-3-azido-4-(3,5-difluorophenyl)-1-((1-(3methoxyphenyl) cyclopropyl)amino)butan-2-ol 77a: Oxirane **74** (150 mg, 0.666 mmol) was dissolved in iPrOH (10 mL) and treated with amine **76a** (435 mg, 2.66 mmol) stirred under reflux for 18 h. The reaction mixture cooled to 23 °C and the volatiles were removed. The crude reside was purified *via* flash chromatography (2% acetone/CH$_2$Cl$_2$).Azide **77a** was isolated as a clear yellow oil (190

mg, 74%); ^{1}H NMR (500 MHz, CDCl$_3$)δ 7.23 (t, *J* = 7.8 Hz, 1H), 6.91 – 6.85 (m, 2H), 6.79 – 6.61 (m, 5H), 3.80 (s, 3H), 3.42 (ddd, *J* = 8.7, 5.3, 3.5 Hz, 1H), 3.00 (dt, *J* = 8.8, 4.2 Hz, 1H), 2.81 (ddd, *J* = 20.3, 12.7, 3.6 Hz, 2H), 2.61 (dd, *J* = 12.0, 8.5 Hz, 1H), 2.47 – 2.38 (m, 1H), 1.02 – 0.85 (m, 4H); ^{13}C NMR (126 MHz, CDCl$_3$) δ 164.05, 163.95, 162.08, 161.98, 159.72, 144.77, 143.32, 129.44, 119.81, 113.63, 112.12, 112.07, 111.96, 111.92, 111.50, 102.00, 101.80, 101.60, 77.35, 77.09, 76.84, 72.30, 55.43, 55.17, 48.21, 42.37, 39.40, 15.87, 15.63; LRMS-ESI (*m/z*) [M+H]$^+$ = 389.1.

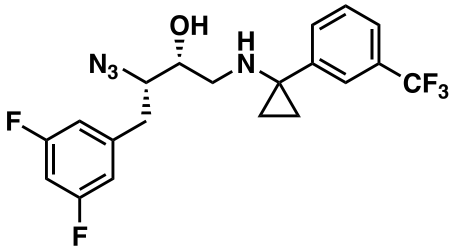

(2*R*,3*S*)-3-azido-4-(3,5-difluorophenyl)-1-((1-(3(trifluoromethyl)phenyl)cyclopropyl) amino)butan-2-ol 77b: Oxirane **74** (150 mg, 0.666 mmol) was treated with amine **76b** (535 mg, 2.66 mmol) in refluxing iPrOH (10 mL) to afford Azide **77b** as a clear yellow oil (80 mg, 31%); ^{1}H NMR (500 MHz, CDCl$_3$) δ 7.56 (td, *J* = 1.8, 1.0 Hz, 1H), 7.54 – 7.43 (m, 3H), 6.76 (dt, *J* = 6.6, 2.1 Hz, 2H), 6.73 – 6.65 (m, 1H), 3.58 – 3.48 (m, 2H), 2.93 (dd, *J* = 14.2, 3.7 Hz, 1H), 2.81 (dd, *J* = 12.3, 3.5 Hz, 1H), 2.72 – 2.59 (m, 2H), 1.20 (d, *J* = 6.1 Hz, 1H), 1.12 – 1.02 (m, 2H), 1.02 – 0.96 (m, 2H); ^{13}C NMR (101 MHz, CDCl$_3$) δ 164.22, 164.09, 161.75, 161.62, 143.76, 141.32, 130.84, 128.95, 124.13, 123.59, 112.23, 112.16, 112.05, 111.98, 102.51, 102.25, 70.62, 65.92, 48.07, 42.21, 36.52, 25.22, 15.90, 15.55; LRMS-ESI (*m/z*) [M+H]$^+$ = 427.1.

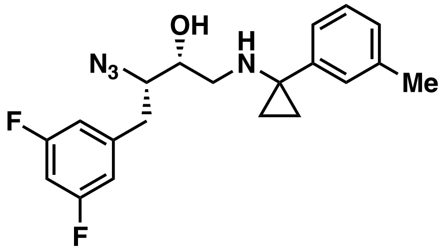

(2*R*,3*S*)-3-azido-4-(3,5-difluorophenyl)-1-((1-(*m*-tolyl)cyclopropyl)amino)butan-2-ol 77c: Oxirane **74** (100 mg, 0.44 mmol) was treated with amine **76c** (258 mg, 1.76 mmol) in refluxing iPrOH (8 mL) to afford Azide **77c** as a clear yellow oil (116 mg, 71%); ^{1}H NMR (400 MHz, CDCl$_3$)

δ 7.28 – 7.18 (m, 2H), 7.12 (dd, *J* = 6.7, 1.5 Hz, 2H), 7.08 – 7.01 (m, 2H), 6.75 – 6.63 (m, 4H), 3.41 (ddd, *J* = 8.7, 5.3, 3.4 Hz, 1H), 3.03 (ddd, *J* = 9.4, 5.3, 3.8 Hz, 1H), 2.82 (ddd, *J* = 15.7, 12.8, 3.6 Hz, 2H), 2.60 (dd, *J* = 12.1, 8.6 Hz, 1H), 2.35 (s, 3H), 1.01 – 0.89 (m, 4H); ^{13}C NMR (101 MHz, $CDCl_3$) δ 164.23, 161.63, 142.78, 137.96, 128.23, 127.34, 124.62, 112.04, 111.80, 101.73, 94.44, 77.27, 76.95, 76.63, 72.10, 55.31, 48.01, 42.28, 39.39, 21.40, 15.62, 15.17; LRMS-ESI (*m/z*) $[M+H]^+$ = 373.1.

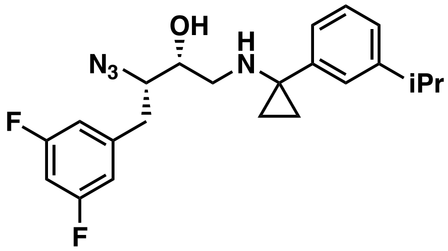

(2*R*,3*S*)-3-azido-4-(3,5-difluorophenyl)-1-((1-(3-isopropylphenyl)cyclopropyl)amino)butan-2-ol 77d: Oxirane **74** (150 mg, 0.66 mmol) was treated with amine **76d** (462 mg, 2.64 mmol) in refluxing iPrOH (10 mL) to afford Azide **77d** as a clear yellow oil (125 mg, 47%); ^{1}H NMR (400 MHz, $CDCl_3$) δ 7.29 (dd, *J* = 8.0, 7.1 Hz, 1H), 7.19 (t, *J* = 1.9 Hz, 1H), 7.17 – 7.11 (m, 2H), 6.82 – 6.75 (m, 2H), 3.58 – 3.48 (m, 2H), 3.00 – 2.89 (m, 2H), 2.89 – 2.84 (m, 1H), 2.75 – 2.61 (m, 2H), 1.29 (d, *J* = 6.9 Hz, 6H), 1.06 – 0.94 (m, 4H); ^{13}C NMR (101 MHz, $CDCl_3$) δ 164.34, 164.21, 161.87, 161.74, 149.23, 142.58, 141.65, 128.51, 125.87, 125.16, 124.93, 112.37, 112.31, 112.19, 112.13, 102.58, 102.33, 102.08, 77.42, 77.10, 76.79, 70.68, 66.20, 48.28, 42.63, 36.68, 34.18, 24.06, 23.90, 15.71, 15.33; LRMS-ESI (*m/z*) $[M+H]^+$ = 401.1.

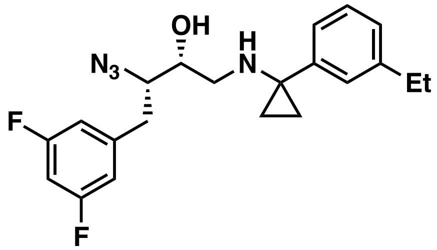

(2*R*,3*S*)-3-azido-4-(3,5-difluorophenyl)-1-((1-(3-ethylphenyl)cyclopropyl)amino)butan-2-ol 77e: Oxirane **74** (145 mg, 0.66 mmol) was treated with amine **76e** (425 mg, 2.64 mmol) in refluxing iPrOH (10 mL) to afford Azide **77e** as a clear yellow oil (145 mg, 57%); ^{1}H NMR (400 MHz, $CDCl_3$) δ 7.29 (t, *J* = 7.5 Hz, 1H), 7.20 – 7.09 (m, 3H), 6.83 – 6.76 (m, 2H), 6.76 – 6.67 (m, 1H), 3.54 (s, 2H), 2.95 (dd, *J* = 14.1, 3.2 Hz, 1H), 2.88 (dd, *J* = 12.4, 3.1 Hz, 1H), 2.75 – 2.61 (m, 4H), 1.28 (t, *J* = 7.6 Hz, 3H), 1.00 (tt, *J* = 6.9, 4.2 Hz, 4H); ^{13}C NMR (101 MHz, $CDCl_3$) δ 164.24, 164.11, 161.77, 161.64, 144.49, 142.54, 141.56, 128.42, 127.14, 126.34, 124.94, 112.27, 112.20, 112.09, 112.02, 102.47, 102.22, 101.97, 77.33, 77.02, 76.70, 70.58, 66.06, 48.17, 42.47, 36.54, 28.82, 15.58, 15.53, 15.17; LRMS-ESI (*m/z*) $[M+H]^+$ = 387.1.

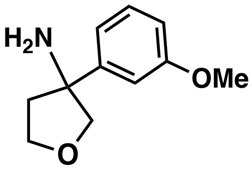

Preparation of 3-(3-methoxyphenyl)tetrahydrofuran-3-amine 83a: In a clean, dry, round bottom flask ketone **78** (0.6 mL, 7.8 mmol) was dissolved in THF (30 mL) and the aryl magnesium bromide **80a** in a solution of THF (0.5 M, 14.04 mmol, 28.08 mL) was added dropwise over 5 minutes at 23 °C. The resulting reaction mixture was refluxed for 0.5 h and cooled to 23 °C. The reaction was quenched with saturated aqueous NH_4Cl and the organic layer was washed with H_2O. The organic layer was removed under reduced pressure and the crude **81a** (1.55 g) was carried forward without further purification. The crude alcohol **81a** was immediately dissolved in CH_2Cl_2 (15 mL) and treated with sodium azide (1.45 g, 7.47 mmol). The resulting heterogenous mixture was subjected to dropwise addition of a solution of TFA (4.6 mL, 59.76 mmol.) and CH_2Cl_2. After 48 h of stirring at 23 °C the mixture was diluted with H_2O and neutralized with saturated aqueous $NaHCO_3$. The crude mixture was extracted with CH_2Cl_2 and dried with Na_2SO_4 followed by removal of the volatiles under reduced pressure. Azide **82a** (1.1 g) was diluted in EtOH (15 mL) and treated with concentrated HCl at 23 °C. A catalytic amount of Pd/C (20% w/w, 220 mg) was added under a hydrogen atmosphere and the resulting mixture was stirred for 24 h at 23 °C. The reaction mixture was filtered through a pad of celite and concentrated to provide amine **83a** as a clear yellow oil (860 mg, 58% over 3 steps); ^{1}H NMR (300 MHz, $CDCl_3$) δ 7.21 (d, *J* = 8.2 Hz, 1H), 7.01 – 6.92 (m, 2H), 6.80 – 6.70 (m, 1H), 4.09 (dd, *J* = 8.7, 7.1 Hz, 1H), 4.00 (q, *J* = 4.8 Hz, 1H), 3.84 (dd, *J* = 12.0, 8.3 Hz, 1H), 3.75 (d, *J* = 2.5 Hz, 4H), 2.37 – 2.24 (m, 1H), 2.11 – 1.98 (m, 1H); ^{13}C NMR (75 MHz, $CDCl_3$) δ 159.53, 146.65, 129.42, 117.84, 111.93, 111.81, 80.42, 67.65, 63.37, 55.23, 41.90.

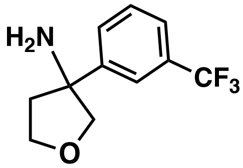

3-(3-(trifluoromethyl)phenyl)tetrahydrofuran-3-amine 83b: Amine **84b** was prepared from ketone **78** (0.6 mL, 7.8 mmol) to afford amine **83b** as a clear yellow oil (751 mg, 64% over 3 steps); ^{1}H NMR (300 MHz, CDCl$_3$) δ 7.73 (d, *J* = 2.7 Hz, 1H), 7.62 (d, *J* = 7.9 Hz, 1H), 7.43 (dd, *J* = 14.2, 6.7 Hz, 2H), 4.21 – 3.95 (m, 2H), 3.92 – 3.75 (m, 2H), 2.33 (td, *J* = 8.7, 4.0 Hz, 1H), 2.10 (ddd, *J* = 12.3, 7.4, 4.1 Hz, 1H), 1.79 (s, 2H); ^{13}C NMR (75 MHz, CDCl$_3$) δ 145.92, 129.11, 128.85, 122.42, 80.52, 67.60, 63.26, 42.28.

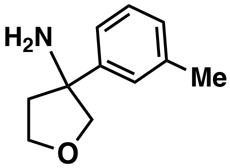

3-(*m*-tolyl)tetrahydrofuran-3-amine 83c: Amine **83c** was prepared from ketone **78** (0.6 mL, 7.8 mmol) to afford amine **83c** as a clear yellow oil (420 mg, 38% over 3 steps); ^{1}H NMR (300 MHz, CDCl$_3$) δ 7.29 – 7.20 (m, 3H), 7.13 – 7.05 (m, 1H), 4.22 – 4.01 (m, 2H), 3.98 – 3.83 (m, 2H), 2.47 – 2.31 (m, 4H), 2.13 (dddd, *J* = 12.4, 7.2, 3.8, 1.1 Hz, 1H); ^{13}C NMR (75 MHz, CDCl$_3$) δ 144.74, 138.09, 128.38, 127.71, 126.38, 122.55, 80.46, 67.71, 63.39, 41.82, 21.69.

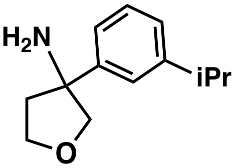

3-(3-isopropylphenyl)tetrahydrofuran-3-amine 83d: Amine **83d** was prepared from ketone **78** (0.4 mL, 5.2 mmol) to afford amine **83d** as a clear yellow oil (660 mg, 63% over 3 steps); ^{1}H NMR (300 MHz, CDCl$_3$) δ 7.35 – 7.23 (m, 3H), 7.15 (dd, *J* = 6.9, 2.0 Hz, 1H), 4.25 – 4.00 (m, 2H), 3.91 (dt, *J* = 9.7, 8.6 Hz, 2H), 2.92 (p, *J* = 6.9 Hz, 1H), 2.48 – 2.31 (m, 1H), 2.13 (dddd, *J* = 12.4, 7.2, 3.9, 1.1 Hz, 1H), 1.73 (s, 2H), 1.26 (dd, *J* = 6.9, 4.0 Hz, 6H); ^{13}C NMR (75 MHz, CDCl$_3$) δ 149.03, 144.81, 128.42, 124.88, 123.86, 123.05, 80.56, 67.71, 63.50, 41.95, 34.41, 24.20.

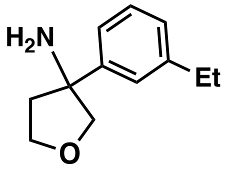

3-(3-ethylphenyl)tetrahydrofuran-3-amine 83e: Amine **83e** was prepared from ketone **78** (310 mg, 3.6 mmol) to afford amine **83e** as a clear yellow oil (268 mg, 39% over 3 steps); ^{1}H NMR (300 MHz, CDCl$_3$) δ 7.27 (ddd, *J* = 8.6, 2.1, 1.1 Hz, 3H), 7.11 (dd, *J* = 5.2, 3.4 Hz, 1H), 4.22 – 4.00 (m, 2H), 3.90 (dt, *J* = 9.7, 8.5 Hz, 2H), 2.66 (q, *J* = 7.7 Hz, 2H), 2.39 (ddd, *J* = 12.5, 9.5, 8.3 Hz, 1H), 2.19 – 2.06 (m, 1H), 1.25 (t, *J* = 7.6 Hz, 3H); ^{13}C NMR (75 MHz, CDCl$_3$) δ 144.85, 144.40, 128.43, 126.44, 125.21, 122.86, 80.51, 67.71, 63.44, 41.91, 29.13, 15.85.

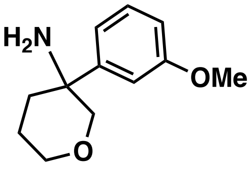

3-(3-methoxyphenyl)tetrahydro-2*H*-pyran-3-amine 83f: Amine **83f** was prepared from ketone **79** (0.60 mL, 6.5 mmol) to afford amine **83f** as clear colorless oil (340 mg, 26% over 3 steps); ^{1}H NMR (400 MHz, CDCl$_3$) δ 7.32 (t, *J* = 7.9 Hz, 1H), 7.07 – 6.98 (m, 2H), 6.87 (ddd, *J* = 8.3, 2.5, 0.9 Hz, 1H), 3.96 (dt, *J* = 11.4, 3.9 Hz, 1H), 3.89 (dd, *J* = 11.9, 1.5 Hz, 1H), 3.83 (s, 3H), 3.67 (d, *J* = 12.0 Hz, 1H), 3.54 (ddd, *J* = 11.2, 10.3, 2.8 Hz, 1H), 2.19 – 2.11 (m, 2H), 2.11 – 1.99 (m, 1H), 1.67 – 1.55 (m, 1H); ^{13}C NMR (101 MHz, CDCl$_3$) δ 159.79, 141.94, 129.72, 118.02, 112.94, 112.28, 73.72, 67.77, 64.14, 55.21, 32.70, 22.27.

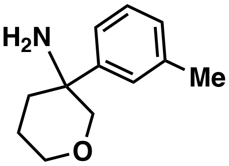

3-(*m*-tolyl)tetrahydro-2*H*-pyran-3-amine 83g: Amine **83g** was prepared from ketone **79** (0.6 mL, 6.5 mmol) to afford amine **83g** as a clear yellow oil (300 mg, 24% over 3 steps); ^{1}H NMR (300 MHz, CDCl$_3$) δ 7.42 – 7.29 (m, 2H), 7.24 (t, *J* = 7.6 Hz, 1H), 7.12 – 7.03 (m, 1H), 3.97 – 3.87 (m, 1H), 3.73 (d, *J* = 11.3 Hz, 1H), 3.64 – 3.44 (m, 2H), 2.37 (d, *J* = 0.8 Hz, 3H), 2.10 (ddd, *J* = 12.7, 11.2, 4.2 Hz, 1H), 2.03 – 1.85 (m, 1H), 1.79 (s, 3H), 1.56 (ddd, *J* = 13.7, 5.7, 2.3 Hz, 1H); ^{13}C

NMR (75 MHz, CDCl3) δ 145.60, 137.80, 128.16, 127.62, 126.31, 122.51, 76.75, 68.21, 52.84, 37.11, 22.58, 21.78.

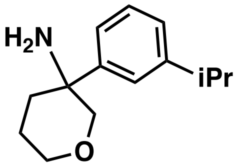

3-(3-isopropylphenyl)tetrahydro-2*H*-pyran-3-amine 83h: Amine **83h** was prepared from ketone **79** (0.8 mL, 8.6 mmol) to afford amine **83h** as a clear yellow oil (270 mg, 13% over 3 steps); ^{1}H NMR (300 MHz, CDCl3) δ 7.37 – 7.19 (m, 4H), 4.06 – 3.80 (m, 2H), 3.67 (d, *J* = 12.0 Hz, 1H), 3.54 (td, *J* = 10.9, 2.9 Hz, 1H), 2.99 – 2.85 (m, 1H), 2.20 – 2.10 (m, 2H), 1.31 – 1.22 (m, 6H).^{13}C NMR (75 MHz, CDCl3) δ 164.13, 149.37, 140.21, 128.65, 126.07, 123.17, 74.00, 67.90, 64.54, 34.40, 32.81, 24.12, 22.50.

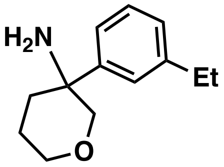

3-(3-ethylphenyl)tetrahydro-2*H*-pyran-3-amine 83i: Amine **83i** was prepared from ketone **79** (0.6 mL, 6.5 mmol) to afford amine **83i** as a clear colorless oil (242 mg, 18% over 3 steps); ^{1}H NMR (300 MHz, CDCl3) δ 7.44 – 7.22 (m, 3H), 7.16 – 7.07 (m, 1H), 3.98 – 3.88 (m, 1H), 3.80 – 3.61 (m, 2H), 3.52 (td, *J* = 10.6, 2.9 Hz, 1H), 2.87 (s, 1H), 2.67 (q, *J* = 7.6 Hz, 2H), 2.17 – 2.08 (m, 1H), 2.08 – 1.92 (m, 1H), 1.92 – 1.81 (m, 1H), 1.64 – 1.52 (m, 1H), 1.25 (td, *J* = 7.6, 0.6 Hz, 3H); ^{13}C NMR (75 MHz, CDCl3) δ 144.68, 144.27, 128.29, 126.57, 125.18, 122.82, 68.20, 53.32, 36.61, 29.18, 22.45, 15.83.

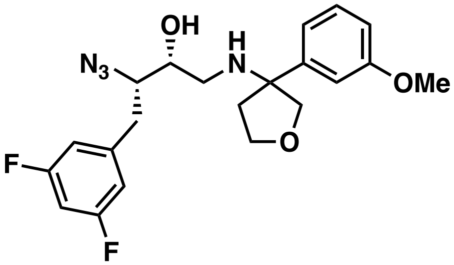

Preparation of (2*R*,3*S*)-3-azido-4-(3,5-difluorophenyl)-1-((3-(3-methoxyphenyl) tetrahydro furan-3-yl)amino)butan-2-ol 84a: In a round bottom flask oxirane **74** (80 mg, 0.35 mmol) was dissolved in iPrOH (10 mL) and treated with selected amine **83a** (110 mg, 0.53 mmol) stirred under reflux for 18 h. The reaction mixture cooled to 23 °C and the volatiles were removed. The crude reside was purified *via* flash chromatography (2% acetone/CH_2Cl_2). Azide **84a** was isolated as a clear colorless oil (31 mg, 57%); ^{1}H NMR (400 MHz, $CDCl_3$) δ 7.33 – 7.23 (m, 1H), 6.93 – 6.79 (m, 3H), 6.77 – 6.66 (m, 3H), 4.14 – 3.98 (m, 3H), 3.84 (d, *J* = 8.9 Hz, 1H), 3.81 (s, 3H), 3.44 (ddd, *J* = 9.1, 6.5, 3.8 Hz, 1H), 3.32 (ddd, *J* = 7.9, 6.4, 3.7 Hz, 1H), 2.90 (dd, *J* = 14.2, 3.7 Hz, 1H), 2.72 – 2.61 (m, 2H), 2.42 – 2.25 (m, 3H);^{13}C NMR (101 MHz, $CDCl_3$) δ 164.05, 161.58, 159.70, 143.36, 141.31, 129.62, 118.94, 113.22, 112.27, 112.03, 102.45, 102.20, 77.26, 76.94, 76.62, 76.35, 71.06, 67.58, 67.04, 65.76, 55.15, 45.14, 36.66, 36.47; LRMS-ESI (*m/z*) $[M+H]^+$ = 419.1.

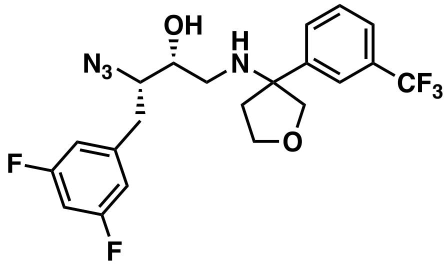

(2*R*,3*S*)-3-azido-4-(3,5-difluorophenyl)-1-((3-(3-(trifluoromethyl)phenyl)tetrahydrofuran-3-yl)amino)butan-2-ol 84b: Oxirane **74** (50 mg, 0.22 mmol) was treated with amine **83b** (100 mg, 0.44 mmol) in refluxing iPrOH (6 mL) to afford Azide **84b** as a yellow oil (22 mg, 24%); ^{1}H NMR (400 MHz, $CDCl_3$) δ 7.56 (dd, *J* = 7.8, 2.3 Hz, 2H), 7.53 – 7.48 (m, 2H), 6.82 (dt, *J* = 6.6, 2.1 Hz, 1H), 6.71 (ddt, *J* = 16.3, 9.1, 2.2 Hz, 3H), 4.17 – 4.00 (m, 3H), 3.87 (dd, *J* = 8.9, 3.1 Hz, 1H), 3.68 – 3.58 (m, 2H), 3.58 – 3.48 (m, 1H), 3.11 (dd, *J* = 14.1, 2.6 Hz, 1H), 2.91 (dd, *J* = 14.1, 3.8 Hz, 1H), 2.76 – 2.61 (m, 2H), 2.55 (dd, *J* = 12.3, 3.8 Hz, 1H), 2.50 – 2.39 (m, 1H), 2.39 – 2.29 (m, 2H). ^{13}C NMR (101 MHz, $CDCl_3$) δ 164.20, 161.60, 142.95, 130.07, 129.15, 128.86, 124.38, 123.29, 112.25, 112.01, 102.28, 72.40, 71.77, 71.16, 71.03, 68.19, 67.46, 67.00, 65.66, 64.61, 45.23, 44.96, 36.76, 36.66, 36.48, 21.91; LRMS-ESI (*m/z*) $[M+H]^+$ = 457.1.

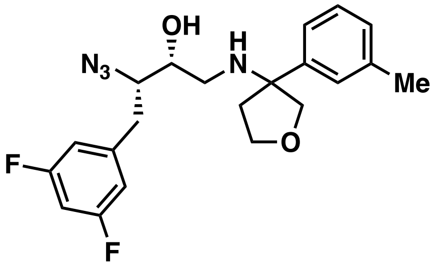

(2*R*,3*S*)-3-azido-4-(3,5-difluorophenyl)-1-((3-(*m*-tolyl)tetrahydrofuran-3-yl)amino)butan-2-ol 84c: Oxirane **74** (80 mg, 0.35 mmol) was treated with amine **83c** (123 mg, 0.70 mmol) in refluxing iPrOH (10 mL) to afford azide **84c** as a clear yellow oil (145 mg, 99%); ^{1}H NMR (400 MHz, CDCl$_3$) δ 7.10 (ddt, *J* = 4.8, 2.4, 0.8 Hz, 6H), 6.77 – 6.72 (m, 3H), 6.72 – 6.64 (m, 3H), 4.17 – 4.08 (m, 3H), 4.08 – 4.06 (m, 1H), 4.06 – 3.96 (m, 2H), 3.85 (dd, *J* = 8.9, 5.1 Hz, 2H), 3.44 (dddd, *J* = 10.6, 9.0, 6.6, 3.8 Hz, 2H), 3.29 (ddd, *J* = 7.7, 6.6, 3.8 Hz, 2H), 2.90 (dd, *J* = 14.1, 3.7 Hz, 2H), 2.71 – 2.63 (m, 3H), 2.46 (dd, *J* = 12.5, 7.4 Hz, 2H), 2.36 – 2.27 (m, 6H); ^{13}C NMR (101 MHz, CDCl$_3$) δ 164.05, 161.58, 141.61, 138.24, 128.46, 128.24, 127.31, 123.70, 112.26, 112.02, 102.45, 102.20, 101.95, 70.96, 70.84, 67.53, 67.03, 65.75, 65.66, 45.07, 44.82, 36.62, 36.45, 21.48; LRMS-ESI (*m/z*) [M+H]$^+$ = 403.1.

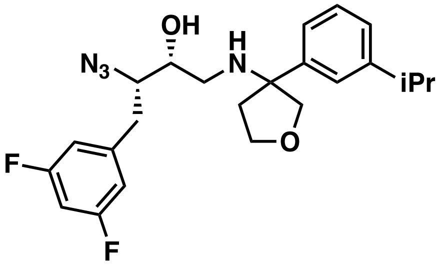

(2*R*,3*S*)-3-azido-4-(3,5-difluorophenyl)-1-((3-(3-isopropylphenyl)tetrahydrofuran-3-yl) amino)butan-2-ol 84d: Oxirane **74** (80 mg, 0.35 mmol) was treated with amine **83d** (144 mg, 0.70 mmol) in refluxing iPrOH (10 mL) to afford Azide **84d** as a clear yellow oil (65 mg, 43%); ^{1}H NMR (400 MHz, CDCl$_3$) δ 7.33 – 7.23 (m, 1H), 7.17 – 7.08 (m, 3H), 6.77 – 6.66 (m, 3H), 4.16 – 4.06 (m, 2H), 4.06 – 3.99 (m, 1H), 3.87 (dd, *J* = 8.9, 5.7 Hz, 1H), 3.47 – 3.40 (m, 1H), 3.33 – 3.24 (m, 1H), 2.91 – 2.85 (m, 1H), 2.72 – 2.55 (m, 2H), 2.43 – 2.29 (m, 3H), 1.25 (d, *J* = 6.9 Hz, 6H).^{13}C NMR (101 MHz, CDCl$_3$); δ 164.04, 161.70, 149.27, 141.58, 128.52, 125.44, 124.87, 124.08, 112.26, 112.02, 102.19, 101.94, 77.25, 76.93, 76.62, 76.45, 76.37, 70.98, 70.88, 67.67, 67.05, 65.81, 65.72, 45.07, 44.82, 36.72, 36.48, 34.10, 23.92; LRMS-ESI (*m/z*) [M+H]$^+$ = 431.1.

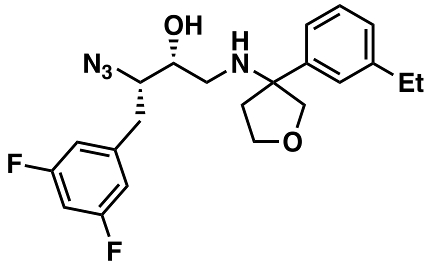

(2*R*,3*S*)-3-azido-4-(3,5-difluorophenyl)-1-((3-(3-ethylphenyl)tetrahydrofuran-3-yl)amino) butan-2-ol 84e: Oxirane **74** (80 mg, 0.35 mmol) was treated with amine **83e** (100 mg, 0.53 mmol) in refluxing iPrOH (8 mL) to afford azide **84e** as a clear yellow oil (140 mg, 97%) ^{1}H NMR (400 MHz, CDCl$_3$)δ 7.30 – 7.23 (m, 1H), 7.16 – 7.08 (m, 3H), 6.77 – 6.66 (m, 3H), 4.17 – 4.05 (m, 2H), 4.05 – 3.97 (m, 1H), 3.90 – 3.82 (m, 1H), 3.49 – 3.39 (m, 1H), 3.34 – 3.25 (m, 1H), 2.90 (dd, *J* = 14.2, 3.7 Hz, 1H), 2.71 – 2.63 (m, 3H), 2.63 – 2.55 (m, 1H), 2.33 (td, *J* = 7.8, 7.4, 2.9 Hz, 2H), 1.24 (t, *J* = 7.6 Hz, 3H).^{13}C NMR (101 MHz, CDCl$_3$) δ 164.05, 161.71, 144.62, 141.65, 128.53, 126.99, 126.18, 123.94, 112.26, 112.01, 102.19, 77.24, 76.93, 76.61, 76.44, 76.35, 70.90, 67.60, 67.04, 65.78, 65.70, 45.09, 44.84, 36.69, 36.47, 28.85, 15.54; LRMS-ESI (*m/z*) [M+H]$^+$ = 417.1.

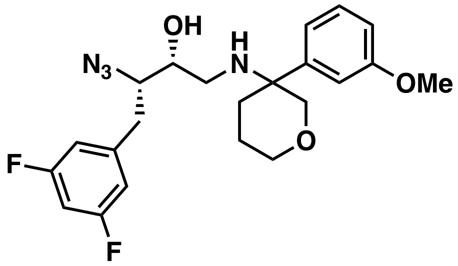

(2*R*,3*S*)-3-azido-4-(3,5-difluorophenyl)-1-((3-(3-methoxyphenyl)tetrahydro-2*H*-pyran-3-yl)amino)butan-2-ol 84f: Oxirane **74** (80 mg, 0.53 mmol) was treated with amine **83f** (110 mg, 0.53 mmol) in refluxing iPrOH (10 m) to afford azide **84f** was as a clear yellow oil (135 mg, 89%); ^{1}H NMR (400 MHz, CDCl$_3$) δ 7.32 – 7.23 (m, 2H), 7.06 – 6.98 (m, 4H), 6.86 – 6.71 (m, 7H), 6.71 – 6.66 (m, 1H), 3.95 (d, *J* = 11.2 Hz, 2H), 3.89 – 3.77 (m, 8H), 3.54 – 3.47 (m, 2H), 3.45 (dd, *J* = 6.5, 1.9 Hz, 1H), 3.41 (qd, *J* = 5.8, 2.7 Hz, 2H), 2.98 – 2.87 (m, 2H), 2.74 – 2.63 (m, 3H), 2.56 (dd, *J* = 12.4, 6.3 Hz, 1H), 2.44 (d, *J* = 4.3 Hz, 0H), 2.16 – 2.09 (m, 1H), 2.07 – 1.98 (m, 2H), 1.68 – 1.59 (m, 2H); ^{13}C NMR (101 MHz, CDCl$_3$) δ 164.05, 161.70, 159.71, 144.57, 144.39, 141.46, 129.45, 118.68, 118.61, 112.89, 112.32, 112.26, 112.08, 112.01, 102.41, 102.16, 101.91, 77.28, 76.96, 76.64, 76.34, 76.01, 71.30, 71.09, 68.03, 65.84, 65.72, 56.16, 55.10, 43.68, 42.80, 36.50, 30.65, 30.23, 22.01; LRMS-ESI (*m/z*) [M+H]$^+$ = 433.1.

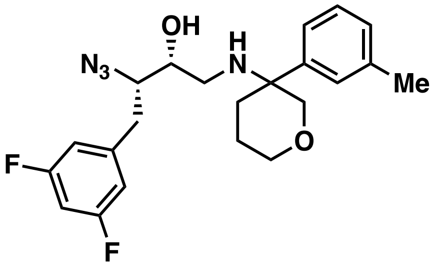

(2*R*,3*S*)-3-azido-4-(3,5-difluorophenyl)-1-((3-(*m*-tolyl)tetrahydro-2*H*-pyran-3-yl)amino) butan-2-ol 84g: Oxirane **74** (80 mg, 0.35 mmol) was treated with amine **83g** (100 mg, 0.53 mmol) in refluxing iPrOH (10 mL) to afford **a**zide **84g** as a clear yellow oil (147 mg, 99%); ^{1}H NMR (400 MHz, $CDCl_3$) δ 7.26 (t, *J* = 2.4 Hz, 6H), 7.10 (dd, *J* = 5.2, 2.4 Hz, 2H), 6.76 (ddd, *J* = 8.1, 3.6, 2.1 Hz, 4H), 6.76 – 6.64 (m, 2H), 4.01 – 3.82 (m, 5H), 3.56 – 3.42 (m, 4H), 3.46 – 3.39 (m, 2H), 2.93 (ddd, *J* = 14.2, 12.1, 3.4 Hz, 2H), 2.74 – 2.62 (m, 3H), 2.56 (dd, *J* = 12.3, 6.4 Hz, 1H), 2.42 (dd, *J* = 12.3, 4.1 Hz, 1H), 2.37 (d, *J* = 3.7 Hz, 6H), 2.16 (q, *J* = 5.6, 5.1 Hz, 4H), 2.11 – 2.00 (m, 2H), 1.88 (s, 1H), 1.93 – 1.82 (m, 1H), 1.69 – 1.59 (m, 2H);^{13}C NMR (101 MHz, $CDCl_3$) δ 164.05, 161.71, 142.70, 142.56, 141.55, 141.47, 138.00, 128.36, 128.09, 127.07, 127.00, 123.44, 123.38, 112.32, 112.26, 112.08, 112.02, 102.40, 102.14, 101.89, 77.33, 77.01, 76.69, 76.35, 76.11, 71.34, 71.13, 68.04, 68.00, 65.94, 65.85, 65.71, 56.04, 43.64, 42.83, 36.50, 36.42, 30.52, 30.25, 22.03, 21.58; LRMS-ESI (*m/z*) $[M+H]^+$ = 417.1.

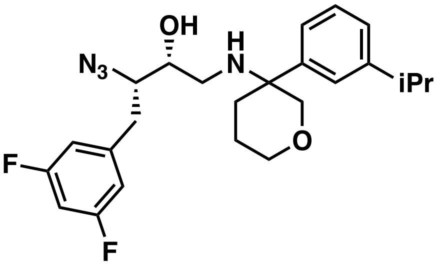

(2*R*,3*S*)-3-azido-4-(3,5-difluorophenyl)-1-((3-(3-isopropylphenyl)tetrahydro-2*H*-pyran-3-yl)amino)butan-2-ol 84h: Oxirane **74** (80 mg, 0.35 mmol) was treated with amine **83h** (115 mg, 0.53 mmol) to afford azide **84h** as a clear yellow oil (140 mg, 90%); ^{1}H NMR (400 MHz, $CDCl_3$) δ 7.37 – 7.23 (m, 6H), 7.20 – 7.13 (m, 2H), 6.81 – 6.64 (m, 5H), 4.02 – 3.94 (m, 2H), 3.88 (td, *J* = 8.8, 4.3 Hz, 2H), 3.56 – 3.48 (m, 3H), 3.48 – 3.40 (m, 4H), 2.94 (dd, *J* = 14.0, 3.6 Hz, 4H), 2.75 –

2.62 (m, 3H), 2.58 (dd, *J* = 12.4, 6.3 Hz, 1H), 2.44 (dd, *J* = 12.4, 4.3 Hz, 1H), 2.24 – 2.11 (m, 3H), 2.11 – 1.99 (m, 2H), 1.95 – 1.84 (m, 2H), 1.70 – 1.61 (m, 2H), 1.27 (ddd, *J* = 7.0, 3.7, 1.6 Hz, 12H); ^{13}C NMR (101 MHz, $CDCl_3$) δ 164.19, 161.72, 149.04, 142.68, 142.51, 128.38, 125.33, 124.58, 124.51, 123.79, 123.73, 112.28, 112.08, 102.39, 102.14, 77.33, 77.02, 76.70, 76.48, 76.19, 71.37, 71.13, 68.00, 65.86, 65.74, 56.23, 43.62, 42.86, 36.49, 34.19, 30.49, 30.15, 24.06, 24.02, 23.91, 23.88, 22.04; LRMS-ESI (*m/z*) [M+H]$^+$ = 445.2.

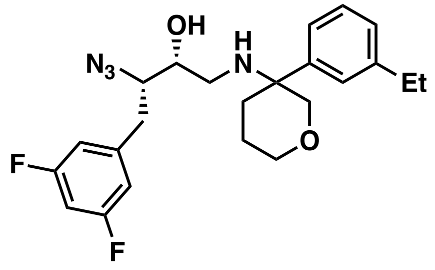

(2*R*,3*S*)-3-azido-4-(3,5-difluorophenyl)-1-((3-(3-ethylphenyl)tetrahydro-2*H*-pyran-3-yl)amino)butan-2-ol 84i: Oxirane **74** (80 mg, 0.35 mmol) was treated with amine **83i** (110 mg, 0.53 mmol) in refluxing iPrOH (10 mL) to afford azide **84i** as a clear yellow oil (132 mg, 88%); ^{1}H NMR (400 MHz, $CDCl_3$) δ 7.31 – 7.23 (m, 5H), 7.16 – 7.09 (m, 2H), 6.79 – 6.68 (m, 4H), 6.71 – 6.63 (m, 1H), 3.96 (dd, *J* = 11.5, 4.0 Hz, 2H), 3.87 (ddd, *J* = 11.3, 8.7, 2.5 Hz, 2H), 3.56 – 3.33 (m, 6H), 2.93 (dt, *J* = 14.2, 3.6 Hz, 2H), 2.74 – 2.61 (m, 6H), 2.56 (dd, *J* = 12.5, 6.2 Hz, 1H), 2.43 (dd, *J* = 12.4, 4.3 Hz, 1H), 2.21 – 2.12 (m, 3H), 2.12 – 2.04 (m, 1H), 2.07 – 1.98 (m, 1H), 1.93 – 1.82 (m, 1H), 1.69 – 1.60 (m, 2H), 1.24 (td, *J* = 7.6, 3.3 Hz, 6H); ^{13}C NMR (101 MHz, $CDCl_3$) δ 164.18, 161.57, 144.40, 142.72, 142.55, 128.41, 126.86, 125.90, 125.83, 123.65, 123.58, 112.31, 112.25, 112.06, 102.40, 102.15, 77.28, 76.96, 76.64, 76.45, 76.09, 71.29, 71.00, 68.03, 65.84, 65.73, 56.13, 43.60, 42.75, 36.51, 30.61, 30.13, 28.95, 22.03, 15.56; LRMS-ESI (*m/z*) [M+H]$^+$ = 431.2.

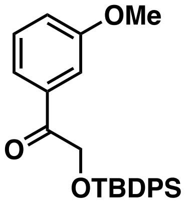

Preparation of 2-((*tert*-butyldiphenylsilyl)oxy)-1-(3-methoxyphenyl)ethan-1-one 91a: In a clean and dry, 2-neck round bottom flask the appropriate aryl magnesium bromide (2.84 mL, 22.41

mmol) is added as a solution in THF (15 mL). The mixture is cooled to 0 °C and a solution of THF (40 mL) and weinreb amide **89** (4.45 g, 12.45 mmol) is added dropwise over 10 minutes. The resulting mixture is stirred for 3 h at 0 °C and quenched with saturated aqueous NH_4Cl. The reaction is diluted H_2O and extracted by EtOAc. The residue was purified *via* column chromatography (5% EtOAc/Hexanes) to provide aryl ketone **91a** was isolated as a clear colorless oil (4.59 g, 91%); ^{1}H NMR (400 MHz, $CDCl_3$) δ 7.75 – 7.67 (m, 4H), 7.45 – 7.32 (m, 8H), 4.91 (s, 2H), 3.82 (s, 3H), 1.11 (d, J = 1.9 Hz, 9H);^{13}C NMR (101 MHz, $CDCl_3$) δ 196.37, 159.67, 136.18, 135.50, 132.86, 129.78, 129.42, 127.72, 120.14, 119.60, 112.01, 77.23, 76.92, 76.60, 67.50, 55.32, 26.62, 19.26.

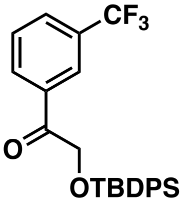

2-((*tert*-butyldiphenylsilyl)oxy)-1-(3-(trifluoromethyl)phenyl)ethan-1-one 91b: Ketone **91b** was prepared from weinreb amide **89** (11.7 g, 32.7 mmol) to afford ketone **91b** as a clear colorless oil (13.0 g, 90%); ^{1}H NMR (400 MHz, $CDCl_3$) δ 7.70 (dd, J = 7.9, 1.6 Hz, 4H), 7.48 – 7.36 (m, 6H), 4.89 (s, 2H), 1.11 (s, 9H);^{13}C NMR (101 MHz, $CDCl_3$) δ 195.91, 135.50, 132.49, 131.18, 129.95, 129.07, 127.81, 125.04, 77.25, 76.94, 76.62, 67.87, 26.59, 19.19.

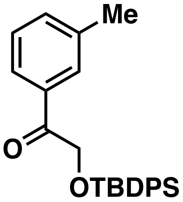

2-((*tert*-butyldiphenylsilyl)oxy)-1-(*m*-tolyl)ethan-1-one 91c: Ketone **91c** was prepared from weinreb amide **89** (7.5 g, 20.9 mmol) to afford ketone **91c** as a clear colorless oil (7.6 g, 94%); ^{1}H NMR (400 MHz, $CDCl_3$) δ 7.76 – 7.69 (m, 4H), 7.46 – 7.35 (m, 6H), 7.33 – 7.23 (m, 1H), 4.91 (s, 2H), 2.36 (s, 3H), 1.12 (s, 9H);^{13}C NMR (101 MHz, $CDCl_3$) δ 196.79, 138.23, 135.52, 133.83, 132.91, 129.77, 128.29, 127.71, 124.88, 77.25, 76.93, 76.61, 67.52, 26.63, 21.21, 19.26.

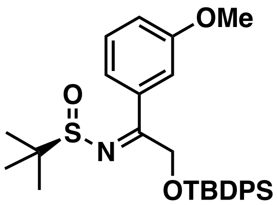

Preparation of (*R*,*E*)-*N*-(2-((*tert*-butyldiphenylsilyl)oxy)-1-(3-methoxyphenyl)ethylidene)-2-methylpropane-2-sulfinamide 92a: The aryl ketone **91a** is dissolved in toluene (200 mL) at 23 °C. The optically active (*R*)-*tert*-butylsulfonamide (4.82 g, 11.4 mmol) is added followed by the dropwise addition of Ti(OEt)$_4$ (11.9 mL, 17.0 mmol). The resulting heterogenous mixture is warmed to 90 °C and stirred for 5 h. The reaction is quenched with brine and the precipitate is filtered through a pad of celite with the aid of EtOAc. The organic layer is concentrated under reduced pressure and subjected immediately to column purification (5% EtOAc/ Hexanes) to provide imine **92a** as clear yellow oil (3.39 g, 60%); ^{1}H NMR (400 MHz, CDCl$_3$) δ 7.62 (td, *J* = 8.0, 1.4 Hz, 4H), 7.46 – 7.34 (m, 7H), 3.79 (s, 3H), 1.24 (d, *J* = 0.9 Hz, 9H), 0.98 (s, 9H); ^{13}C NMR (101 MHz, CDCl$_3$) δ 179.40, 157.88, 135.56, 132.60, 129.81, 127.70, 77.23, 77.12, 76.92, 76.60, 55.22, 26.59, 22.45, 19.12.

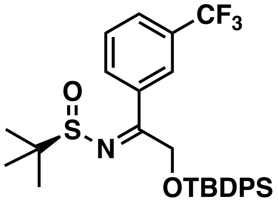

(*R*,*E*)-*N*-(2-((*tert*-butyldiphenylsilyl)oxy)-1-(3-(trifluoromethyl)phenyl)ethylidene)-2-methylpropane-2-sulfinamide 92b: Imine **92b** was prepared from ketone **91b** (4.40 g, 9.95 mmol) to afford imine **92b** as a clear yellow oil (3.9 g, 72%) ^{1}H NMR (400 MHz, CDCl$_3$) δ 7.65 – 7.49 (m, 5H), 7.47 – 7.32 (m, 7H), 1.24 (s, 9H), 0.95 (s, 9H).^{13}C NMR (101 MHz, CDCl$_3$) δ 176.23, 135.55, 135.50, 132.30, 131.69, 130.29, 129.95, 128.49, 127.81, 127.76, 127.30, 77.27, 76.95, 76.63, 61.35, 58.07, 26.53, 22.53, 19.00.

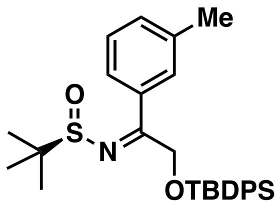

(*R*,*E*)-*N*-(2-((*tert*-butyldiphenylsilyl)oxy)-1-(*m*-tolyl)ethylidene)-2-methylpropane-2-sulfinamide 92c: Imine **92c** was prepared from ketone **91c** (7.8 g, 20.0 mmol) to afford imine **92c** as a clear orange oil (4.9 g, 50%) ^{1}H NMR (400 MHz, CDCl$_3$) δ 7.67 – 7.58 (m, 4H), 7.46 – 7.33 (m, 7H), 7.25 (d, *J* = 4.7 Hz, 2H), 2.35 (s, 3H), 1.24 (d, *J* = 2.1 Hz, 10H), 0.98 (s, 9H).^{13}C NMR (101 MHz, CDCl$_3$) δ 168.92, 137.61, 135.70, 132.75, 129.91, 127.97, 127.82, 127.79, 77.34, 77.03, 76.71, 26.68, 22.57, 21.41, 19.21.

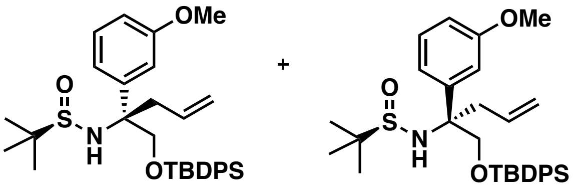

(*R*)-93a

Major

(*S*)-93a

Minor

(*R*)-*N*-((*R*)-1-((*tert*-butyldiphenylsilyl)oxy)-2-(3-methoxyphenyl)pent-4-en-2-yl)-2-methylpropane-2-sulfinamide 93a: The silyloxy ketimine **92a** is immediately diluted in CH$_2$Cl$_2$ (35 mL) and cooled to 0 °C. A mixture of allyl magnesium bromide (1.0 M in Et$_2$O, 31.5 mmol, 31.5 mL) in CH$_2$Cl$_2$ (35 mL) is treated by dropwise addition over 10 minutes of the ketimine **92a** and CH$_2$Cl$_2$ at 0 °C. The resulting mixture is stirred for 0.5 h and then quenched by saturated NH$_4$Cl. The reaction mixture is extracted with CH$_2$Cl$_2$ and the organic layer is dried with Na$_2$SO$_4$. Upon removal of the volatiles the crude is purified *via* flash column chromatography (10% EtOAc/Hexanes). *N*-sulfinyl amine **93a** was isolated as a clear colorless oil as a mixture of diastereomers (1.42 g, 96%); ^{1}H NMR (400 MHz, CDCl$_3$) δ 7.72 (ddd, *J* = 12.8, 7.8, 1.6 Hz, 5H), 7.61 – 7.52 (m, 4H), 7.48 – 7.44 (m, 2H), 7.44 – 7.38 (m, 8H), 7.36 (dd, *J* = 7.6, 1.7 Hz, 4H), 7.24 (d, *J* = 10.9 Hz, 2H), 7.17 (t, *J* = 7.9 Hz, 1H), 6.97 – 6.87 (m, 4H), 6.85 – 6.74 (m, 2H), 6.27 (s, 1H), 5.98 (s, 1H), 5.68 (ddt, *J* = 18.1, 9.6, 6.4 Hz, 1H), 4.93 – 4.83 (m, 2H), 4.24 (s, 1H), 4.15 –

4.08 (m, 1H), 3.76 (d, *J* = 6.9 Hz, 3H), 2.13 (ddd, *J* = 13.7, 11.8, 4.8 Hz, 1H), 1.97 (ddd, *J* = 13.8, 11.9, 4.8 Hz, 1H), 1.37 (s, 9H), 1.27 (s, 9H), 1.14 (s, 9H), 1.02 (s, 9H); ^{13}C NMR (101 MHz, $CDCl_3$) δ 159.55, 138.13, 135.87, 135.69, 135.57, 135.32, 130.25, 129.73, 129.42, 129.12, 128.51, 128.01, 127.70, 125.16, 119.54, 119.24, 114.50, 113.33, 112.34, 77.36, 77.04, 76.72, 68.62, 64.48, 56.32, 55.19, 27.74, 26.87, 26.58, 22.89, 22.57, 19.24; LRMS-ESI (*m/z*) $[M+H]^+$ = 550.2.

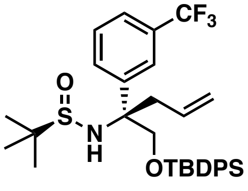

(*R*)-93b

Major

+

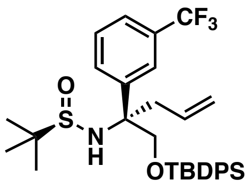

(*S*)-93b

Minor

(*R*)-*N*-((*R*)-1-((*tert*-butyldiphenylsilyl)oxy)-2-(3-(trifluoromethyl)phenyl)pent-4-en-2-yl)-2-methylpropane-2-sulfinamide 93b: *N*-Sulfinyl amine **93b** was prepared from ketimine **92b** (3.5 g, 6.41 mmol) to afford *N*-sulfinyl amine **93b** as a clear colorless oil as a mixture of diastereomers (3.33 g, 89%); ^{1}H NMR (400 MHz, $CDCl_3$) δ 7.60 – 7.30 (m, 14H), 5.45 (ddt, *J* = 17.2, 9.9, 7.2 Hz, 1H), 5.28 (d, *J* = 1.9 Hz, 1H), 5.15 – 5.01 (m, 2H), 4.22 (s, 1H), 4.19 – 4.09 (m, 2H), 4.01 (d, *J* = 10.2 Hz, 1H), 2.79 (d, *J* = 6.9 Hz, 2H), 1.26 (s, 9H), 0.99 (s, 9H); ^{13}C NMR (101 MHz, $CDCl_3$) δ 143.38, 135.61, 135.54, 132.65, 132.31, 131.79, 130.87, 129.76, 128.43, 127.67, 127.63, 124.42, 123.96, 120.88, 77.27, 76.95, 76.63, 68.70, 63.81, 60.27, 56.55, 53.31, 42.12, 26.67, 26.54, 22.74, 20.93, 19.06, 14.09.

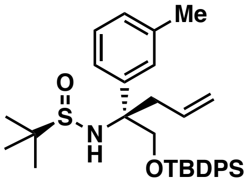

(*R*)-93c

Major

+

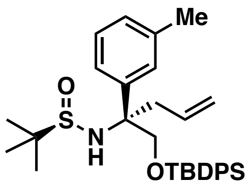

(*S*)-93c

Minor

(*R*)-*N*-((*R*)-**1-((*tert*-butyldiphenylsilyl)oxy)-2-(*m*-tolyl)pent-4-en-2-yl)-2-methylpropane-2-sulfinamide 93c**: *N*-Sulfinyl amine **93c** was prepared from ketimine **92c** (4.10 g, 8.34 mmol) to afford *N*-sulfinyl amine **93c** a clear colorless oil (4.0 g, 91%); ^{1}H NMR (400 MHz, $CDCl_3$) δ 7.61 – 7.48 (m, 5H), 7.44 – 7.31 (m, 7H), 7.24 – 7.18 (m, 3H), 5.53 – 5.40 (m, 1H), 5.07 (dd, *J* = 17.1, 2.0 Hz, 1H), 5.00 (dd, *J* = 10.2, 2.2 Hz, 1H), 4.19 (s, 1H), 4.09 (d, *J* = 10.1 Hz, 1H), 4.04 (d, *J* = 10.0 Hz, 1H), 2.79 (qd, *J* = 14.0, 7.3 Hz, 2H), 2.32 (s, 3H), 1.25 (s, 9H), 1.02 (s, 9H); ^{13}C NMR (101 MHz, $CDCl_3$) δ 137.33, 135.75, 135.64, 133.02, 132.64, 129.59, 128.13, 127.83, 127.55, 124.51, 119.98, 77.25, 76.93, 76.61, 68.66, 63.70, 56.30, 42.25, 26.74, 22.84, 21.57, 19.14.

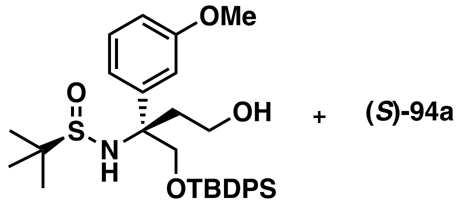

(*R*)-94a

(*R*)-*N*-((*R*)-1-((*tert*-butyldiphenylsilyl)oxy)-2-(3-methoxyphenyl)pent-4-en-2-yl)-2-methylpropane-2-sulfinamide (*R*-94a) The *N*-sulfinyl amine **(*R*)-93a** (3.09 mmol, 1.7 g)was dissolved in a 1:1 mixture of MeOH:CH_2Cl_2 (50 mL) and cooled to -78 °C. A stream of ozone was bubbled through the reaction mixture until the reaction was complete by TLC. Oxygen was bubbled into the reaction mixture to remove excess ozone. At the same temperature $NaBH_4$ (15.45 mmol, 584 mg) was added to reaction mixture portiowise and the reaction was slowly warmed to 23 °C. The reaction was quenched with water and extracted with CH_2Cl_2. The organic layer was dried with Na_2SO_4 and concentrated under reduced pressure. The resulting residue was purified by column chromatography (30% EtOAc/Hexanes). The product **(*R*)-94a** was isolated as a mixture of diastereomers as a semi-solid (1.33 g, 81%). ^{1}H NMR (500 MHz, $CDCl_3$) δ 7.45 (d, *J* = 1.3 Hz, 2H), 7.44 – 7.36 (m, 7H), 7.35 – 7.26 (m, 7H), 4.60 (s, 1H), 3.97 (dd, *J* = 10.3, 1.0 Hz, 2H), 3.91 – 3.85 (m, 2H), 3.77 (s, 3H), 2.45 (ddd, *J* = 14.6, 9.5, 4.3 Hz, 3H), 2.37 – 2.29 (m, 2H), 1.29 (s, 7H), 0.93 (s, 7H). ^{13}C NMR (126 MHz, $CDCl_3$) δ 159.65, 143.05, 129.59, 119.27, 113.73, 113.36, 112.99, 112.89, 77.38, 77.13, 76.87, 68.06, 67.06, 66.78, 55.87, 55.22, 39.77, 22.55, 22.42.

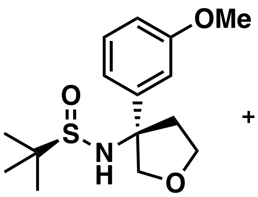

+ **(*S*)-96a**

(*R*)-96a

(*R*)-*N*-((*R*)-3-(3-methoxyphenyl)tetrahydrofuran-3-yl)-2-methylpropane-2-sulfinamide (*R*-96a) The alcohol **(*R*)-94a** (2.3 mmol, 1.3 g) was dissolved in THF (25 mL) at 23 °C. A solution of TBAF (1M in THF, 2.9 mmol, 2.9 mL) was added dropwise at 23 °C and stirred at the same temperature for 3 h. After the completion of the reaction, H_2O (50 mL) was added and EtOAc was used to extract the organic layer. The organic layer was dried by Na_2SO_4 and concentrated. The crude diol was taken to the next step without further purification. The diol was diluted in CH_2Cl_2 (5 mL) at 23 °C. The resulting mixture was treated with TsCl (3.16 mmol, 662 mg), 4-dimethylpyridine (10 mol%, 20 mg), and triethylamine (3.08 mmol, 0.44 mL) at 23 °C. The reaction mixture was allowed to stir for 12 h at 23 °C and then poured over saturated $NaHCO_3$. The organic layer was extracted by CH_2Cl_2 and dried by Na_2SO_4. The volatiles were removed and the crude was purified by flash column chromatography (2% MeOH/CH_2Cl_2). The spirocycle was isolated a mixture of diastereomers as a yellow oil (160 mg, 34% over 2 steps). ^{1}H NMR (500 MHz, $CDCl_3$) δ 7.28 – 7.22 (m, 2H), 6.99 – 6.92 (m, 3H), 6.84 – 6.78 (m, 2H), 4.22 (dd, *J* = 9.1, 1.2 Hz, 1H), 4.06 (dd, *J* = 23.4, 8.8 Hz, 3H), 3.92 (td, *J* = 8.7, 5.0 Hz, 1H), 3.77 (s, 4H), 2.55 – 2.45 (m, 2H), 2.36 (ddd, *J* = 12.9, 8.9, 7.3 Hz, 1H), 1.15 (s, 9H). ^{13}C NMR (126 MHz, $CDCl_3$) δ 159.64, 143.04, 129.59, 119.26, 113.35, 112.88, 77.38, 77.13, 76.87, 68.06, 66.78, 55.87, 55.22, 39.78, 22.55, 22.42.

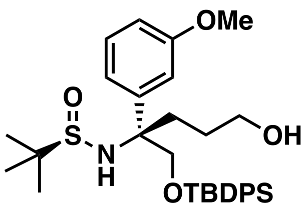

+ **(*S*)-97a**

(*R*)-97a

(*R*)-*N*-((*R*)-1-((*tert*-butyldiphenylsilyl)oxy)-5-hydroxy-2-(3-methoxyphenyl)pentan-2-yl)-2-methylpropane-2-sulfinamide (*R*-97a) In a flame-dried flask the *N*-sulfinyl amine **(*R*)-97a** was dissolved in THF (6 mL) and cooled to 0 °C. A solution of 9-BBN (0.5 in PhMe, 10.5 mmol, 21.3 mL) was added dropwise over 5 minutes at 0 °C. The reaction mixture was slowly warmed to room temperature and stirred for 15 h. The heterogenous mixture was cooled to 0 °C and aqueous 6M NaOH (10 mL) and H_2O_2 (30% w/w, 8.2 mL) was added in a subsequent manner. The resulting mixture was allowed to warm up to 23 °C and stirred for an additional 12 h. Upon completion EtOAc was added and the organic layer was washed with brine. The organic layer was dried with Na_2SO_4 and concentrated. The crude material was purified by column chromatography (50% EtOAc/Hexanes). The product was isolated as a mixture of diastereomers as a clear colorless oil (2.0 g, 99%). ^{1}H NMR (400 MHz, $CDCl_3$) δ 7.51 – 7.28 (m, 12H), 6.96 – 6.89 (m, 2H), 4.18 – 4.07 (m, 3H), 4.00 – 3.87 (m, 2H), 3.81 (d, *J* = 4.9 Hz, 2H), 3.77 (s, 4H), 1.92 – 1.84 (m, 8H), 1.66 – 1.56 (m, 7H), 1.28 (s, 11H), 0.97 (s, 9H). ^{13}C NMR (101 MHz, $CDCl_3$) δ 135.65, 135.51, 129.58, 127.54, 77.23, 77.12, 76.91, 76.59, 71.69, 36.27, 26.69, 22.78, 19.92, 14.10.

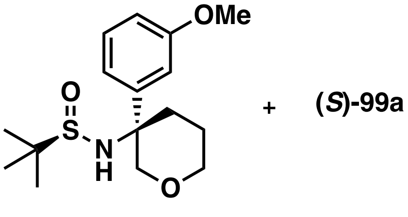

(*R*)-99a

(*R*)-*N*-((*R*)-3-(3-methoxyphenyl)tetrahydro-2*H*-pyran-3-yl)-2-methylpropane-2-sulfinamide (*R*-99a) Identical conditions to prepare the spirocycle **(*R*)-96a** were used to furnish the desired spirocyclic (245 mg, 79% over 2 steps). ^{1}H NMR (500 MHz, $CDCl_3$) δ 7.68 (dd, *J* = 8.1, 5.1 Hz, 3H), 7.32 – 7.19 (m, 5H), 6.90 – 6.83 (m, 2H), 6.83 – 6.75 (m, 3H), 4.14 – 4.06 (m, 1H), 3.95 – 3.85 (m, 4H), 3.76 (s, 5H), 2.41 (d, *J* = 3.2 Hz, 5H), 1.87 – 1.75 (m, 2H), 1.28 (s, 9H).^{13}C NMR (126 MHz, $CDCl_3$) δ 159.82, 159.56, 144.79, 143.35, 142.18, 132.91, 132.85, 129.84, 129.80, 129.41, 127.81, 118.95, 118.09, 113.24, 112.67, 112.41, 112.12, 77.39, 77.13, 76.88, 70.25, 68.81, 66.24, 65.10, 64.13, 60.35, 56.69, 56.46, 55.19, 55.16, 36.65, 31.89, 23.49, 23.23, 22.83, 22.66, 21.61, 14.19.

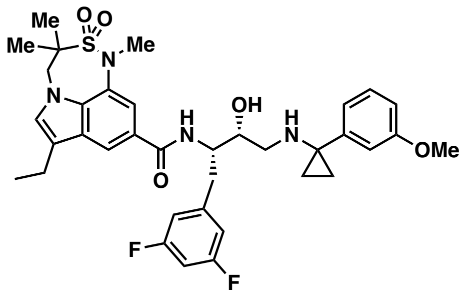

Preparation of BACE1 inhibitor *N*-((2*S*,3*R*)-1-(3,5-difluorophenyl)-3-hydroxy-4-((1-(3methoxyphenyl)cyclopropyl) amino)butan-2-yl)-7-ethyl-1,3,3-trimethyl-3,4-dihydro-1*H*-[1,2,5]thiadiazepino[3,4,5-*hi*] indole-9-carboxamide 2,2-dioxide 111a: In a dry, clean 2-neck round bottom flask the 7,6,5-tricyclic indole **105** (16 mg, 0.44 mmol) was dissolved in CH_2Cl_2 (5 mL) at 23 °C. The resulting mixture is treated with triethylamine (0.03 mL, 0.25 mmol) and HATU (24 mg, 0.064 mmol) and stirred for 1 h at 23 °C. Amine **77a** (18 mg, 0.049 mmol) was added as a solution in CH_2Cl_2 dropwise over 1 h at 23 °C. The reaction mixture was stirred for an additional 36 h at 23 °C. The mixture was poured over a saturated solution of $NaHCO_3$ and extracted with CH_2Cl_2 The organic layer was dried with Na_2SO_4 and purified by flash chromatography (1% MeOH/CH_2Cl_2). Inhibitor **111a** was isolated as a white solid (11.23 mg, 37%); ^{1}H NMR (500 MHz, $CDCl_3$) δ 7.61 (d, *J* = 1.5 Hz, 1H), 7.30 (d, *J* = 1.5 Hz, 1H), 7.18 (d, *J* = 8.1 Hz, 1H), 6.92 – 6.86 (m, 2H), 6.84 – 6.78 (m, 4H), 6.73 (ddd, *J* = 8.2, 2.5, 1.0 Hz, 2H), 6.67 – 6.61 (m, 2H), 6.52 (d, *J* = 9.0 Hz, 1H), 4.11 (d, *J* = 1.1 Hz, 2H), 3.76 (s, 3H), 3.51 (s, 4H), 3.06 (dd, *J* = 14.2, 5.0 Hz, 2H), 2.94 (dd, *J* = 14.3, 8.1 Hz, 2H), 2.77 – 2.68 (m, 5H), 1.56 (s, 6H), 1.29 (d, *J* = 7.5 Hz, 3H), 1.03 (dd, *J* = 11.9, 7.6 Hz, 2H), 0.93 (td, *J* = 5.9, 3.1 Hz, 2H); LRMS-ESI (*m/z*) $[M+H]^+$ = 681.2.

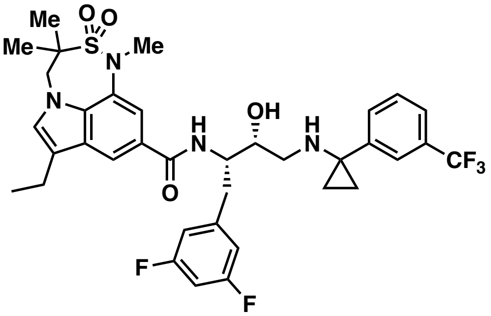

***N*-((2*S*,3*R*)-1-(3,5-difluorophenyl)-3-hydroxy-4-((1-(3-(trifluoromethyl)phenyl) cyclopropyl) amino)butan-2-yl)-7-ethyl-1,3,3-trimethyl-3,4-dihydro-1*H*-[1,2,5]thiadiazepino[3,4,5-*hi*] indole-9-carboxamide 2,2-dioxide 111b**: Inhibitor **111b** was prepared from acid **105** (13 mg, 0.40

mmol) and amine **77b** (18 mg, 0.044 mmol) to afford inhibitor **111b** as a white solid (14.8 mg, 52%); ^{1}H NMR (500 MHz, $CDCl_3$) δ 7.62 (d, *J* = 1.5 Hz, 1H), 7.55 – 7.49 (m, 2H), 7.43 – 7.36 (m, 2H), 7.29 (s, 1H), 6.84 – 6.78 (m, 3H), 6.64 (t, *J* = 2.4 Hz, 1H), 6.49 (d, *J* = 8.9 Hz, 1H), 4.15 – 4.07 (m, 6H), 3.09 (dd, *J* = 14.2, 4.8 Hz, 2H), 2.98 – 2.90 (m, 2H), 2.75 – 2.67 (m, 4H), 2.66 (d, *J* = 8.7 Hz, 1H), 1.55 (d, *J* = 2.2 Hz, 6H), 1.29 (t, *J* = 7.5 Hz, 6H), 1.08 – 1.02 (m, 3H), 0.94 (dt, *J* = 6.5, 4.1 Hz, 2H); LRMS-ESI (*m/z*) $[M+H]^+$ = 719.2.

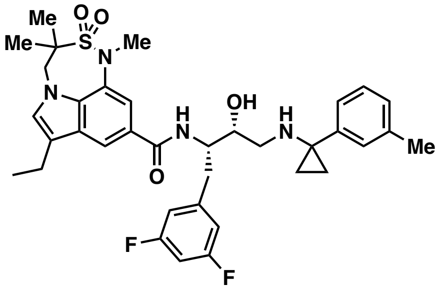

***N*-((2*S*,3*R*)-1-(3,5-difluorophenyl)-3-hydroxy-4-((1-(*m*-tolyl)cyclopropyl)amino)butan-2-yl)-7-ethyl-1,3,3-trimethyl-3,4-dihydro-1*H*-[1,2,5]thiadiazepino[3,4,5-*hi*]indole-9-carboxamide 2,2-dioxide 111c**: Inhibitor **111c** was prepared from acid **105** (22 mg, 0.065 mmol) and amine **77c** (25 mg, 0.072 mmol) to afford inhibitor **111c** as a white solid (19 mg, 40%); ^{1}H NMR (500 MHz, $CDCl_3$) δ 7.68 (dd, *J* = 8.1, 5.1 Hz, 3H), 7.32 – 7.19 (m, 5H), 6.90 – 6.83 (m, 2H), 6.83 – 6.75 (m, 3H), 4.14 – 4.06 (m, 1H), 3.95 – 3.85 (m, 4H), 3.76 (s, 5H), 2.41 (d, *J* = 3.2 Hz, 5H), 1.87 – 1.75 (m, 2H), 1.28 (m, 9H).

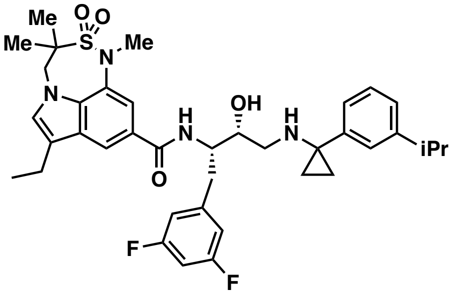

***N*-((2*S*,3*R*)-1-(3,5-difluorophenyl)-3-hydroxy-4-((1-(3-isopropylphenyl)cyclopropyl)amino) butan-2-yl)-7-ethyl-1,3,3-trimethyl-3,4-dihydro-1*H*-[1,2,5]thiadiazepino[3,4,5-*hi*]indole-9-carboxamide 2,2-dioxide 111d**: Inhibitor **111d** was prepared from acid **105** (10 mg, 0.030 mmol) and amine **77d** (11 mg, 0.031 mmol) to afford inhibitor **111d** as a white solid (6.2 mg, 38%); ^{1}H NMR (500 MHz, $CDCl_3$) δ 7.65 (s, 1H), 7.23 – 7.15 (m, 3H), 7.14 – 7.09 (m, 2H), 7.05 (d, *J* = 7.7 Hz, 2H), 6.81 (d, *J* = 4.6 Hz, 3H), 6.66 – 6.57 (m, 3H), 4.11 (s, 2H), 3.50 (s, 3H), 3.06 – 2.92 (m, 4H), 2.73 (dt, *J* = 15.1, 6.9 Hz, 5H), 1.56 (d, *J* = 3.0 Hz, 5H), 1.30 (t, *J* = 7.5 Hz, 4H), 1.18 (dd, *J* = 6.9, 5.0 Hz, 6H), 1.04 (s, 1H), 1.02 (d, *J* = 6.9 Hz, 2H), 0.98 – 0.91 (m, 2H).

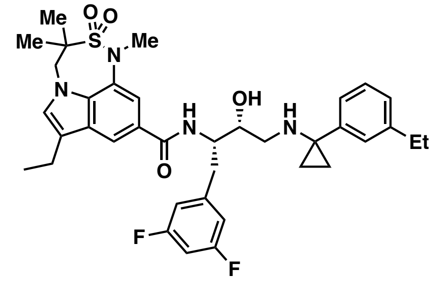

***N*-((2*S*,3*R*)-1-(3,5-difluorophenyl)-4-((1-(3-ethylphenyl)cyclopropyl)amino)-3-hydroxy butan-2-yl)-7-ethyl-1,3,3-trimethyl-3,4-dihydro-1*H*-[1,2,5]thiadiazepino[3,4,5-*hi*]indole-9-carboxamide 2,2-dioxide 111e**: Inhibitor **111e** was prepared from acid **105** (29 mg, 0.086 mmol) and amine **77e** (32 mg, 0.088 mmol) to afford inhibitor **111e** as a white solid (29.3 mg, 49%); ^{1}H NMR (500 MHz, CDCl$_3$) δ 7.66 (d, *J* = 1.5 Hz, 1H), 7.31 (d, *J* = 1.5 Hz, 1H), 7.20 (t, *J* = 7.5 Hz, 1H), 7.17 – 7.11 (m, 2H), 7.03 (dt, *J* = 7.5, 1.5 Hz, 1H), 6.84 – 6.74 (m, 4H), 6.65 – 6.58 (m, 1H), 4.11 (s, 2H), 3.49 (s, 3H), 2.99 (dd, *J* = 14.2, 5.0 Hz, 1H), 2.88 (dd, *J* = 14.2, 8.5 Hz, 1H), 2.78 – 2.67 (m, 4H), 2.58 (q, *J* = 7.6 Hz, 2H), 1.55 (s, 6H), 1.29 (t, *J* = 7.5 Hz, 3H), 1.17 (t, *J* = 7.6 Hz, 3H), 1.07 – 0.99 (m, 3H), 0.98 – 0.91 (m, 1H); LRMS-ESI (*m/z*) [M+H]$^+$ = 680.1.

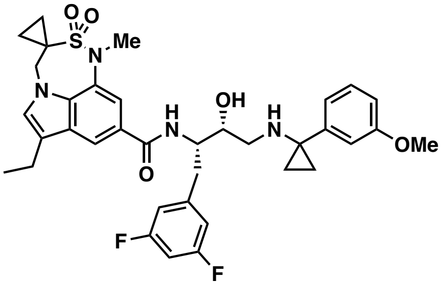

***N*-((2*S*,3*R*)-1-(3,5-difluorophenyl)-3-hydroxy-4-((1-(3-methoxyphenyl)cyclopropyl)amino) butan-2-yl)-7'-ethyl-1'-methyl-1'*H*,4'*H*-spiro[cyclopropane-1,3'-[1,2,5]thiadiazepino [3,4,5-*hi*]indole]-9'-carboxamide 2',2'-dioxide 112a**: Inhibitor **112a** was prepaed from acid **110** (15 mg, 0.042 mmol) and amine **77a** (17 mg, 0.047 mmol) to afford inhibitor **112a** as white solid (10.9 mg, 38%); ^{1}H NMR (500 MHz, CDCl$_3$) δ 7.75 (d, *J* = 1.5 Hz, 1H), 7.37 (d, *J* = 1.5 Hz, 1H), 7.20 (t, *J* = 8.1 Hz, 1H), 6.94 – 6.89 (m, 2H), 6.84 – 6.71 (m, 6H), 6.65 – 6.57 (m, 2H), 4.27 (s, 2H), 3.75

(s, 3H), 3.43 (s, 3H), 3.16 (q, *J* = 7.3 Hz, 2H), 3.05 (dd, *J* = 14.2, 4.7 Hz, 2H), 2.92 – 2.82 (m, 2H), 2.82 – 2.72 (m, 5H), 2.70 (dd, *J* = 7.5, 1.0 Hz, 1H), 1.31 (t, *J* = 7.3 Hz, 3H), 1.13 – 1.03 (m, 4H), 1.03 – 0.95 (m, 4H); LRMS-ESI (*m/z*) $[M+H]^+$ = 679.2.

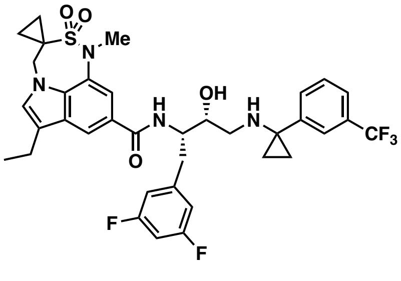

***N*-((2*S*,3*R*)-1-(3,5-difluorophenyl)-3-hydroxy-4-((1-(3-(trifluoromethyl)phenyl)cyclopropyl) amino)butan-2-yl)-7'-ethyl-1'-methyl-1'*H*,4'*H*-spiro[cyclopropane-1,3'-[1,2,5]thiadiazepino [3,4,5-*hi*]indole]-9'-carboxamide 2',2'-dioxide 112b**: Inhibitor **112b** was prepared from acid **110** (13.2 mg, 0.040 mmol) and amine **77b** (18 mg, 0.044 mmol) to afford inhibitor **112b** as a white solid (12.2 mg, 43%); ^{1}H NMR (500 MHz, $CDCl_3$) δ 7.76 (d, *J* = 1.5 Hz, 1H), 7.52 (d, *J* = 7.5 Hz, 2H), 7.43 – 7.38 (m, 2H), 7.35 (s, 1H), 6.84 – 6.81 (m, 1H), 6.79 (d, *J* = 14.5 Hz, 2H), 6.68 – 6.62 (m, 1H), 6.47 (d, *J* = 8.9 Hz, 1H), 4.28 (d, *J* = 4.8 Hz, 2H), 3.43 (s, 2H), 3.10 (dd, *J* = 14.2, 4.9 Hz, 1H), 2.95 (dd, *J* = 14.5, 8.5 Hz, 1H), 2.77 – 2.62 (m, 5H), 1.33 – 1.31 (m, 1H), 1.29 (t, *J* = 7.5 Hz, 2H), 1.25 (s, 2H), 1.13 (td, *J* = 10.0, 6.2 Hz, 2H), 1.09 – 0.91 (m, 6H); LRMS-ESI (*m/z*) $[M+H]^+$ = 717.2.

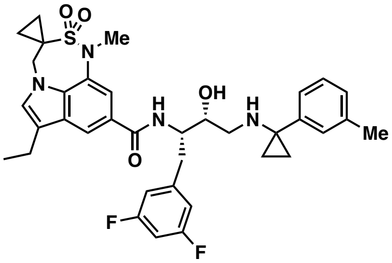

***N*-((2*S*,3*R*)-1-(3,5-difluorophenyl)-3-hydroxy-4-((1-(*m*-tolyl)cyclopropyl)amino)butan-2-yl)-7'-ethyl-1'-methyl-1'*H*,4'*H*-spiro[cyclopropane-1,3'-[1,2,5]thiadiazepino[3,4,5-*hi*]indole]-9'-carboxamide 2',2'-dioxide 112c**: Inhibitor **112c** was prepared from acid **110** (22 mg, 0.065 mmol) and amine **77c** (25 mg, 0.072 mmol) to afford inhibitor **112c** as a white solid (19 mg, 45%); ^{1}H

NMR (400 MHz, $CDCl_3$) δ 7.69 (s, 2H), 7.52 (s, 1H), 6.99 (s, 1H), 6.86 (d, *J* = 6.9 Hz, 3H), 6.80 (s, 3H), 6.67 (t, *J* = 9.0 Hz, 3H), 4.29 (s, 2H), 3.55 (s, 3H), 3.04 (s, 4H), 2.75 (s, 2H), 2.73 (s, 1H), 2.30 (s, 3H), 1.31 (m, 6H), 0.84 (m, 4H).

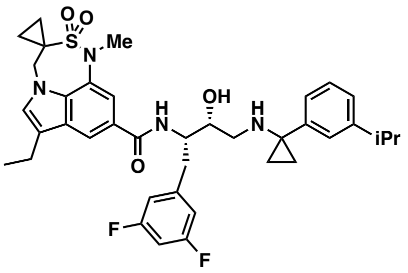

***N*-((2*S*,3*R*)-1-(3,5-difluorophenyl)-3-hydroxy-4-((1-(3-isopropylphenyl)cyclopropyl)amino)butan-2-yl)-7'-ethyl-1'-methyl-1'*H*,4'*H*-spiro[cyclopropane-1,3'-[1,2,5]thiadiazepino[3,4,5-*hi*]indole]-9'-carboxamide 2',2'-dioxide 112d**: Inhibitor **112d** was prepared from acid **110** (7.9 mg, 0.023 mmol) and amine **77d** (9.0 mg, 0.024 mmol) to afford inhibitor **112d** as a white solid (8.4 mg, 40%); ^{1}H NMR (500 MHz, $CDCl_3$) δ 7.79 (s, 1H), 7.38 (s, 1H), 7.22 – 7.14 (m, 2H), 7.08 – 7.02 (m, 1H), 6.85 – 6.76 (m, 3H), 6.68 – 6.61 (m, 2H), 4.28 (d, *J* = 11.8 Hz, 2H), 3.44 (s, 2H), 3.07 – 2.91 (m, 3H), 2.79 (s, 7H), 2.74 (ddd, *J* = 11.7, 6.0, 2.1 Hz, 4H), 1.31 – 1.23 (m, 4H), 1.19 – 1.14 (m, 4H), 1.04 – 0.98 (m, 4H), 0.97 – 0.87 (m, 3H).

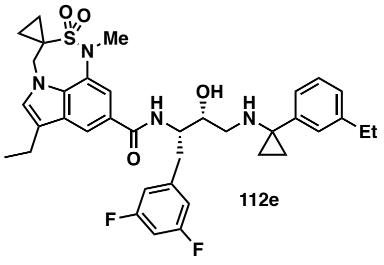

112e

***N*-((2*S*,3*R*)-1-(3,5-difluorophenyl)-4-((1-(3-ethylphenyl)cyclopropyl)amino)-3-hydroxybutan-2-yl)-7'-ethyl-1'-methyl-1'*H*,4'*H*-spiro[cyclopropane-1,3'-[1,2,5]thiadiazepino[3,4,5-*hi*]indole]-9'-carboxamide 2',2'-dioxide 112e**: Inhibitor **112e** was prepared from acid **110** (18 mg, 0.054 mmol) and amine **77e** (20 mg, 0.055 mmol) to afford inhibitor **112e** as a white solid (17.3 mg, 47%); ^{1}H NMR (500 MHz, $CDCl_3$) δ 7.79 (d, *J* = 1.5 Hz, 1H), 7.38 (d, *J* = 1.5 Hz, 1H), 7.20 (t, *J* = 7.5 Hz, 1H), 7.17 – 7.10 (m, 2H), 7.02 (d, *J* = 7.5 Hz, 1H), 6.82 – 6.75 (m, 3H), 6.72 (d, *J*

= 8.9 Hz, 1H), 6.67 – 6.59 (m, 1H), 4.28 (d, J = 5.9 Hz, 2H), 3.56 (dt, J = 6.7, 4.4 Hz, 1H), 3.02 (dd, J = 14.2, 5.1 Hz, 1H), 2.93 (dd, J = 14.2, 8.2 Hz, 1H), 2.78 – 2.69 (m, 4H), 2.58 (q, J = 7.6 Hz, 2H), 1.29 (t, J = 7.5 Hz, 5H), 1.17 (t, J = 7.6 Hz, 3H), 1.06 – 0.91 (m, 6H).

APPENDIX A. NMR SPECTRA

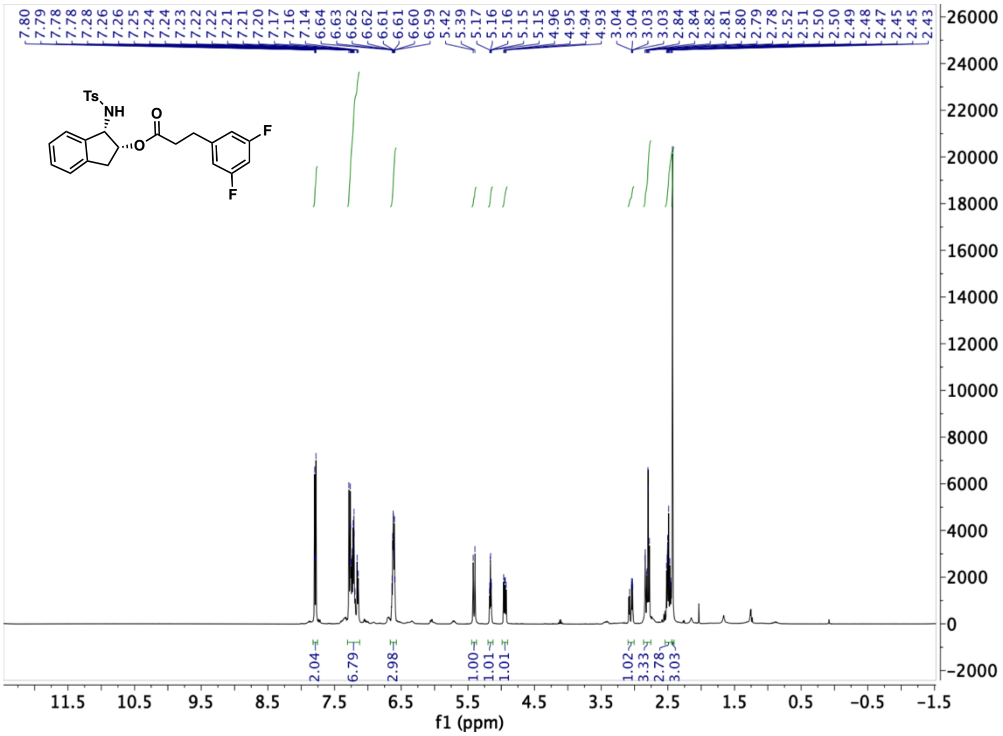

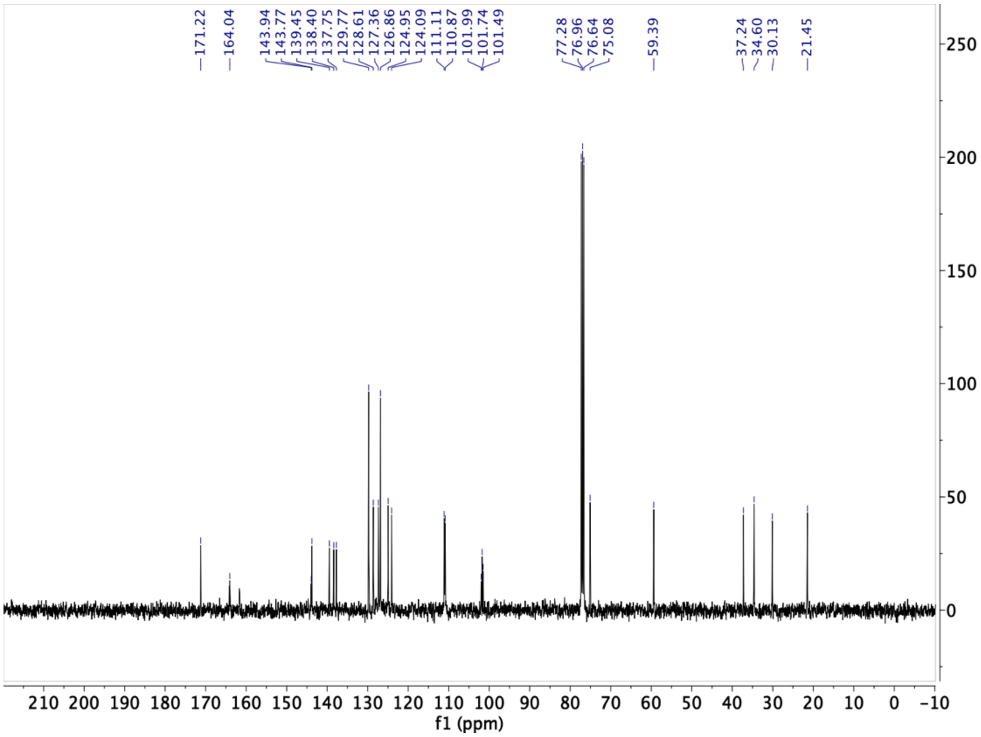

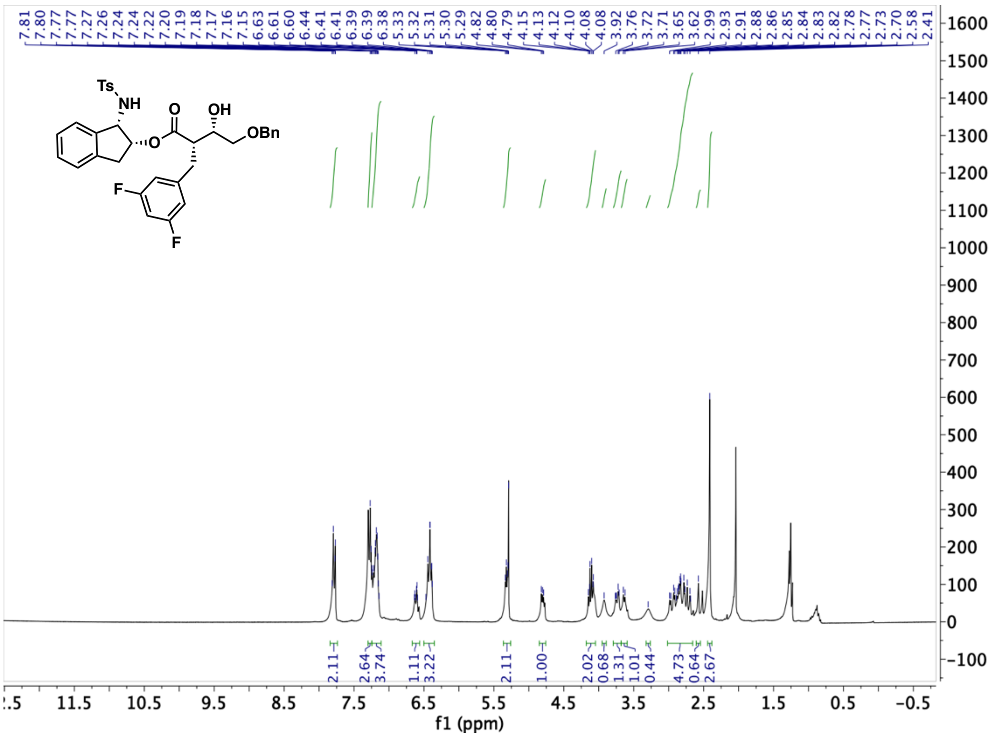
7.81
7.80
7.77
7.77
7.26
7.24
7.24
7.22
7.20
7.19
7.18
7.17
7.16
7.15
6.63
6.61
6.60
6.44
6.41
6.41
6.39
6.39
6.38
5.33
5.32
5.31
5.30
5.29
4.82
4.80
4.79
4.15
4.13
4.12
4.10
4.08
4.08
3.92
3.76
3.72
3.71
3.65
3.62
2.99
2.93
2.91
2.88
2.86
2.85
2.84
2.83
2.82
2.78
2.77
2.73
2.70
2.58
2.41
Ts
NH
O
OH
O
OBn
F
F
2.11
2.64
3.74
1.11
3.22
2.11
1.00
2.02
0.68
1.31
1.01
0.44
4.73
0.64
2.67
1600
1500
1400
1300
1200
1100
1000
900
800
700
600
500
400
300
200
100
0
−100
.5
11.5
10.5
9.5
8.5
7.5
6.5
5.5
4.5
3.5
2.5
1.5
0.5
−0.5
f1 (ppm)

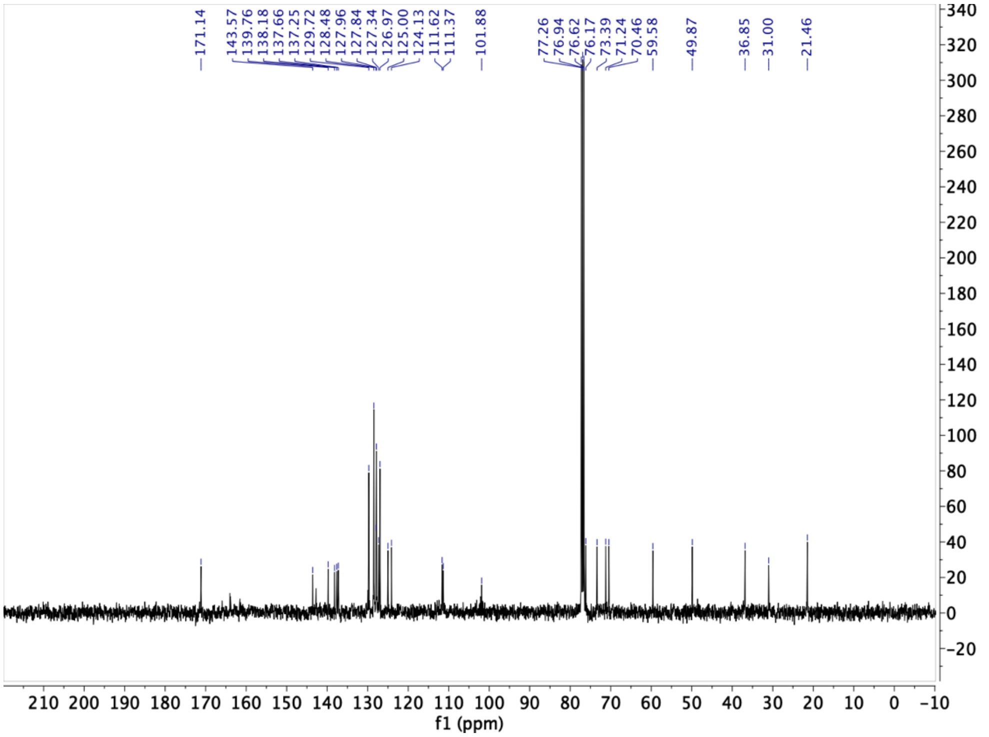
171.14
143.57
139.76
138.18
137.66
137.25
129.72
128.48
127.96
127.84
127.34
126.97
125.00
124.13
111.62
111.37
101.88
77.26
76.94
76.62
76.17
73.39
71.24
70.46
59.58
49.87
36.85
31.00
21.46
340
320
300
280
260
240
220
200
180
160
140
120
100
80
60
40
20
0
−20
210
200
190
180
170
160
150
140
130
120
110
100
90
80
70
60
50
40
30
20
10
0
−10
f1 (ppm)

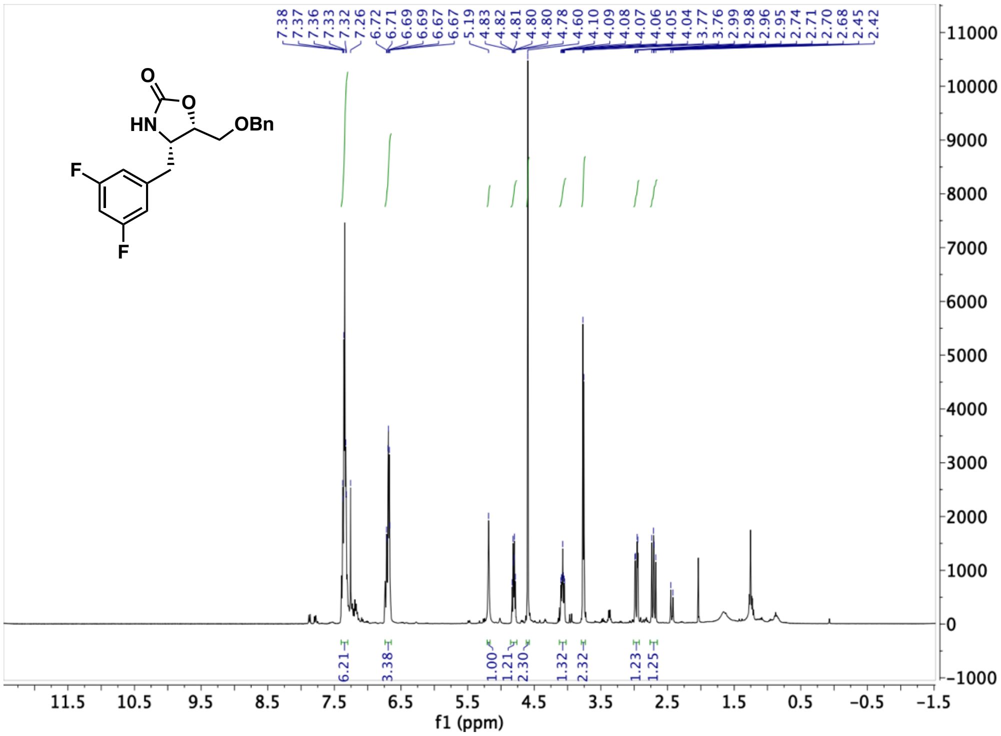
7.38
7.37
7.36
7.33
7.32
7.26
6.72
6.71
6.69
6.69
6.67
6.67
5.19
4.83
4.82
4.81
4.80
4.80
4.78
4.60
4.10
4.09
4.08
4.07
4.06
4.05
4.04
3.77
3.76
2.99
2.98
2.96
2.95
2.74
2.71
2.70
2.68
2.45
2.42
O
O
HN
OBn
F
F
6.21
3.38
1.00
1.21
2.30
1.32
2.32
1.23
1.25
11000
10000
9000
8000
7000
6000
5000
4000
3000
2000
1000
0
−1000
11.5
10.5
9.5
8.5
7.5
6.5
5.5
4.5
3.5
2.5
1.5
0.5
−0.5
−1.5
f1 (ppm)

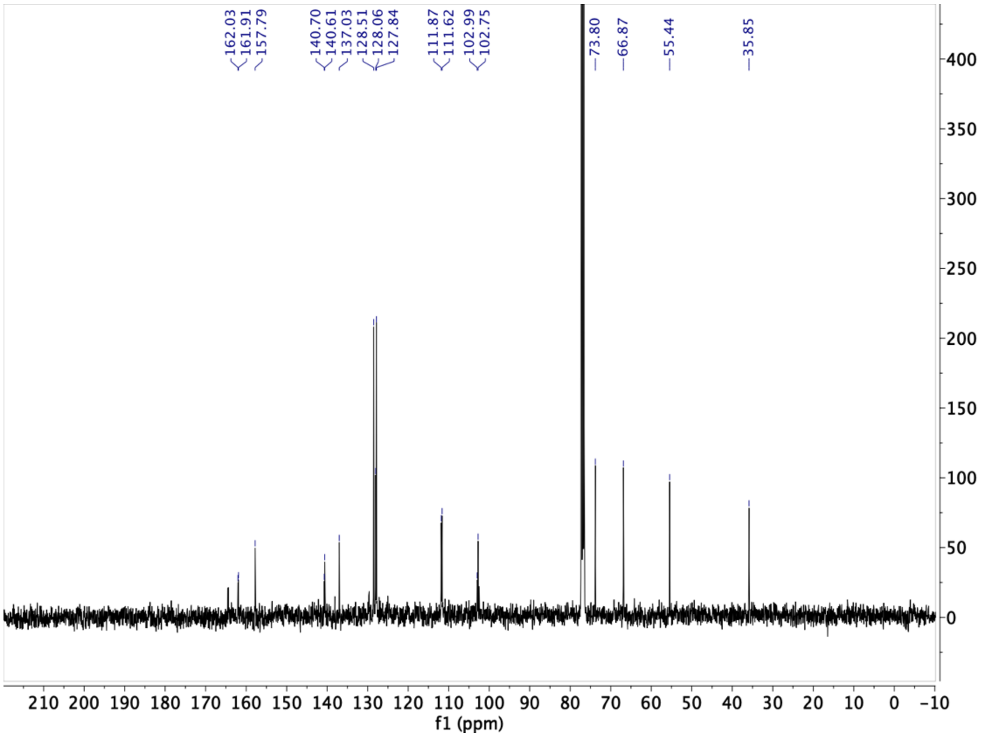
162.03
161.91
157.79
140.70
140.61
137.03
128.51
128.06
127.84
111.87
111.62
102.99
102.75
73.80
66.87
55.44
35.85
400
350
300
250
200
150
100
50
0
210
200
190
180
170
160
150
140
130
120
110
100
90
80
70
60
50
40
30
20
10
0
−10
f1 (ppm)

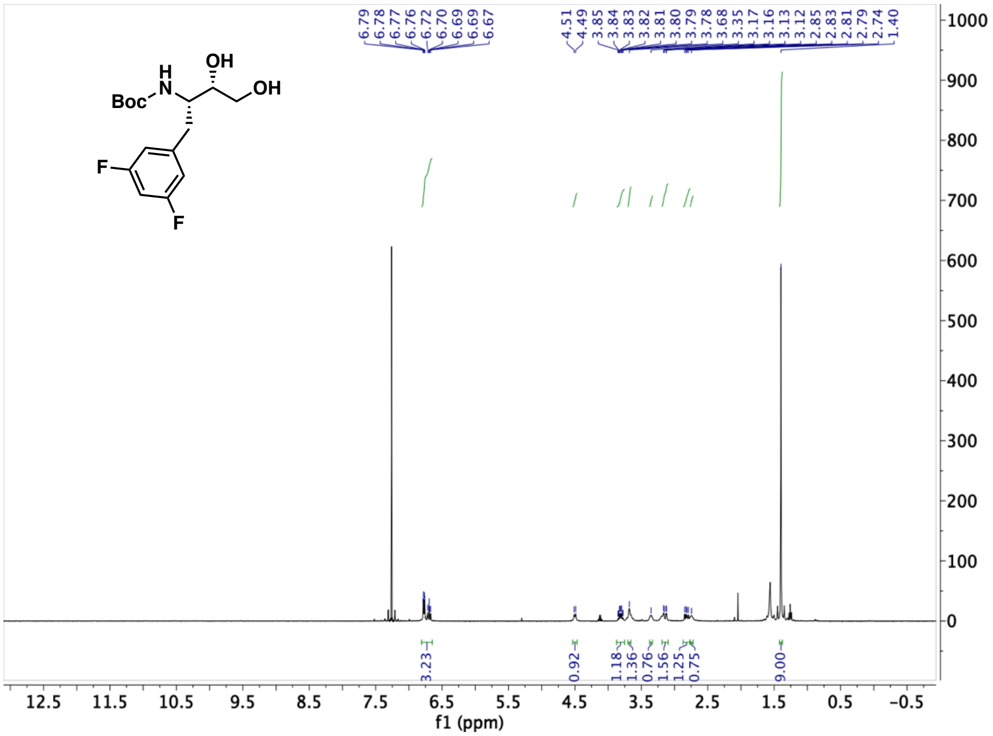
6.79
6.78
6.77
6.76
6.72
6.70
6.69
6.69
6.67
4.51
4.49
3.85
3.84
3.83
3.82
3.81
3.80
3.79
3.78
3.68
3.35
3.17
3.16
3.13
3.12
2.85
2.83
2.81
2.79
2.74
1.40
OH
H
Boc
N
OH
F
F
3.23
0.92
1.18
1.36
0.76
1.56
1.25
0.75
9.00
12.5
11.5
10.5
9.5
8.5
7.5
6.5
5.5
4.5
3.5
2.5
1.5
0.5
-0.5
f1 (ppm)
1000
900
800
700
600
500
400
300
200
100
0

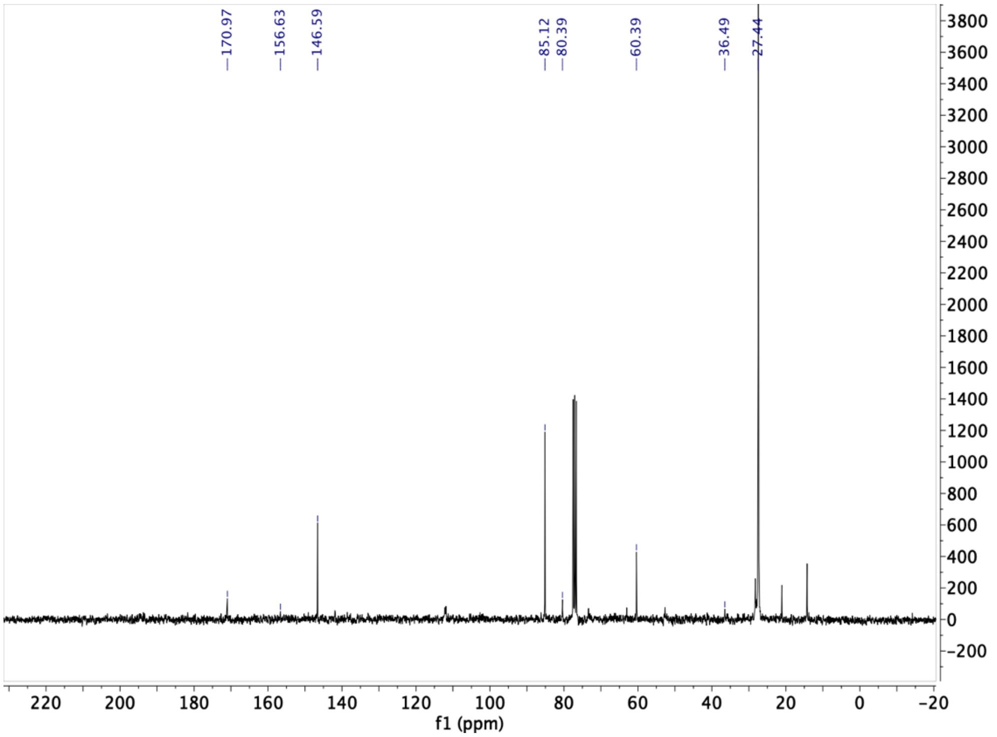
170.97
156.63
146.59
85.12
80.39
60.39
36.49
27.44
220
200
180
160
140
120
100
80
60
40
20
0
-20
f1 (ppm)
3800
3600
3400
3200
3000
2800
2600
2400
2200
2000
1800
1600
1400
1200
1000
800
600
400
200
0
-200

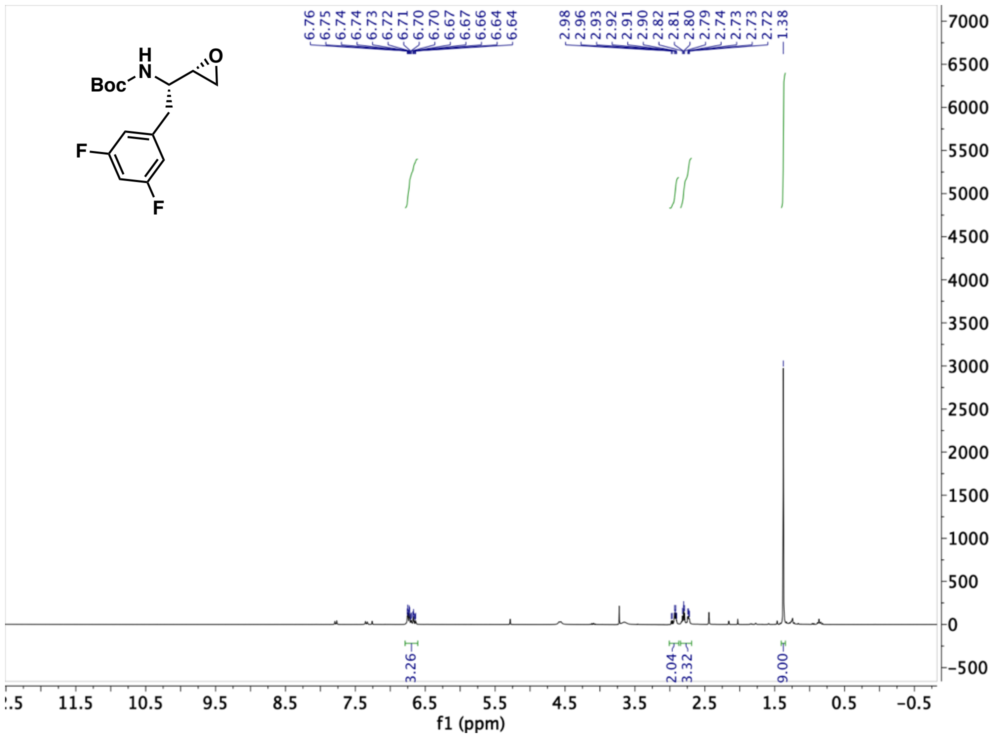
6.76
6.75
6.74
6.74
6.73
6.72
6.71
6.70
6.70
6.67
6.67
6.66
6.64
6.64
2.98
2.96
2.93
2.92
2.91
2.90
2.82
2.81
2.80
2.79
2.74
2.73
2.73
2.72
1.38
H
N
Boc
O
F
F
3.26
2.04
3.32
9.00
7000
6500
6000
5500
5000
4500
4000
3500
3000
2500
2000
1500
1000
500
0
-500
11.5
10.5
9.5
8.5
7.5
6.5
5.5
4.5
3.5
2.5
1.5
0.5
-0.5
f1 (ppm)

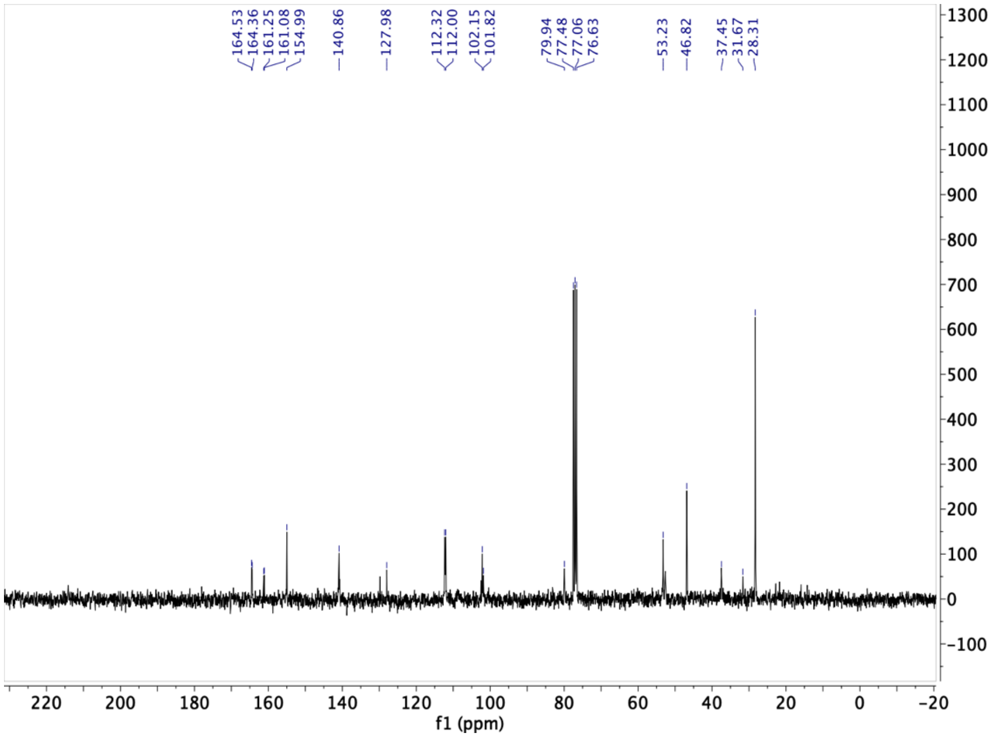
164.53
164.36
161.25
161.08
154.99
140.86
127.98
112.32
112.00
102.15
101.82
79.94
77.48
77.06
76.63
53.23
46.82
37.45
31.67
28.31
1300
1200
1100
1000
900
800
700
600
500
400
300
200
100
0
-100
220
200
180
160
140
120
100
80
60
40
20
0
-20
f1 (ppm)

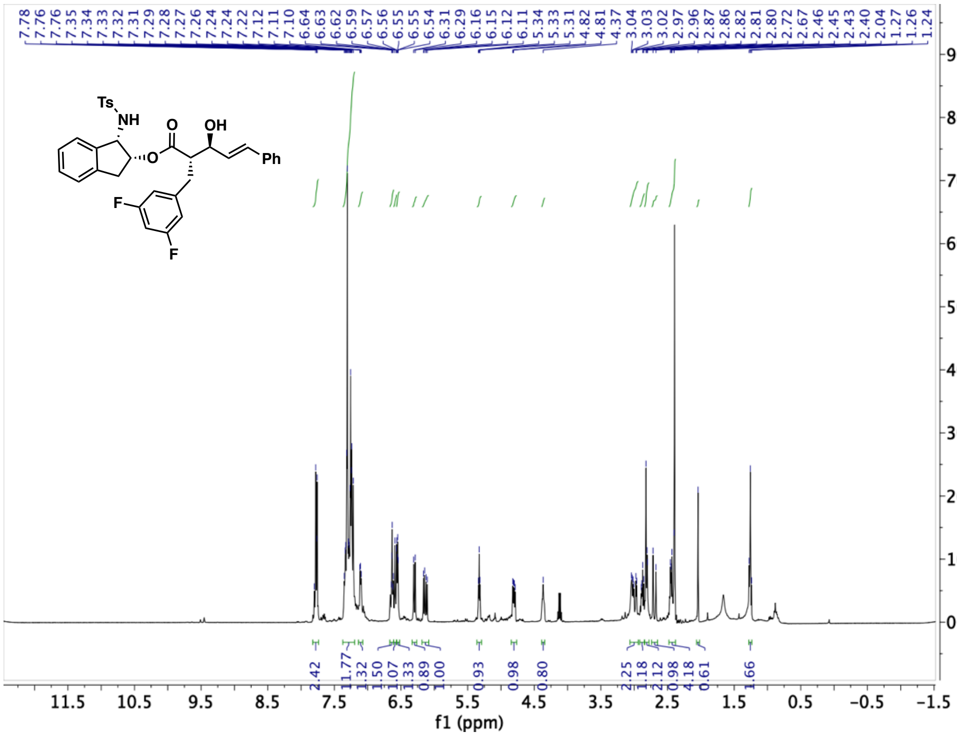
7.78
7.76
7.35
7.34
7.33
7.32
7.31
7.29
7.28
7.27
7.26
7.24
7.24
7.22
7.12
7.11
7.10
6.64
6.63
6.62
6.59
6.57
6.56
6.55
6.55
6.54
6.31
6.29
6.16
6.15
6.12
6.11
5.34
5.33
5.31
4.82
4.81
4.37
3.04
3.03
3.02
2.97
2.96
2.87
2.86
2.82
2.81
2.80
2.72
2.67
2.46
2.45
2.43
2.40
2.04
1.27
1.26
1.24
Ts
NH
O
OH
O
Ph
F
F
2.42
11.77
1.32
1.50
1.07
1.33
0.89
1.00
0.93
0.98
0.80
2.25
1.18
2.12
0.98
4.18
0.61
1.66
9000
8000
7000
6000
5000
4000
3000
2000
1000
0
11.5
10.5
9.5
8.5
7.5
6.5
5.5
4.5
3.5
2.5
1.5
0.5
-0.5
-1.5
f1 (ppm)

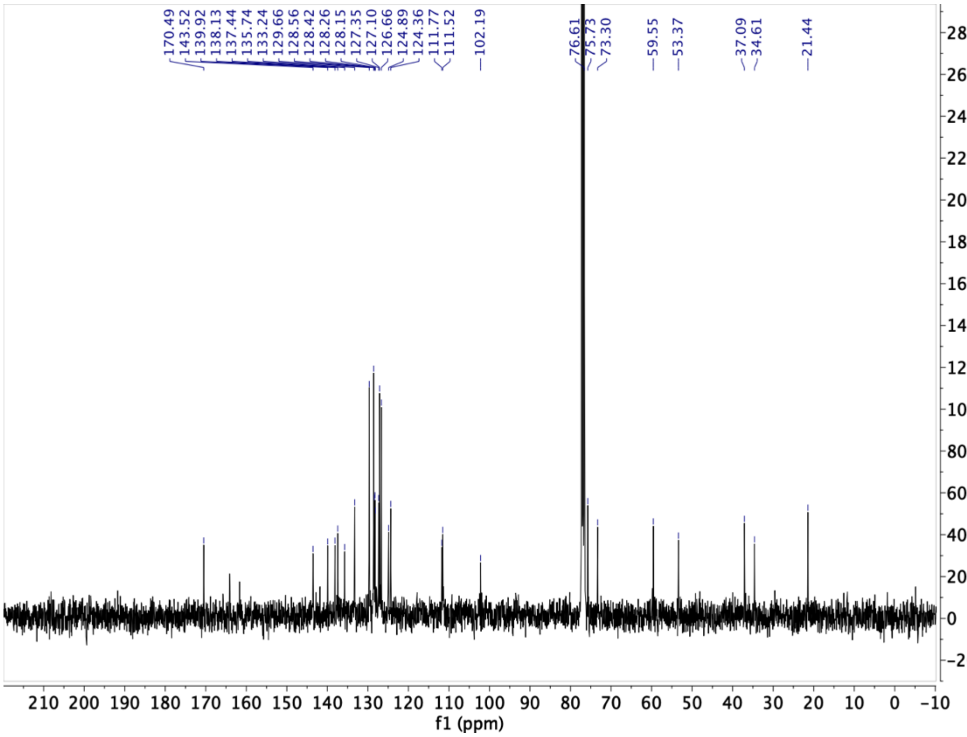
170.49
143.52
139.92
138.13
137.44
135.74
133.24
129.66
128.56
128.42
128.26
128.15
127.35
127.10
126.66
124.89
124.36
111.77
111.52
102.19
76.61
75.73
73.30
59.55
53.37
37.09
34.61
21.44
280
260
240
220
200
180
160
140
120
100
80
60
40
20
0
-20
210
200
190
180
170
160
150
140
130
120
110
100
90
80
70
60
50
40
30
20
10
0
-10
f1 (ppm)

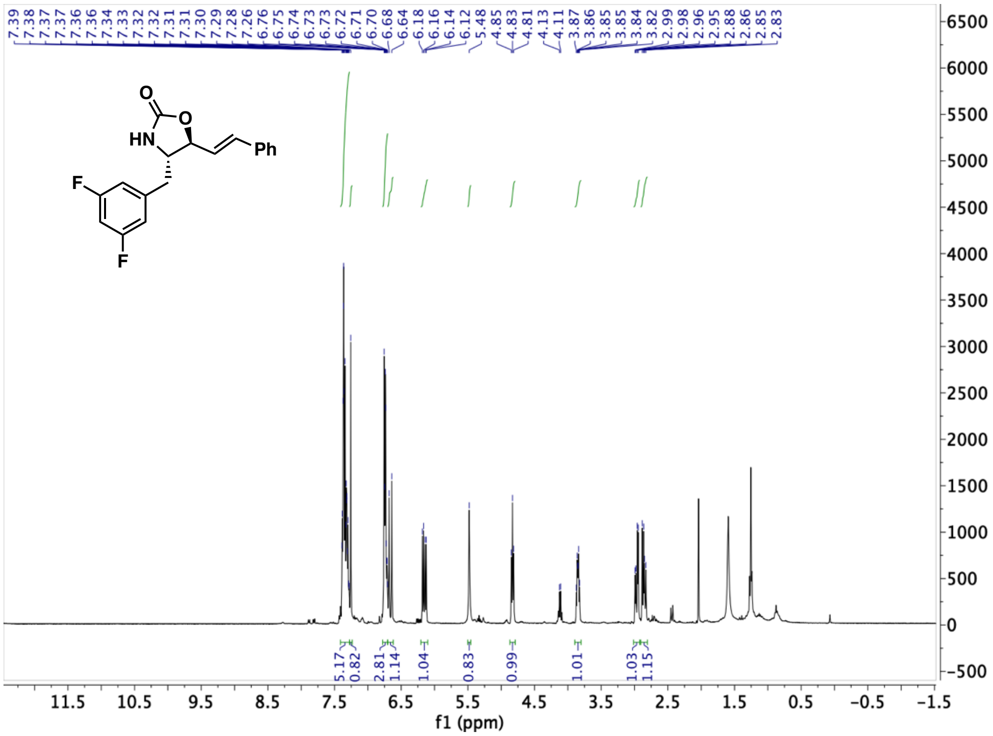
7.39
7.38
7.37
7.37
7.36
7.36
7.34
7.33
7.32
7.32
7.31
7.31
7.30
7.29
7.28
7.26
6.76
6.75
6.74
6.73
6.73
6.72
6.71
6.70
6.68
6.64
6.18
6.16
6.14
6.12
5.48
4.85
4.83
4.81
4.13
4.11
3.87
3.86
3.85
3.85
3.84
3.82
2.99
2.98
2.96
2.95
2.88
2.86
2.85
2.83
O
O
HN
Ph
F
F
5.17
0.82
2.81
1.14
1.04
0.83
0.99
1.01
1.03
1.15
6500
6000
5500
5000
4500
4000
3500
3000
2500
2000
1500
1000
500
0
−500
11.5
10.5
9.5
8.5
7.5
6.5
5.5
4.5
3.5
2.5
1.5
0.5
−0.5
−1.5
f1 (ppm)

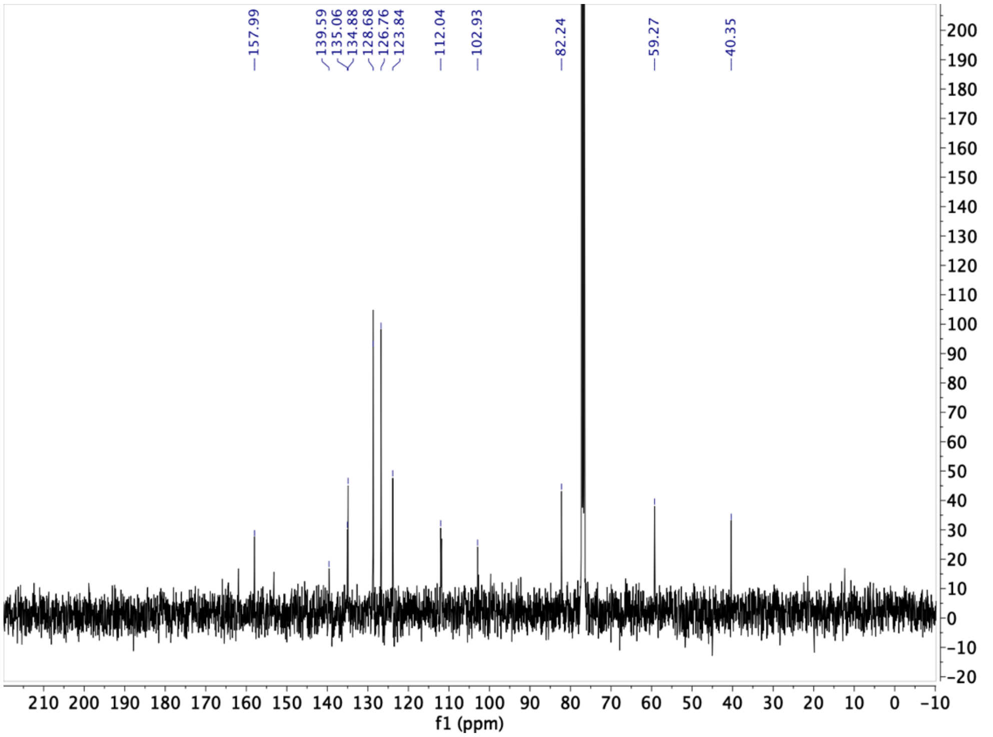
157.99
139.59
135.06
134.88
128.68
126.76
123.84
112.04
102.93
82.24
59.27
40.35
200
190
180
170
160
150
140
130
120
110
100
90
80
70
60
50
40
30
20
10
0
−10
−20
210
200
190
180
170
160
150
140
130
120
110
100
90
80
70
60
50
40
30
20
10
0
−10
f1 (ppm)

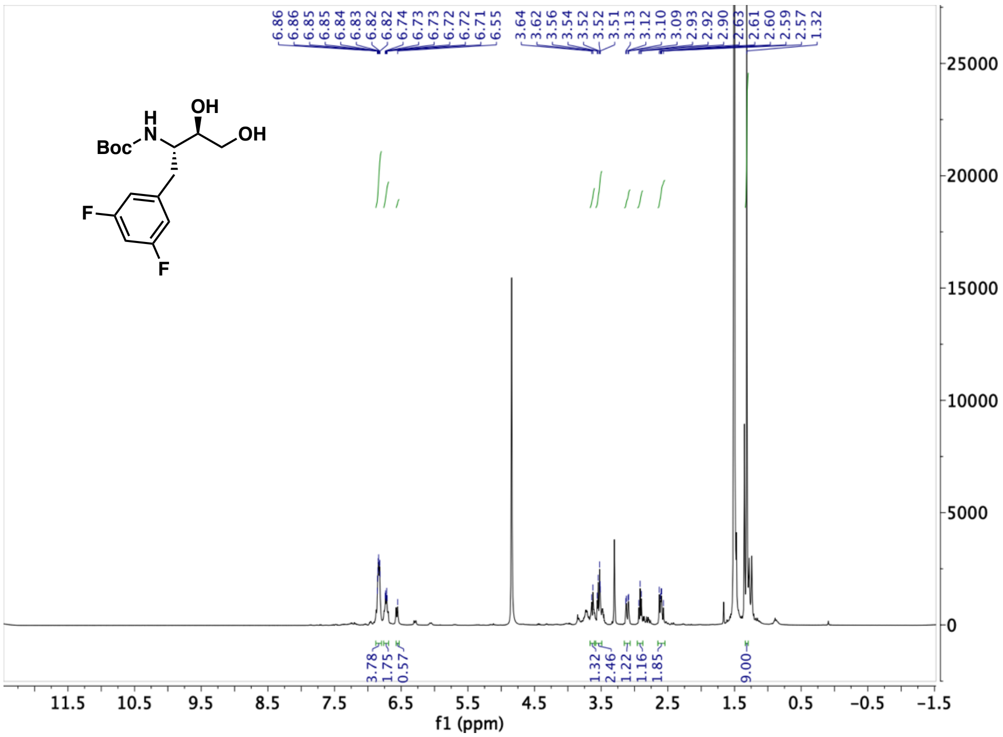
6.86
6.86
6.85
6.84
6.83
6.82
6.82
6.74
6.73
6.73
6.72
6.72
6.71
6.55
3.64
3.62
3.56
3.54
3.52
3.52
3.51
3.13
3.12
3.10
3.09
2.93
2.92
2.90
2.63
2.61
2.60
2.59
2.57
1.32
Boc
H
N
OH
OH
F
F
3.78
1.75
0.57
1.32
2.46
1.22
1.16
1.85
9.00
25000
20000
15000
10000
5000
0
11.5
10.5
9.5
8.5
7.5
6.5
5.5
4.5
3.5
2.5
1.5
0.5
−0.5
−1.5
f1 (ppm)

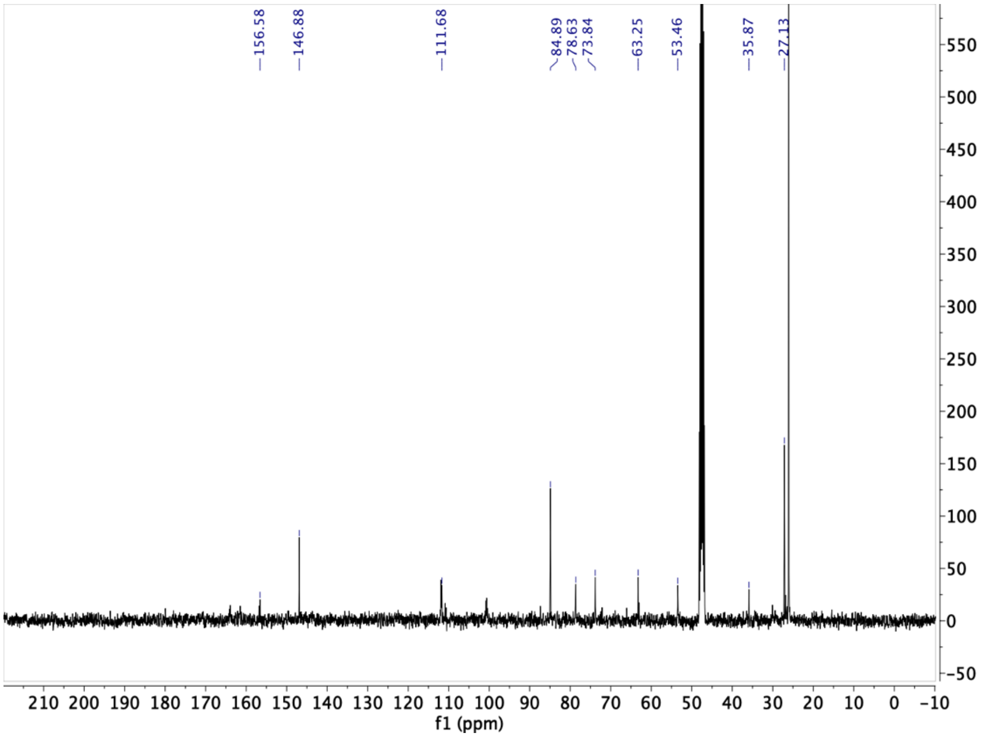
156.58
146.88
111.68
84.89
78.63
73.84
63.25
53.46
35.87
27.13
550
500
450
400
350
300
250
200
150
100
50
0
−50
210
200
190
180
170
160
150
140
130
120
110
100
90
80
70
60
50
40
30
20
10
0
−10
f1 (ppm)

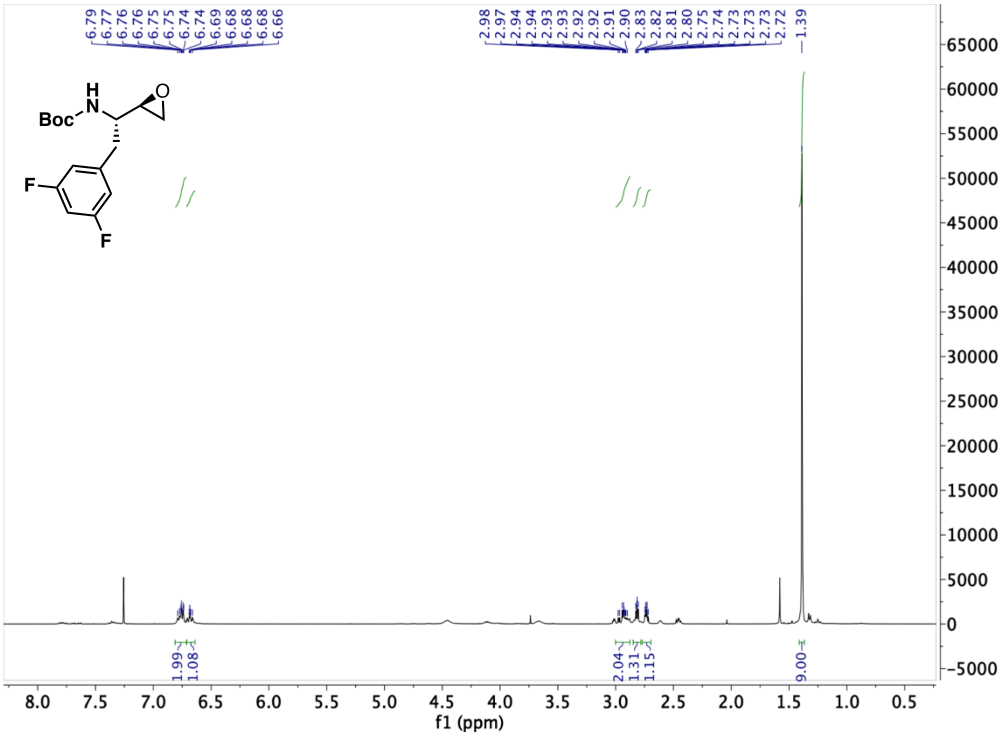
6.79
6.77
6.76
6.76
6.75
6.75
6.74
6.74
6.69
6.68
6.68
6.68
6.66
2.98
2.97
2.94
2.94
2.93
2.93
2.92
2.92
2.91
2.90
2.83
2.82
2.81
2.80
2.75
2.74
2.73
2.73
2.73
2.72
1.39
H
N
Boc
O
F
F
1.99
1.08
2.04
1.31
1.15
9.00
65000
60000
55000
50000
45000
40000
35000
30000
25000
20000
15000
10000
5000
0
−5000
8.0
7.5
7.0
6.5
6.0
5.5
5.0
4.5
4.0
3.5
3.0
2.5
2.0
1.5
1.0
0.5
f1 (ppm)

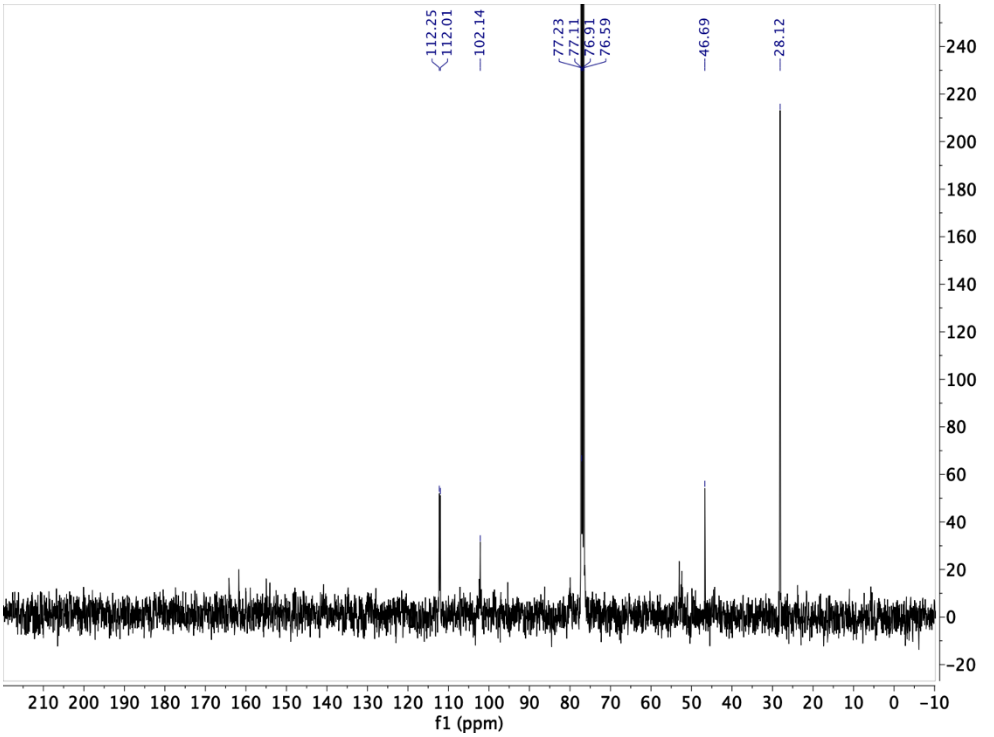
112.25
112.01
102.14
77.23
77.11
76.91
76.59
46.69
28.12
240
220
200
180
160
140
120
100
80
60
40
20
0
−20
210
200
190
180
170
160
150
140
130
120
110
100
90
80
70
60
50
40
30
20
10
0
−10
f1 (ppm)

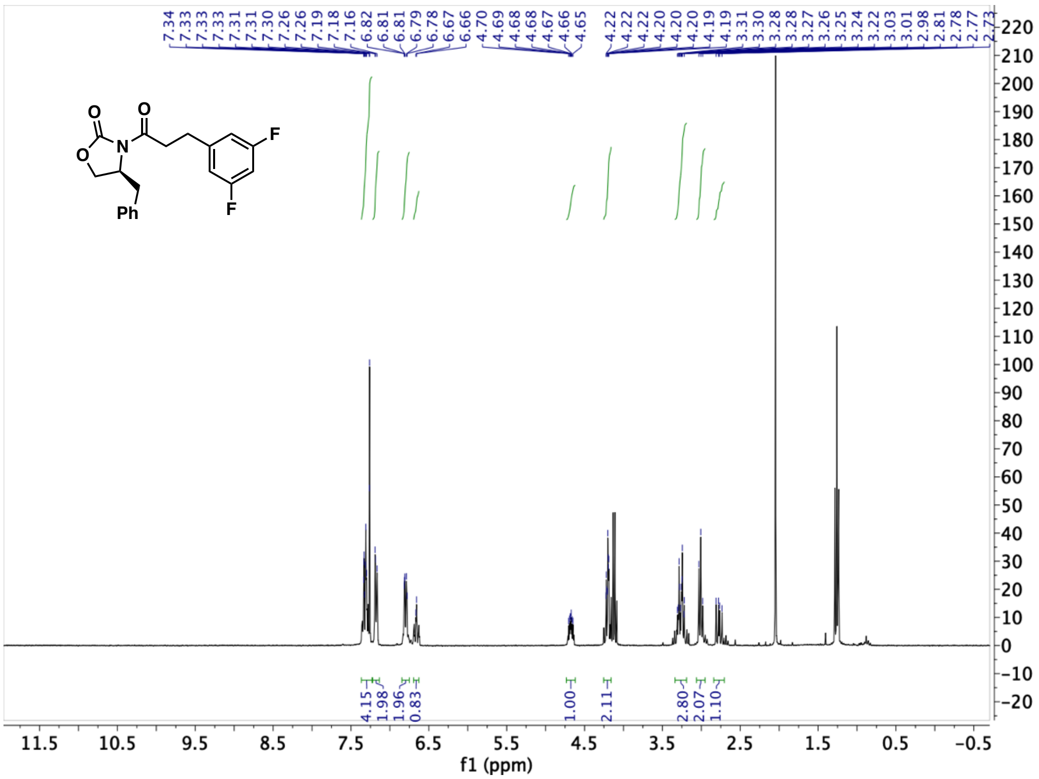
7.34
7.33
7.33
7.31
7.31
7.30
7.26
7.19
7.18
7.16
6.82
6.81
6.81
6.79
6.78
6.67
6.66
4.70
4.69
4.68
4.68
4.67
4.66
4.65
4.22
4.22
4.22
4.20
4.20
4.20
4.19
4.19
3.31
3.30
3.28
3.28
3.27
3.26
3.25
3.24
3.22
3.03
3.01
2.98
2.81
2.78
2.77
2.73
O
O
N
O
F
F
Ph
4.15
1.98
1.96
0.83
1.00
2.11
2.80
2.07
1.10
220
210
200
190
180
170
160
150
140
130
120
110
100
90
80
70
60
50
40
30
20
10
0
-10
-20
11.5
10.5
9.5
8.5
7.5
6.5
5.5
4.5
3.5
2.5
1.5
0.5
-0.5
f1 (ppm)

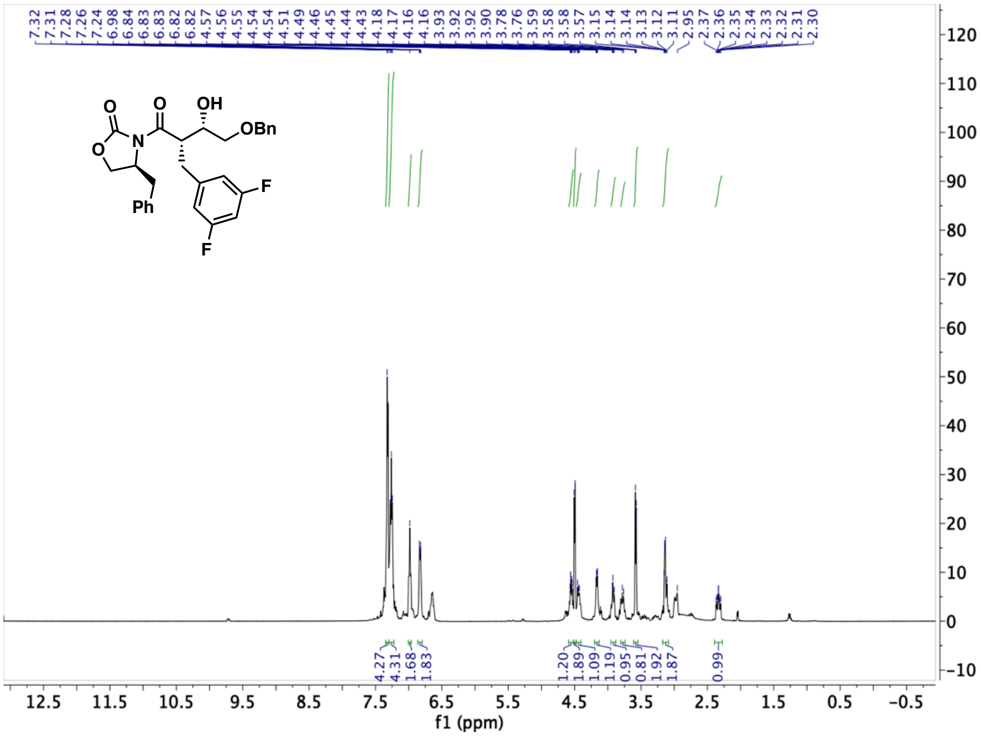
7.32
7.31
7.28
7.26
7.24
6.98
6.84
6.83
6.83
6.82
6.82
4.57
4.56
4.55
4.54
4.54
4.51
4.49
4.46
4.45
4.44
4.43
4.18
4.17
4.16
4.16
3.93
3.92
3.92
3.90
3.78
3.76
3.59
3.58
3.58
3.57
3.15
3.14
3.14
3.13
3.12
3.11
2.95
2.37
2.36
2.35
2.34
2.33
2.32
2.31
2.30
O
O
OH
OBn
N
O
Ph
F
F
4.27
4.31
1.68
1.83
1.20
1.89
1.09
1.19
0.95
0.81
1.92
1.87
0.99
12.5
11.5
10.5
9.5
8.5
7.5
6.5
5.5
4.5
3.5
2.5
1.5
0.5
-0.5
f1 (ppm)
120
110
100
90
80
70
60
50
40
30
20
10
0
-10

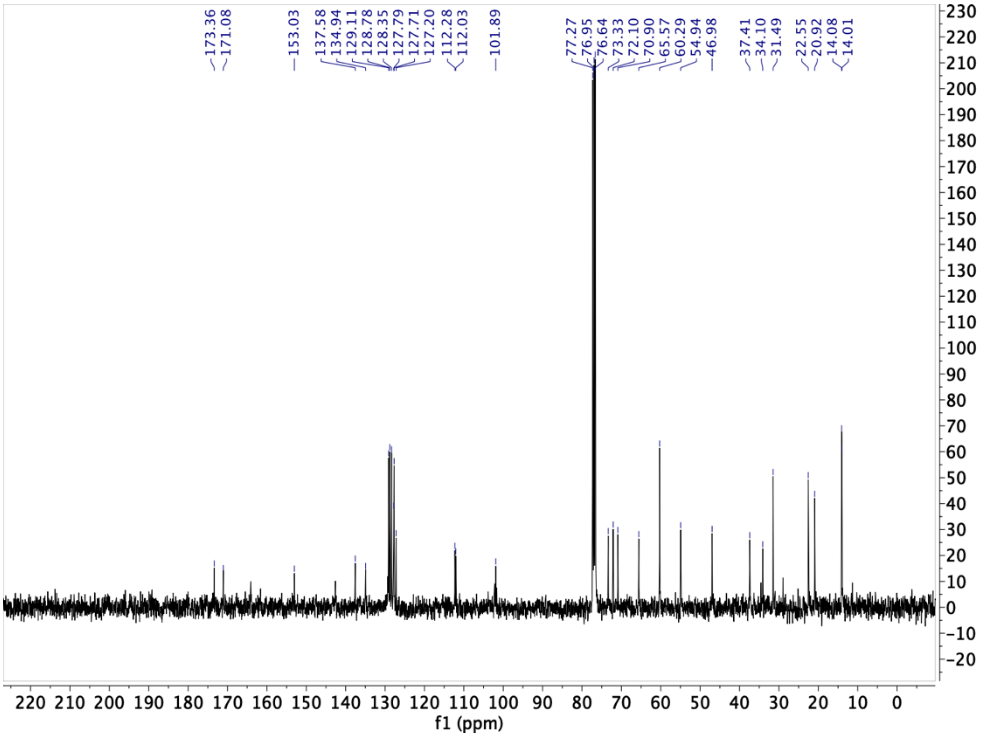
173.36
171.08
153.03
137.58
134.94
129.11
128.78
128.35
127.79
127.71
127.20
112.28
112.03
101.89
77.27
76.95
76.64
73.33
72.10
70.90
65.57
60.29
54.94
46.98
37.41
34.10
31.49
22.55
20.92
14.08
14.01
220
210
200
190
180
170
160
150
140
130
120
110
100
90
80
70
60
50
40
30
20
10
0
f1 (ppm)
230
220
210
200
190
180
170
160
150
140
130
120
110
100
90
80
70
60
50
40
30
20
10
0
-10
-20

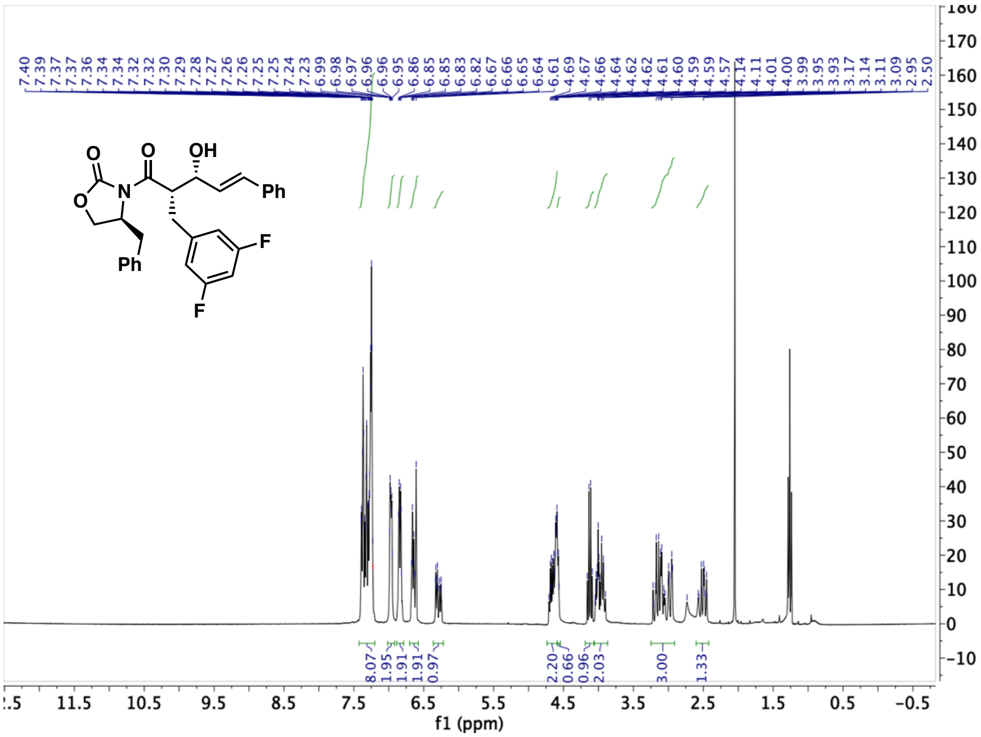
7.40
7.39
7.37
7.37
7.36
7.34
7.34
7.32
7.32
7.30
7.29
7.28
7.27
7.26
7.25
7.25
7.24
7.23
6.99
6.98
6.97
6.96
6.96
6.95
6.86
6.85
6.85
6.83
6.82
6.67
6.66
6.65
6.64
6.61
4.69
4.67
4.66
4.64
4.62
4.61
4.60
4.59
4.59
4.57
4.14
4.11
4.01
4.00
3.99
3.95
3.93
3.17
3.14
3.11
3.09
2.95
2.50
O
O
OH
N
Ph
O
Ph
F
F
8.07
1.95
1.91
1.91
0.97
2.20
0.66
0.96
2.03
3.00
1.33
f1 (ppm)

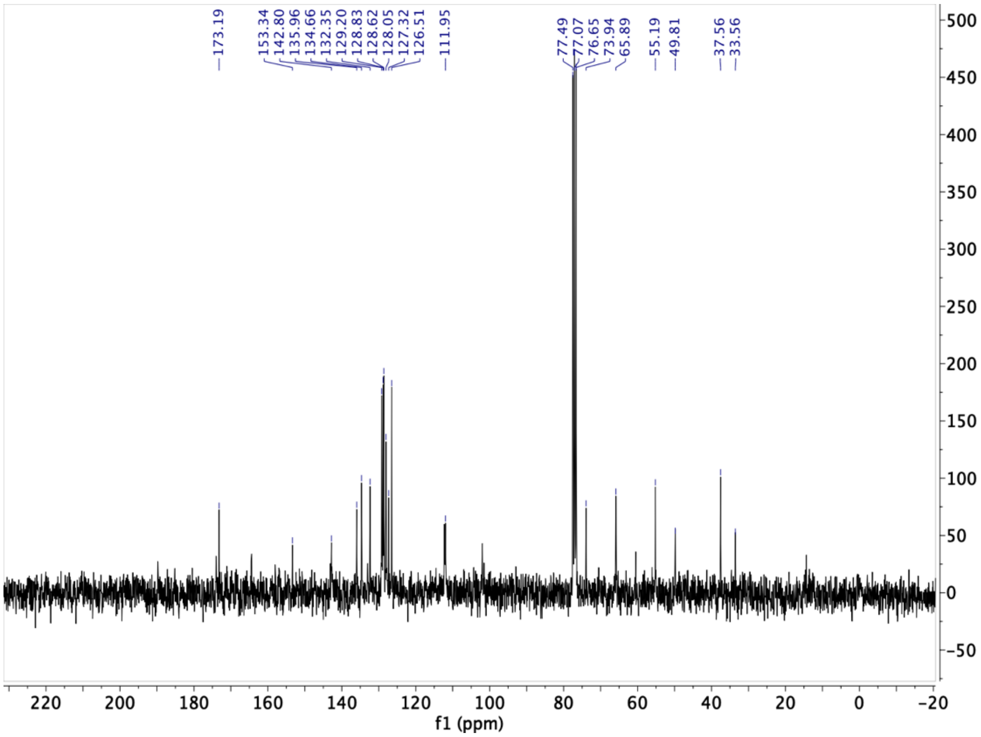
173.19
153.34
142.80
135.96
134.66
132.35
129.20
128.83
128.62
128.05
127.32
126.51
111.95
77.49
77.07
76.65
73.94
65.89
55.19
49.81
37.56
33.56
f1 (ppm)

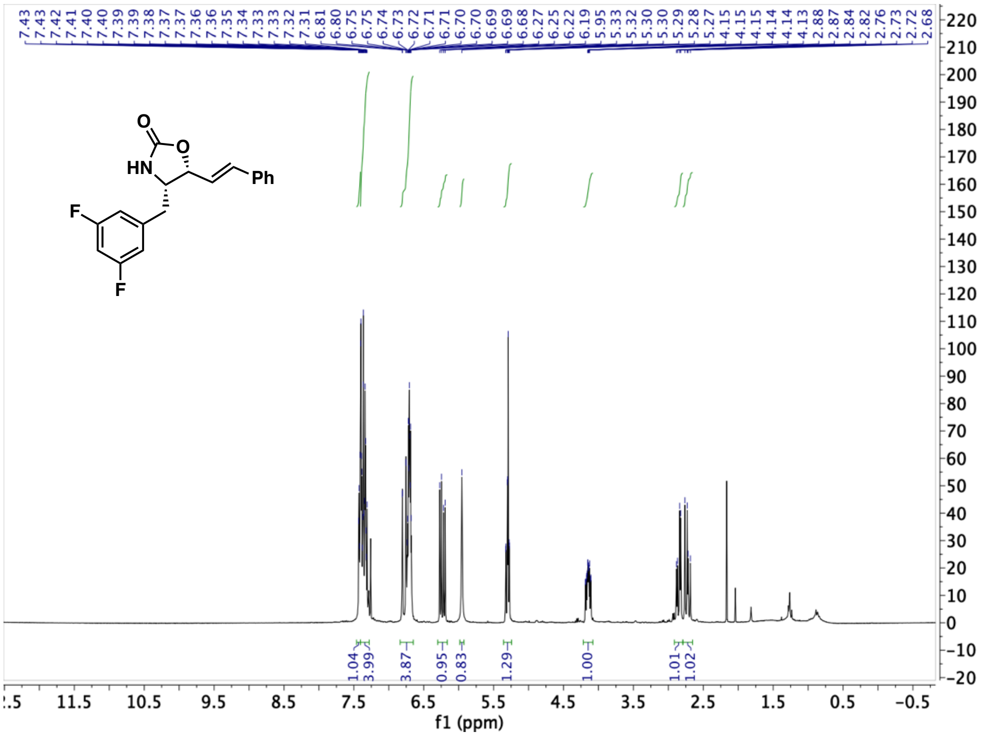
7.43
7.43
7.42
7.41
7.40
7.40
7.39
7.39
7.38
7.37
7.37
7.36
7.35
7.34
7.33
7.33
7.32
7.31
6.81
6.80
6.75
6.74
6.73
6.72
6.71
6.71
6.70
6.69
6.68
6.27
6.25
6.22
6.19
5.95
5.33
5.32
5.30
5.30
5.29
5.28
5.27
4.15
4.15
4.15
4.14
4.14
4.13
2.88
2.87
2.84
2.82
2.76
2.73
2.72
2.68
O
HN
O
Ph
F
F
1.04
3.99
3.87
0.95
0.83
1.29
1.00
1.01
1.02
.5
11.5
10.5
9.5
8.5
7.5
6.5
5.5
4.5
3.5
2.5
1.5
0.5
-0.5
f1 (ppm)
220
210
200
190
180
170
160
150
140
130
120
110
100
90
80
70
60
50
40
30
20
10
0
-10
-20

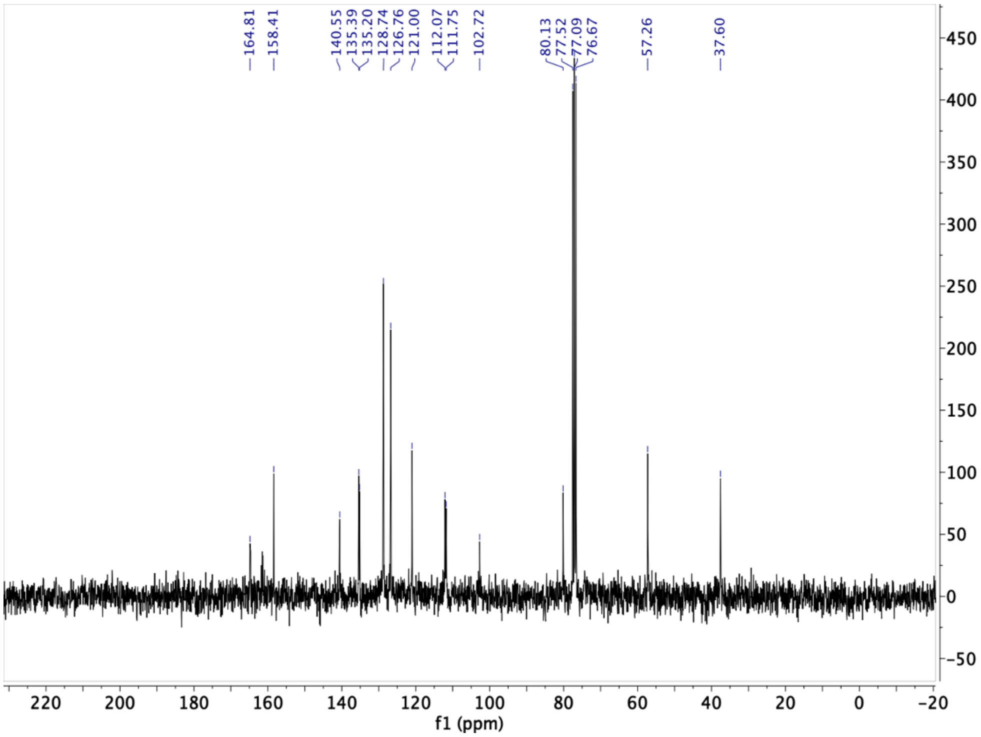
164.81
158.41
140.55
135.39
135.20
128.74
126.76
121.00
112.07
111.75
102.72
80.13
77.52
77.09
76.67
57.26
37.60
220
200
180
160
140
120
100
80
60
40
20
0
-20
f1 (ppm)
450
400
350
300
250
200
150
100
50
0
-50

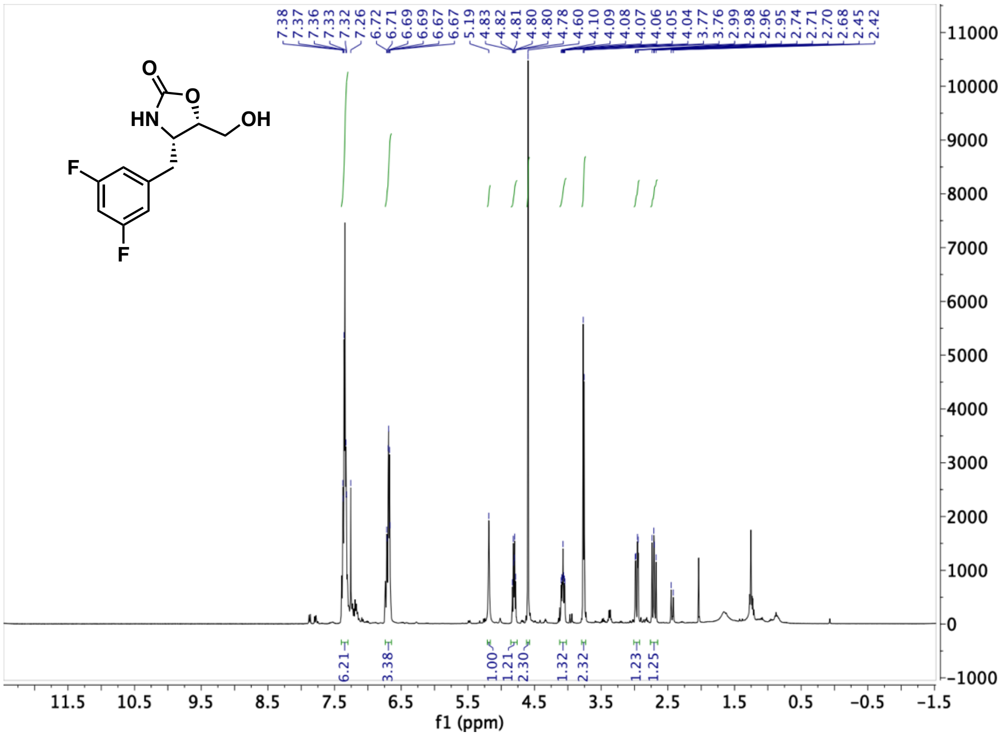
7.38
7.37
7.36
7.33
7.32
7.26
6.72
6.71
6.69
6.69
6.67
6.67
5.19
4.83
4.82
4.81
4.80
4.80
4.78
4.60
4.10
4.09
4.08
4.07
4.06
4.05
4.04
3.77
3.76
2.99
2.98
2.96
2.95
2.74
2.71
2.70
2.68
2.45
2.42
O
O
HN
OH
F
F
6.21
3.38
1.00
1.21
2.30
1.32
2.32
1.23
1.25
11000
10000
9000
8000
7000
6000
5000
4000
3000
2000
1000
0
−1000
11.5
10.5
9.5
8.5
7.5
6.5
5.5
4.5
3.5
2.5
1.5
0.5
−0.5
−1.5
f1 (ppm)

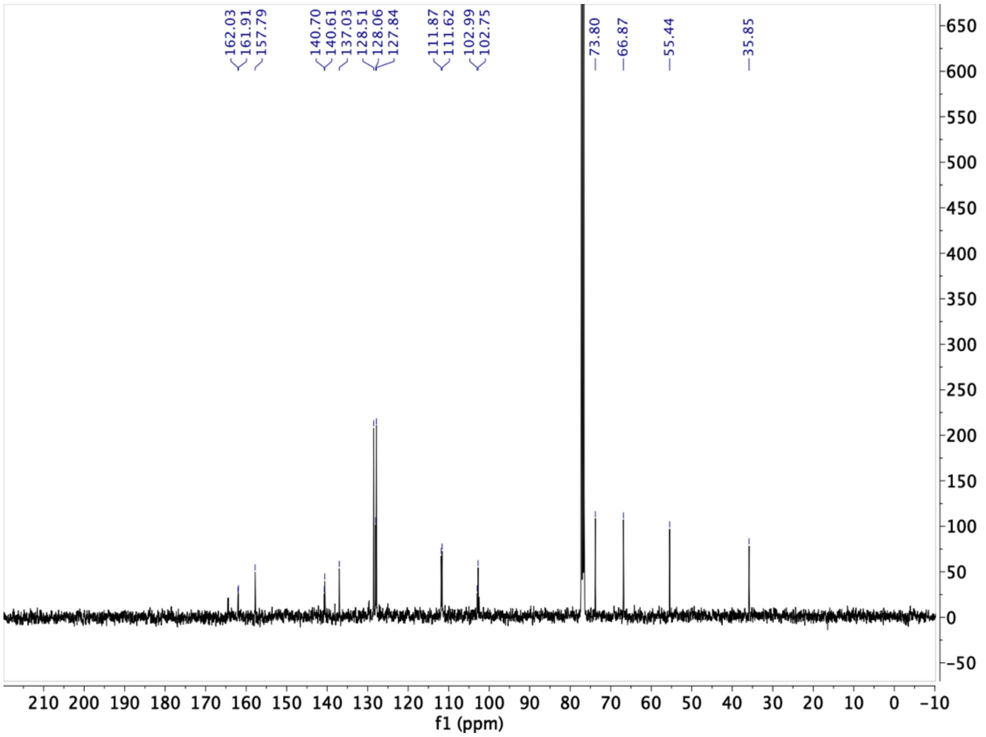
162.03
161.91
157.79
140.70
140.61
137.03
128.51
128.06
127.84
111.87
111.62
102.99
102.75
73.80
66.87
55.44
35.85
650
600
550
500
450
400
350
300
250
200
150
100
50
0
−50
210
200
190
180
170
160
150
140
130
120
110
100
90
80
70
60
50
40
30
20
10
0
−10
f1 (ppm)

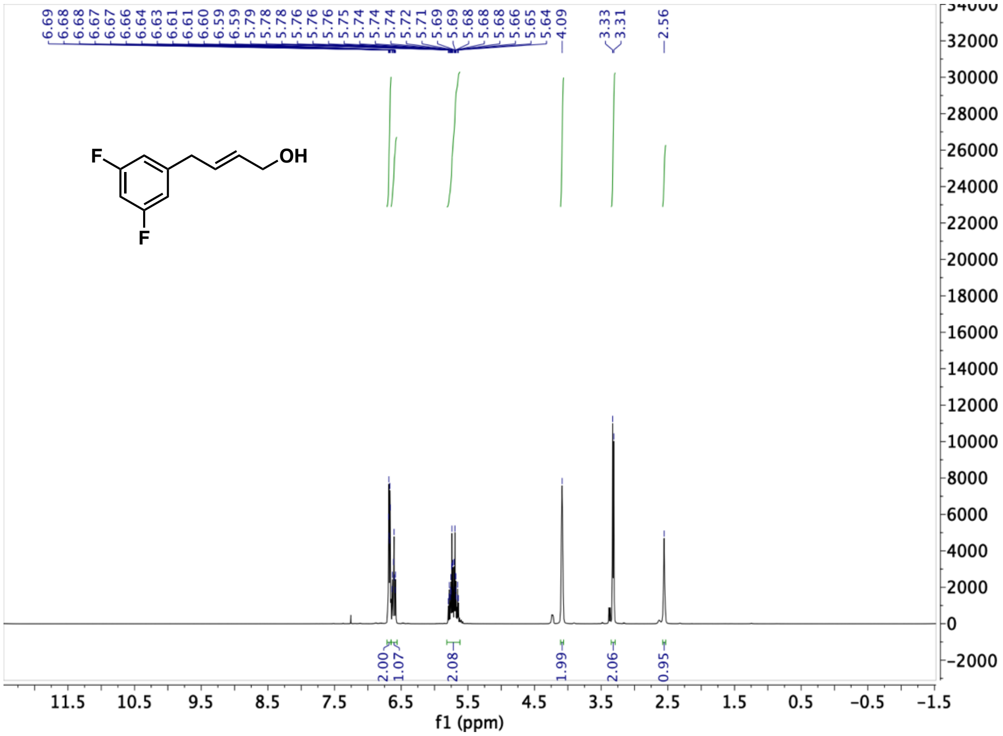
6.69
6.68
6.67
6.67
6.66
6.64
6.63
6.61
6.61
6.60
6.59
6.59
6.59
5.79
5.78
5.78
5.76
5.76
5.75
5.74
5.74
5.74
5.72
5.71
5.69
5.69
5.68
5.68
5.68
5.66
5.65
5.64
4.09
3.33
3.31
2.56
F
F
OH
2.00
1.07
2.08
1.99
2.06
0.95
11.5 10.5 9.5 8.5 7.5 6.5 5.5 4.5 3.5 2.5 1.5 0.5 −0.5 −1.5
f1 (ppm)
34000 32000 30000 28000 26000 24000 22000 20000 18000 16000 14000 12000 10000 8000 6000 4000 2000 0 −2000

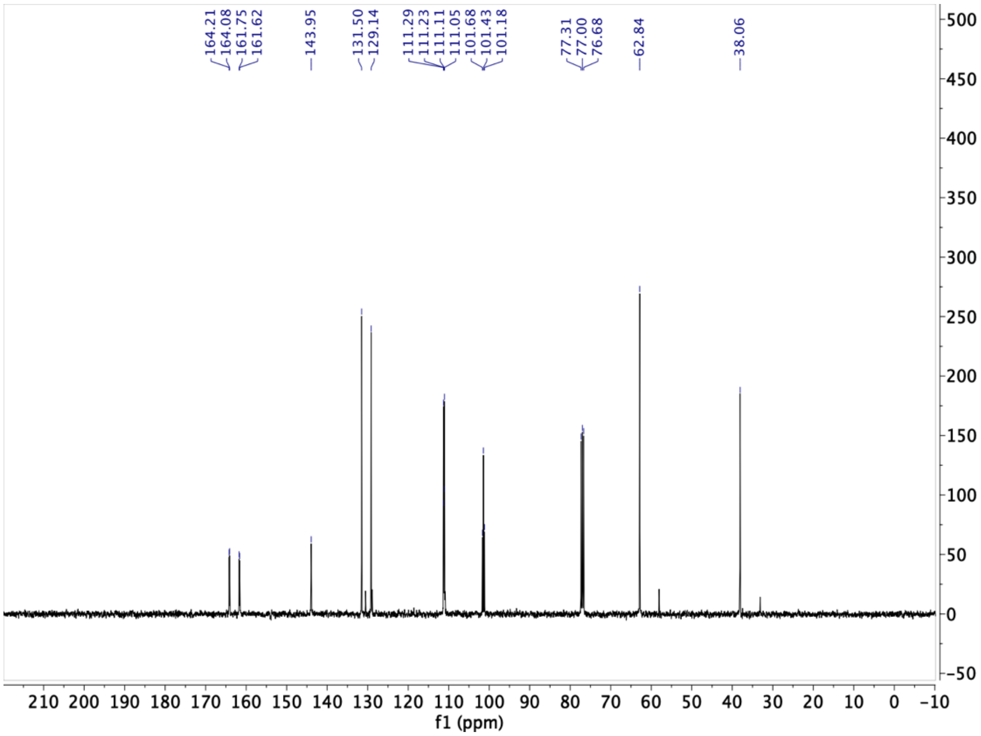
164.21
164.08
161.75
161.62
143.95
131.50
129.14
111.29
111.23
111.11
111.05
101.68
101.43
101.18
77.31
77.00
76.68
62.84
38.06
210 200 190 180 170 160 150 140 130 120 110 100 90 80 70 60 50 40 30 20 10 0 −10
f1 (ppm)
500 450 400 350 300 250 200 150 100 50 0 −50

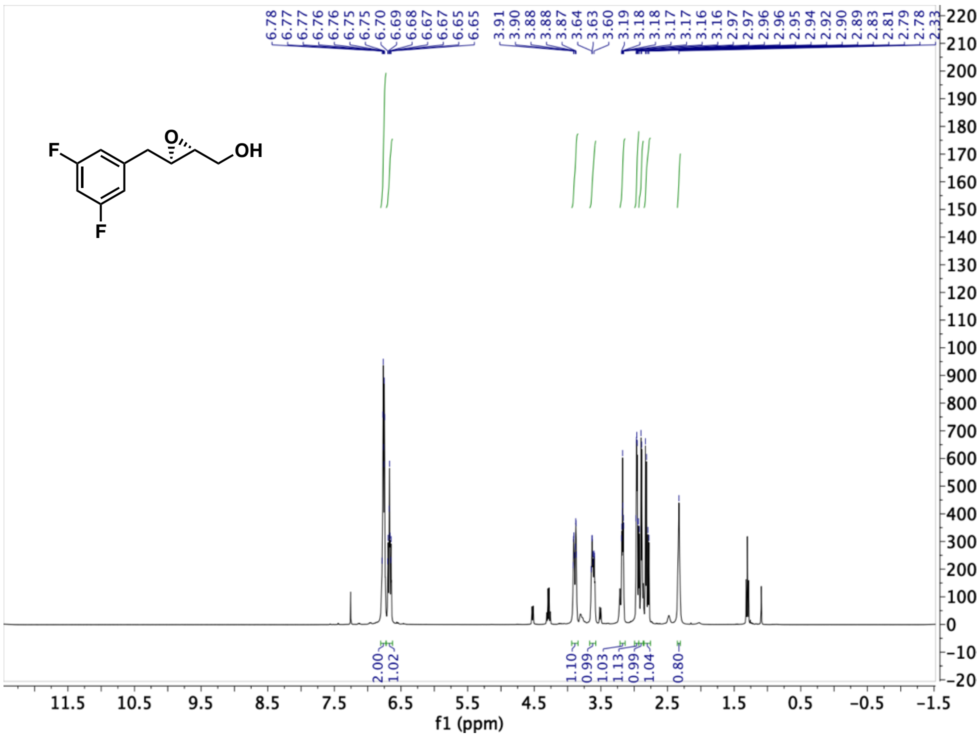
6.78
6.77
6.76
6.76
6.75
6.75
6.70
6.69
6.68
6.67
6.67
6.65
6.65
3.91
3.90
3.88
3.88
3.87
3.64
3.63
3.60
3.19
3.18
3.18
3.17
3.17
3.16
3.16
2.97
2.97
2.96
2.96
2.95
2.94
2.92
2.90
2.89
2.83
2.81
2.79
2.78
2.33
F
O
OH
F
2.00
1.02
1.10
0.99
1.03
1.13
0.99
1.04
0.80
f1 (ppm)
11.5
10.5
9.5
8.5
7.5
6.5
5.5
4.5
3.5
2.5
1.5
0.5
−0.5
−1.5
22000
21000
20000
19000
18000
17000
16000
15000
14000
13000
12000
11000
10000
9000
8000
7000
6000
5000
4000
3000
2000
1000
0
−1000
−2000

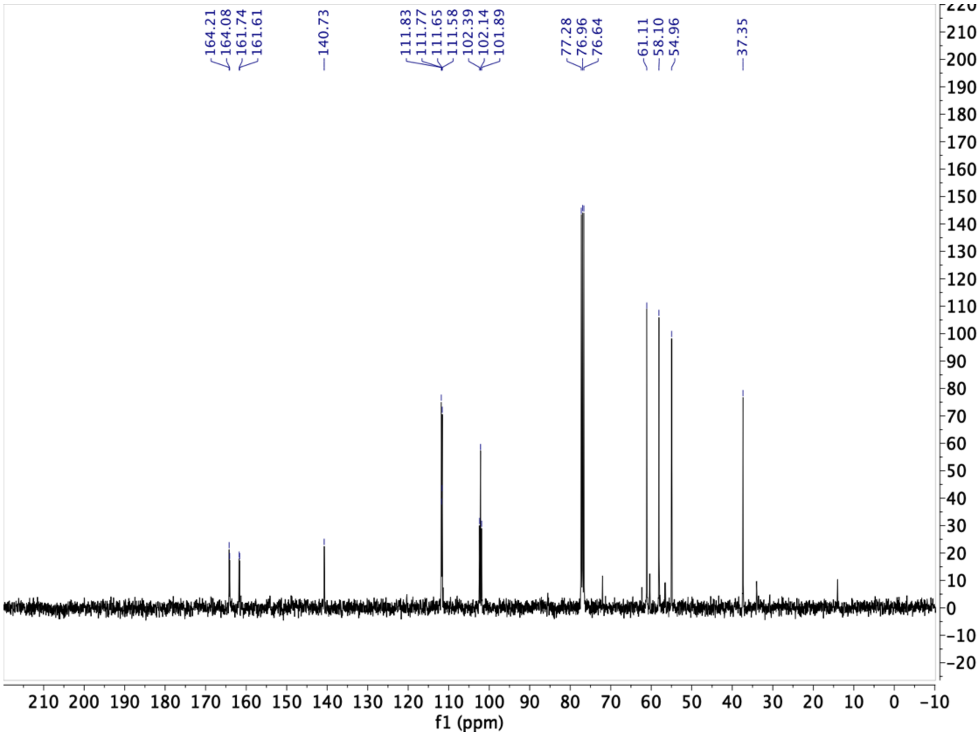
164.21
164.08
161.74
161.61
140.73
111.83
111.77
111.65
111.58
102.39
102.14
101.89
77.28
76.96
76.64
61.11
58.10
54.96
37.35
f1 (ppm)
210
200
190
180
170
160
150
140
130
120
110
100
90
80
70
60
50
40
30
20
10
0
−10
220
210
200
190
180
170
160
150
140
130
120
110
100
90
80
70
60
50
40
30
20
10
0
−10
−20

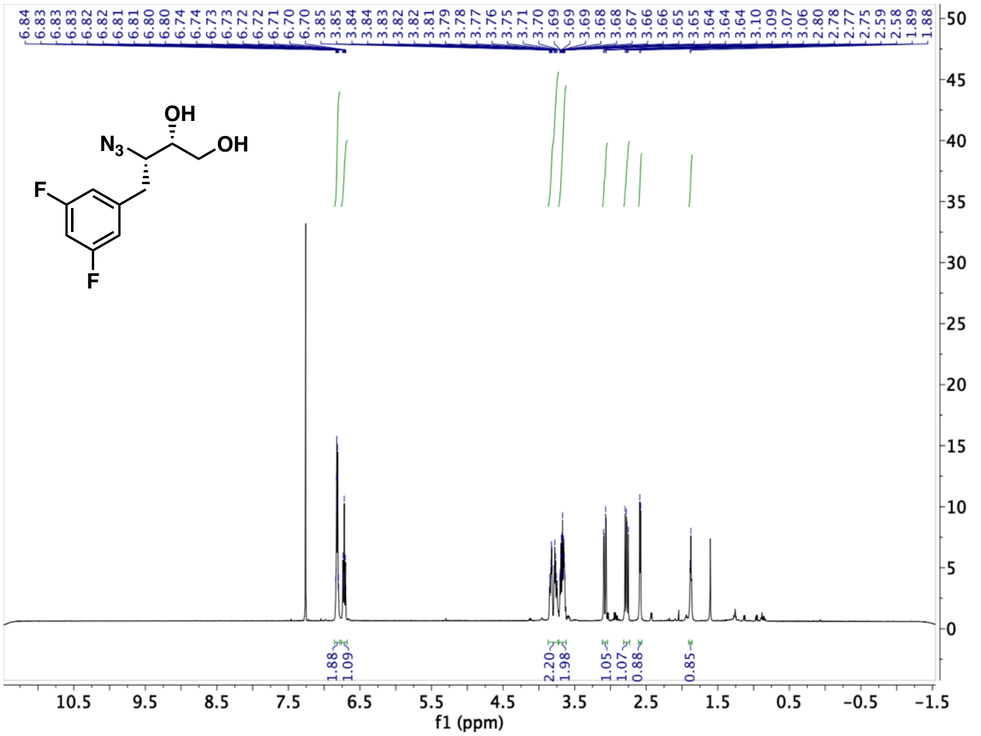
6.84
6.83
6.83
6.82
6.82
6.81
6.81
6.80
6.74
6.73
6.73
6.72
6.72
6.71
6.70
6.70
3.85
3.85
3.84
3.84
3.83
3.82
3.82
3.81
3.79
3.78
3.77
3.76
3.75
3.71
3.70
3.69
3.69
3.69
3.68
3.68
3.67
3.66
3.66
3.65
3.65
3.64
3.64
3.64
3.10
3.09
3.07
3.06
2.80
2.78
2.77
2.75
2.59
2.58
1.89
1.88
OH
N_3
OH
F
F
1.88
1.09
2.20
1.98
1.05
1.07
0.88
0.85
10.5
9.5
8.5
7.5
6.5
5.5
4.5
3.5
2.5
1.5
0.5
−0.5
−1.5
f1 (ppm)
50
45
40
35
30
25
20
15
10
5
0

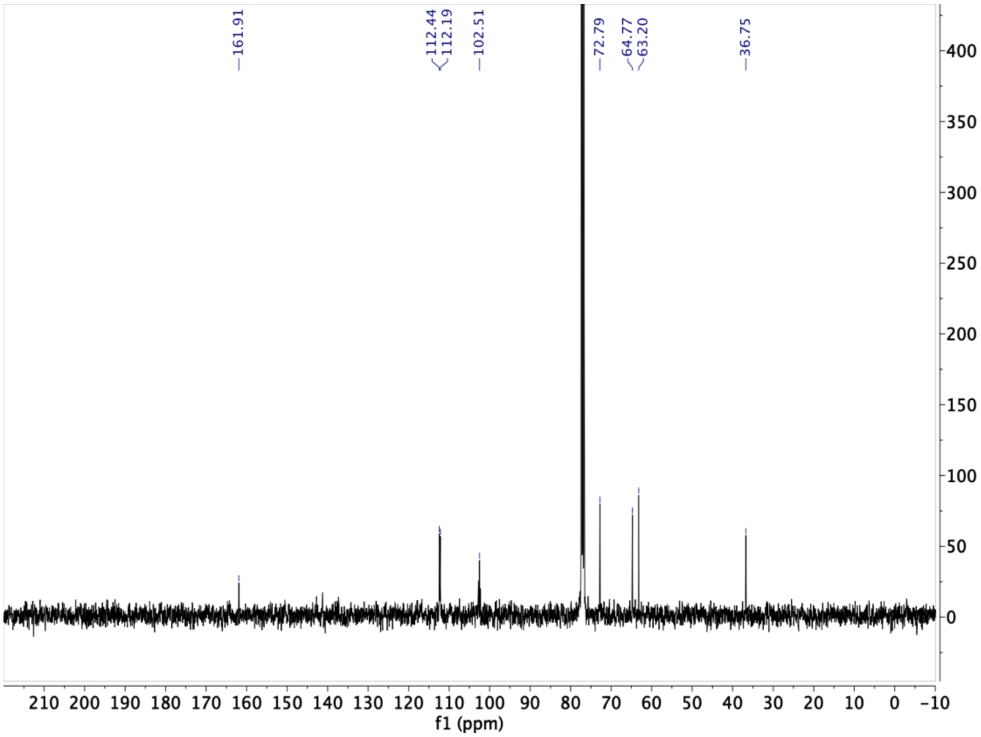
161.91
112.44
112.19
102.51
72.79
64.77
63.20
36.75
210
200
190
180
170
160
150
140
130
120
110
100
90
80
70
60
50
40
30
20
10
0
−10
f1 (ppm)
400
350
300
250
200
150
100
50
0

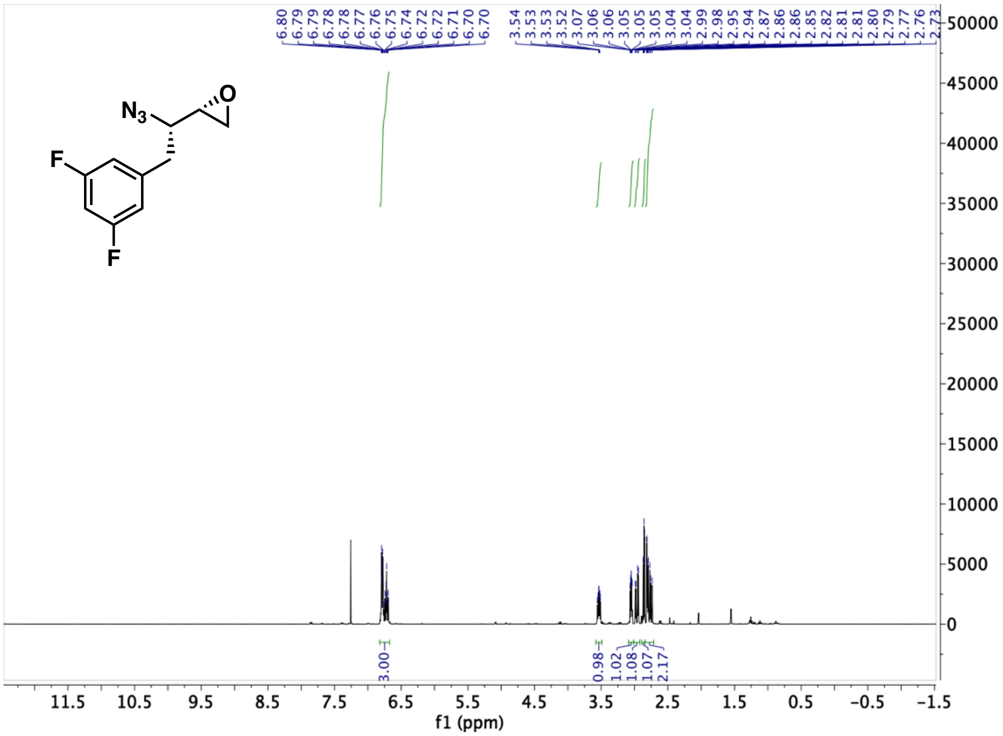
6.80
6.79
6.79
6.78
6.78
6.77
6.76
6.75
6.74
6.72
6.72
6.71
6.70
6.70
3.54
3.53
3.53
3.52
3.07
3.06
3.06
3.05
3.05
3.05
3.04
3.04
2.99
2.98
2.95
2.94
2.87
2.86
2.86
2.85
2.82
2.81
2.80
2.79
2.77
2.76
2.73
N3
O
F
F
3.00
0.98
1.02
1.08
1.07
2.17
f1 (ppm)

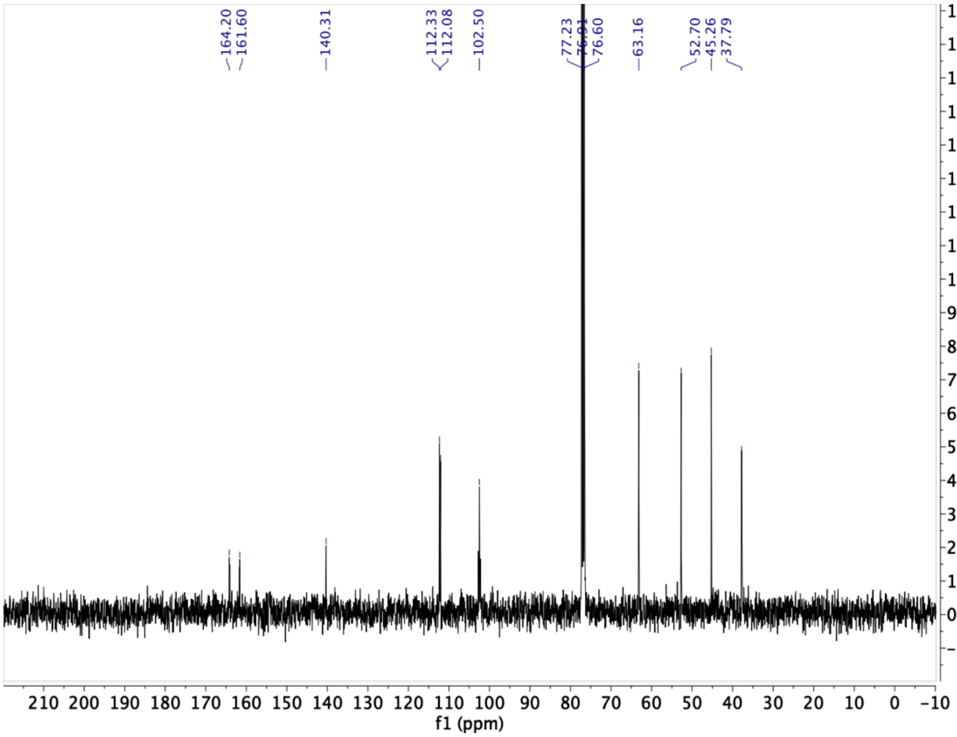
164.20
161.60
140.31
112.33
112.08
102.50
77.23
76.91
76.60
63.16
52.70
45.26
37.79
f1 (ppm)

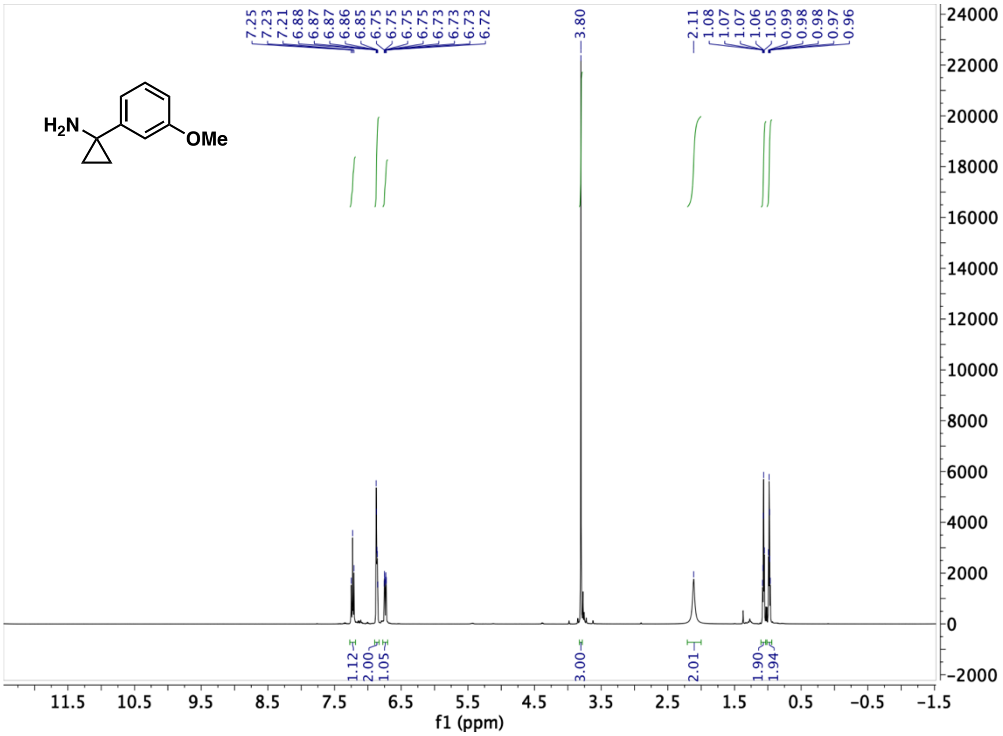
7.25
7.23
7.21
6.88
6.87
6.87
6.86
6.85
6.75
6.75
6.75
6.75
6.73
6.73
6.72
3.80
2.11
1.08
1.07
1.07
1.06
1.05
0.99
0.98
0.98
0.97
0.96
H_2N
OMe
1.12
2.00
1.05
3.00
2.01
1.90
1.94
24000
22000
20000
18000
16000
14000
12000
10000
8000
6000
4000
2000
0
-2000
11.5
10.5
9.5
8.5
7.5
6.5
5.5
4.5
3.5
2.5
1.5
0.5
-0.5
-1.5
f1 (ppm)

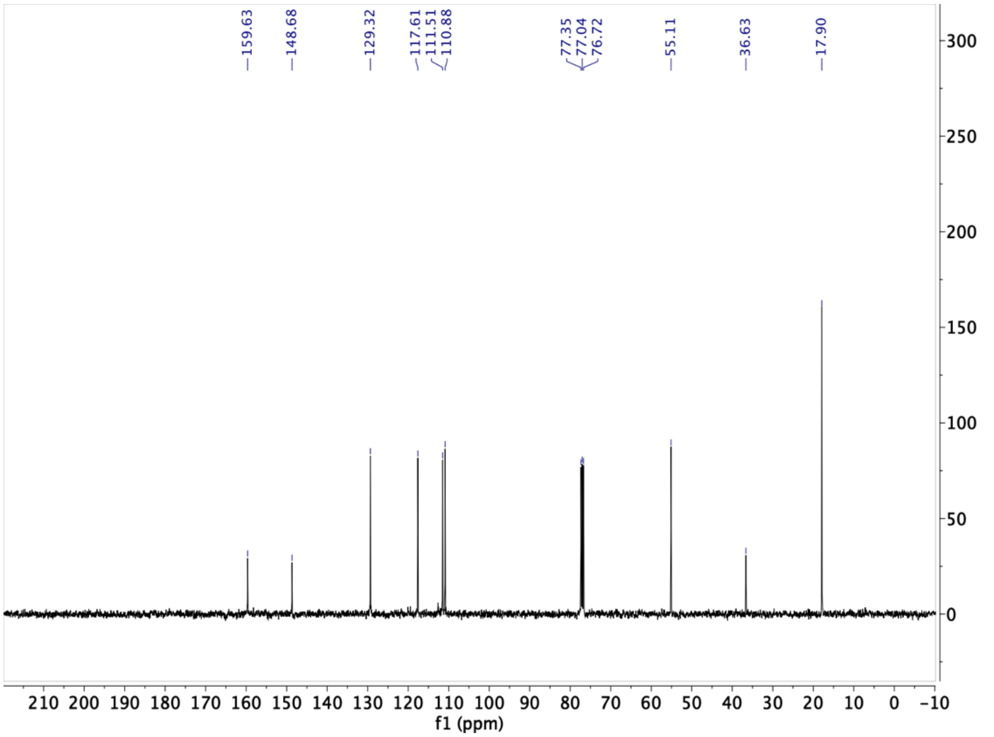
159.63
148.68
129.32
117.61
111.51
110.88
77.35
77.04
76.72
55.11
36.63
17.90
300
250
200
150
100
50
0
210
200
190
180
170
160
150
140
130
120
110
100
90
80
70
60
50
40
30
20
10
0
-10
f1 (ppm)

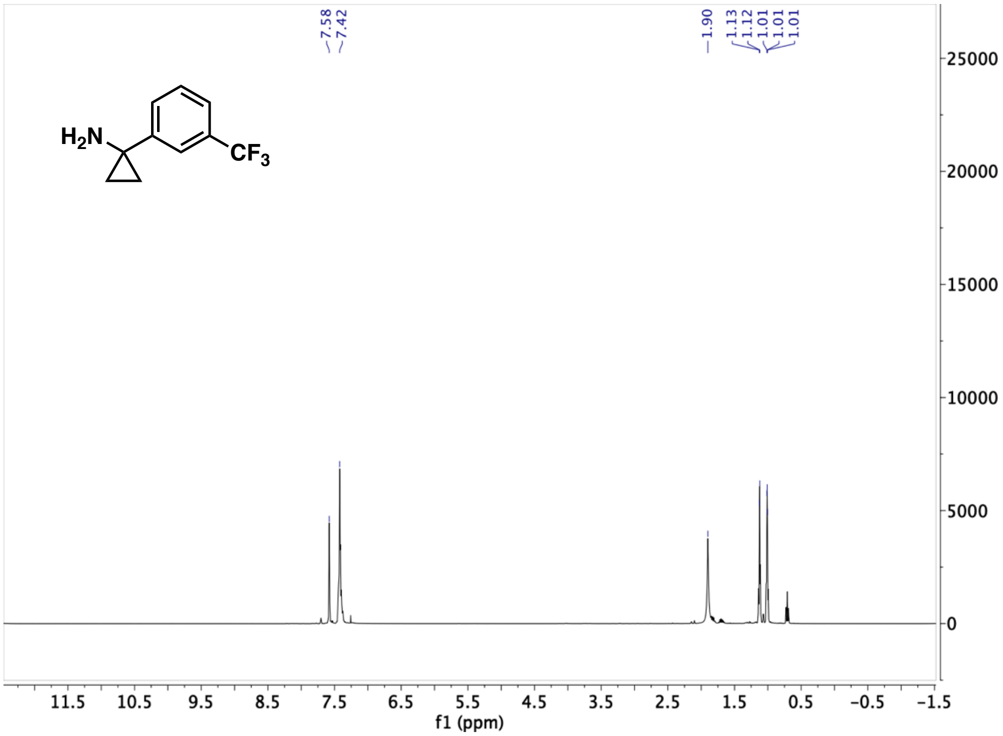
7.58
7.42
1.90
1.13
1.12
1.01
1.01
1.01
H_2N
CF_3
25000
20000
15000
10000
5000
0
11.5
10.5
9.5
8.5
7.5
6.5
5.5
4.5
3.5
2.5
1.5
0.5
−0.5
−1.5
f1 (ppm)

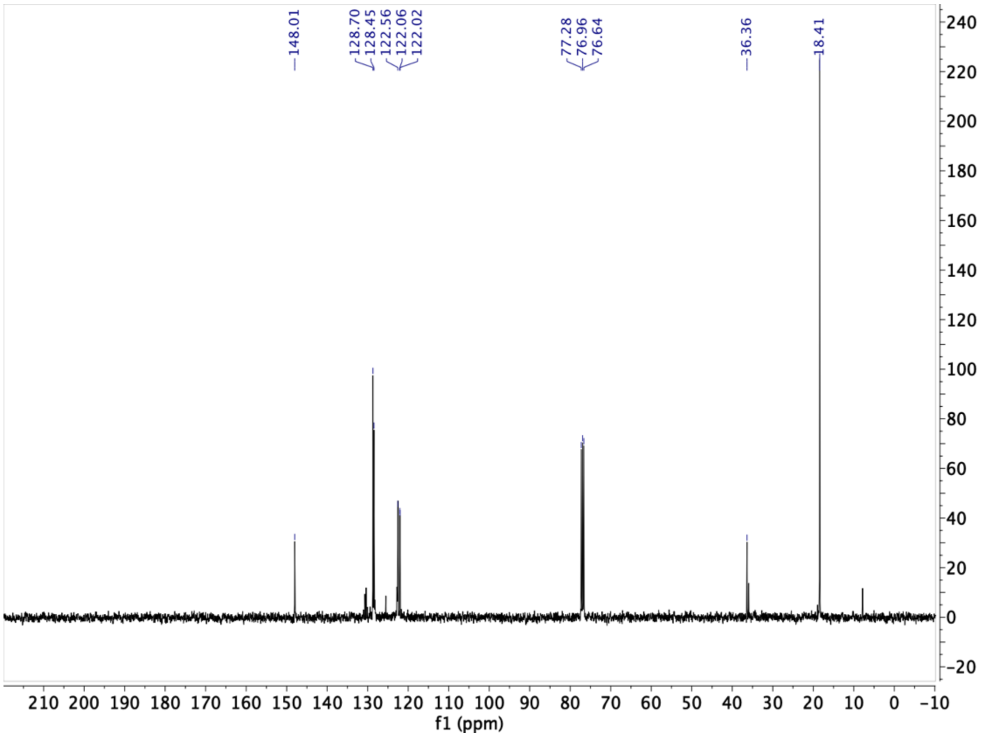
148.01
128.70
128.45
122.56
122.06
122.02
77.28
76.96
76.64
36.36
18.41
240
220
200
180
160
140
120
100
80
60
40
20
0
−20
210
200
190
180
170
160
150
140
130
120
110
100
90
80
70
60
50
40
30
20
10
0
−10
f1 (ppm)

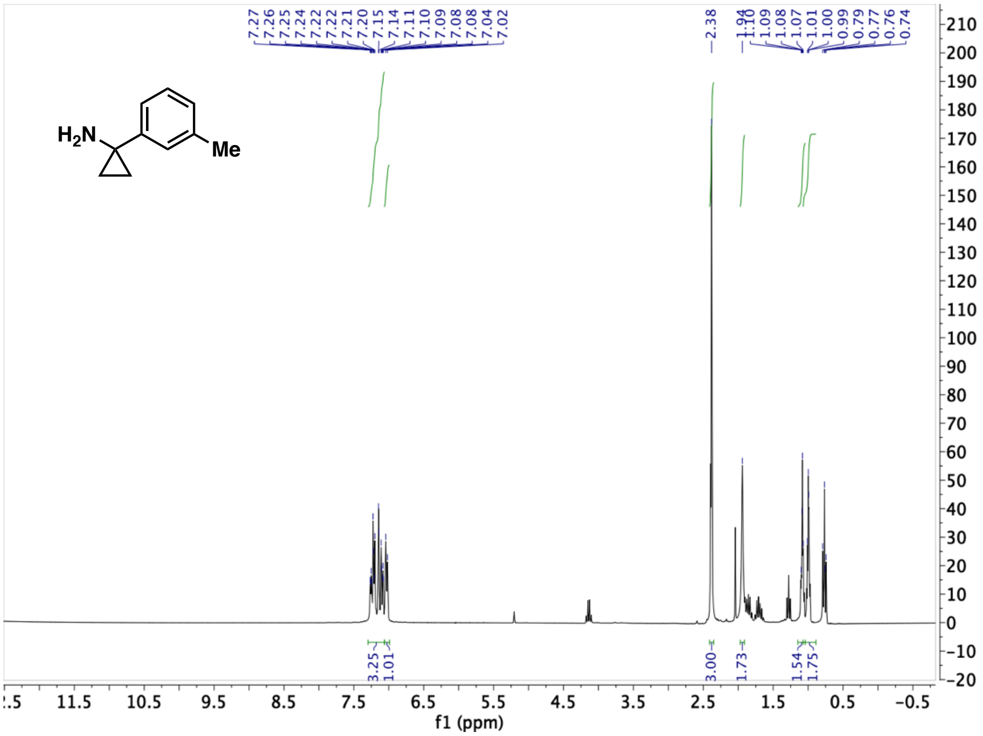
7.27
7.26
7.25
7.24
7.22
7.22
7.21
7.20
7.15
7.14
7.11
7.10
7.09
7.08
7.08
7.04
7.02
2.38
1.94
1.10
1.09
1.08
1.07
1.01
1.00
0.99
0.79
0.77
0.76
0.74
H2N
Me
3.25
1.01
3.00
1.73
1.54
1.75
f1 (ppm)

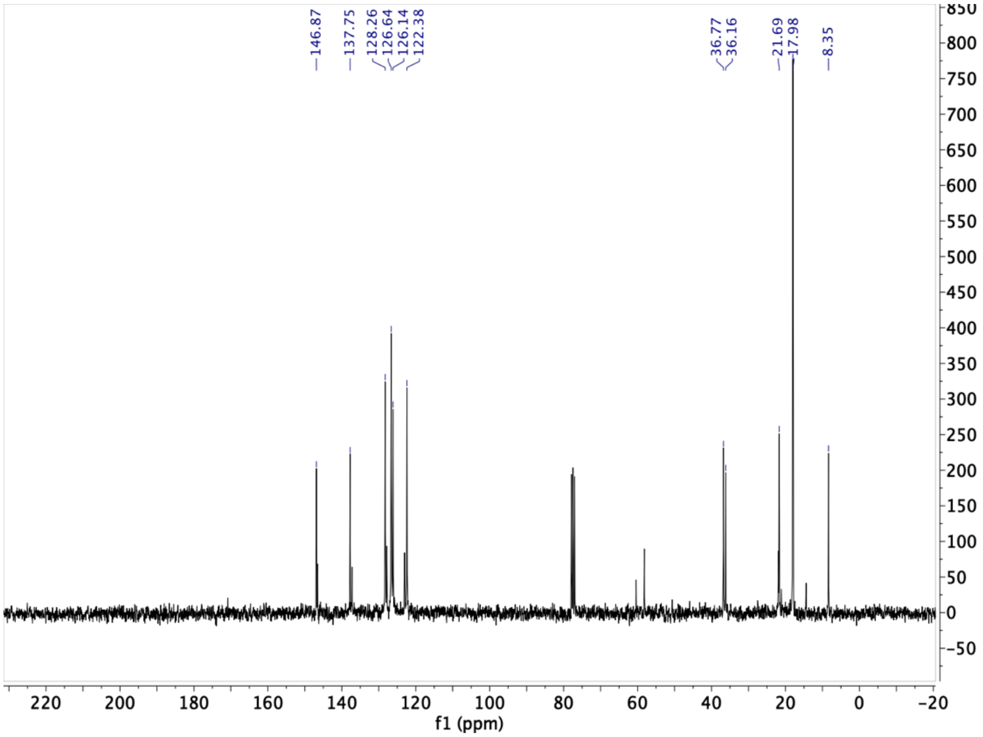
146.87
137.75
128.26
126.64
126.14
122.38
36.77
36.16
21.69
17.98
8.35
f1 (ppm)

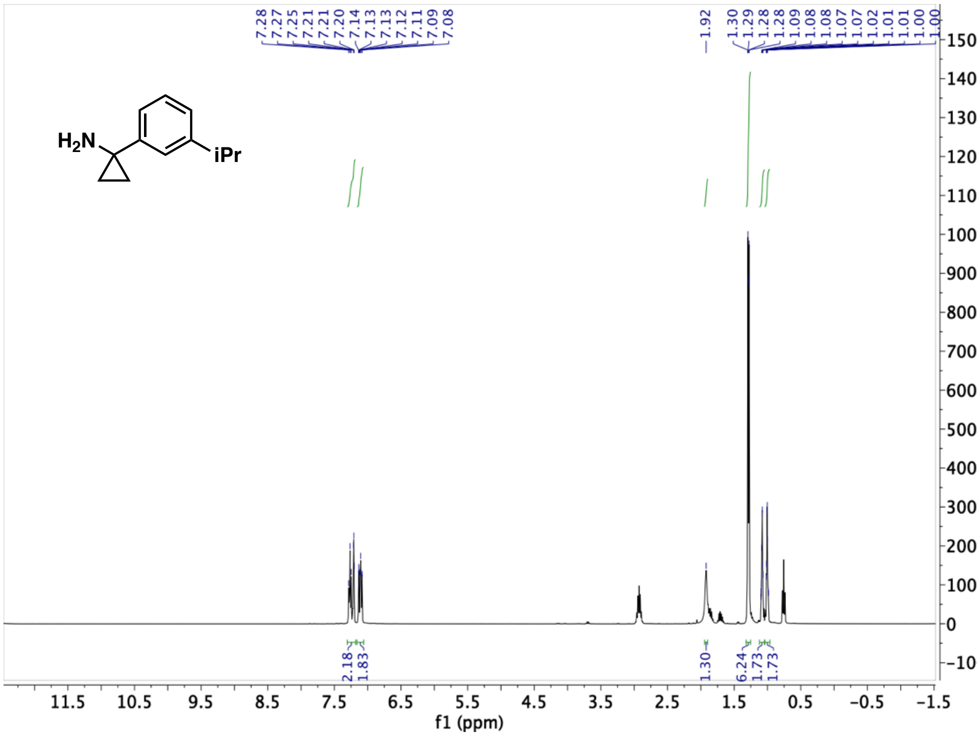
H2N
iPr
7.28
7.27
7.25
7.21
7.21
7.20
7.14
7.13
7.13
7.12
7.11
7.09
7.08
1.92
1.30
1.29
1.28
1.28
1.09
1.08
1.08
1.07
1.07
1.02
1.01
1.01
1.00
1.00
2.18
1.83
1.30
6.24
1.73
1.73
15000
14000
13000
12000
11000
10000
9000
8000
7000
6000
5000
4000
3000
2000
1000
0
−1000
11.5 10.5 9.5 8.5 7.5 6.5 5.5 4.5 3.5 2.5 1.5 0.5 −0.5 −1.5
f1 (ppm)

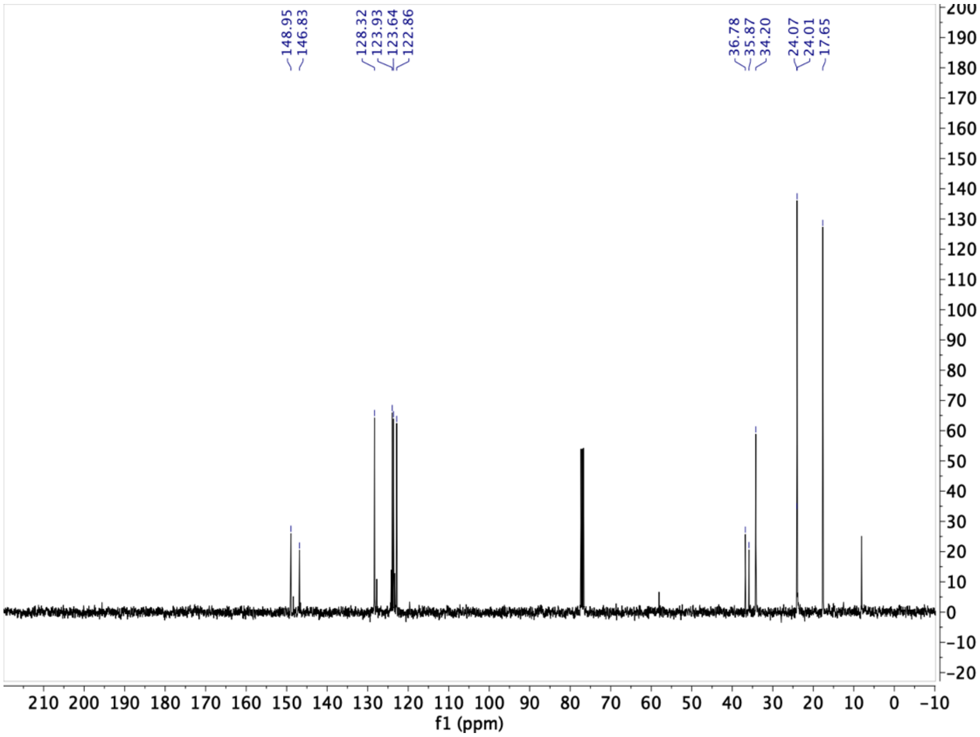
148.95
146.83
128.32
123.93
123.64
122.86
36.78
35.87
34.20
24.07
24.01
17.65
200
190
180
170
160
150
140
130
120
110
100
90
80
70
60
50
40
30
20
10
0
−10
−20
210 200 190 180 170 160 150 140 130 120 110 100 90 80 70 60 50 40 30 20 10 0 −10
f1 (ppm)

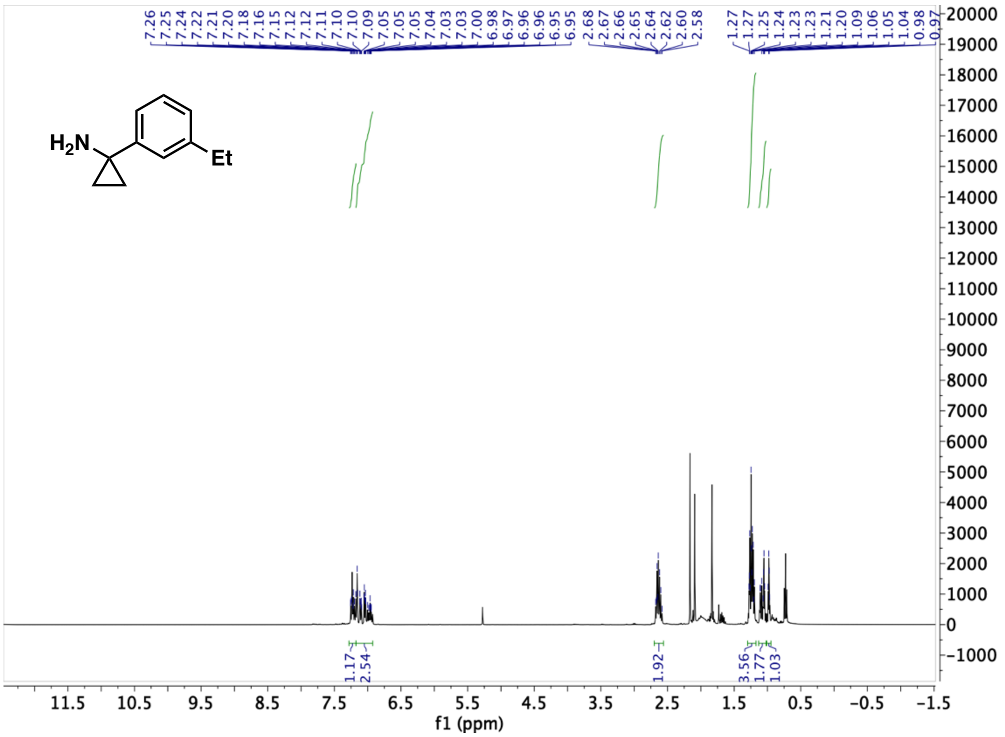
7.26
7.25
7.24
7.22
7.21
7.20
7.18
7.16
7.15
7.12
7.12
7.11
7.10
7.10
7.09
7.05
7.05
7.04
7.03
7.03
7.00
6.98
6.97
6.96
6.96
6.95
6.95
2.68
2.67
2.66
2.65
2.64
2.62
2.60
2.58
1.27
1.27
1.25
1.24
1.23
1.23
1.21
1.20
1.09
1.06
1.05
1.04
0.98
0.97
H_2N
Et
1.17
2.54
1.92
3.56
1.77
1.03
f1 (ppm)

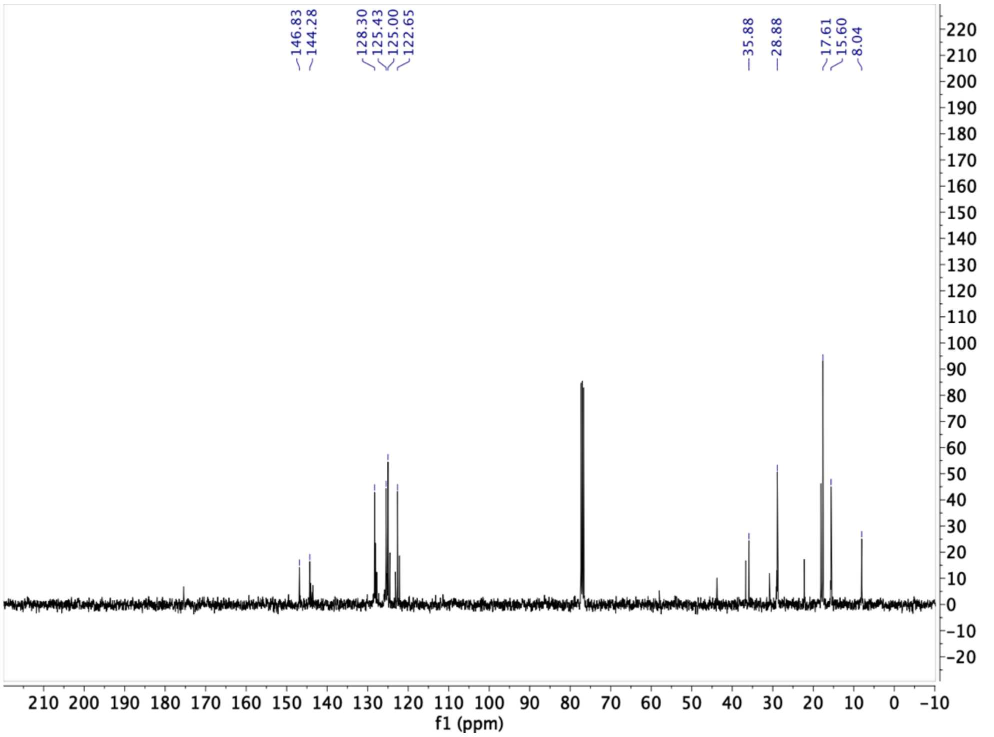
146.83
144.28
128.30
125.43
125.00
122.65
35.88
28.88
17.61
15.60
8.04
f1 (ppm)

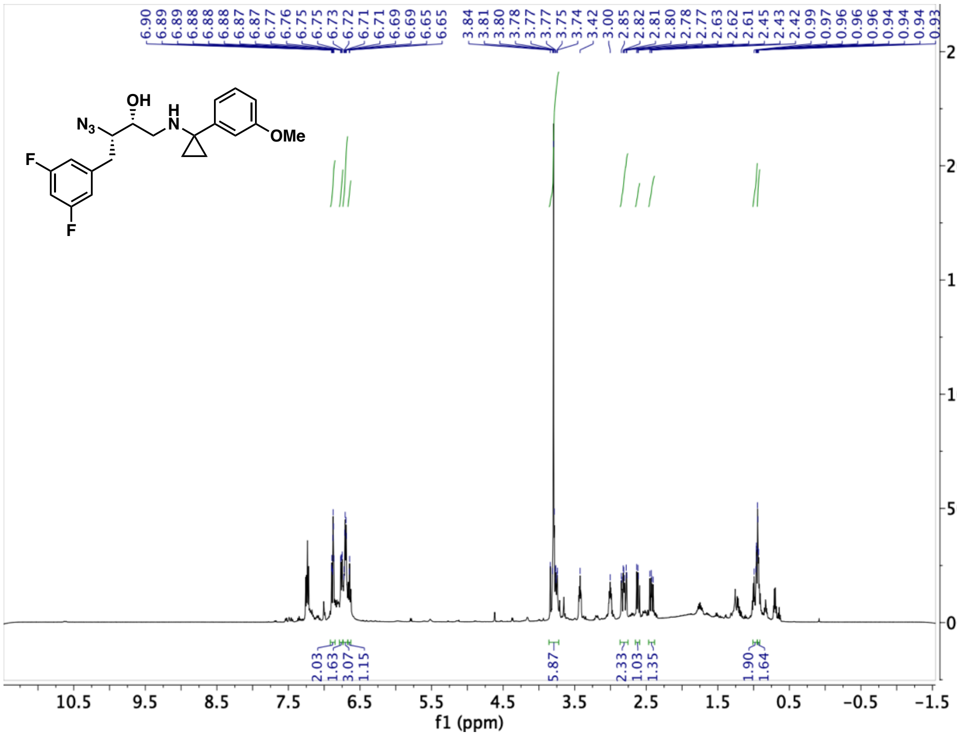
6.90
6.89
6.89
6.88
6.88
6.88
6.87
6.87
6.77
6.76
6.75
6.75
6.73
6.72
6.71
6.71
6.69
6.69
6.65
6.65
3.84
3.81
3.80
3.78
3.77
3.77
3.75
3.74
3.42
3.00
2.85
2.82
2.81
2.80
2.78
2.77
2.63
2.62
2.62
2.61
2.45
2.43
2.42
0.99
0.97
0.96
0.96
0.94
0.94
0.94
0.93
OH
N3
H
N
OMe
F
F
2.03
1.63
3.07
1.15
5.87
2.33
1.03
1.35
1.90
1.64
250
200
150
100
50
0
10.5
9.5
8.5
7.5
6.5
5.5
4.5
3.5
2.5
1.5
0.5
−0.5
−1.5
f1 (ppm)

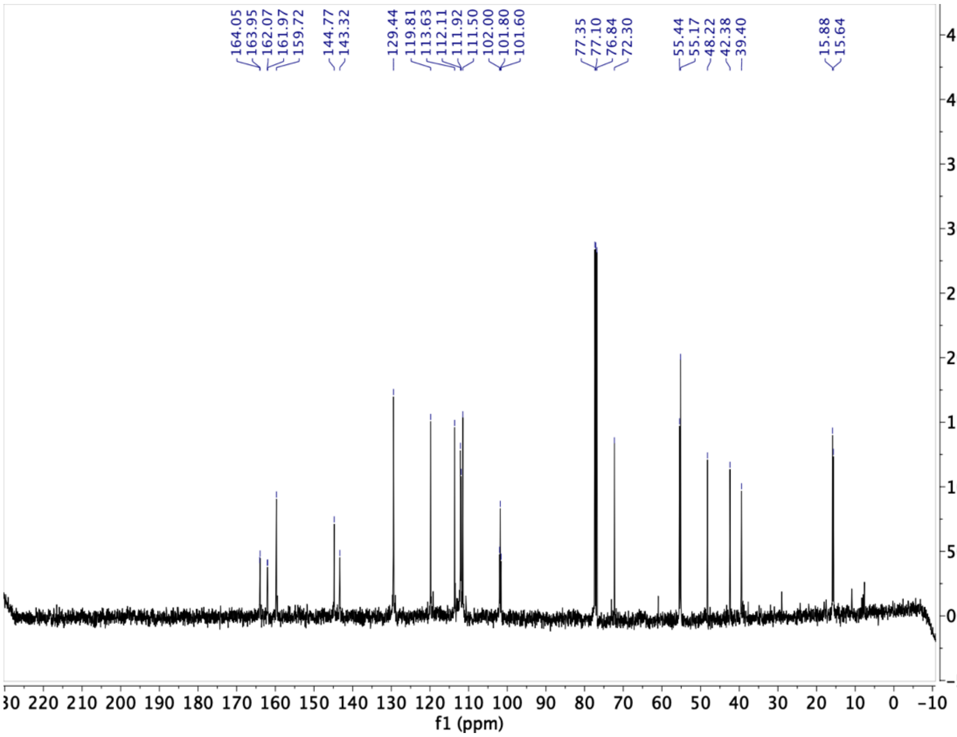
164.05
163.95
162.07
161.97
159.72
144.77
143.32
129.44
119.81
113.63
112.11
111.92
111.50
102.00
101.80
101.60
77.35
77.10
76.84
72.30
55.44
55.17
48.22
42.38
39.40
15.88
15.64
450
400
350
300
250
200
150
100
50
0
−50
30
220
210
200
190
180
170
160
150
140
130
120
110
100
90
80
70
60
50
40
30
20
10
0
−10
f1 (ppm)

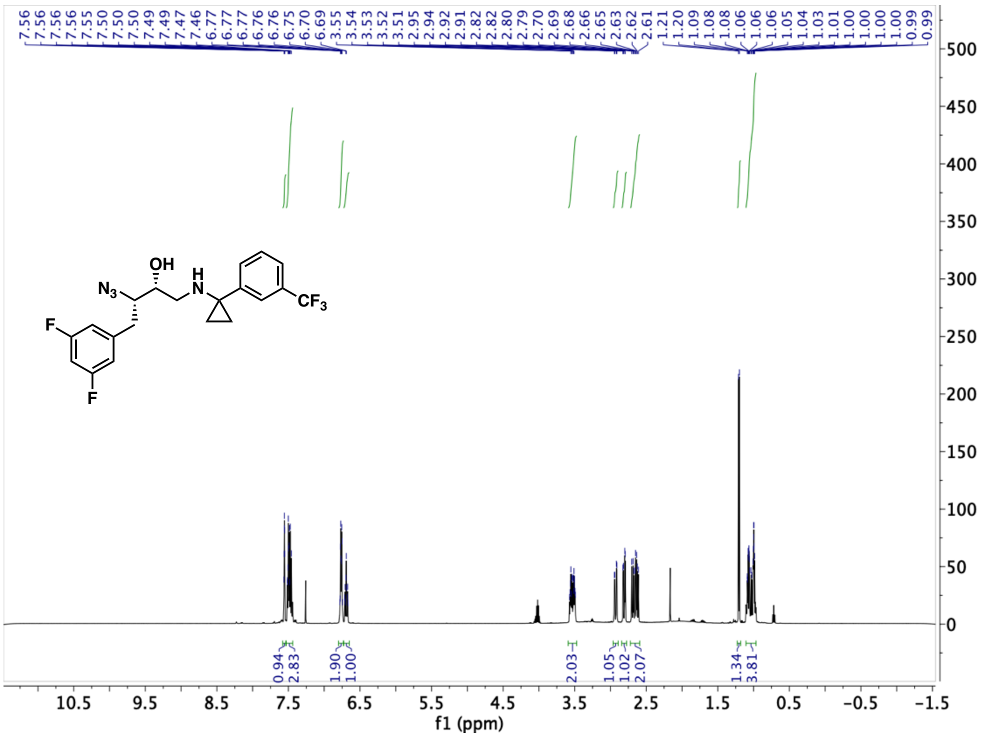
7.56
7.56
7.56
7.56
7.55
7.50
7.50
7.50
7.49
7.49
7.47
7.46
6.77
6.77
6.77
6.76
6.76
6.75
6.70
6.69
3.55
3.54
3.53
3.52
3.51
2.95
2.94
2.92
2.91
2.82
2.82
2.80
2.79
2.70
2.69
2.68
2.66
2.65
2.63
2.62
2.61
1.21
1.20
1.09
1.08
1.08
1.06
1.06
1.06
1.05
1.04
1.03
1.01
1.00
1.00
1.00
0.99
0.99
OH
N3
H
N
CF3
F
F
0.94
2.83
1.90
1.00
2.03
1.05
1.02
2.07
1.34
3.81
10.5
9.5
8.5
7.5
6.5
5.5
4.5
3.5
2.5
1.5
0.5
−0.5
−1.5
f1 (ppm)
500
450
400
350
300
250
200
150
100
50
0

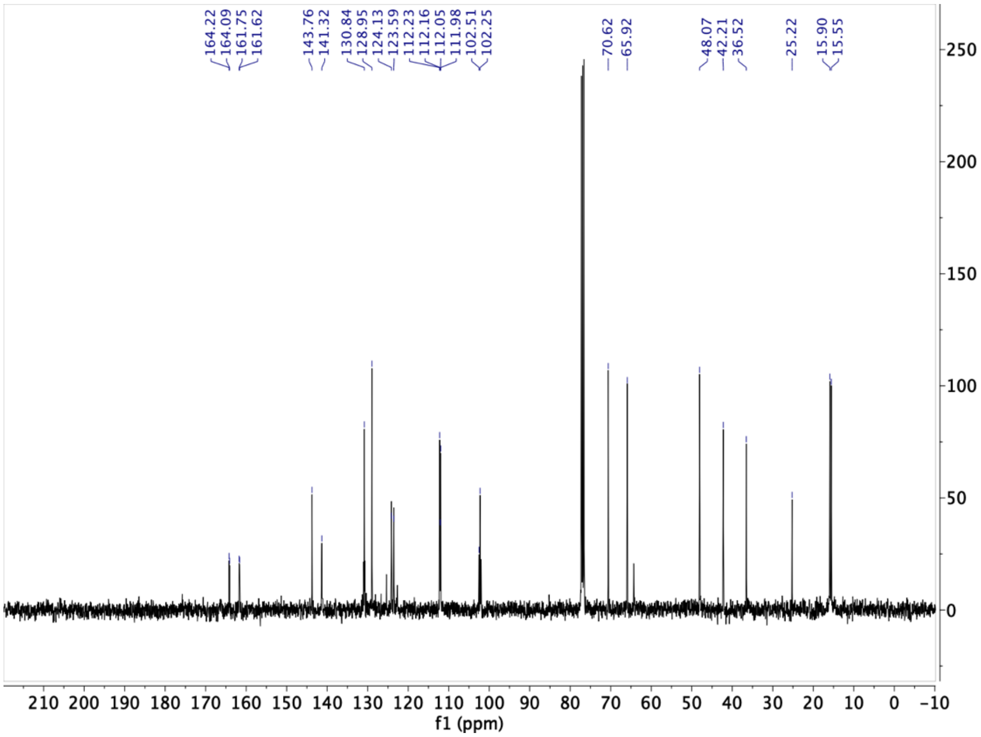
164.22
164.09
161.75
161.62
143.76
141.32
130.84
128.95
124.13
123.59
112.23
112.16
112.05
111.98
102.51
102.25
70.62
65.92
48.07
42.21
36.52
25.22
15.90
15.55
210
200
190
180
170
160
150
140
130
120
110
100
90
80
70
60
50
40
30
20
10
0
−10
f1 (ppm)
250
200
150
100
50
0

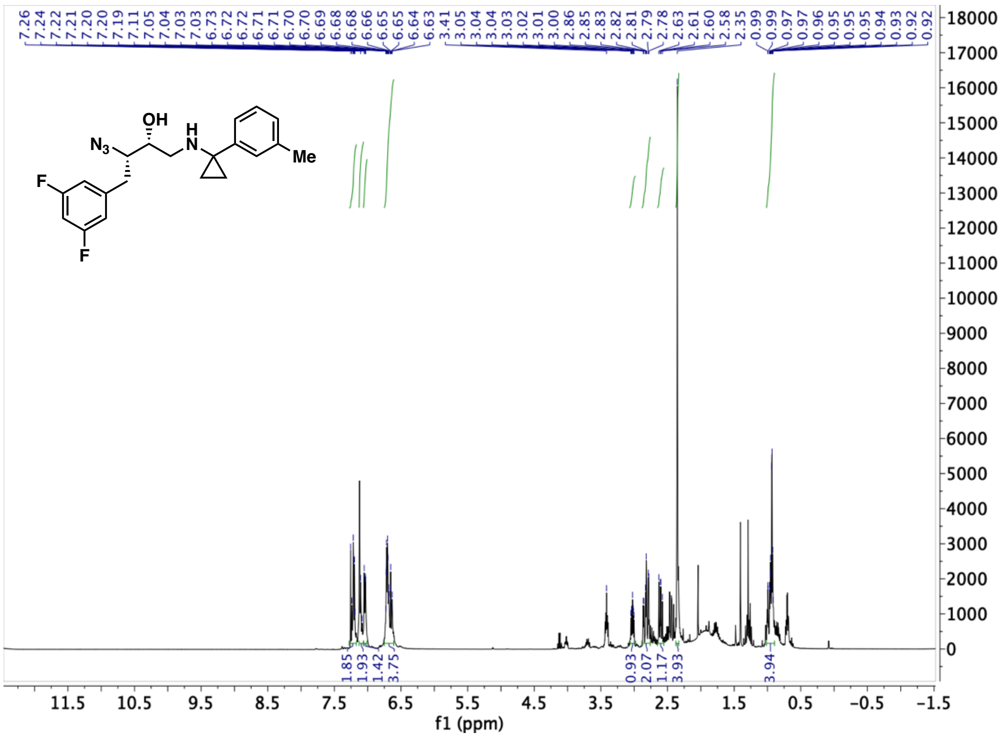
7.26
7.24
7.22
7.21
7.20
7.20
7.19
7.11
7.05
7.04
7.03
7.03
6.73
6.72
6.72
6.71
6.70
6.70
6.69
6.68
6.68
6.66
6.65
6.65
6.64
6.63
3.41
3.05
3.04
3.04
3.03
3.02
3.01
3.00
2.86
2.85
2.83
2.82
2.81
2.79
2.78
2.63
2.61
2.60
2.58
2.35
0.99
0.99
0.97
0.96
0.95
0.95
0.95
0.94
0.93
0.92
0.92
OH
H
N
N_3
F
F
Me
1.85
1.93
1.42
3.75
0.93
2.07
1.17
3.93
3.94
11.5
10.5
9.5
8.5
7.5
6.5
5.5
4.5
3.5
2.5
1.5
0.5
−0.5
−1.5
f1 (ppm)
18000
17000
16000
15000
14000
13000
12000
11000
10000
9000
8000
7000
6000
5000
4000
3000
2000
1000
0

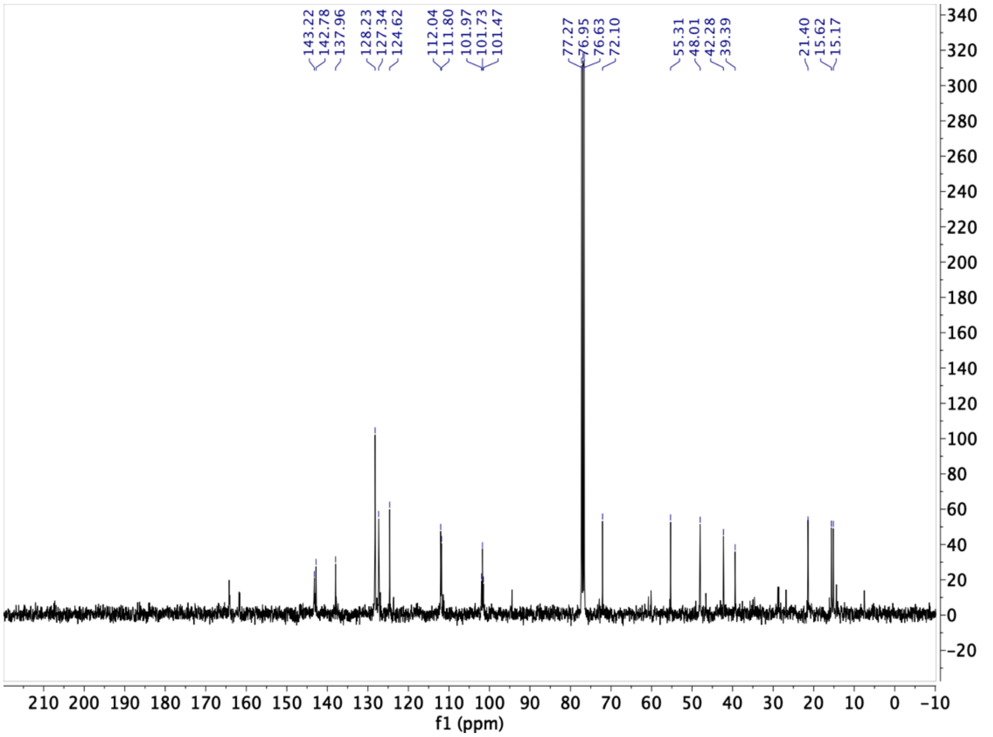
143.22
142.78
137.96
128.23
127.34
124.62
112.04
111.80
101.97
101.73
101.47
77.27
76.95
76.63
72.10
55.31
48.01
42.28
39.39
21.40
15.62
15.17
210
200
190
180
170
160
150
140
130
120
110
100
90
80
70
60
50
40
30
20
10
0
−10
f1 (ppm)
340
320
300
280
260
240
220
200
180
160
140
120
100
80
60
40
20
0
−20

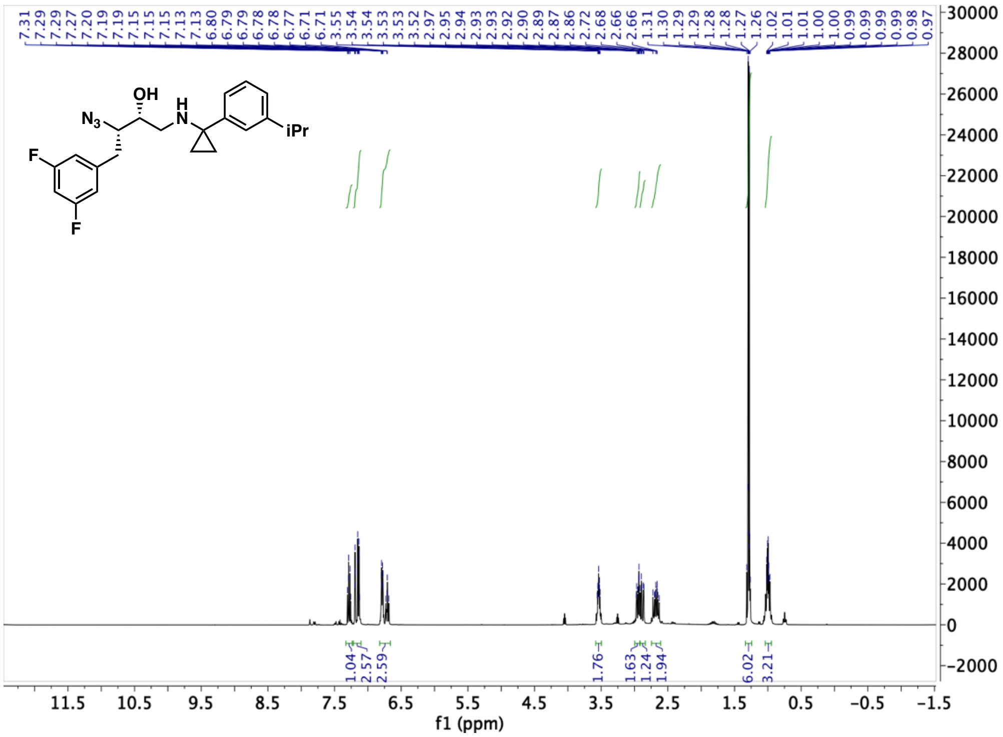
7.31
7.29
7.29
7.27
7.20
7.19
7.19
7.15
7.15
7.15
7.13
7.13
6.80
6.79
6.79
6.78
6.77
6.71
6.71
3.55
3.54
3.54
3.53
3.53
3.52
2.97
2.95
2.94
2.93
2.93
2.92
2.90
2.89
2.87
2.86
2.72
2.68
2.66
2.66
1.31
1.30
1.29
1.29
1.28
1.28
1.27
1.26
1.02
1.01
1.01
1.00
1.00
0.99
0.99
0.99
0.98
0.97
OH
H
N
N_3
iPr
F
F
1.04
2.57
2.59
1.76
1.63
1.24
1.94
6.02
3.21
30000
28000
26000
24000
22000
20000
18000
16000
14000
12000
10000
8000
6000
4000
2000
0
−2000
11.5
10.5
9.5
8.5
7.5
6.5
5.5
4.5
3.5
2.5
1.5
0.5
−0.5
−1.5
f1 (ppm)

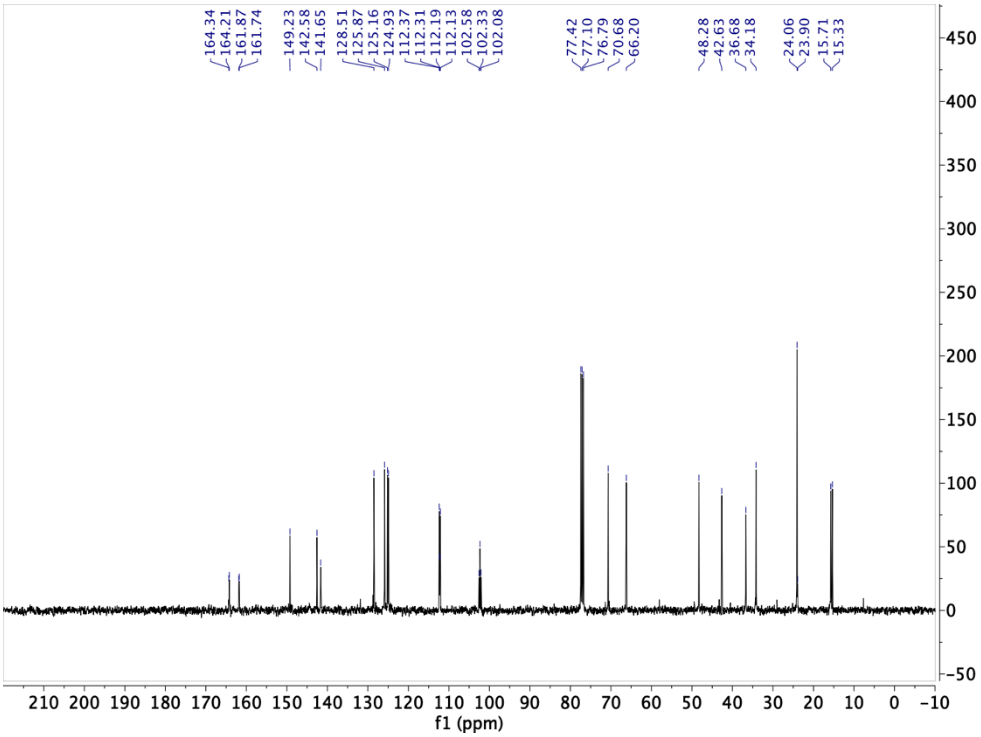
164.34
164.21
161.87
161.74
149.23
142.58
141.65
128.51
125.87
125.16
124.93
112.37
112.31
112.19
112.13
102.58
102.33
102.08
77.42
77.10
76.79
70.68
66.20
48.28
42.63
36.68
34.18
24.06
23.90
15.71
15.33
450
400
350
300
250
200
150
100
50
0
−50
210
200
190
180
170
160
150
140
130
120
110
100
90
80
70
60
50
40
30
20
10
0
−10
f1 (ppm)

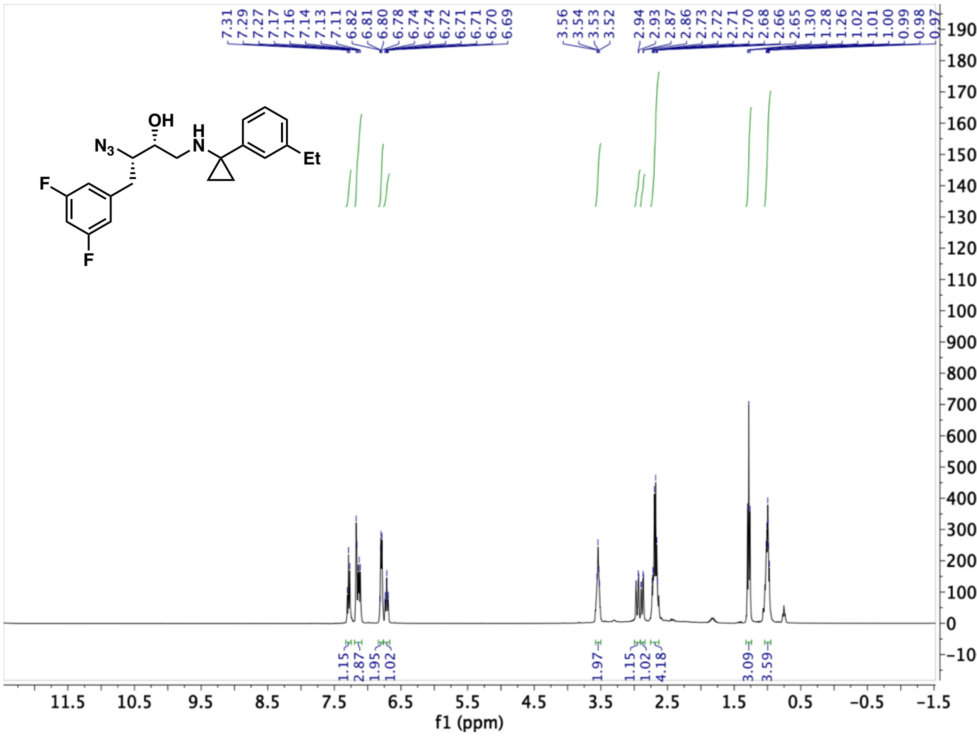
7.31
7.29
7.27
7.17
7.16
7.14
7.13
7.11
6.82
6.81
6.80
6.78
6.74
6.74
6.72
6.71
6.70
6.69
3.56
3.54
3.53
3.52
2.94
2.93
2.87
2.86
2.73
2.72
2.71
2.70
2.68
2.66
2.65
1.30
1.28
1.26
1.02
1.01
1.00
0.99
0.98
0.97
OH
H
N
N_3
Et
F
F
1.15
2.87
1.95
1.02
1.97
1.15
1.02
4.18
3.09
3.59
19000
18000
17000
16000
15000
14000
13000
12000
11000
10000
9000
8000
7000
6000
5000
4000
3000
2000
1000
0
−1000
11.5
10.5
9.5
8.5
7.5
6.5
5.5
4.5
3.5
2.5
1.5
0.5
−0.5
−1.5
f1 (ppm)

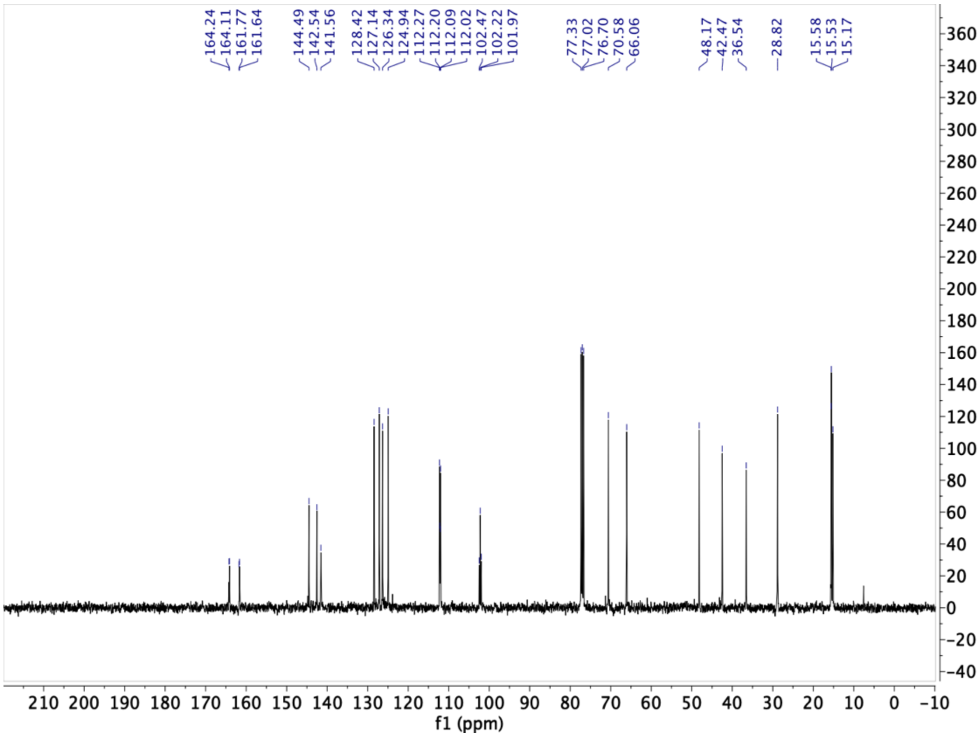
164.24
164.11
161.77
161.64
144.49
142.54
141.56
128.42
127.14
126.34
124.94
112.27
112.20
112.09
112.02
102.47
102.22
101.97
77.33
77.02
76.70
70.58
66.06
48.17
42.47
36.54
28.82
15.58
15.53
15.17
360
340
320
300
280
260
240
220
200
180
160
140
120
100
80
60
40
20
0
−20
−40
210
200
190
180
170
160
150
140
130
120
110
100
90
80
70
60
50
40
30
20
10
0
−10
f1 (ppm)

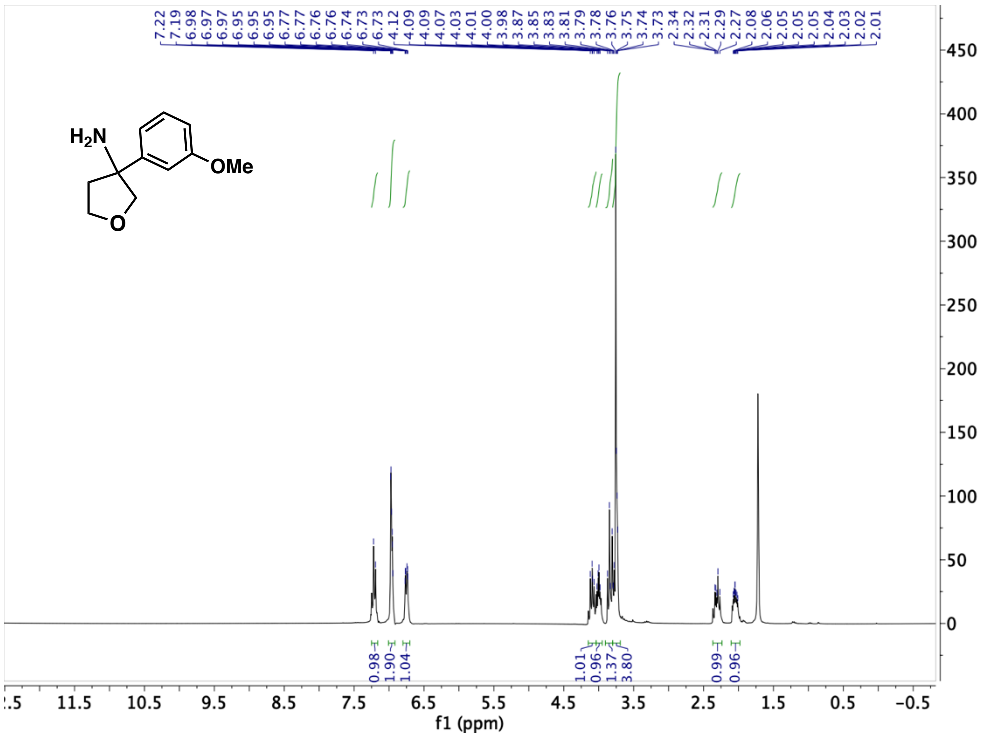
7.22
7.19
6.98
6.97
6.97
6.95
6.95
6.95
6.77
6.77
6.76
6.76
6.74
6.73
6.73
4.12
4.09
4.09
4.07
4.03
4.01
4.00
3.98
3.87
3.85
3.83
3.81
3.79
3.78
3.76
3.75
3.74
3.73
2.34
2.32
2.31
2.29
2.27
2.08
2.06
2.05
2.05
2.05
2.04
2.03
2.02
2.01
H_2N
OMe
O
0.98
1.90
1.04
1.01
0.96
1.37
3.80
0.99
0.96
450
400
350
300
250
200
150
100
50
0
12.5
11.5
10.5
9.5
8.5
7.5
6.5
5.5
4.5
3.5
2.5
1.5
0.5
−0.5
f1 (ppm)

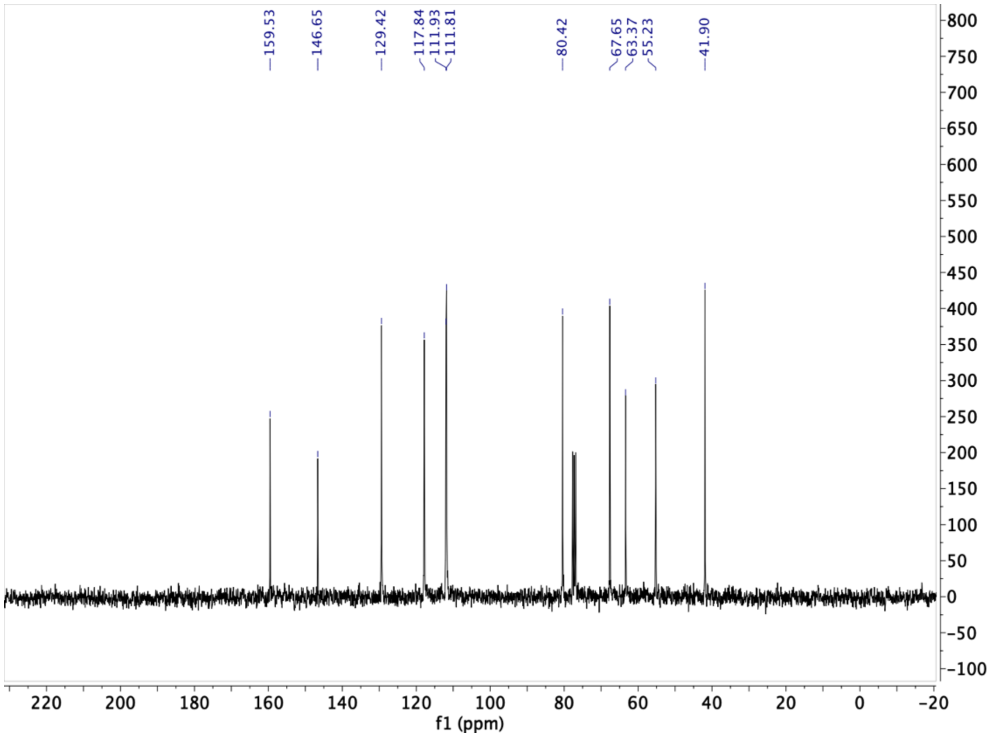
159.53
146.65
129.42
117.84
111.93
111.81
80.42
67.65
63.37
55.23
41.90
800
750
700
650
600
550
500
450
400
350
300
250
200
150
100
50
0
−50
−100
220
200
180
160
140
120
100
80
60
40
20
0
−20
f1 (ppm)

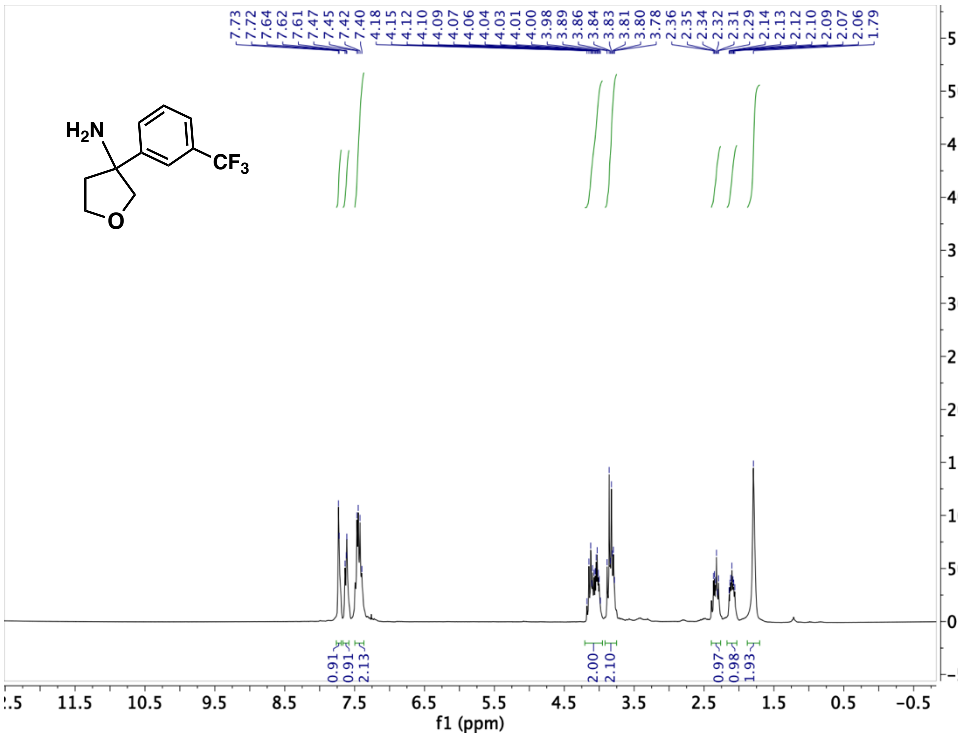
7.73
7.72
7.64
7.62
7.61
7.47
7.45
7.42
7.40
4.18
4.15
4.12
4.10
4.09
4.07
4.06
4.04
4.03
4.01
4.00
3.98
3.89
3.86
3.84
3.83
3.81
3.80
3.78
2.36
2.35
2.34
2.32
2.31
2.29
2.14
2.13
2.12
2.10
2.09
2.07
2.06
1.79
H2N
CF3
O
0.91
0.91
2.13
2.00
2.10
0.97
0.98
1.93
550
500
450
400
350
300
250
200
150
100
50
0
-50
11.5
10.5
9.5
8.5
7.5
6.5
5.5
4.5
3.5
2.5
1.5
0.5
-0.5
f1 (ppm)

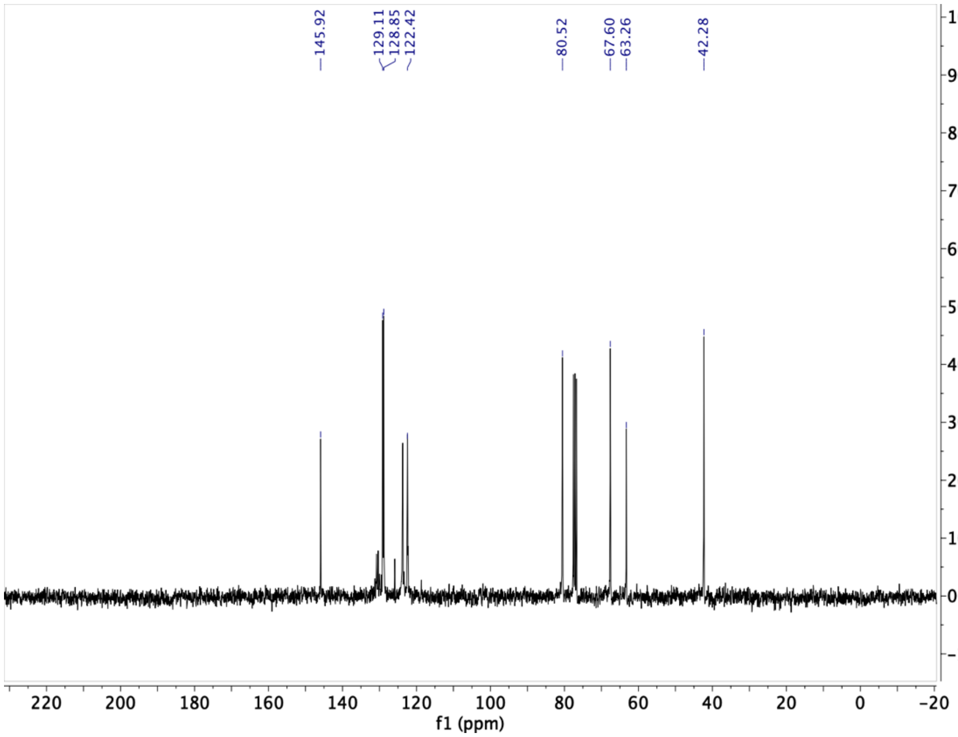
145.92
129.11
128.85
122.42
80.52
67.60
63.26
42.28
1000
900
800
700
600
500
400
300
200
100
0
-100
220
200
180
160
140
120
100
80
60
40
20
0
-20
f1 (ppm)

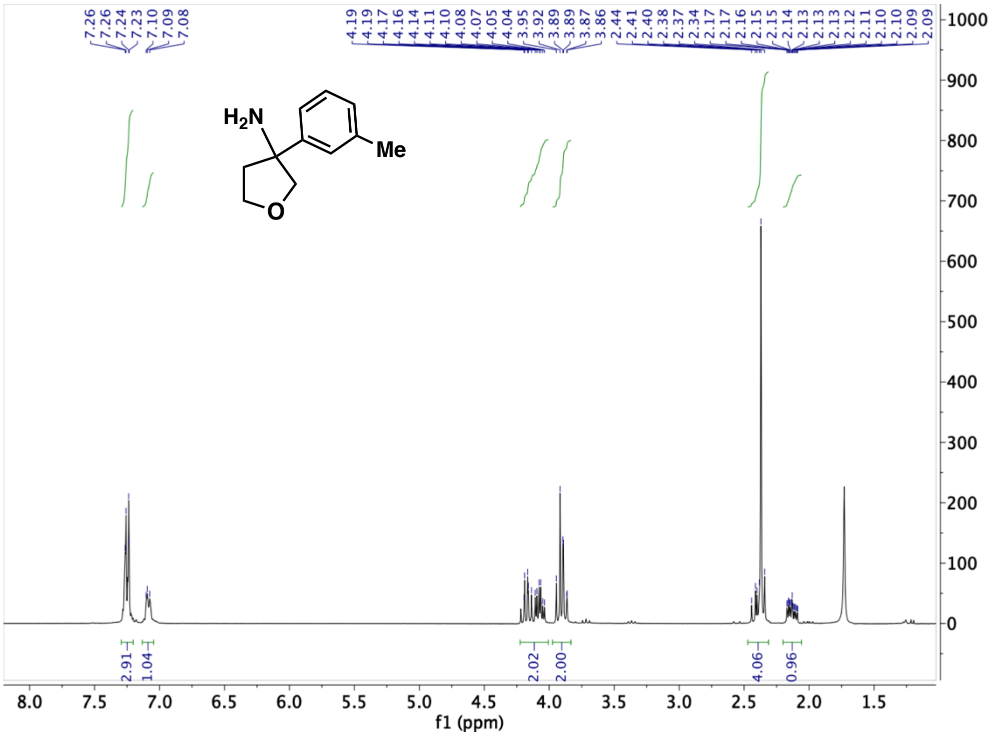
7.26
7.26
7.24
7.23
7.10
7.09
7.08
4.19
4.19
4.17
4.16
4.14
4.11
4.10
4.08
4.07
4.05
4.04
3.95
3.92
3.89
3.89
3.87
3.86
2.44
2.41
2.40
2.38
2.37
2.34
2.17
2.17
2.16
2.15
2.15
2.14
2.13
2.13
2.13
2.12
2.11
2.10
2.09
2.09
H_2N
Me
O
2.91
1.04
2.02
2.00
4.06
0.96
8.0
7.5
7.0
6.5
6.0
5.5
5.0
4.5
4.0
3.5
3.0
2.5
2.0
1.5
f1 (ppm)
1000
900
800
700
600
500
400
300
200
100
0

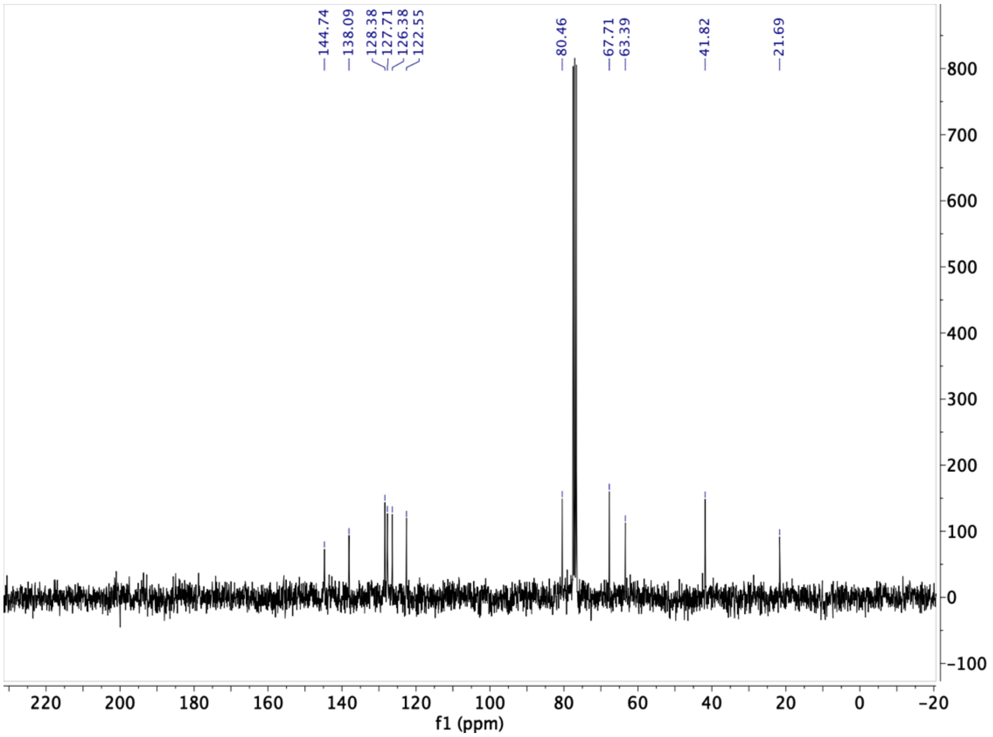
144.74
138.09
128.38
127.71
126.38
122.55
80.46
67.71
63.39
41.82
21.69
220
200
180
160
140
120
100
80
60
40
20
0
−20
f1 (ppm)
800
700
600
500
400
300
200
100
0
−100

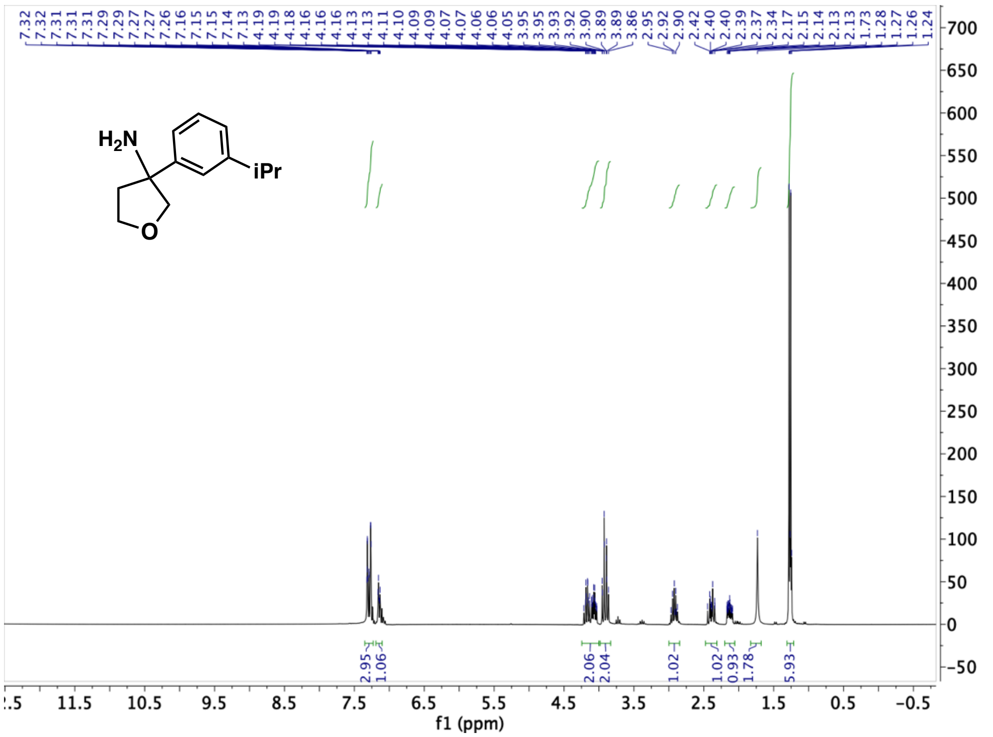
7.32
7.32
7.31
7.31
7.31
7.29
7.27
7.27
7.26
7.16
7.15
7.15
7.14
7.13
4.19
4.19
4.18
4.16
4.16
4.16
4.13
4.13
4.11
4.10
4.09
4.09
4.07
4.07
4.06
4.05
3.95
3.95
3.93
3.92
3.90
3.89
3.89
3.86
2.95
2.92
2.90
2.42
2.40
2.40
2.39
2.37
2.34
2.17
2.15
2.14
2.13
2.13
1.73
1.28
1.27
1.26
1.24
H2N
iPr
O
2.95
1.06
2.06
2.04
1.02
1.02
0.93
1.78
5.93
12.5
11.5
10.5
9.5
8.5
7.5
6.5
5.5
4.5
3.5
2.5
1.5
0.5
−0.5
f1 (ppm)
700
650
600
550
500
450
400
350
300
250
200
150
100
50
0
−50

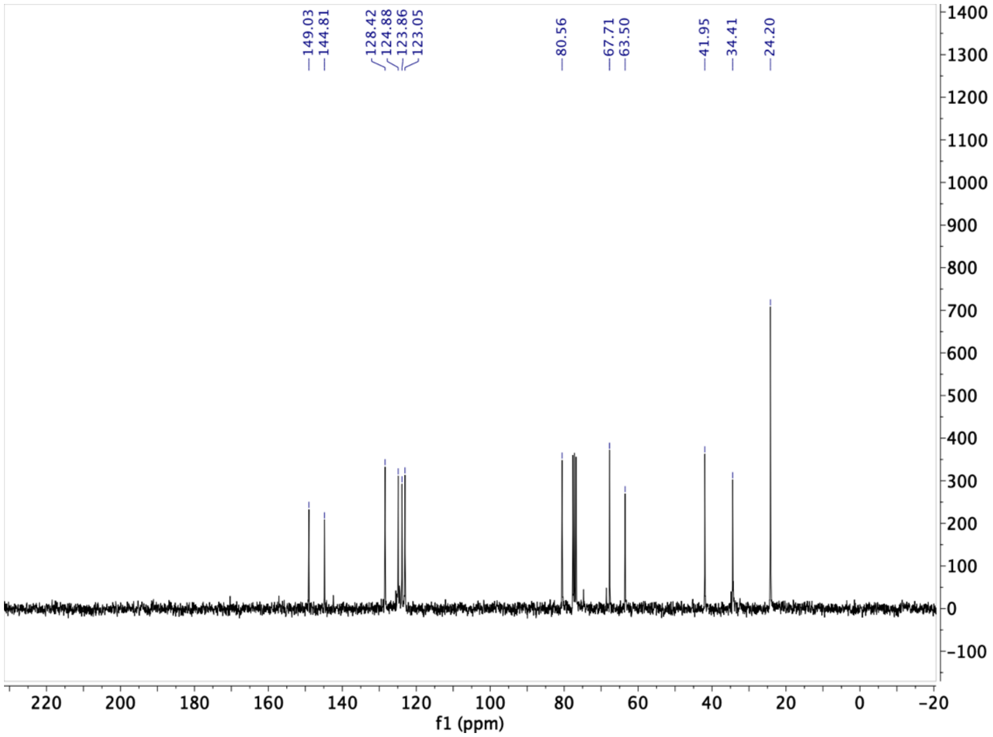
149.03
144.81
128.42
124.88
123.86
123.05
80.56
67.71
63.50
41.95
34.41
24.20
220
200
180
160
140
120
100
80
60
40
20
0
−20
f1 (ppm)
1400
1300
1200
1100
1000
900
800
700
600
500
400
300
200
100
0
−100

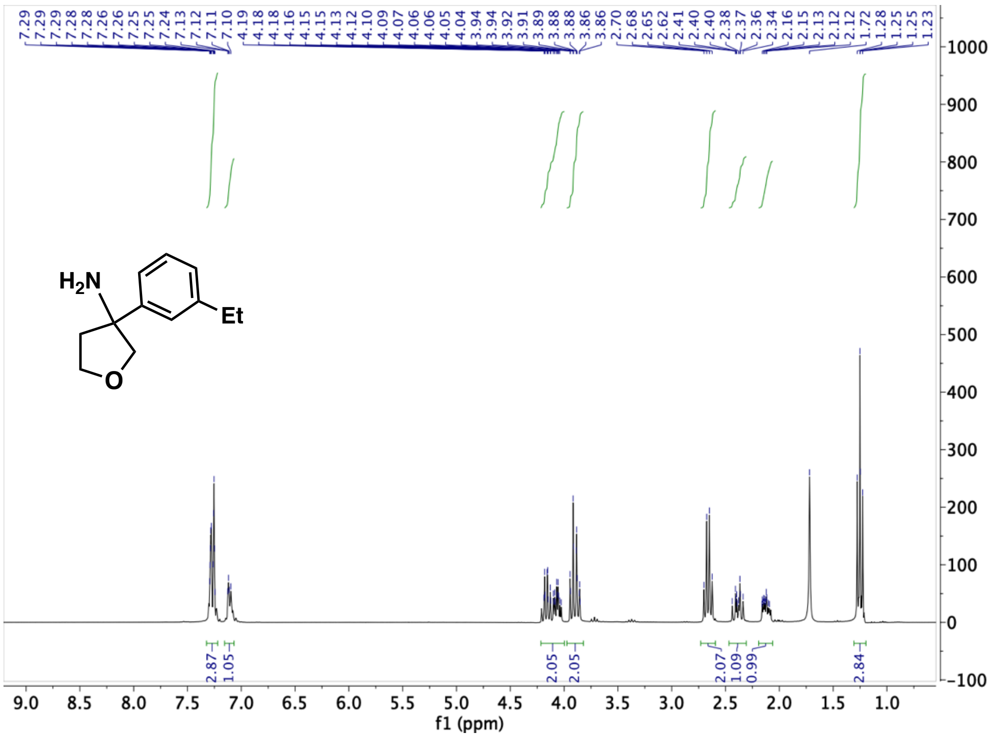
7.29
7.29
7.29
7.28
7.28
7.26
7.25
7.25
7.24
7.13
7.12
7.11
7.10
4.19
4.18
4.18
4.16
4.15
4.15
4.13
4.12
4.10
4.09
4.07
4.06
4.06
4.05
4.04
3.94
3.94
3.92
3.91
3.89
3.88
3.88
3.86
2.70
2.68
2.65
2.62
2.41
2.40
2.38
2.37
2.36
2.34
2.16
2.15
2.13
2.12
2.12
2.12
1.72
1.28
1.25
1.25
1.23
H2N
Et
O
2.87
1.05
2.05
2.05
2.07
1.09
0.99
2.84
9.0
8.5
8.0
7.5
7.0
6.5
6.0
5.5
5.0
4.5
4.0
3.5
3.0
2.5
2.0
1.5
1.0
f1 (ppm)
1000
900
800
700
600
500
400
300
200
100
0
-100

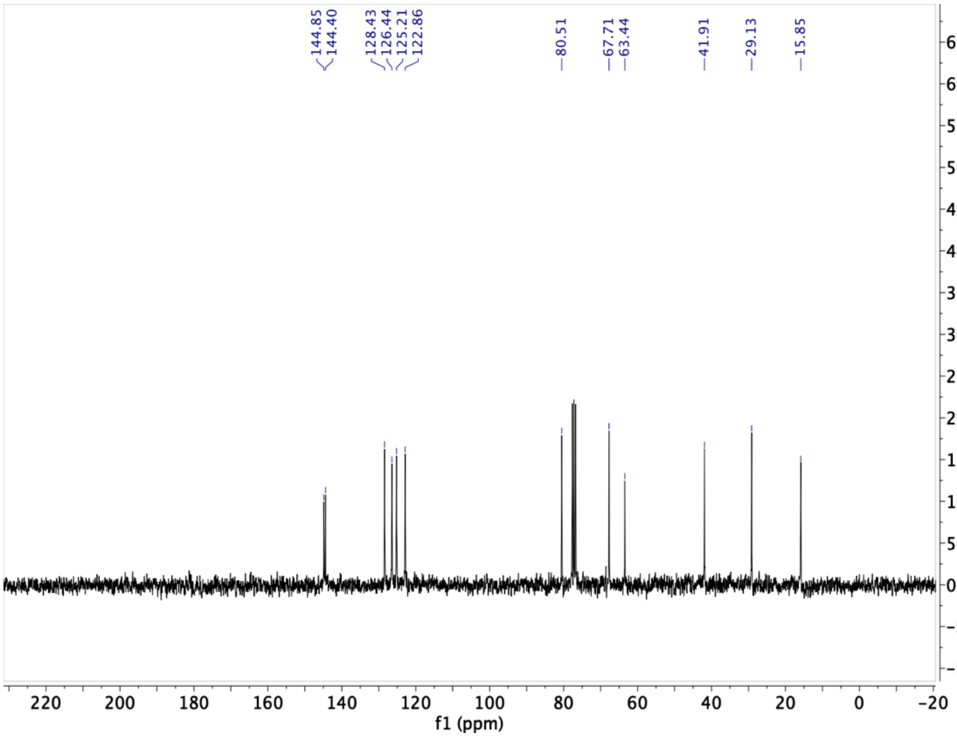
144.85
144.40
128.43
126.44
125.21
122.86
80.51
67.71
63.44
41.91
29.13
15.85
220
200
180
160
140
120
100
80
60
40
20
0
-20
f1 (ppm)
650
600
550
500
450
400
350
300
250
200
150
100
50
0
-50
-100

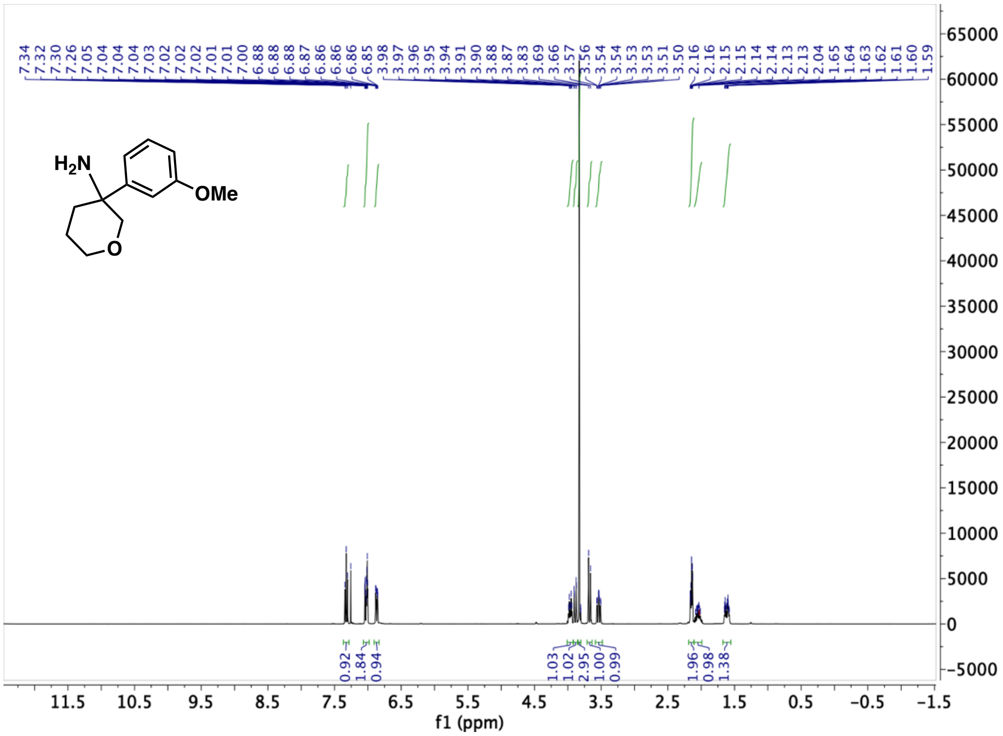
7.34 7.32 7.30 7.26 7.05 7.04 7.04 7.03 7.02 7.02 7.02 7.01 7.01 7.00 6.88 6.88 6.87 6.86 6.86 6.86 6.85 3.98 3.97 3.96 3.95 3.94 3.91 3.90 3.88 3.87 3.83 3.69 3.66 3.57 3.56 3.54 3.54 3.53 3.53 3.51 3.50 2.16 2.16 2.15 2.15 2.14 2.14 2.13 2.13 2.04 1.65 1.64 1.63 1.62 1.61 1.60 1.59
H2N
OMe
O
0.92 1.84 0.94
1.03 1.02 2.95 1.00 0.99
1.96 0.98 1.38
65000 60000 55000 50000 45000 40000 35000 30000 25000 20000 15000 10000 5000 0 -5000
11.5 10.5 9.5 8.5 7.5 6.5 5.5 4.5 3.5 2.5 1.5 0.5 -0.5 -1.5
f1 (ppm)

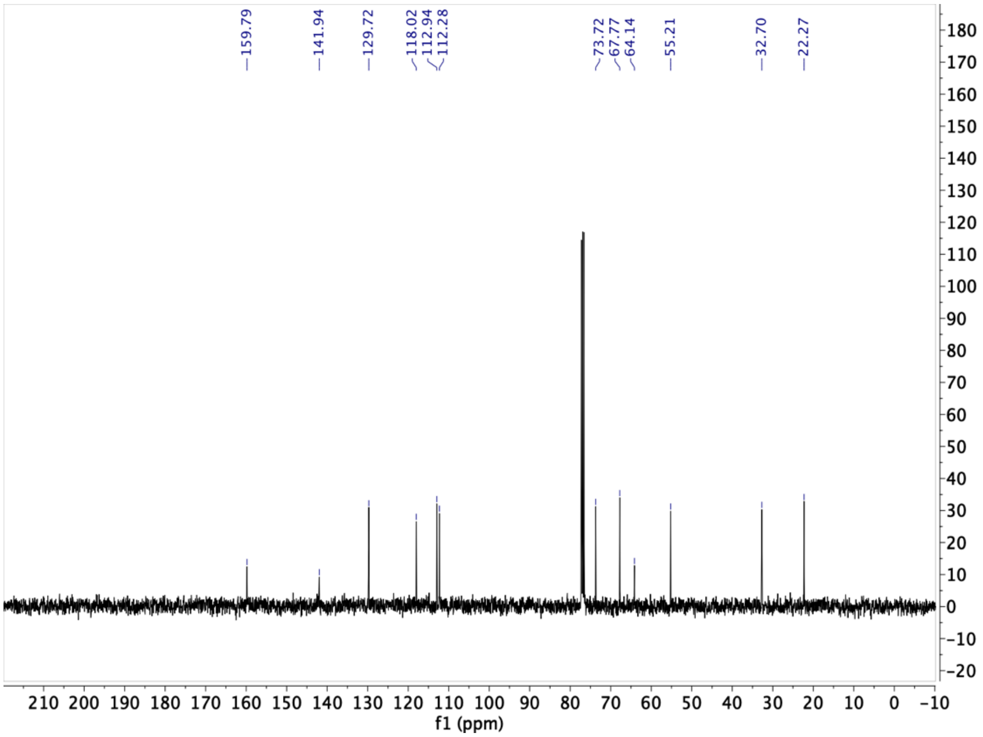
159.79
141.94
129.72
118.02 112.94 112.28
73.72 67.77 64.14
55.21
32.70
22.27
180 170 160 150 140 130 120 110 100 90 80 70 60 50 40 30 20 10 0 -10 -20
210 200 190 180 170 160 150 140 130 120 110 100 90 80 70 60 50 40 30 20 10 0 -10
f1 (ppm)

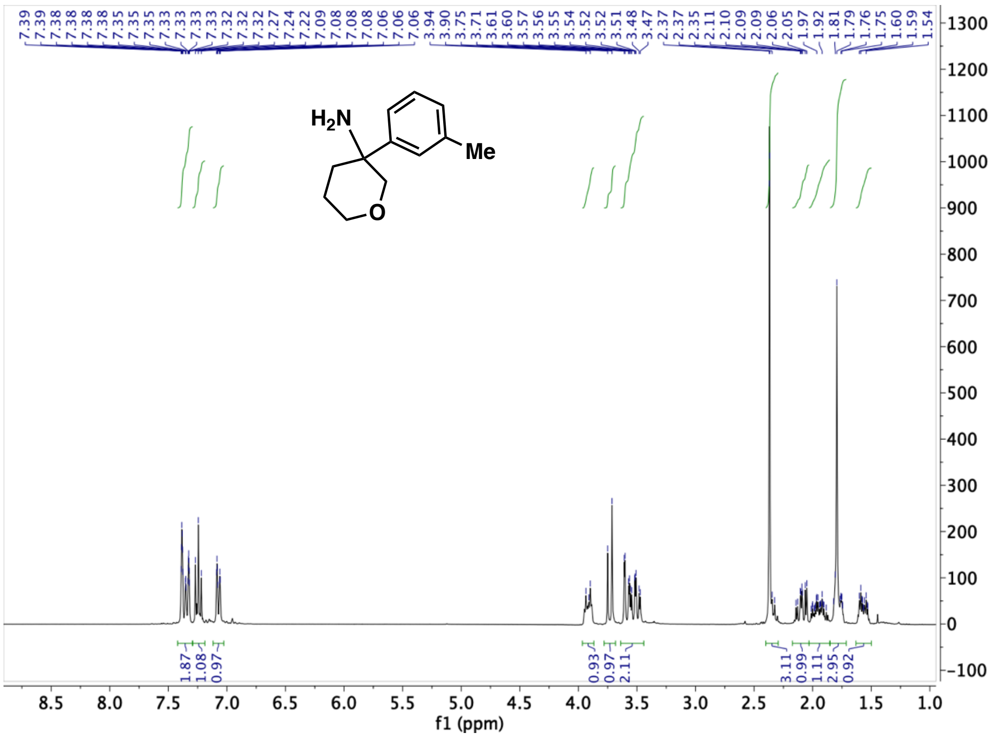
7.39
7.39
7.38
7.38
7.38
7.38
7.35
7.35
7.33
7.33
7.33
7.33
7.32
7.32
7.32
7.27
7.24
7.22
7.09
7.08
7.08
7.06
7.06
7.06
3.94
3.90
3.75
3.71
3.61
3.60
3.57
3.56
3.55
3.54
3.52
3.52
3.51
3.48
3.47
2.37
2.37
2.35
2.11
2.10
2.09
2.09
2.06
2.05
1.97
1.92
1.81
1.79
1.76
1.75
1.60
1.59
1.54
H2N
Me
O
1.87
1.08
0.97
0.93
0.97
2.11
3.11
0.99
1.11
2.95
0.92
1300
1200
1100
1000
900
800
700
600
500
400
300
200
100
0
-100
8.5
8.0
7.5
7.0
6.5
6.0
5.5
5.0
4.5
4.0
3.5
3.0
2.5
2.0
1.5
1.0
f1 (ppm)

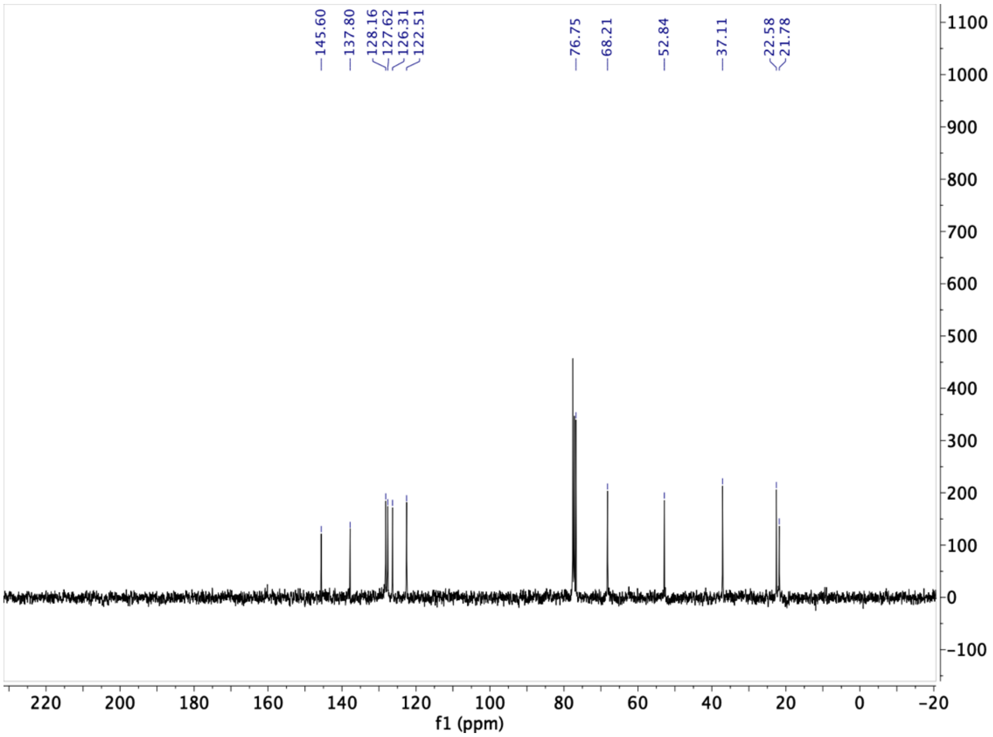
145.60
137.80
128.16
127.62
126.31
122.51
76.75
68.21
52.84
37.11
22.58
21.78
1100
1000
900
800
700
600
500
400
300
200
100
0
-100
220
200
180
160
140
120
100
80
60
40
20
0
-20
f1 (ppm)

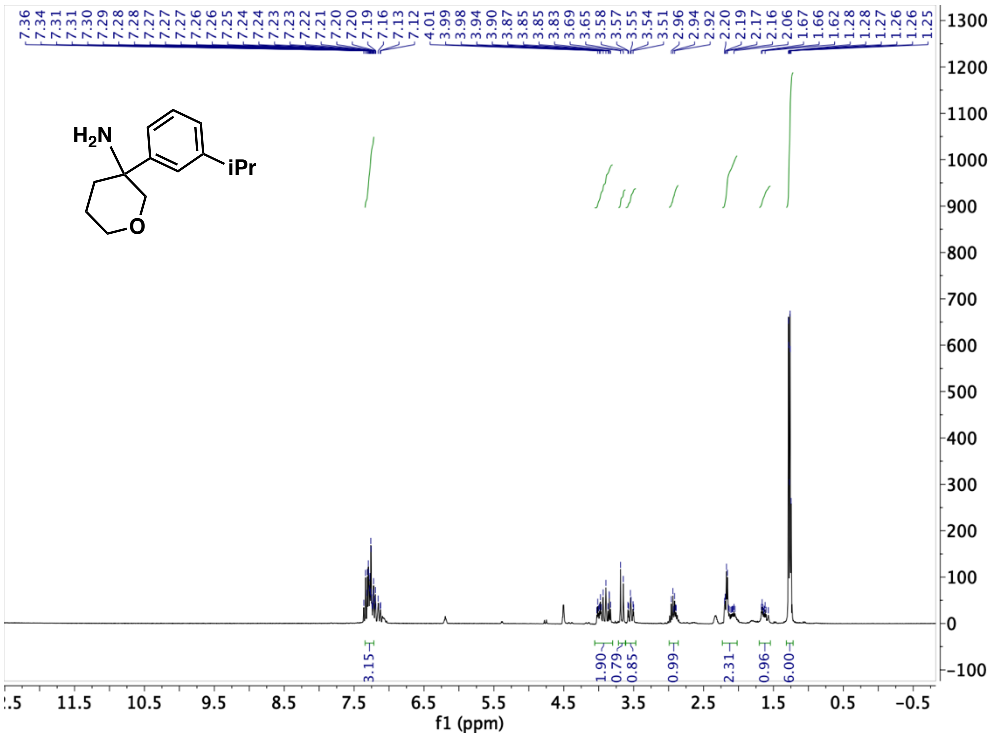
7.36
7.34
7.31
7.30
7.29
7.28
7.28
7.27
7.27
7.27
7.26
7.26
7.25
7.24
7.24
7.23
7.23
7.22
7.21
7.20
7.20
7.19
7.16
7.13
7.12
4.01
3.99
3.98
3.94
3.90
3.87
3.85
3.85
3.83
3.69
3.65
3.58
3.57
3.55
3.54
3.51
2.96
2.94
2.92
2.20
2.19
2.17
2.16
2.06
1.67
1.66
1.62
1.28
1.28
1.27
1.26
1.25
H2N
iPr
O
3.15
1.90
0.79
0.85
0.99
2.31
0.96
6.00
f1 (ppm)
12.5
11.5
10.5
9.5
8.5
7.5
6.5
5.5
4.5
3.5
2.5
1.5
0.5
-0.5
1300
1200
1100
1000
900
800
700
600
500
400
300
200
100
0
-100

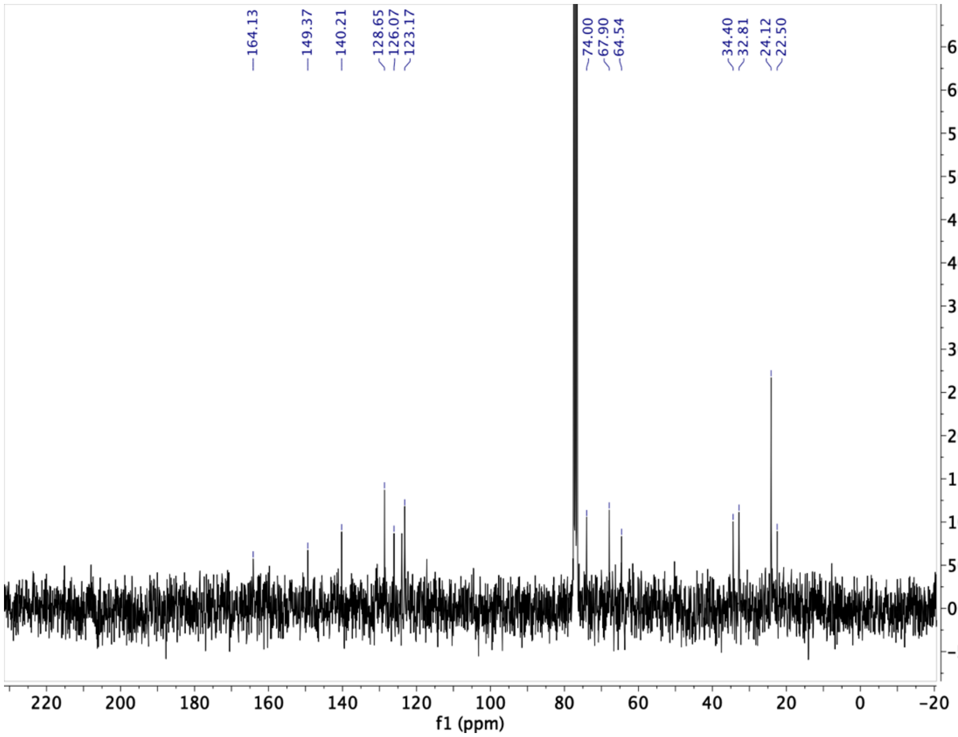
164.13
149.37
140.21
128.65
126.07
123.17
74.00
67.90
64.54
34.40
32.81
24.12
22.50
f1 (ppm)
220
200
180
160
140
120
100
80
60
40
20
0
-20
650
600
550
500
450
400
350
300
250
200
150
100
50
0
-50

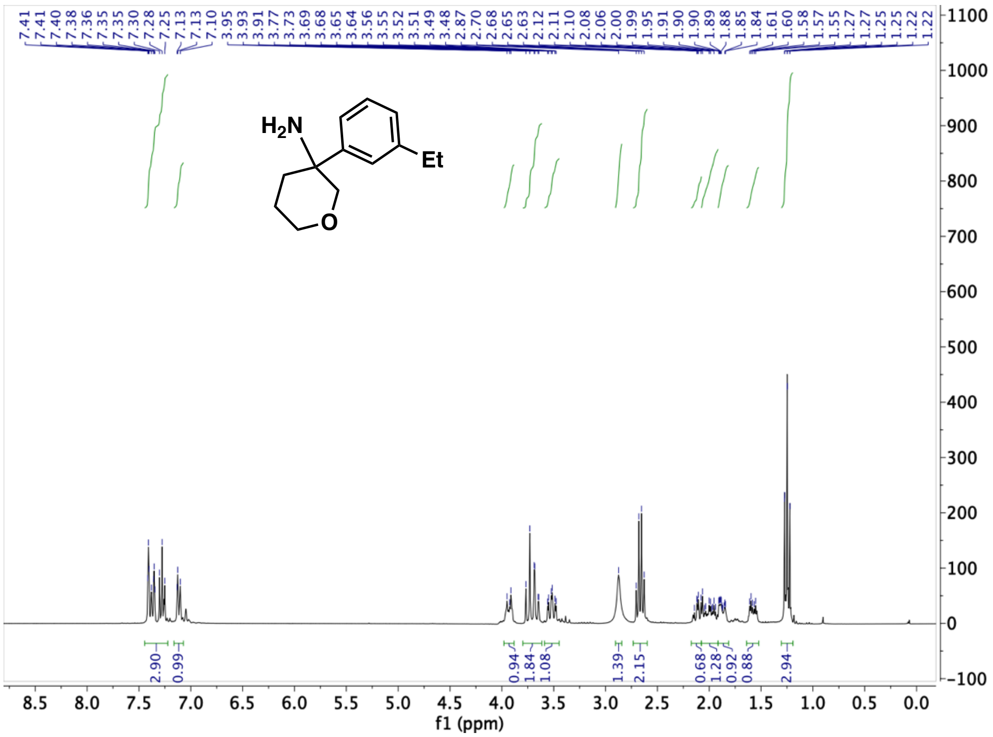
7.41
7.41
7.40
7.38
7.36
7.35
7.35
7.30
7.28
7.25
7.13
7.13
7.10
3.95
3.93
3.91
3.77
3.73
3.69
3.68
3.65
3.64
3.56
3.55
3.52
3.51
3.49
3.48
2.87
2.70
2.68
2.65
2.63
2.12
2.11
2.10
2.08
2.06
2.00
1.99
1.95
1.91
1.90
1.90
1.89
1.88
1.85
1.84
1.61
1.60
1.58
1.57
1.55
1.27
1.27
1.25
1.22
1.22
H2N
Et
O
2.90
0.99
0.94
1.84
1.08
1.39
2.15
0.68
1.28
0.92
0.88
2.94
8.5
8.0
7.5
7.0
6.5
6.0
5.5
5.0
4.5
4.0
3.5
3.0
2.5
2.0
1.5
1.0
0.5
0.0
f1 (ppm)
1100
1000
900
800
700
600
500
400
300
200
100
0
-100

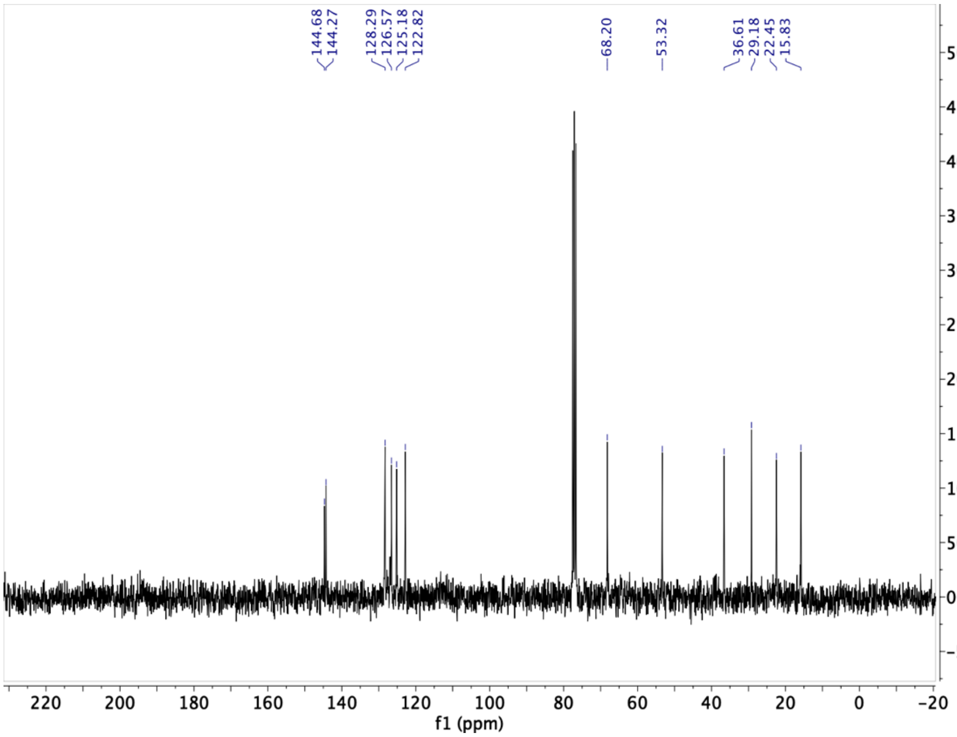
144.68
144.27
128.29
126.57
125.18
122.82
68.20
53.32
36.61
29.18
22.45
15.83
220
200
180
160
140
120
100
80
60
40
20
0
-20
f1 (ppm)
500
450
400
350
300
250
200
150
100
50
0
-50

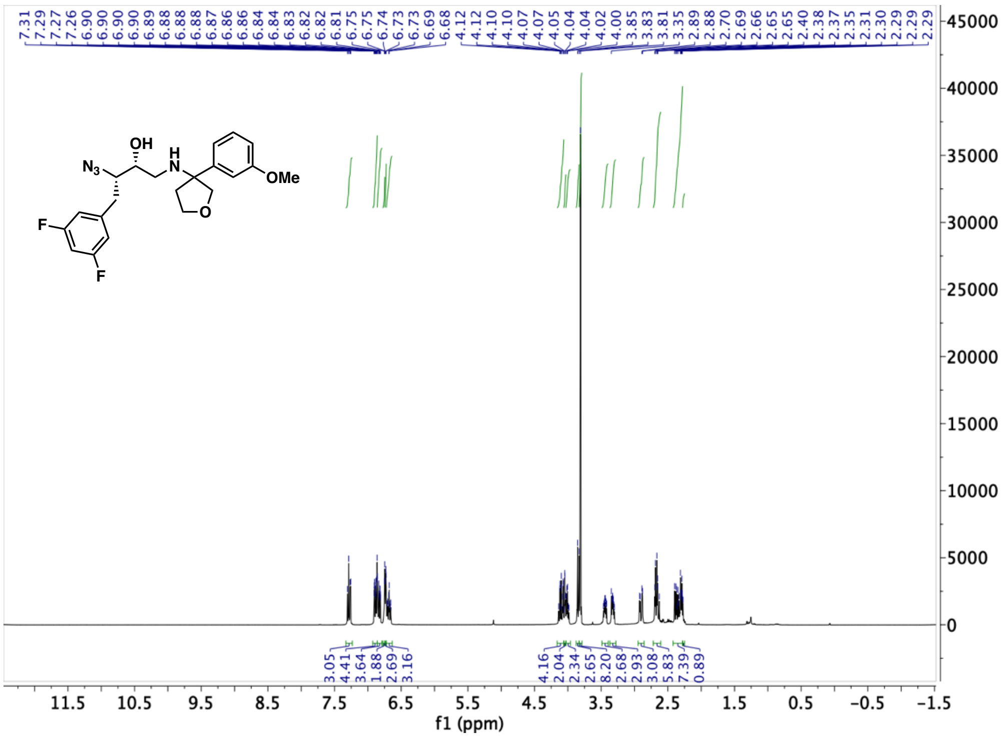
7.31
7.29
7.27
7.26
6.90
6.90
6.90
6.89
6.88
6.88
6.88
6.87
6.86
6.86
6.84
6.84
6.83
6.82
6.82
6.81
6.75
6.74
6.73
6.69
6.68
4.12
4.12
4.10
4.10
4.07
4.05
4.04
4.04
4.02
4.00
3.85
3.83
3.81
3.35
2.89
2.88
2.70
2.69
2.66
2.65
2.65
2.40
2.38
2.37
2.35
2.31
2.30
2.29
2.29
2.29
OH
N3
H
N
OMe
O
F
F
45000
40000
35000
30000
25000
20000
15000
10000
5000
0
3.05
4.41
3.64
1.88
2.69
3.16
4.16
2.04
2.34
2.65
8.20
2.68
2.93
3.08
5.83
7.39
0.89
11.5
10.5
9.5
8.5
7.5
6.5
5.5
4.5
3.5
2.5
1.5
0.5
−0.5
−1.5
f1 (ppm)

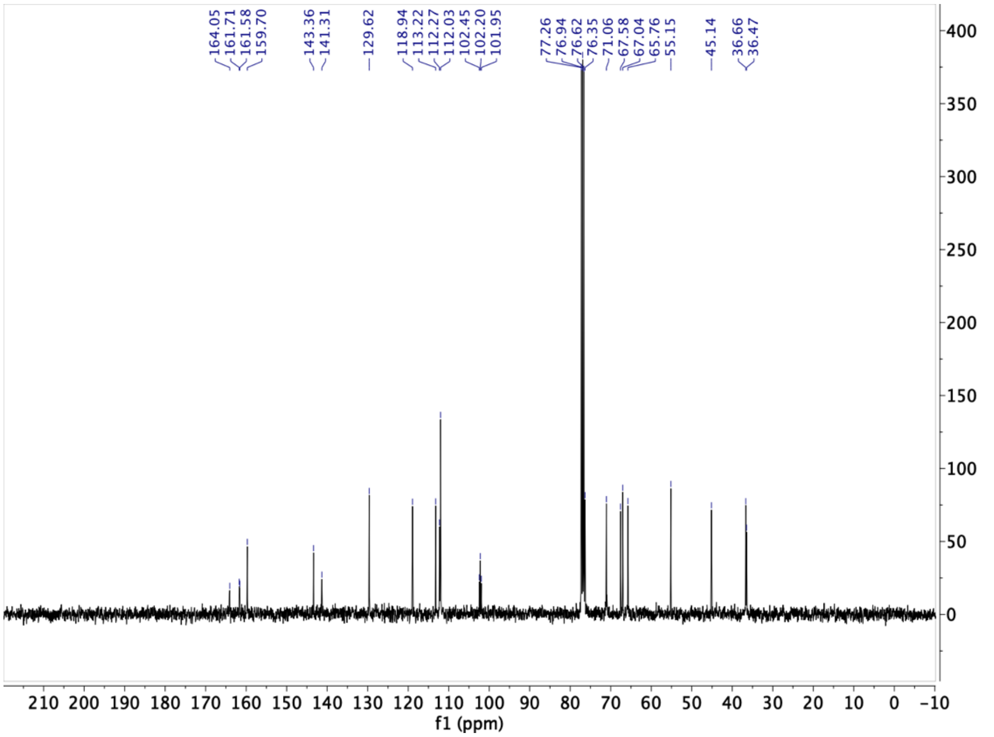
164.05
161.71
161.58
159.70
143.36
141.31
129.62
118.94
113.22
112.27
112.03
102.45
102.20
101.95
77.26
76.94
76.62
76.35
71.06
67.58
67.04
65.76
55.15
45.14
36.66
36.47
400
350
300
250
200
150
100
50
0
210
200
190
180
170
160
150
140
130
120
110
100
90
80
70
60
50
40
30
20
10
0
−10
f1 (ppm)

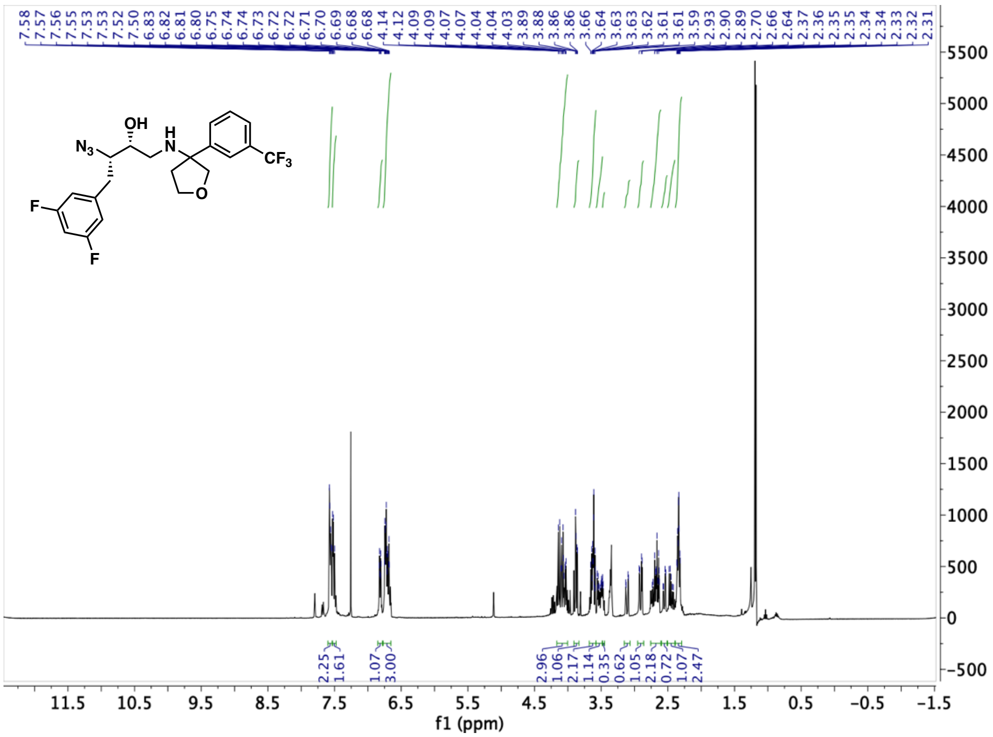
7.58
7.57
7.56
7.55
7.53
7.53
7.52
7.50
6.83
6.82
6.81
6.80
6.75
6.74
6.74
6.73
6.72
6.72
6.71
6.70
6.69
6.68
6.68
4.14
4.12
4.09
4.09
4.07
4.07
4.04
4.04
4.03
3.89
3.88
3.86
3.86
3.66
3.64
3.63
3.63
3.62
3.61
3.61
3.59
2.93
2.90
2.89
2.70
2.66
2.64
2.37
2.36
2.35
2.35
2.34
2.33
2.32
2.31
OH
H
N
N_3
CF_3
O
F
F
2.25
1.61
1.07
3.00
2.96
1.06
2.17
1.14
0.35
0.62
1.05
2.18
0.72
1.07
2.47
5500
5000
4500
4000
3500
3000
2500
2000
1500
1000
500
0
-500
11.5
10.5
9.5
8.5
7.5
6.5
5.5
4.5
3.5
2.5
1.5
0.5
-0.5
-1.5
f1 (ppm)

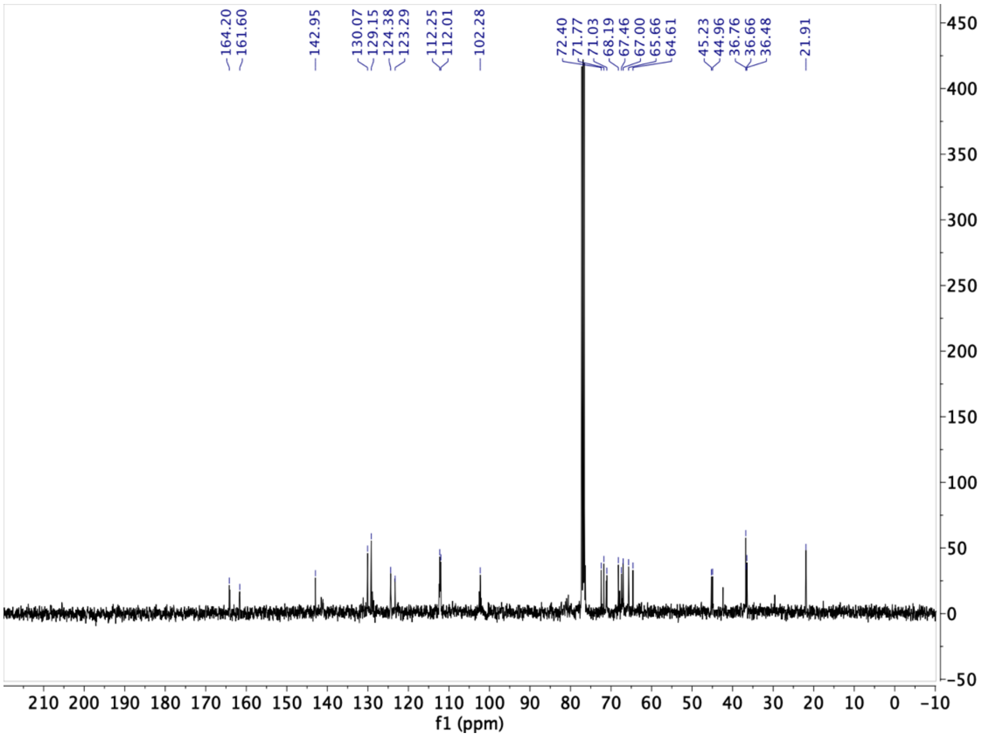
164.20
161.60
142.95
130.07
129.15
124.38
123.29
112.25
112.01
102.28
72.40
71.77
71.03
68.19
67.46
67.00
65.66
64.61
45.23
44.96
36.76
36.66
36.48
21.91
450
400
350
300
250
200
150
100
50
0
-50
210
200
190
180
170
160
150
140
130
120
110
100
90
80
70
60
50
40
30
20
10
0
-10
f1 (ppm)

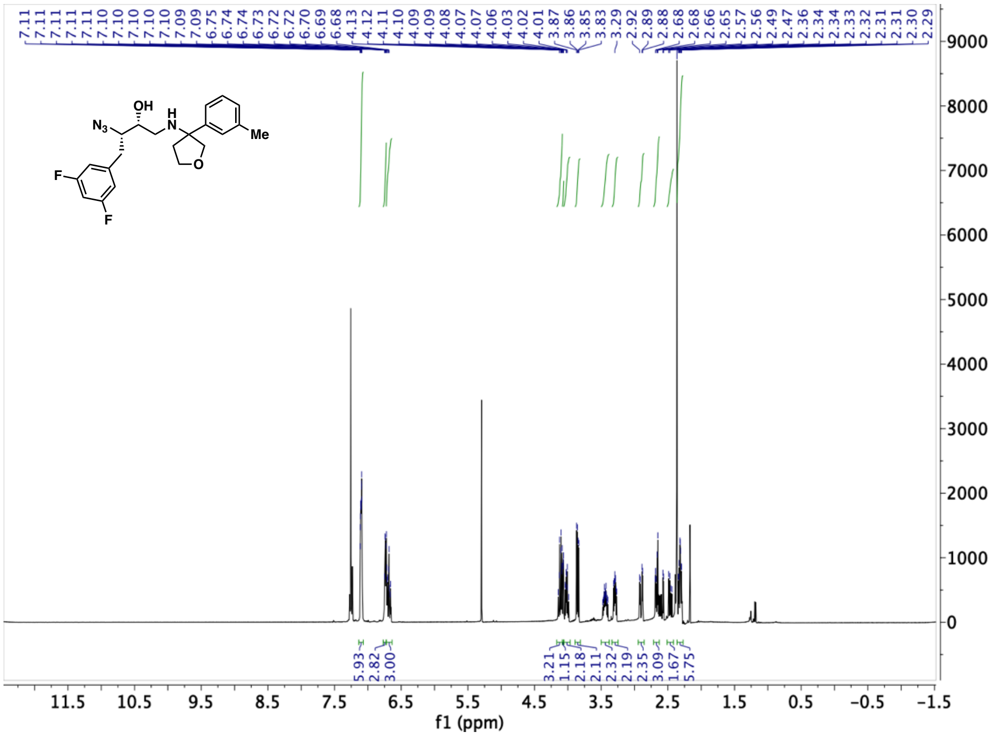
7.11
7.11
7.11
7.11
7.10
7.10
7.10
7.09
7.09
6.75
6.74
6.74
6.73
6.72
6.72
6.70
6.69
6.68
4.13
4.12
4.11
4.10
4.09
4.09
4.08
4.07
4.07
4.06
4.03
4.02
4.01
3.87
3.86
3.85
3.83
3.29
2.92
2.89
2.88
2.68
2.68
2.66
2.65
2.57
2.56
2.49
2.47
2.36
2.34
2.33
2.32
2.32
2.31
2.30
2.29
OH
H
N
N3
Me
O
F
F
9000
8000
7000
6000
5000
4000
3000
2000
1000
0
5.93
2.82
3.00
3.21
1.15
2.18
2.11
2.32
2.19
2.35
3.09
1.67
5.75
11.5
10.5
9.5
8.5
7.5
6.5
5.5
4.5
3.5
2.5
1.5
0.5
−0.5
−1.5
f1 (ppm)

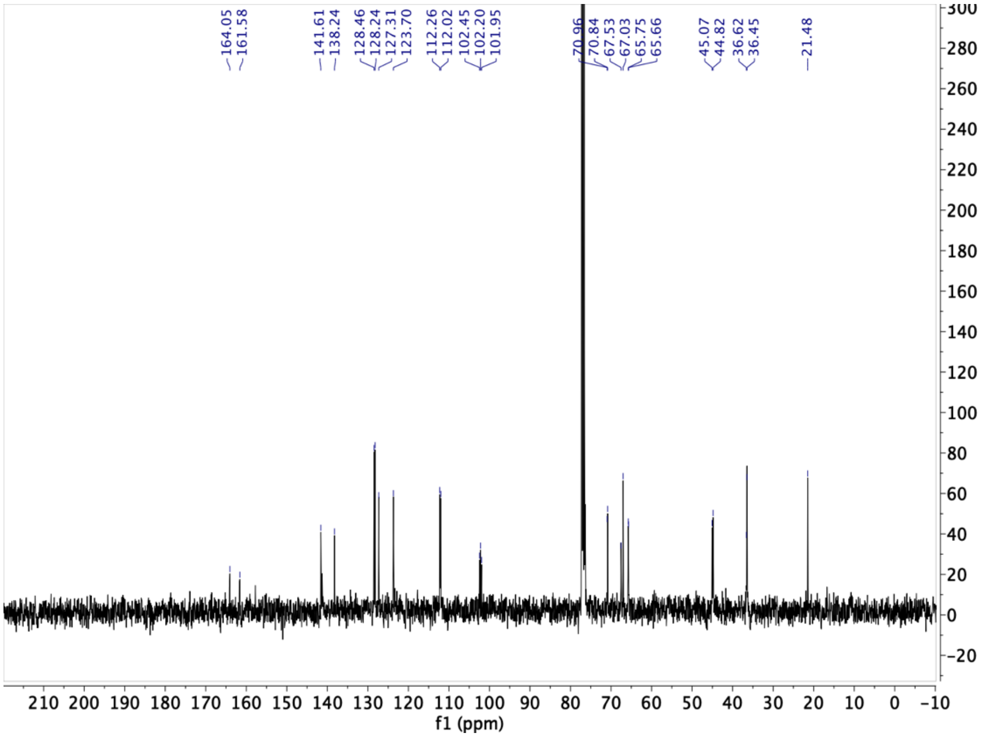
164.05
161.58
141.61
138.24
128.46
128.24
127.31
123.70
112.26
112.02
102.45
102.20
101.95
70.96
70.84
67.53
67.03
65.75
65.66
45.07
44.82
36.62
36.45
21.48
300
280
260
240
220
200
180
160
140
120
100
80
60
40
20
0
−20
210
200
190
180
170
160
150
140
130
120
110
100
90
80
70
60
50
40
30
20
10
0
−10
f1 (ppm)

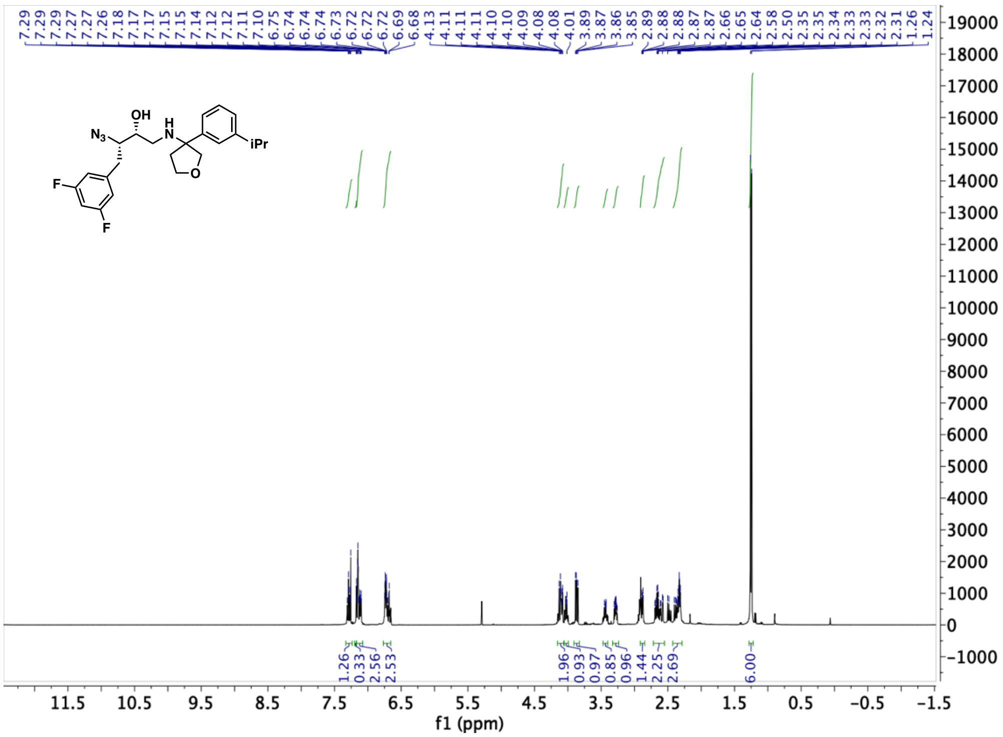
7.29 7.29 7.27 7.27 7.26 7.18 7.17 7.17 7.15 7.15 7.14 7.12 7.12 7.11 7.10 6.75 6.74 6.74 6.74 6.73 6.72 6.72 6.72 6.69 6.68 4.13 4.11 4.11 4.11 4.10 4.09 4.08 4.08 4.01 3.89 3.87 3.86 3.85 2.89 2.88 2.88 2.87 2.87 2.66 2.65 2.64 2.58 2.50 2.35 2.35 2.34 2.33 2.33 2.32 2.31 1.26 1.24
OH
N3
H
N
iPr
O
F
F
1.26 0.33 2.56 2.53
1.96 0.93 0.97 0.85 0.96 1.44 2.25 2.69
6.00
11.5 10.5 9.5 8.5 7.5 6.5 5.5 4.5 3.5 2.5 1.5 0.5 −0.5 −1.5
f1 (ppm)
19000 18000 17000 16000 15000 14000 13000 12000 11000 10000 9000 8000 7000 6000 5000 4000 3000 2000 1000 0 −1000

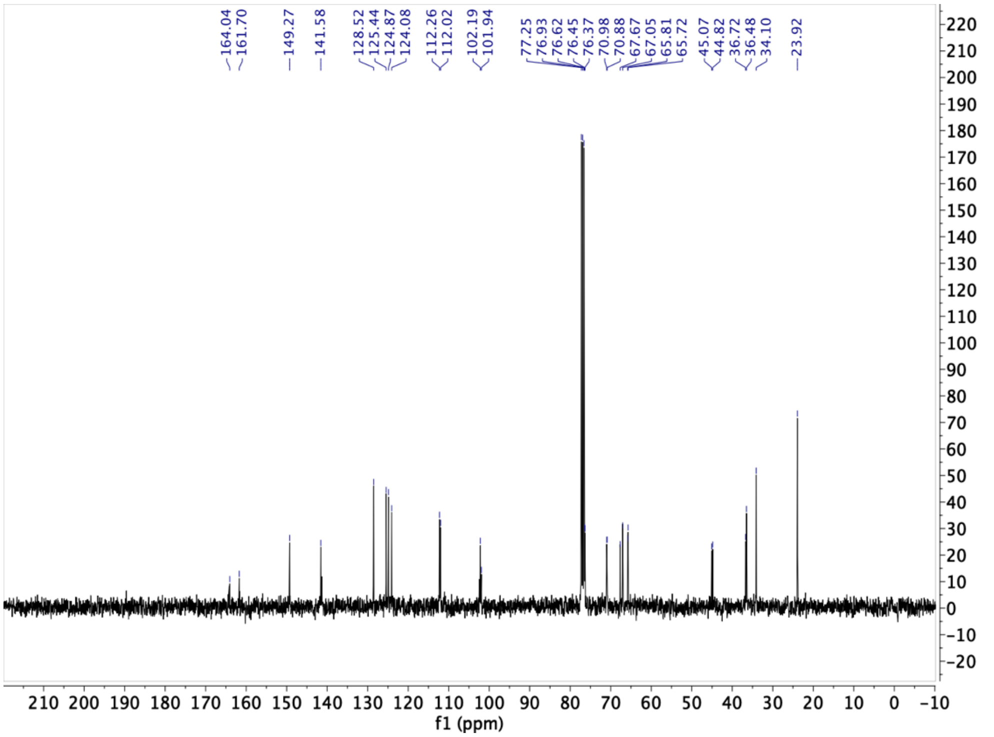
164.04 161.70 149.27 141.58 128.52 125.44 124.87 124.08 112.26 112.02 102.19 101.94 77.25 76.93 76.62 76.45 76.37 70.98 70.88 67.67 67.05 65.81 65.72 45.07 44.82 36.72 36.48 34.10 23.92
210 200 190 180 170 160 150 140 130 120 110 100 90 80 70 60 50 40 30 20 10 0 −10
f1 (ppm)
220 210 200 190 180 170 160 150 140 130 120 110 100 90 80 70 60 50 40 30 20 10 0 −10 −20

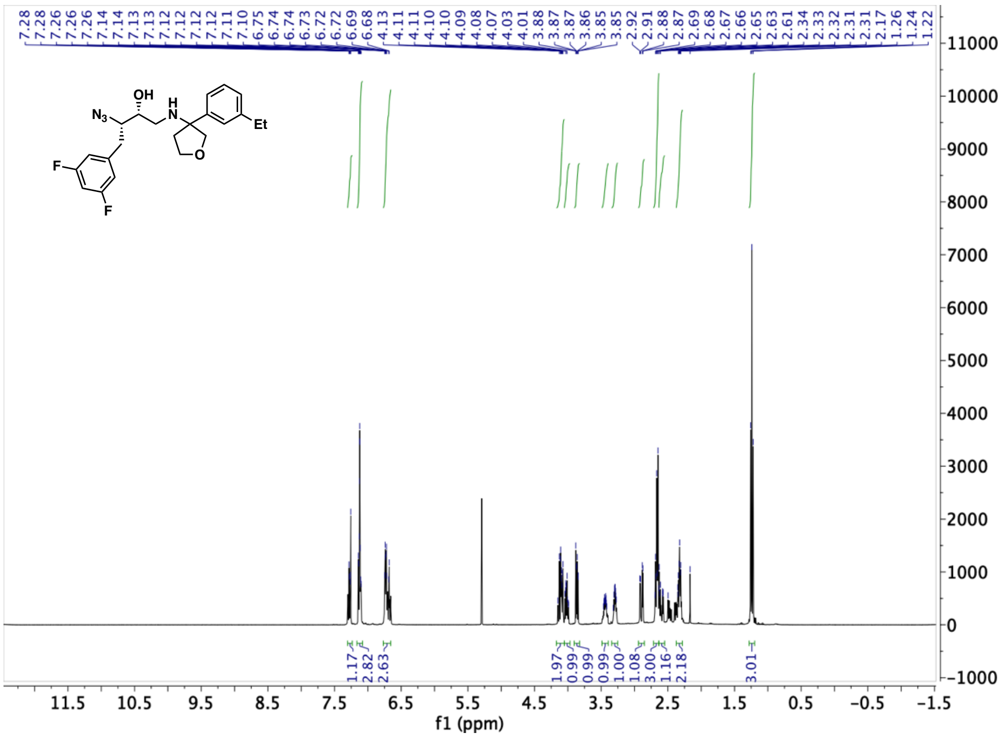
7.28
7.28
7.26
7.26
7.14
7.13
7.13
7.12
7.12
7.12
7.12
7.11
7.10
6.75
6.74
6.74
6.73
6.72
6.72
6.69
6.68
4.13
4.11
4.11
4.10
4.10
4.09
4.08
4.07
4.03
4.01
3.88
3.87
3.87
3.86
3.85
3.85
2.92
2.91
2.88
2.87
2.69
2.68
2.67
2.66
2.65
2.65
2.63
2.61
2.34
2.33
2.32
2.31
2.31
2.17
1.26
1.24
1.22
OH
N3
H
N
Et
O
F
F
1.17
2.82
2.63
1.97
0.99
0.99
0.99
1.00
1.08
3.00
1.16
2.18
3.01
11000
10000
9000
8000
7000
6000
5000
4000
3000
2000
1000
0
-1000
11.5
10.5
9.5
8.5
7.5
6.5
5.5
4.5
3.5
2.5
1.5
0.5
-0.5
-1.5
f1 (ppm)

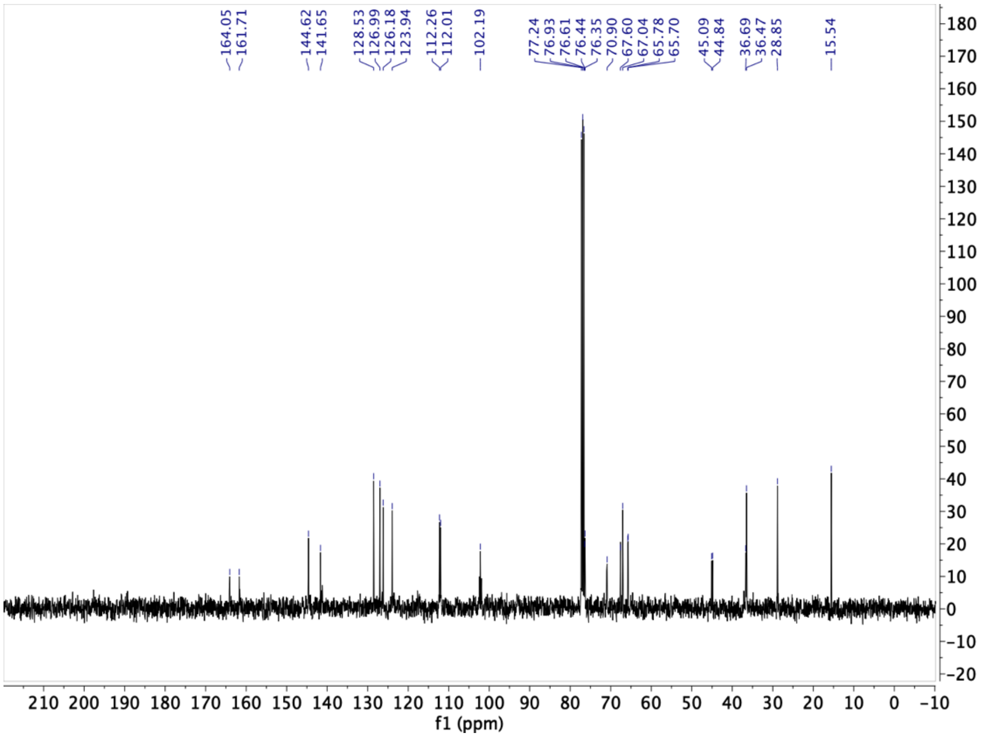
164.05
161.71
144.62
141.65
128.53
126.99
126.18
123.94
112.26
112.01
102.19
77.24
76.93
76.61
76.44
76.35
70.90
67.60
67.04
65.78
65.70
45.09
44.84
36.69
36.47
28.85
15.54
180
170
160
150
140
130
120
110
100
90
80
70
60
50
40
30
20
10
0
-10
-20
210
200
190
180
170
160
150
140
130
120
110
100
90
80
70
60
50
40
30
20
10
0
-10
f1 (ppm)

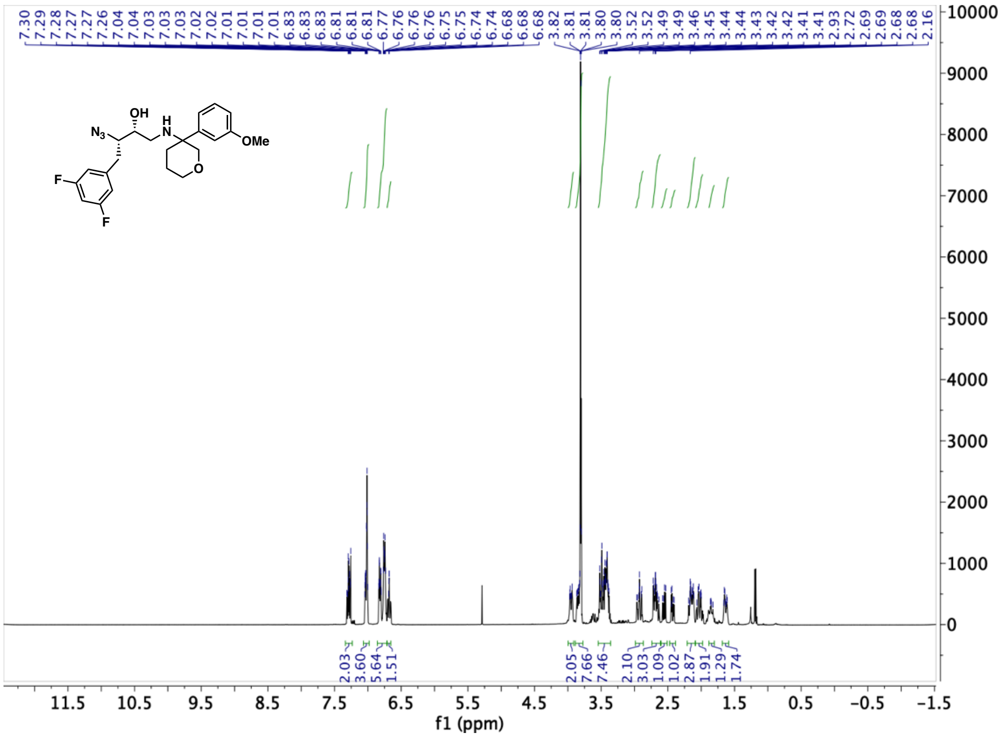
7.30 7.29 7.28 7.27 7.27 7.26 7.04 7.03 7.03 7.03 7.02 7.02 7.01 7.01 7.01 6.83 6.83 6.83 6.81 6.81 6.81 6.77 6.76 6.76 6.76 6.75 6.75 6.74 6.74 6.68 6.68 3.82 3.81 3.81 3.80 3.80 3.52 3.52 3.49 3.49 3.46 3.45 3.44 3.44 3.43 3.42 3.42 3.41 3.41 2.93 2.72 2.69 2.69 2.68 2.68 2.16
OH
H
N
N_3
OMe
O
F
F
2.03
3.60
5.64
1.51
2.05
7.66
7.46
2.10
3.03
1.09
1.02
2.87
1.91
1.29
1.74
10000
9000
8000
7000
6000
5000
4000
3000
2000
1000
0
11.5 10.5 9.5 8.5 7.5 6.5 5.5 4.5 3.5 2.5 1.5 0.5 −0.5 −1.5
f1 (ppm)

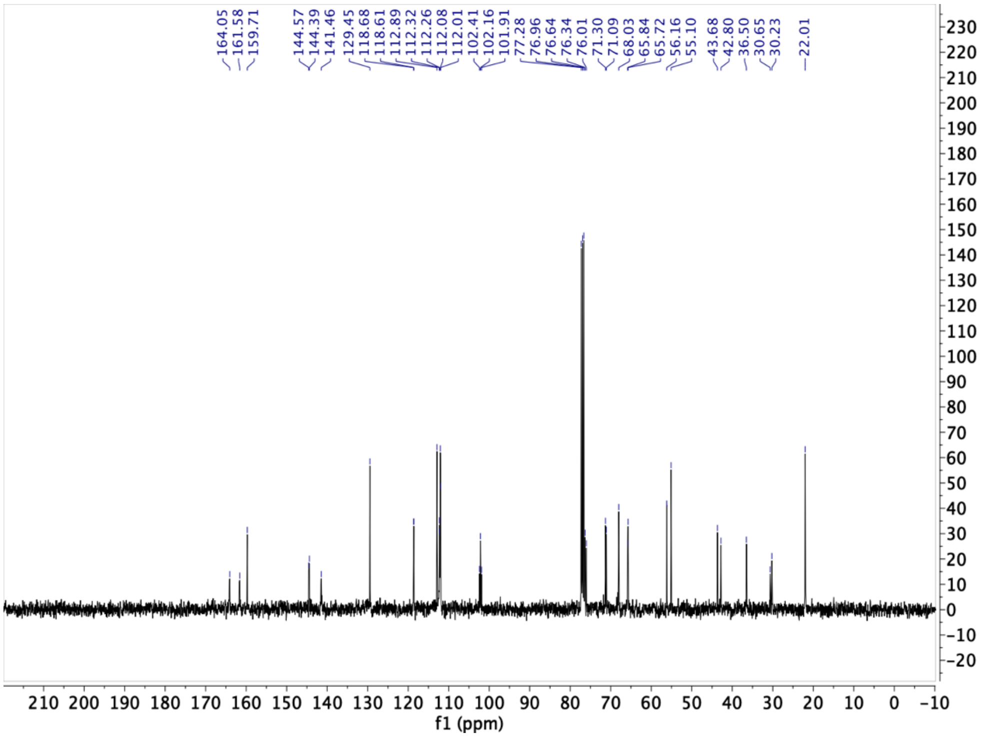
164.05 161.58 159.71 144.57 144.39 141.46 129.45 118.68 118.61 112.89 112.32 112.26 112.08 112.01 102.41 102.16 101.91 77.28 76.96 76.64 76.34 76.01 71.30 71.09 68.03 65.84 65.72 56.16 55.10 43.68 42.80 36.50 30.65 30.23 22.01
230
220
210
200
190
180
170
160
150
140
130
120
110
100
90
80
70
60
50
40
30
20
10
0
−10
−20
210 200 190 180 170 160 150 140 130 120 110 100 90 80 70 60 50 40 30 20 10 0 −10
f1 (ppm)

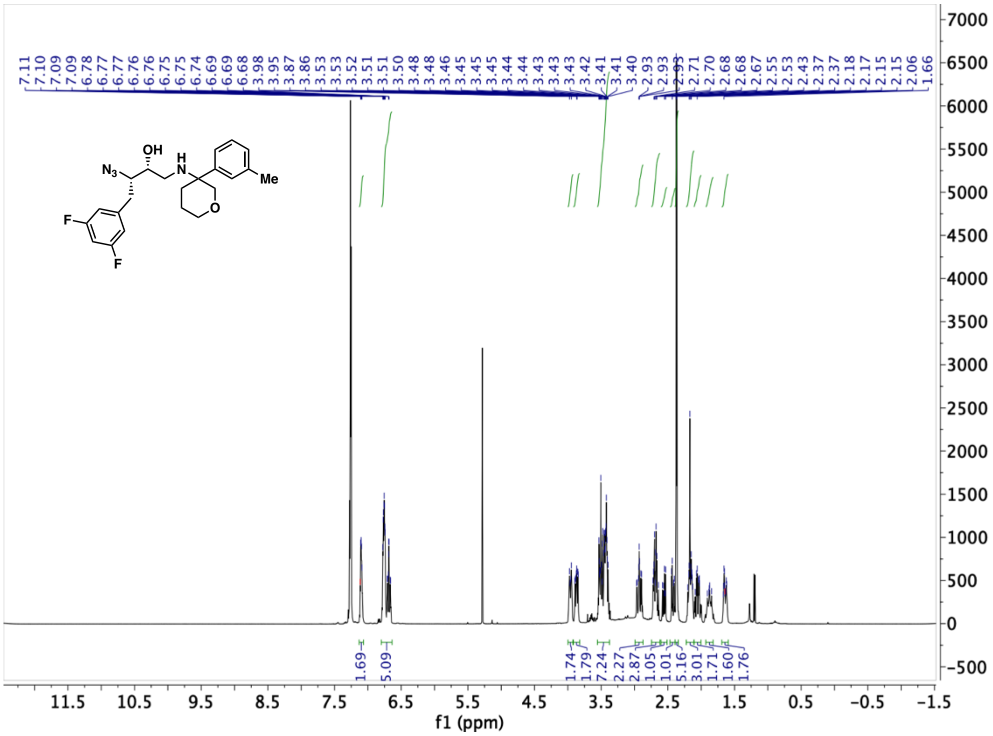
7.11
7.10
7.09
7.09
6.78
6.77
6.76
6.76
6.75
6.75
6.74
6.69
6.69
6.68
3.98
3.95
3.87
3.86
3.53
3.53
3.52
3.51
3.51
3.50
3.48
3.48
3.46
3.45
3.45
3.44
3.44
3.43
3.43
3.43
3.42
3.41
3.41
3.40
2.93
2.93
2.93
2.71
2.70
2.68
2.67
2.55
2.53
2.43
2.37
2.37
2.18
2.17
2.15
2.06
1.66
OH
N3
H
N
Me
O
F
F
1.69
5.09
1.74
1.79
7.24
2.27
2.87
1.05
1.01
5.16
3.01
1.71
1.60
1.76
7000
6500
6000
5500
5000
4500
4000
3500
3000
2500
2000
1500
1000
500
0
−500
11.5
10.5
9.5
8.5
7.5
6.5
5.5
4.5
3.5
2.5
1.5
0.5
−0.5
−1.5
f1 (ppm)

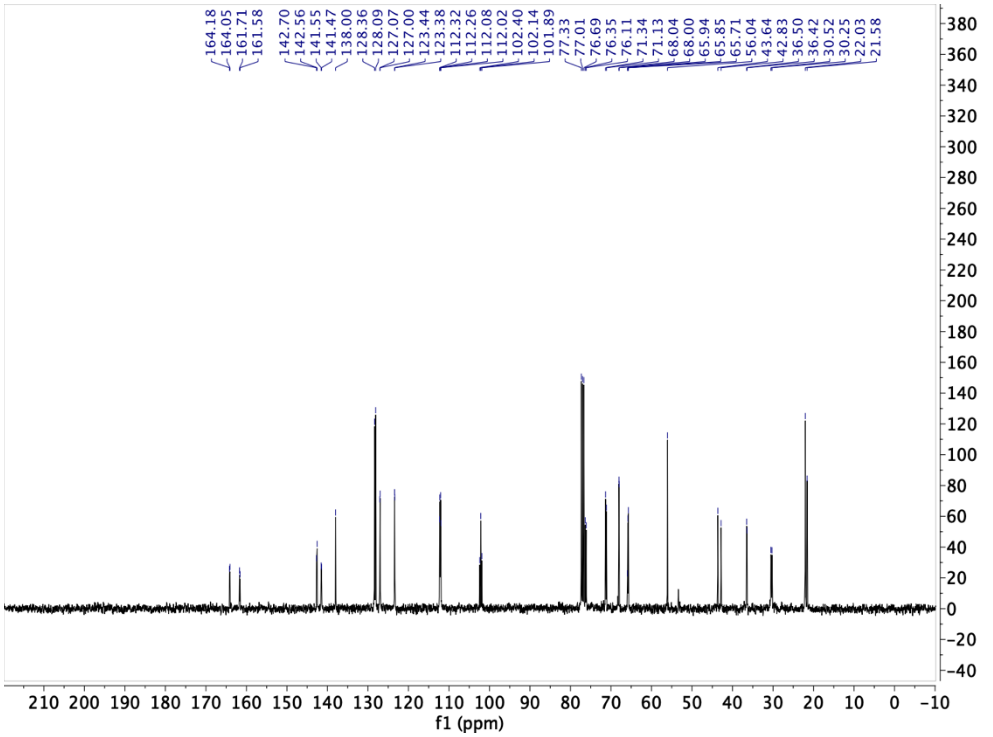
164.18
164.05
161.71
161.58
142.70
142.56
141.55
141.47
138.00
128.36
128.09
127.07
127.00
123.44
123.38
112.32
112.26
112.08
112.02
102.40
102.14
101.89
77.33
77.01
76.69
76.35
76.11
71.34
71.13
68.04
68.00
65.94
65.85
65.71
56.04
43.64
42.83
36.50
36.42
30.52
30.25
22.03
21.58
380
360
340
320
300
280
260
240
220
200
180
160
140
120
100
80
60
40
20
0
−20
−40
210
200
190
180
170
160
150
140
130
120
110
100
90
80
70
60
50
40
30
20
10
0
−10
f1 (ppm)

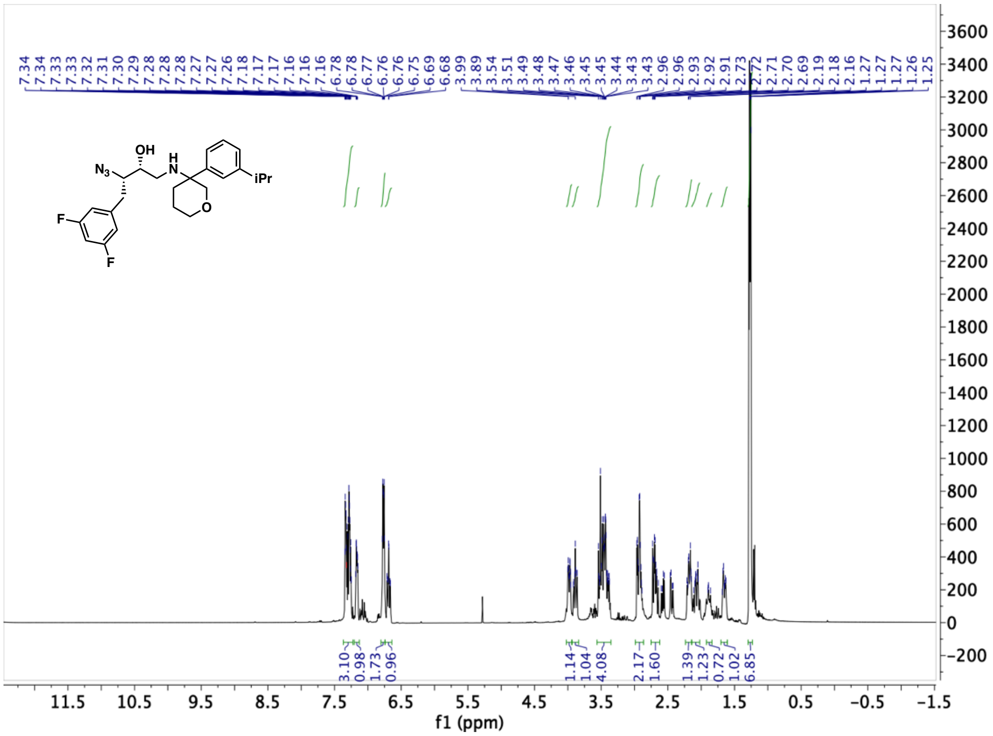
7.34
7.34
7.33
7.32
7.31
7.30
7.29
7.28
7.28
7.28
7.27
7.27
7.26
7.18
7.17
7.17
7.16
7.16
7.16
6.78
6.77
6.76
6.76
6.75
6.69
6.68
3.99
3.89
3.54
3.51
3.49
3.48
3.47
3.46
3.45
3.45
3.44
3.43
2.96
2.96
2.93
2.92
2.91
2.73
2.72
2.71
2.70
2.69
2.19
2.18
2.16
1.27
1.27
1.26
1.25
OH
N3
H
N
iPr
O
F
F
3.10
0.98
1.73
0.96
1.14
1.04
4.08
2.17
1.60
1.39
1.23
0.72
1.02
6.85
3600
3400
3200
3000
2800
2600
2400
2200
2000
1800
1600
1400
1200
1000
800
600
400
200
0
-200
11.5
10.5
9.5
8.5
7.5
6.5
5.5
4.5
3.5
2.5
1.5
0.5
-0.5
-1.5
f1 (ppm)

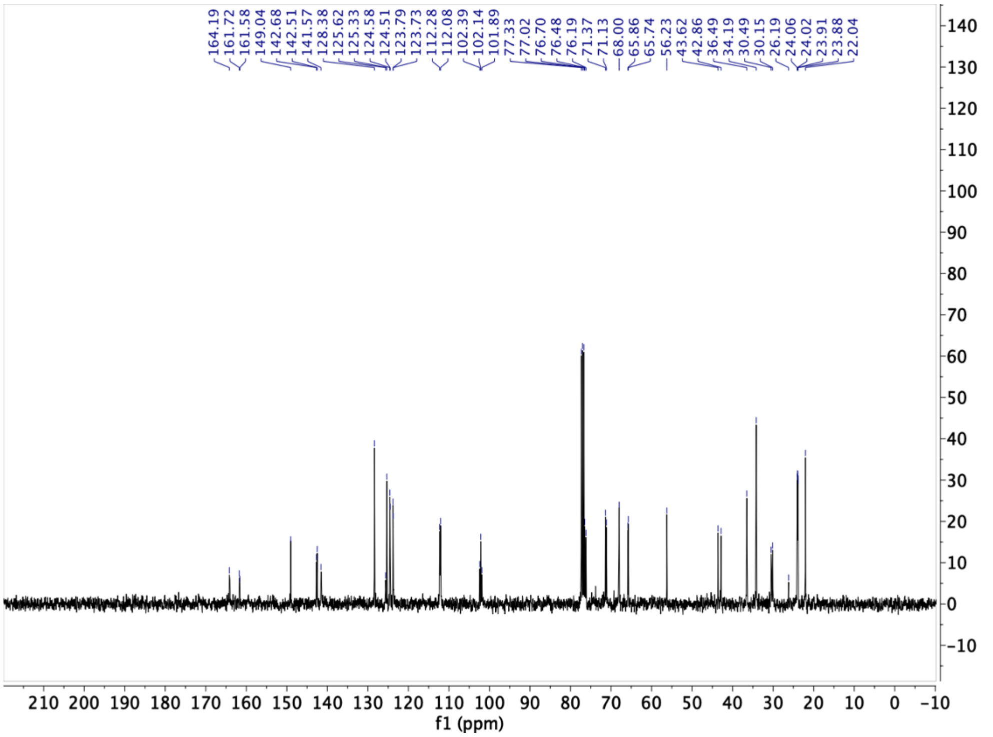
164.19
161.72
161.58
149.04
142.68
142.51
141.57
128.38
125.62
125.33
124.58
124.51
123.79
123.73
112.28
112.08
102.39
102.14
101.89
77.33
77.02
76.70
76.48
76.19
71.37
71.13
68.00
65.86
65.74
56.23
43.62
42.86
36.49
34.19
30.49
30.15
26.19
24.06
24.02
23.91
23.88
22.04
140
130
120
110
100
90
80
70
60
50
40
30
20
10
0
-10
210
200
190
180
170
160
150
140
130
120
110
100
90
80
70
60
50
40
30
20
10
0
-10
f1 (ppm)

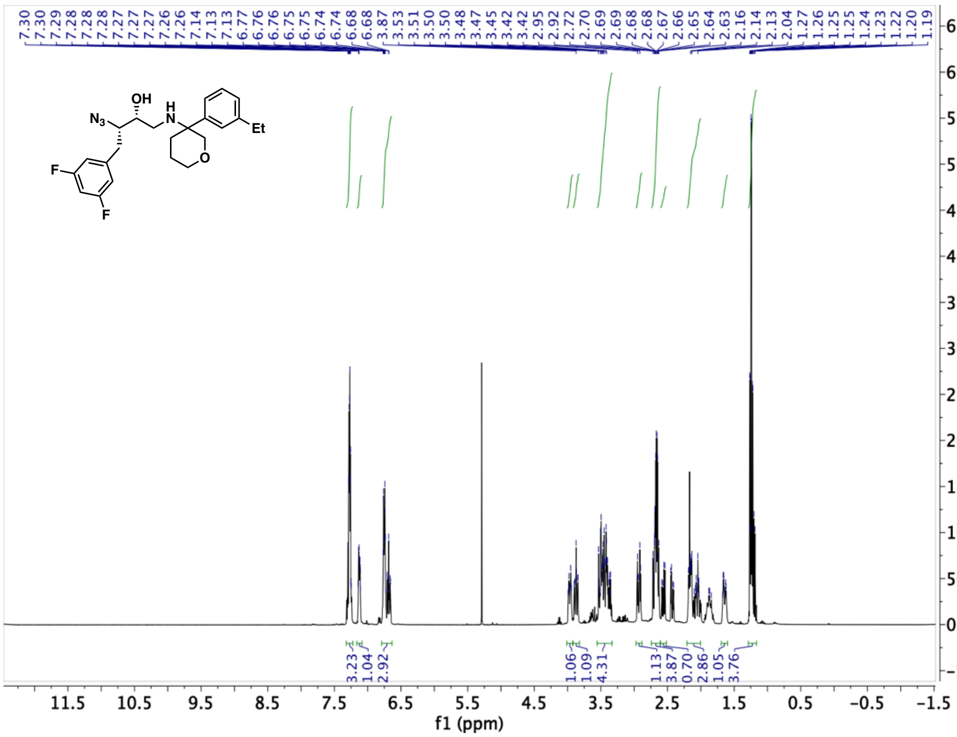
7.30
7.30
7.29
7.28
7.28
7.27
7.27
7.27
7.26
7.26
7.14
7.13
7.13
6.77
6.76
6.75
6.75
6.74
6.74
6.68
6.68
3.87
3.53
3.51
3.50
3.50
3.48
3.47
3.45
3.42
3.42
2.95
2.92
2.72
2.70
2.69
2.69
2.68
2.68
2.67
2.66
2.65
2.64
2.63
2.16
2.14
2.13
2.04
1.27
1.26
1.25
1.25
1.24
1.23
1.22
1.20
1.19
OH
H
N
N3
Et
O
F
F
3.23
1.04
2.92
1.06
1.09
4.31
1.13
3.87
0.70
2.86
1.05
3.76
11.5
10.5
9.5
8.5
7.5
6.5
5.5
4.5
3.5
2.5
1.5
0.5
-0.5
-1.5
f1 (ppm)
6500
6000
5500
5000
4500
4000
3500
3000
2500
2000
1500
1000
500
0
-500

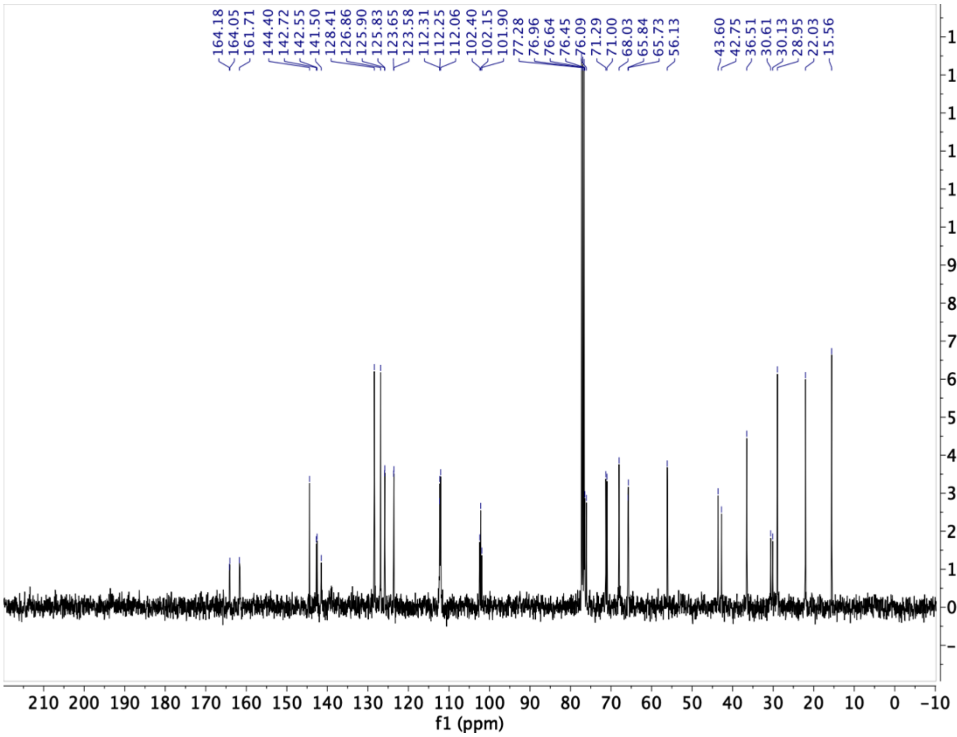
164.18
164.05
161.71
144.40
142.72
142.55
141.50
128.41
126.86
125.90
125.83
123.65
123.58
112.31
112.25
112.06
102.40
102.15
101.90
77.28
76.96
76.64
76.45
76.09
71.29
71.00
68.03
65.84
65.73
56.13
43.60
42.75
36.51
30.61
30.13
28.95
22.03
15.56
210
200
190
180
170
160
150
140
130
120
110
100
90
80
70
60
50
40
30
20
10
0
-10
f1 (ppm)
150
140
130
120
110
100
90
80
70
60
50
40
30
20
10
0
-10

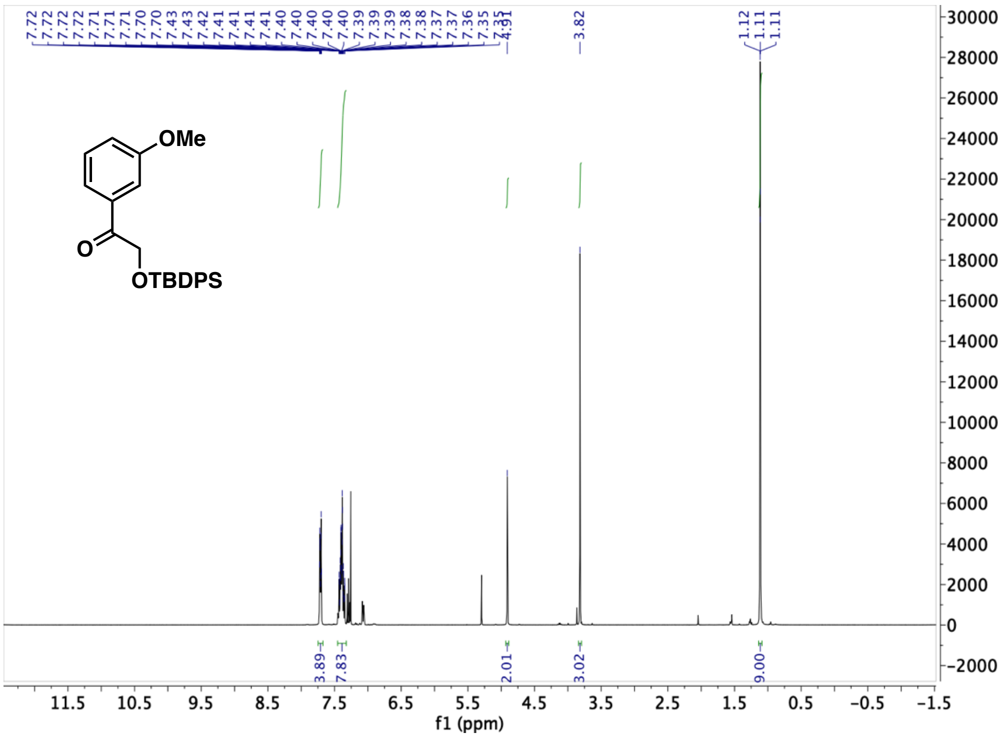
7.72
7.72
7.72
7.72
7.71
7.71
7.71
7.70
7.43
7.43
7.42
7.41
7.41
7.41
7.40
7.40
7.40
7.40
7.39
7.39
7.39
7.38
7.38
7.37
7.36
7.35
4.91
3.82
1.12
1.11
1.11
OMe
O
OTBDPS
3.89
7.83
2.01
3.02
9.00
f1 (ppm)

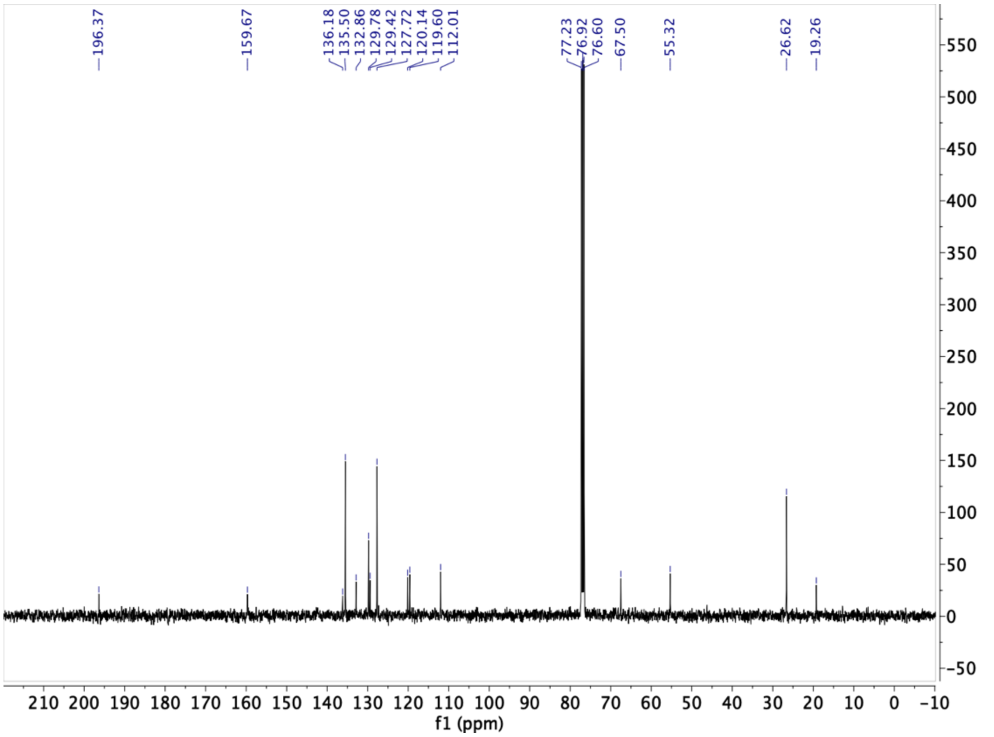
196.37
159.67
136.18
135.50
132.86
129.78
129.42
127.72
120.14
119.60
112.01
77.23
76.92
76.60
67.50
55.32
26.62
19.26
f1 (ppm)

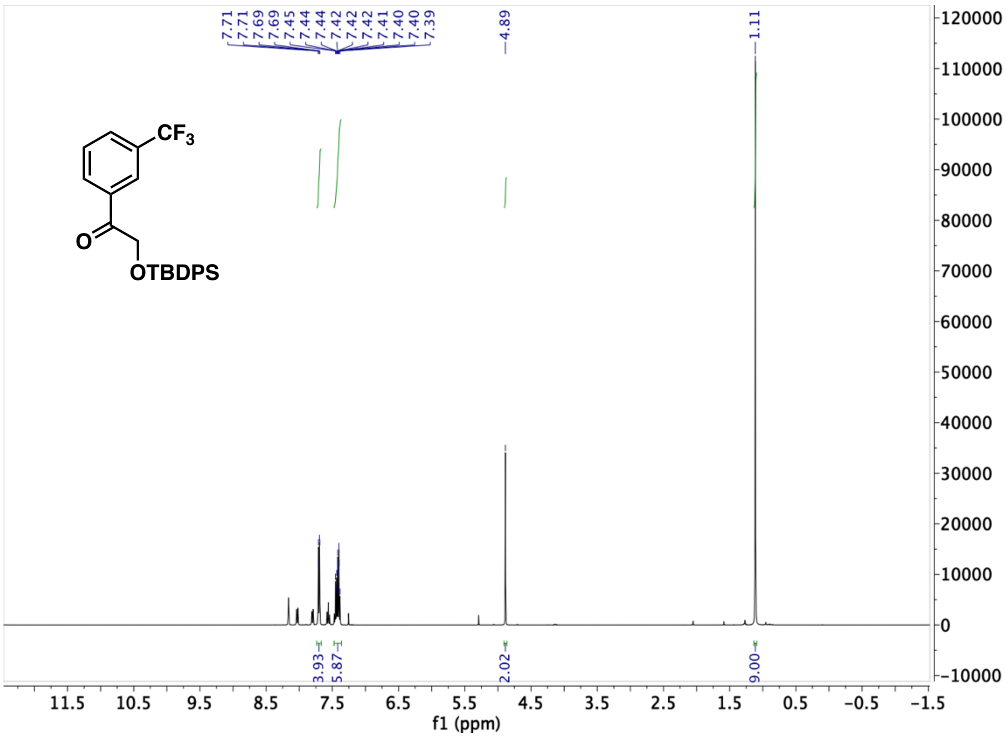
CF3
O
OTBDPS
7.71
7.71
7.69
7.69
7.45
7.44
7.44
7.42
7.42
7.42
7.41
7.40
7.40
7.39
4.89
1.11
3.93
5.87
2.02
9.00
120000
110000
100000
90000
80000
70000
60000
50000
40000
30000
20000
10000
0
−10000
11.5
10.5
9.5
8.5
7.5
6.5
5.5
4.5
3.5
2.5
1.5
0.5
−0.5
−1.5
f1 (ppm)

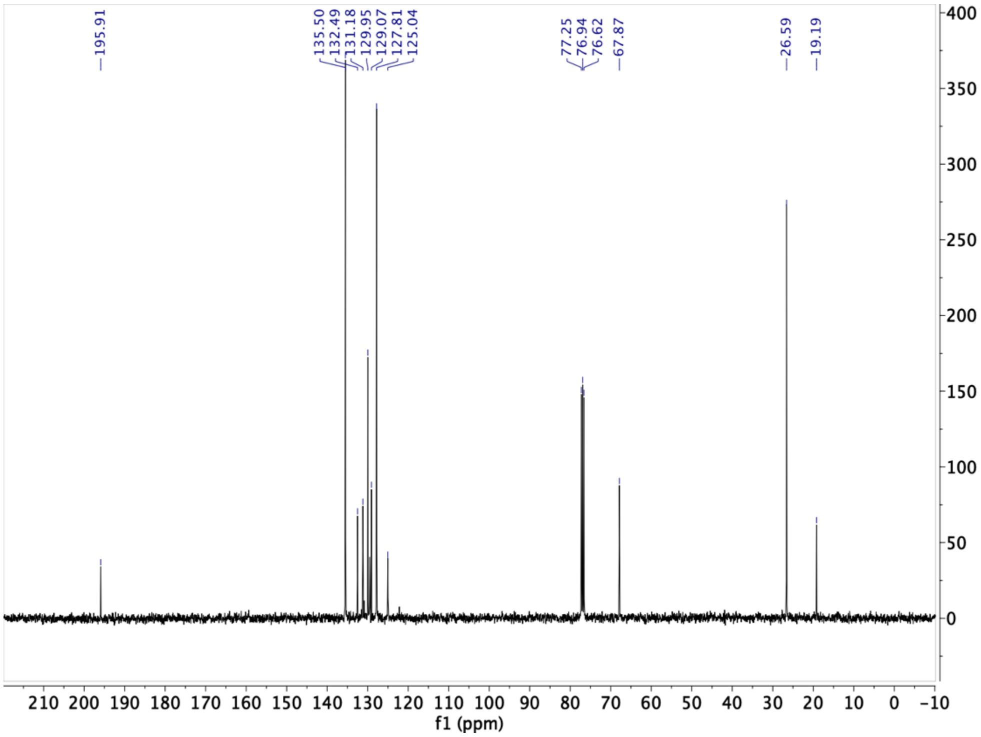
195.91
135.50
132.49
131.18
129.95
129.07
127.81
125.04
77.25
76.94
76.62
67.87
26.59
19.19
400
350
300
250
200
150
100
50
0
210
200
190
180
170
160
150
140
130
120
110
100
90
80
70
60
50
40
30
20
10
0
−10
f1 (ppm)

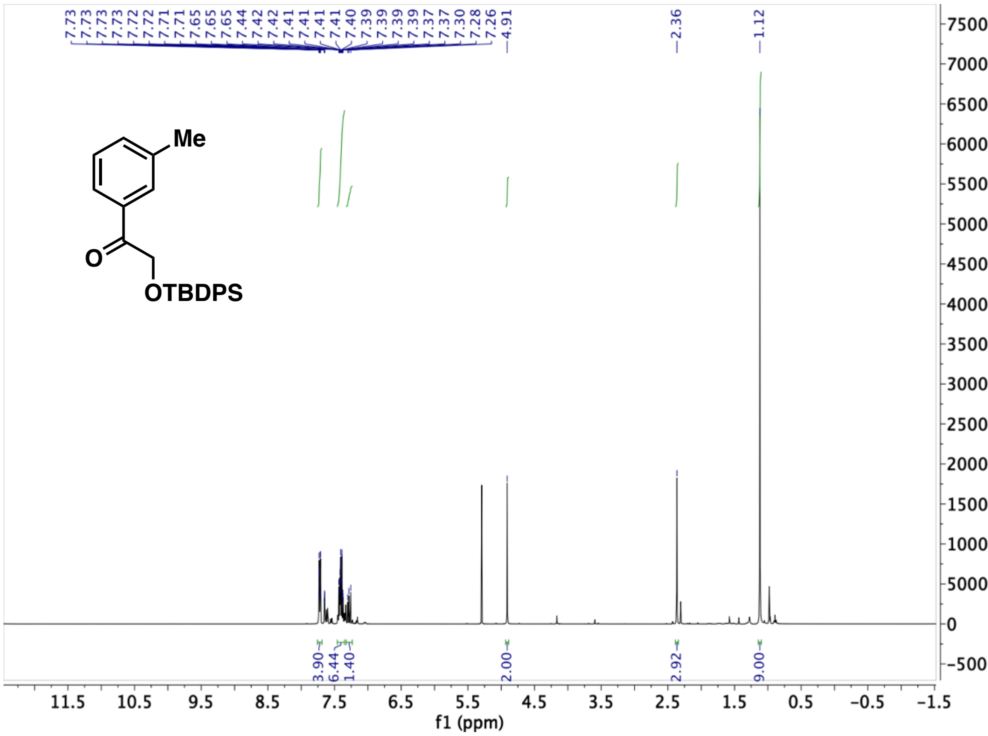
7.73
7.73
7.73
7.72
7.72
7.71
7.71
7.65
7.65
7.44
7.42
7.42
7.41
7.41
7.41
7.40
7.39
7.39
7.39
7.37
7.30
7.28
7.26
4.91
2.36
1.12
Me
O
OTBDPS
3.90
6.44
1.40
2.00
2.92
9.00
f1 (ppm)

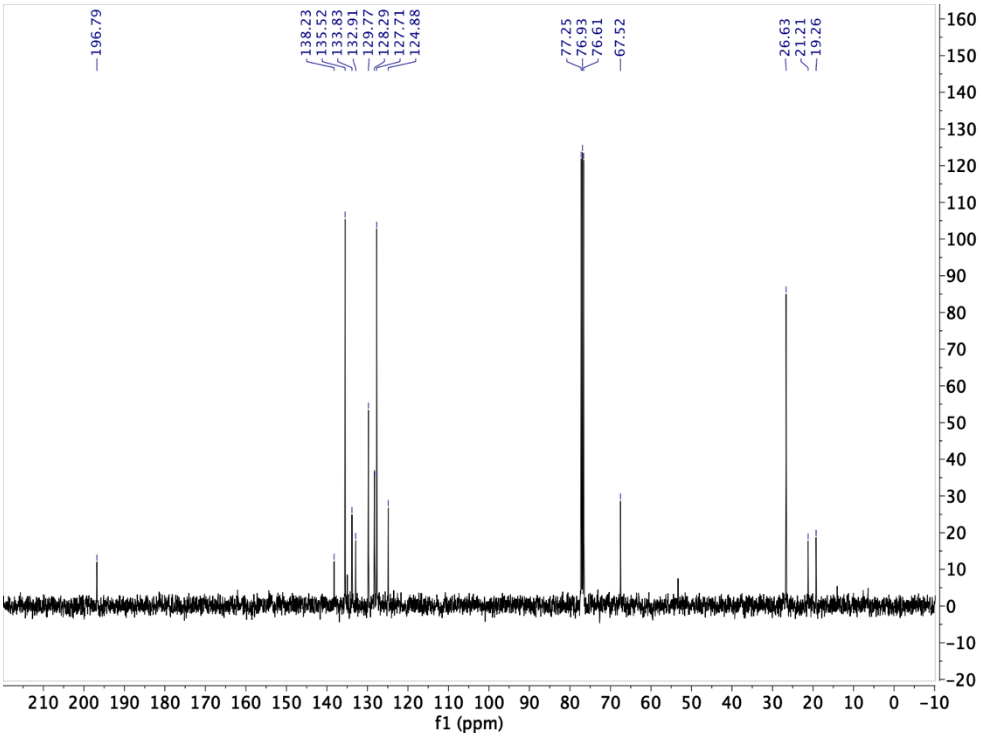
196.79
138.23
135.52
133.83
132.91
129.77
128.29
127.71
124.88
77.25
76.93
76.61
67.52
26.63
21.21
19.26
f1 (ppm)

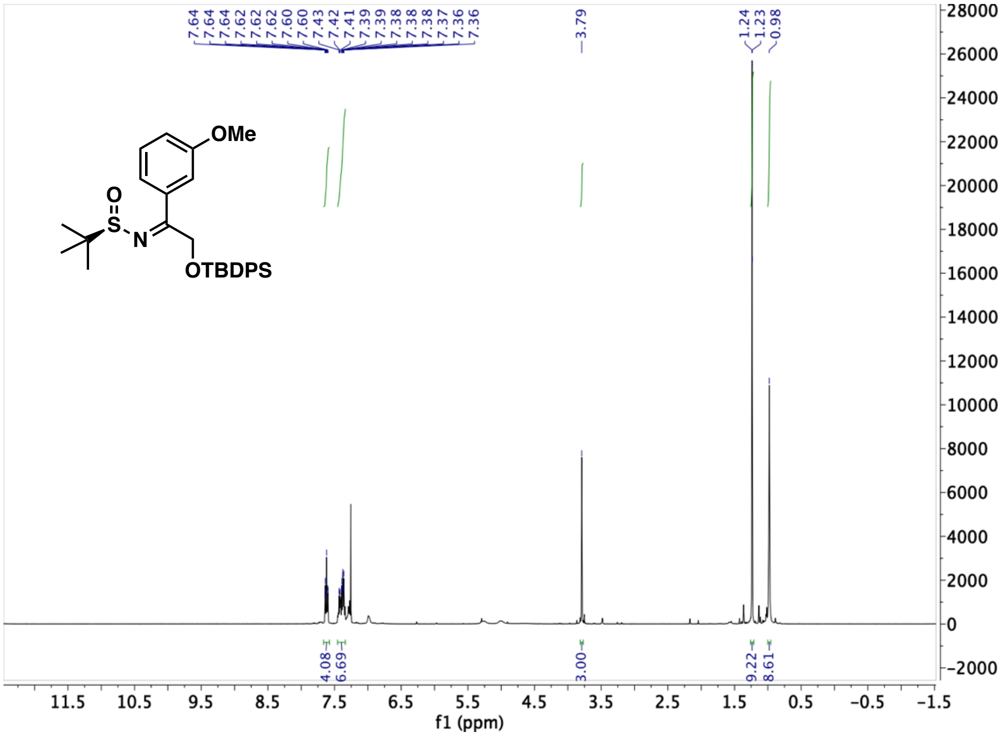
7.64
7.64
7.62
7.62
7.62
7.60
7.60
7.43
7.42
7.41
7.39
7.39
7.38
7.38
7.38
7.37
7.36
7.36
3.79
1.24
1.23
0.98
OMe
O
S
N
OTBDPS
4.08
6.69
3.00
9.22
8.61
28000
26000
24000
22000
20000
18000
16000
14000
12000
10000
8000
6000
4000
2000
0
-2000
11.5
10.5
9.5
8.5
7.5
6.5
5.5
4.5
3.5
2.5
1.5
0.5
-0.5
-1.5
f1 (ppm)

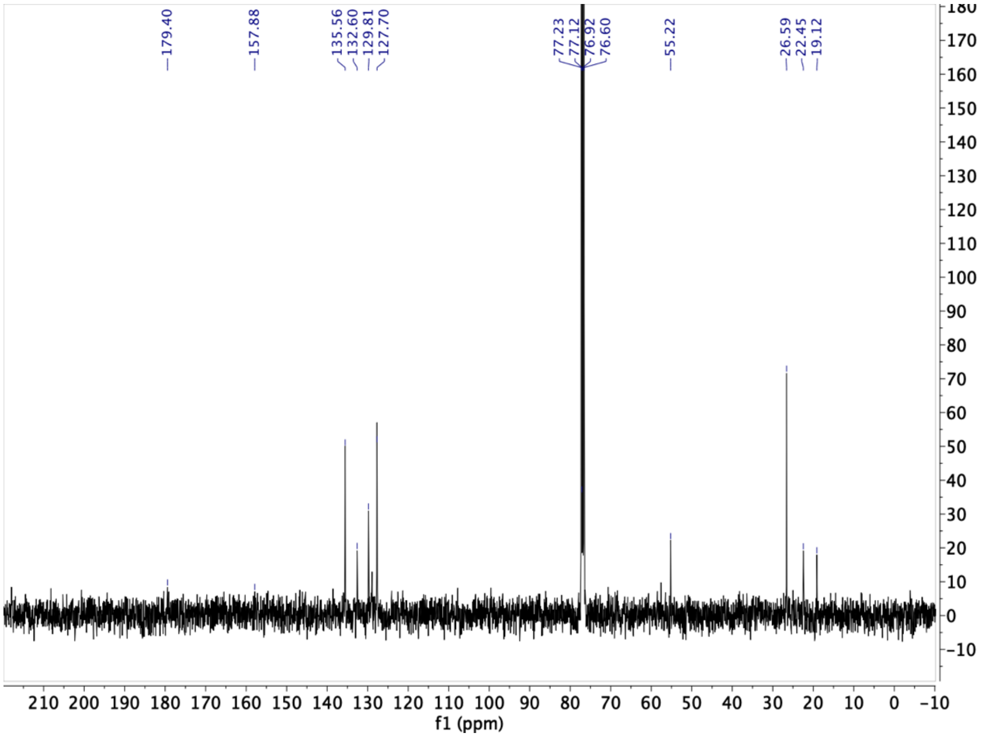
179.40
157.88
135.56
132.60
129.81
127.70
77.23
77.12
76.92
76.60
55.22
26.59
22.45
19.12
180
170
160
150
140
130
120
110
100
90
80
70
60
50
40
30
20
10
0
-10
210
200
190
180
170
160
150
140
130
120
110
100
90
80
70
60
50
40
30
20
10
0
-10
f1 (ppm)

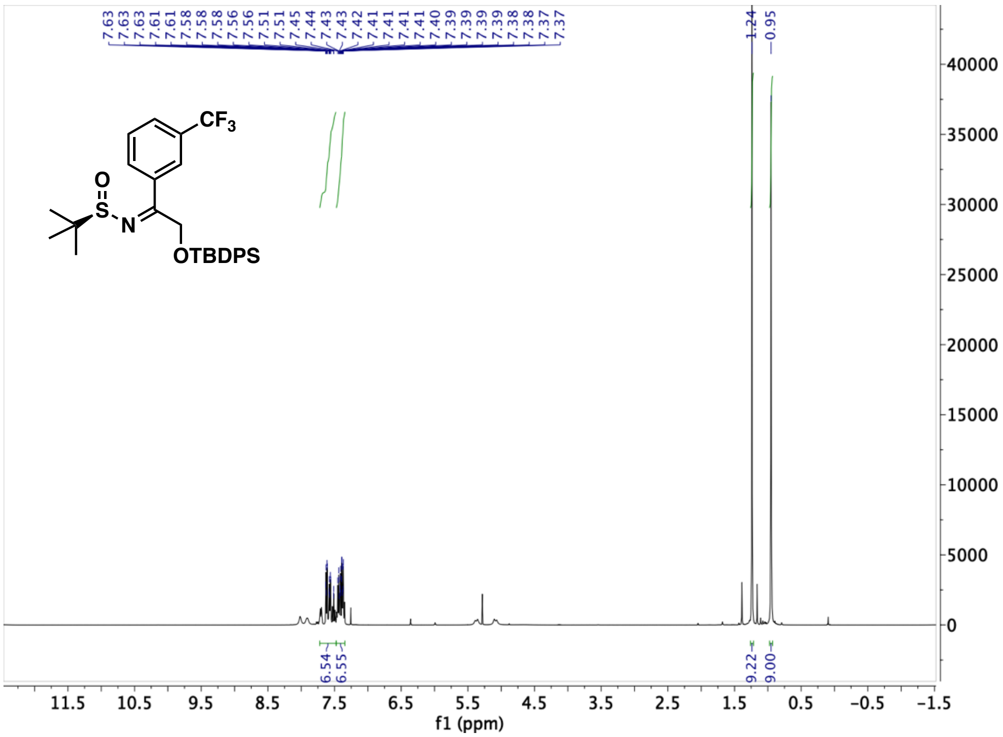
7.63
7.63
7.61
7.58
7.58
7.58
7.56
7.56
7.51
7.51
7.45
7.44
7.43
7.43
7.42
7.41
7.41
7.41
7.40
7.39
7.39
7.39
7.38
7.37
7.37
1.24
0.95
CF3
O
S
N
OTBDPS
6.54
6.55
9.22
9.00
40000
35000
30000
25000
20000
15000
10000
5000
0
11.5
10.5
9.5
8.5
7.5
6.5
5.5
4.5
3.5
2.5
1.5
0.5
−0.5
−1.5
f1 (ppm)

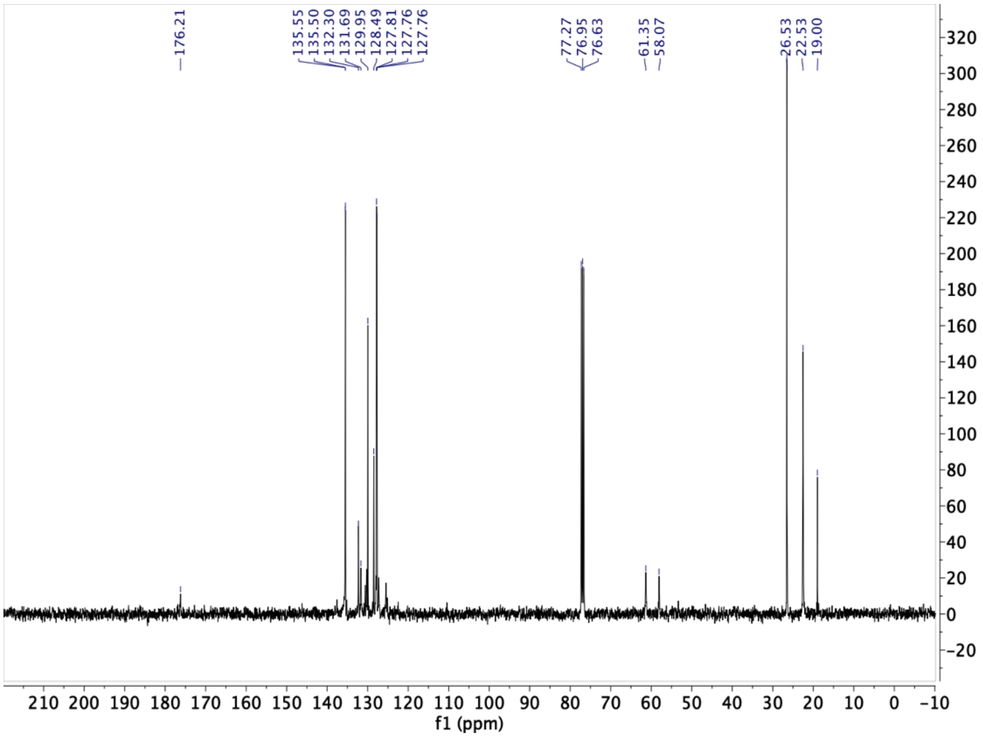
176.21
135.55
135.50
132.30
131.69
129.95
128.49
127.81
127.76
77.27
76.95
76.63
61.35
58.07
26.53
22.53
19.00
320
300
280
260
240
220
200
180
160
140
120
100
80
60
40
20
0
−20
210
200
190
180
170
160
150
140
130
120
110
100
90
80
70
60
50
40
30
20
10
0
−10
f1 (ppm)

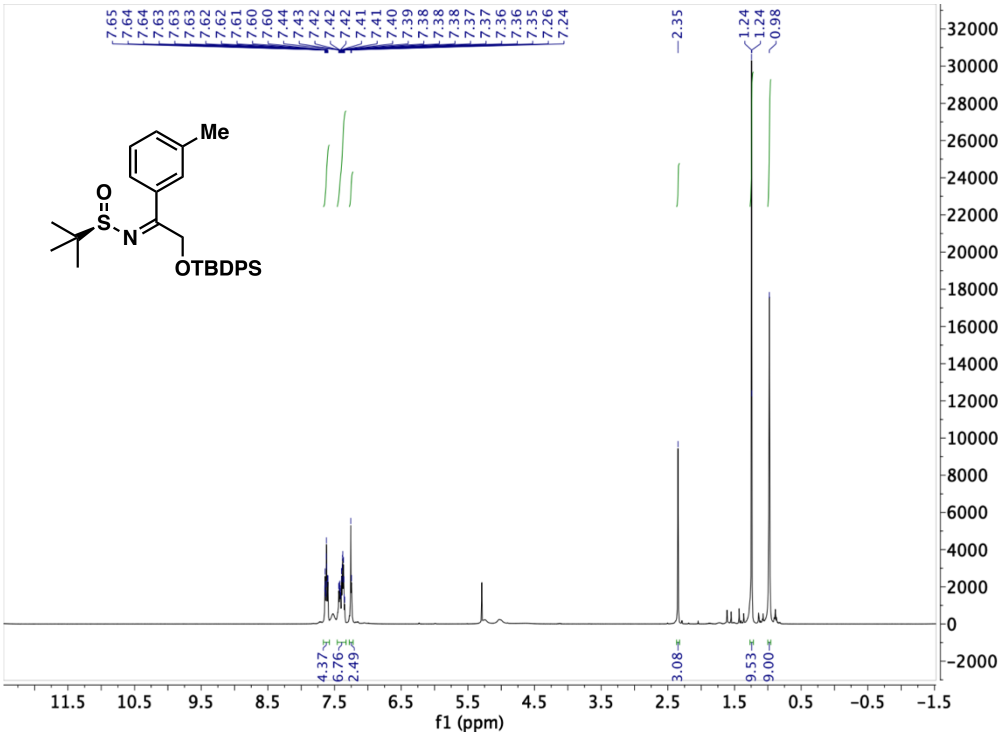
7.65
7.64
7.63
7.63
7.63
7.62
7.61
7.60
7.60
7.44
7.43
7.42
7.42
7.42
7.41
7.40
7.39
7.38
7.38
7.38
7.37
7.36
7.35
7.26
7.24
2.35
1.24
1.24
0.98
Me
O
S
N
OTBDPS
4.37
6.76
2.49
3.08
9.53
9.00
32000
30000
28000
26000
24000
22000
20000
18000
16000
14000
12000
10000
8000
6000
4000
2000
0
-2000
11.5
10.5
9.5
8.5
7.5
6.5
5.5
4.5
3.5
2.5
1.5
0.5
-0.5
-1.5
f1 (ppm)

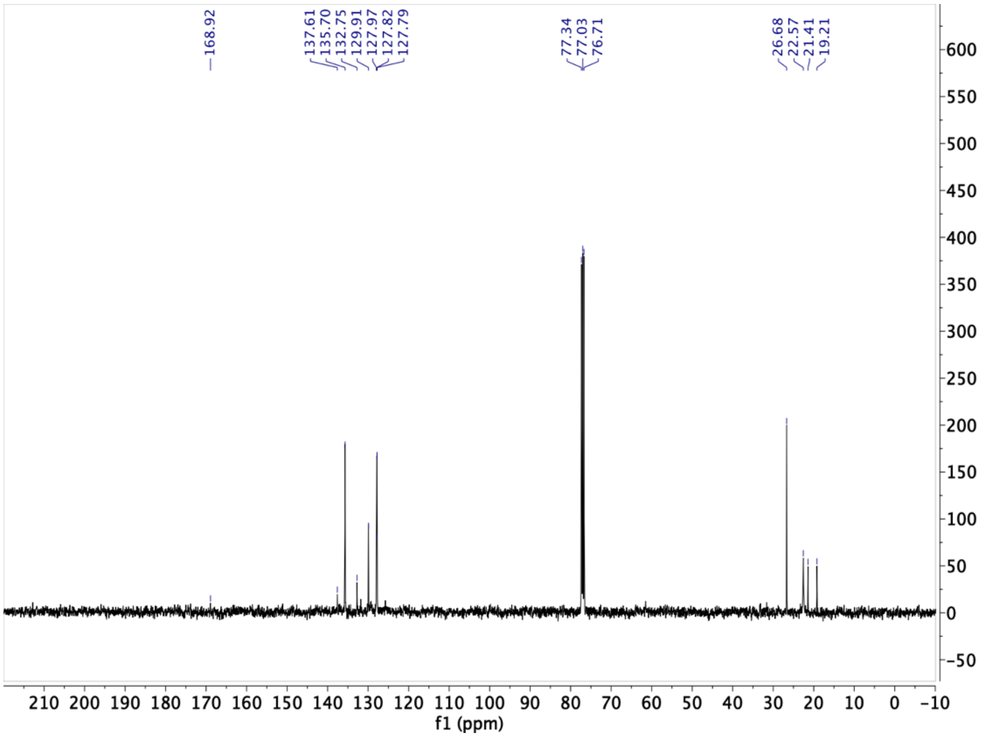
168.92
137.61
135.70
132.75
129.91
127.97
127.82
127.79
77.34
77.03
76.71
26.68
22.57
21.41
19.21
600
550
500
450
400
350
300
250
200
150
100
50
0
-50
210
200
190
180
170
160
150
140
130
120
110
100
90
80
70
60
50
40
30
20
10
0
-10
f1 (ppm)

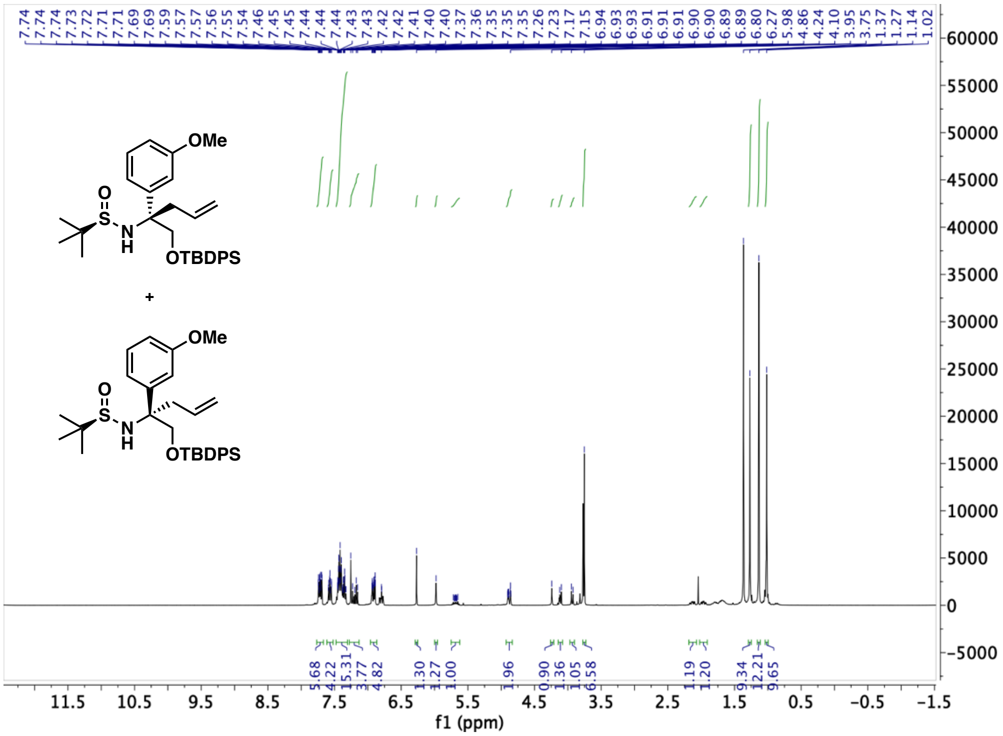
7.74
7.74
7.73
7.72
7.71
7.71
7.69
7.69
7.59
7.57
7.57
7.56
7.55
7.54
7.46
7.45
7.45
7.44
7.44
7.43
7.43
7.42
7.42
7.41
7.40
7.40
7.37
7.36
7.35
7.35
7.35
7.26
7.23
7.17
7.15
6.94
6.93
6.93
6.91
6.91
6.91
6.90
6.90
6.89
6.89
6.80
6.27
5.98
4.86
4.24
4.10
3.95
3.75
1.37
1.27
1.14
1.02
OMe
O
S
N
H
OTBDPS
+
OMe
O
S
N
H
OTBDPS
5.68
4.22
15.31
3.77
4.82
1.30
1.27
1.00
1.96
0.90
1.36
1.05
6.58
1.19
1.20
9.34
12.21
9.65
60000
55000
50000
45000
40000
35000
30000
25000
20000
15000
10000
5000
0
−5000
11.5
10.5
9.5
8.5
7.5
6.5
5.5
4.5
3.5
2.5
1.5
0.5
−0.5
−1.5
f1 (ppm)

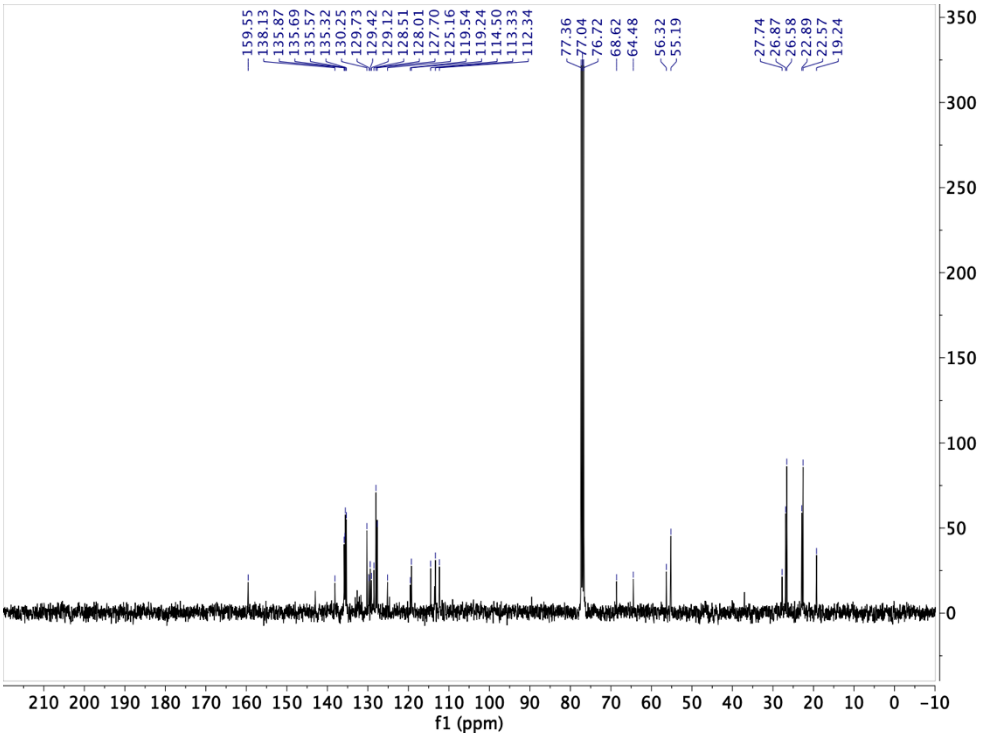
159.55
138.13
135.87
135.69
135.57
135.32
130.25
129.73
129.42
129.12
128.51
128.01
127.70
125.16
119.54
119.24
114.50
113.33
112.34
77.36
77.04
76.72
68.62
64.48
56.32
55.19
27.74
26.87
26.58
22.89
22.57
19.24
350
300
250
200
150
100
50
0
210
200
190
180
170
160
150
140
130
120
110
100
90
80
70
60
50
40
30
20
10
0
−10
f1 (ppm)

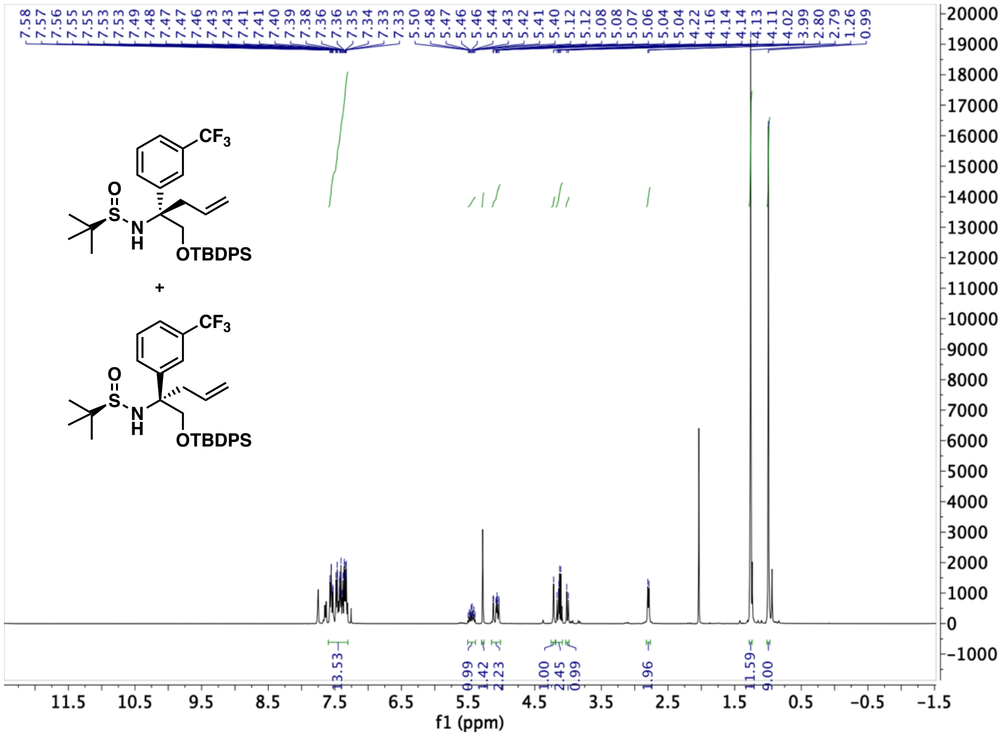
7.58
7.57
7.56
7.55
7.55
7.53
7.53
7.49
7.48
7.47
7.47
7.46
7.43
7.43
7.41
7.41
7.40
7.39
7.38
7.36
7.36
7.35
7.34
7.33
7.33
5.50
5.48
5.47
5.46
5.46
5.44
5.43
5.42
5.41
5.40
5.12
5.12
5.08
5.07
5.06
5.04
5.04
4.22
4.16
4.14
4.14
4.13
4.11
4.02
3.99
2.80
2.79
1.26
0.99
CF3
O
S
N
H
OTBDPS
+
CF3
O
S
N
H
OTBDPS
13.53
0.99
1.42
2.23
1.00
2.45
0.99
1.96
11.59
9.00
11.5
10.5
9.5
8.5
7.5
6.5
5.5
4.5
3.5
2.5
1.5
0.5
−0.5
−1.5
f1 (ppm)
20000
19000
18000
17000
16000
15000
14000
13000
12000
11000
10000
9000
8000
7000
6000
5000
4000
3000
2000
1000
0
−1000

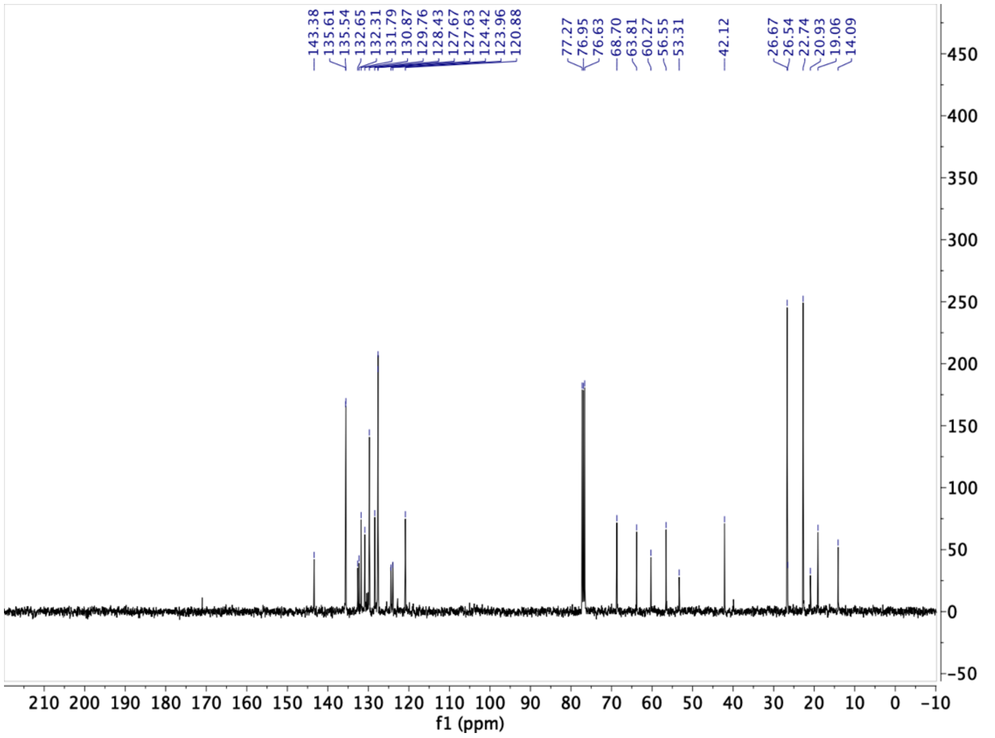
143.38
135.61
135.54
132.65
132.31
131.79
130.87
129.76
128.43
127.67
127.63
124.42
123.96
120.88
77.27
76.95
76.63
68.70
63.81
60.27
56.55
53.31
42.12
26.67
26.54
22.74
20.93
19.06
14.09
210
200
190
180
170
160
150
140
130
120
110
100
90
80
70
60
50
40
30
20
10
0
−10
f1 (ppm)
450
400
350
300
250
200
150
100
50
0
−50

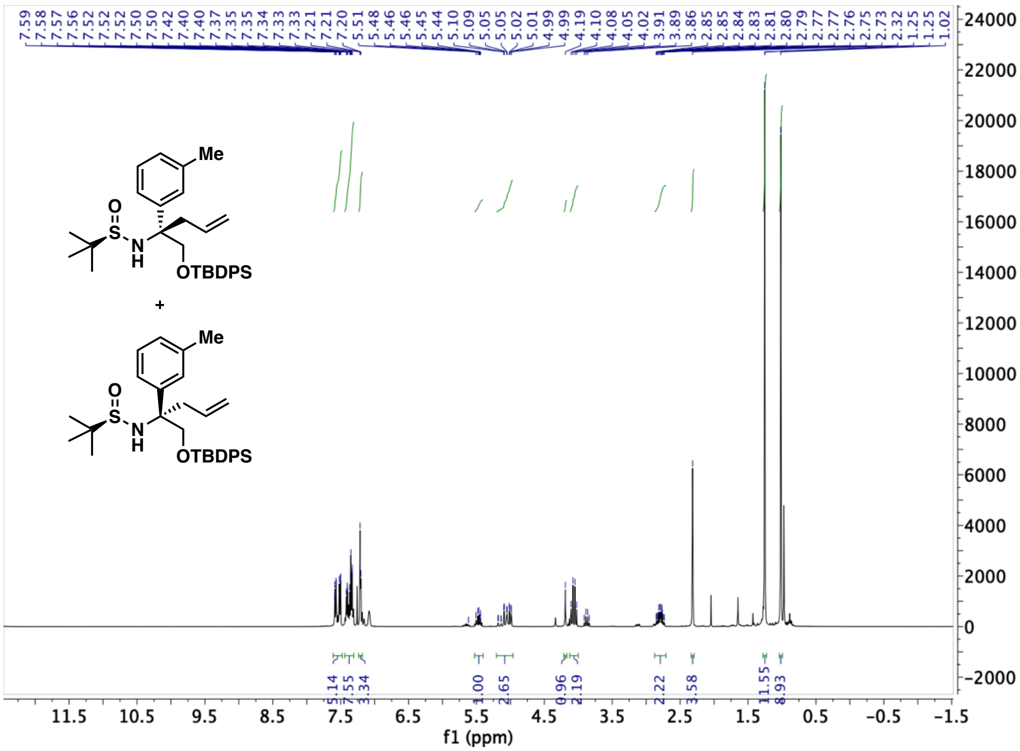
7.59
7.58
7.56
7.52
7.52
7.52
7.50
7.42
7.40
7.37
7.35
7.34
7.33
7.33
7.21
7.20
5.51
5.48
5.46
5.45
5.44
5.10
5.09
5.05
5.05
5.02
5.01
4.99
4.99
4.19
4.10
4.08
4.05
4.02
3.91
3.89
3.86
2.85
2.85
2.84
2.83
2.81
2.80
2.79
2.77
2.77
2.76
2.75
2.73
2.32
1.25
1.25
1.02
Me
O
S
N
H
OTBDPS
+
Me
O
S
N
H
OTBDPS
5.14
7.55
3.34
1.00
2.65
0.96
2.19
2.22
3.58
11.55
8.93
24000
22000
20000
18000
16000
14000
12000
10000
8000
6000
4000
2000
0
−2000
11.5
10.5
9.5
8.5
7.5
6.5
5.5
4.5
3.5
2.5
1.5
0.5
−0.5
−1.5
f1 (ppm)

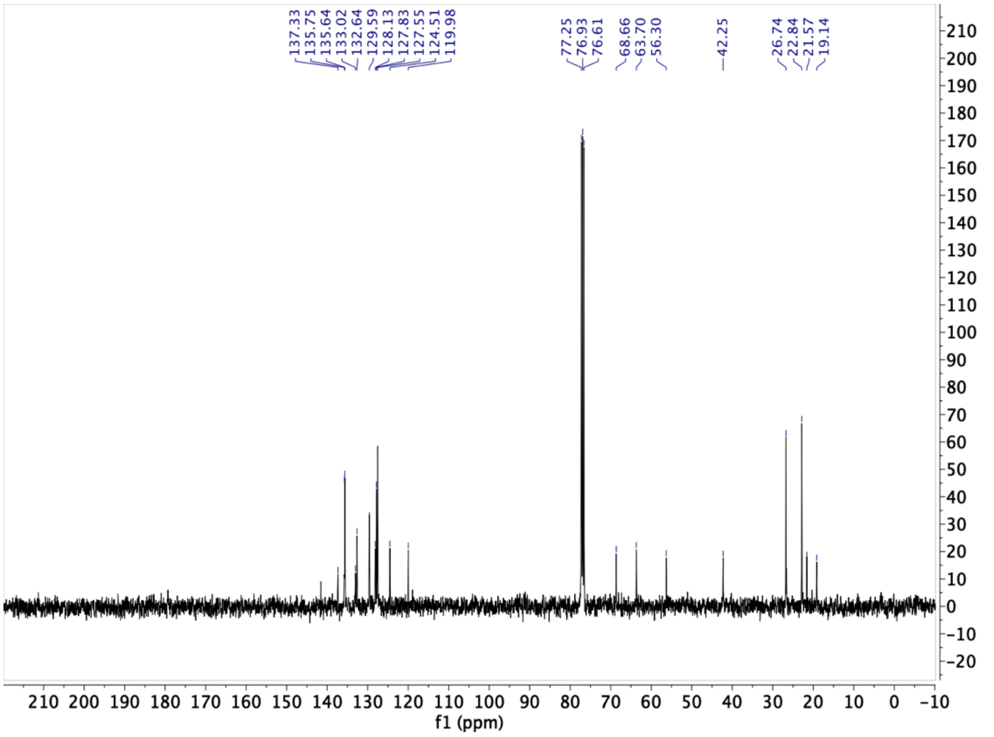
137.33
135.75
135.64
133.02
132.64
129.59
128.13
127.83
127.55
124.51
119.98
77.25
76.93
76.61
68.66
63.70
56.30
42.25
26.74
22.84
21.57
19.14
210
200
190
180
170
160
150
140
130
120
110
100
90
80
70
60
50
40
30
20
10
0
−10
−20
210
200
190
180
170
160
150
140
130
120
110
100
90
80
70
60
50
40
30
20
10
0
−10
f1 (ppm)

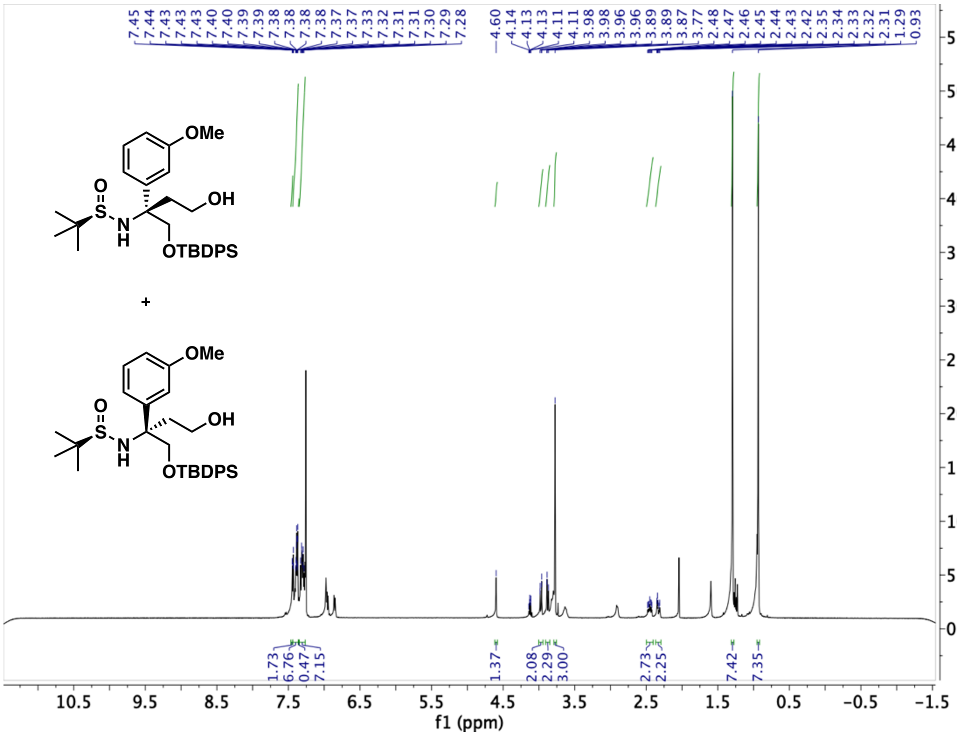
7.45
7.44
7.43
7.43
7.43
7.40
7.40
7.39
7.39
7.38
7.38
7.38
7.38
7.37
7.37
7.33
7.32
7.31
7.31
7.30
7.29
7.28
4.60
4.14
4.13
4.13
4.11
4.11
3.98
3.98
3.96
3.96
3.89
3.89
3.87
3.77
2.48
2.47
2.46
2.45
2.44
2.43
2.42
2.35
2.34
2.33
2.32
2.31
1.29
0.93
OMe
O
S
N
H
OH
OTBDPS
+
OMe
O
S
N
H
OH
OTBDPS
1.73
6.76
0.47
7.15
1.37
2.08
2.29
3.00
2.73
2.25
7.42
7.35
10.5
9.5
8.5
7.5
6.5
5.5
4.5
3.5
2.5
1.5
0.5
−0.5
−1.5
f1 (ppm)
55
50
45
40
35
30
25
20
15
10
5
0

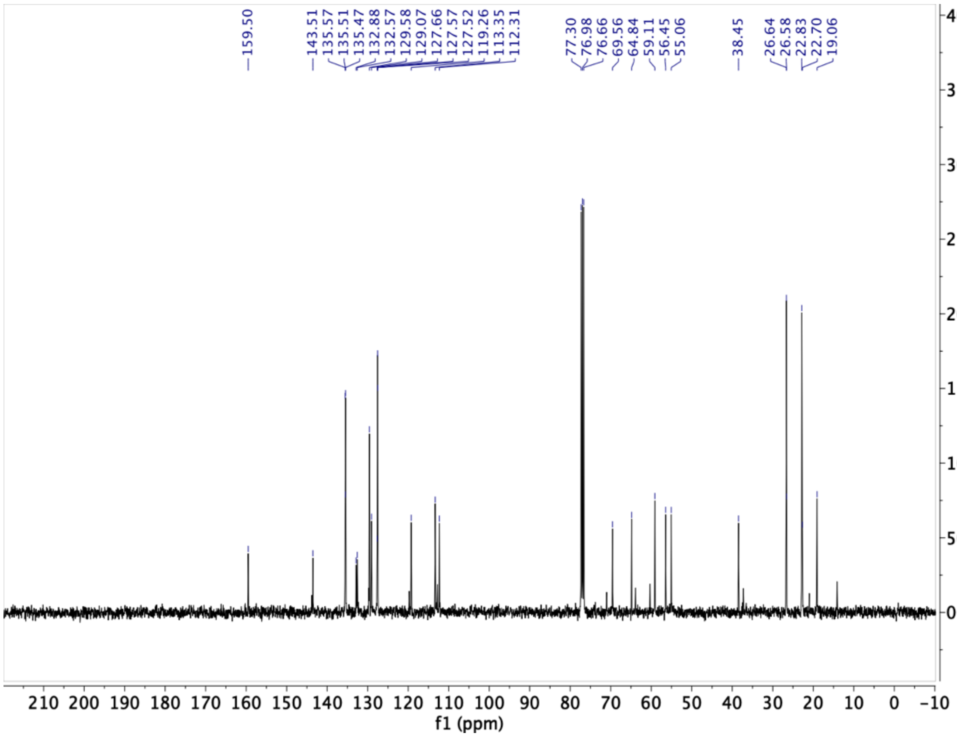
159.50
143.51
135.57
135.51
135.47
132.88
132.57
129.58
129.07
127.66
127.57
127.52
119.26
113.35
112.31
77.30
76.98
76.66
69.56
64.84
59.11
56.45
55.06
38.45
26.64
26.58
22.83
22.70
19.06
210
200
190
180
170
160
150
140
130
120
110
100
90
80
70
60
50
40
30
20
10
0
−10
f1 (ppm)
400
350
300
250
200
150
100
50
0

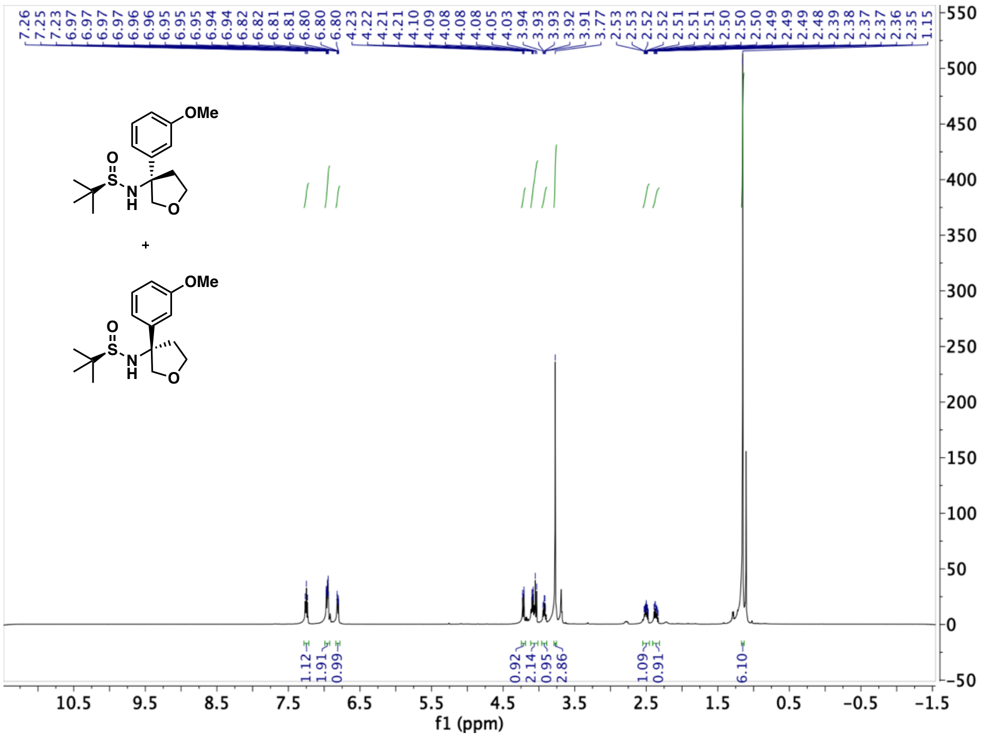
7.26
7.25
7.23
6.97
6.97
6.97
6.97
6.96
6.96
6.95
6.95
6.95
6.94
6.94
6.82
6.82
6.81
6.81
6.80
6.80
6.80
4.23
4.22
4.21
4.21
4.10
4.09
4.08
4.08
4.08
4.05
4.03
3.94
3.93
3.93
3.92
3.91
3.77
2.53
2.53
2.52
2.52
2.51
2.51
2.51
2.50
2.50
2.50
2.49
2.49
2.49
2.48
2.39
2.38
2.37
2.37
2.36
2.35
1.15
OMe
O
S
N
H
O
+
OMe
O
S
N
H
O
1.12
1.91
0.99
0.92
2.14
0.95
2.86
1.09
0.91
6.10
550
500
450
400
350
300
250
200
150
100
50
0
−50
10.5
9.5
8.5
7.5
6.5
5.5
4.5
3.5
2.5
1.5
0.5
−0.5
−1.5
f1 (ppm)

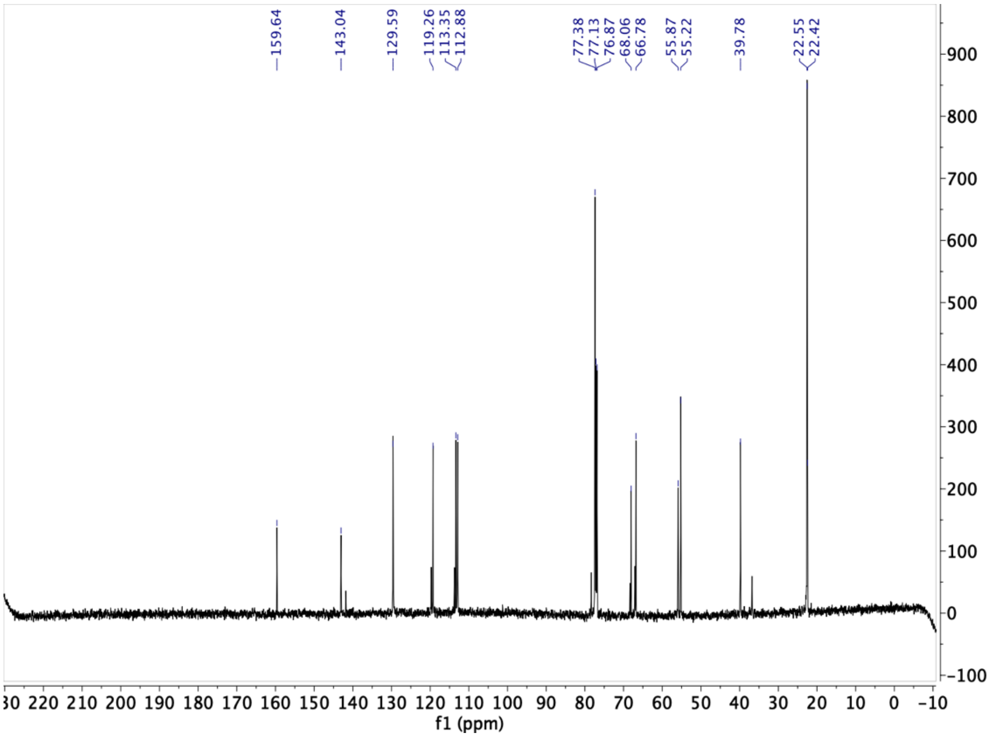
159.64
143.04
129.59
119.26
113.35
112.88
77.38
77.13
76.87
68.06
66.78
55.87
55.22
39.78
22.55
22.42
900
800
700
600
500
400
300
200
100
0
−100
30
220
210
200
190
180
170
160
150
140
130
120
110
100
90
80
70
60
50
40
30
20
10
0
−10
f1 (ppm)

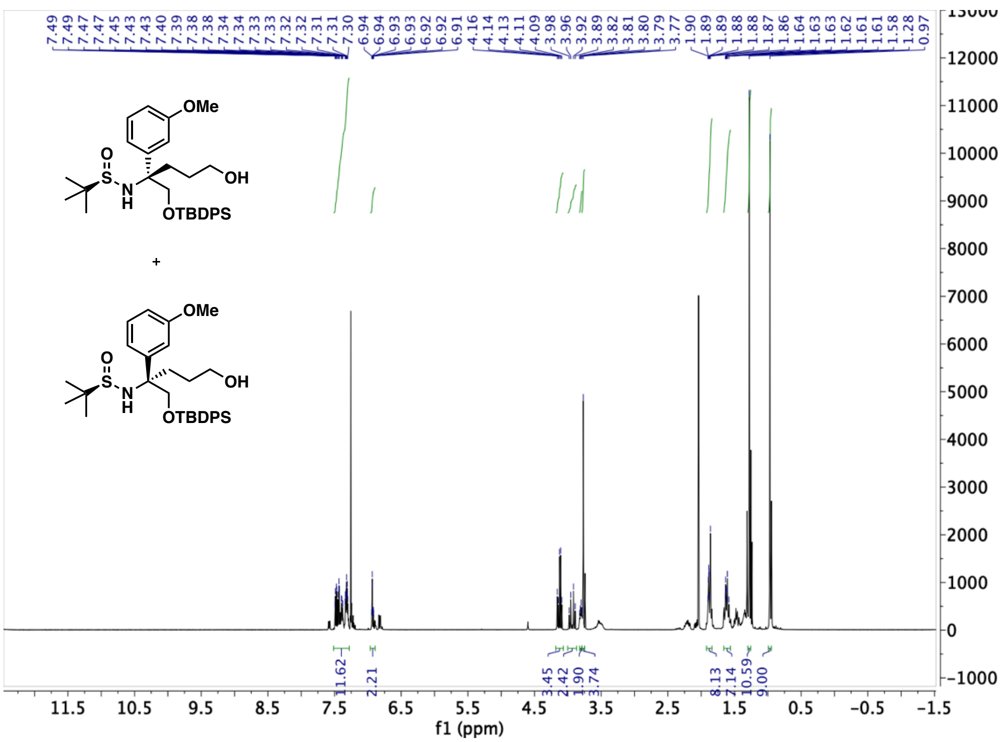
7.49
7.49
7.47
7.45
7.43
7.43
7.40
7.39
7.38
7.38
7.34
7.33
7.33
7.32
7.31
7.31
7.30
6.94
6.94
6.93
6.93
6.92
6.92
6.91
4.16
4.14
4.13
4.11
4.09
3.98
3.96
3.92
3.89
3.82
3.81
3.80
3.79
3.77
1.90
1.89
1.89
1.88
1.88
1.87
1.86
1.64
1.63
1.63
1.62
1.61
1.61
1.58
1.28
0.97
OMe
O
S
N
H
OH
OTBDPS
+
OMe
O
S
N
H
OH
OTBDPS
11.62
2.21
3.45
2.42
1.90
3.74
8.13
7.14
10.59
9.00
13000
12000
11000
10000
9000
8000
7000
6000
5000
4000
3000
2000
1000
0
-1000
11.5
10.5
9.5
8.5
7.5
6.5
5.5
4.5
3.5
2.5
1.5
0.5
-0.5
-1.5
f1 (ppm)

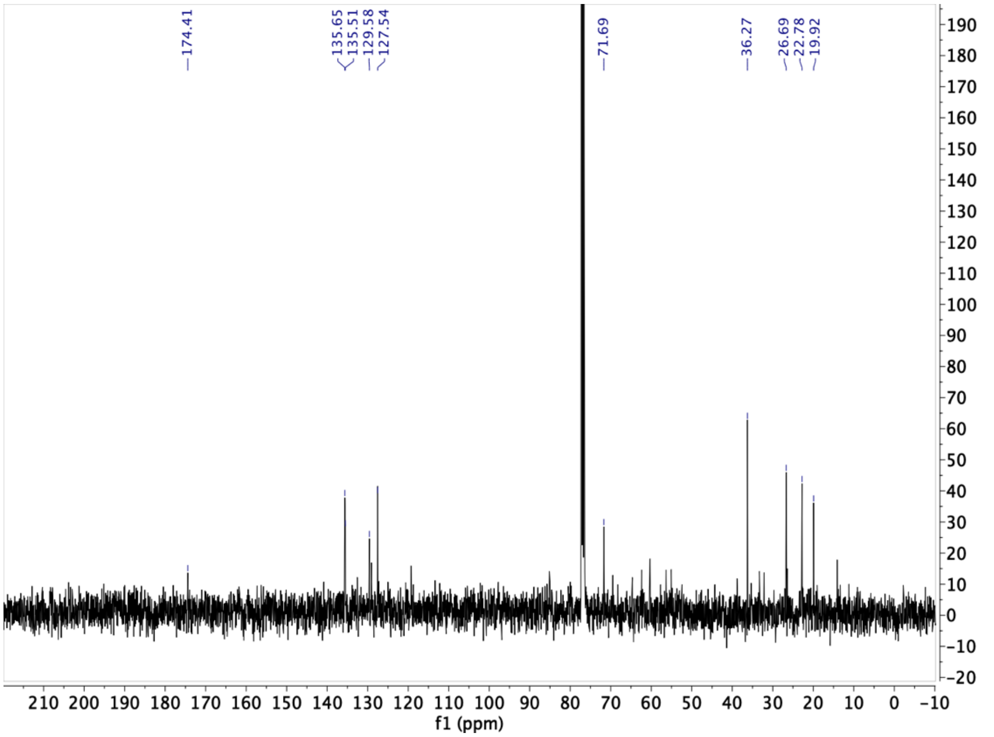
174.41
135.65
135.51
129.58
127.54
71.69
36.27
26.69
22.78
19.92
190
180
170
160
150
140
130
120
110
100
90
80
70
60
50
40
30
20
10
0
-10
-20
210
200
190
180
170
160
150
140
130
120
110
100
90
80
70
60
50
40
30
20
10
0
-10
f1 (ppm)

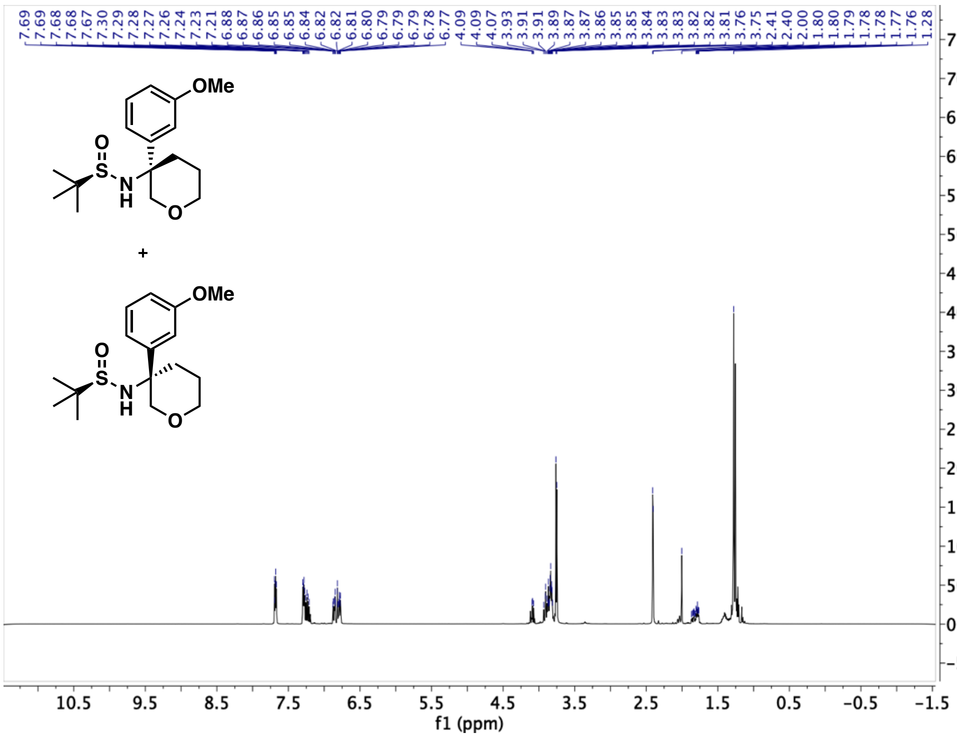
7.69 7.69 7.68 7.68 7.67 7.30 7.29 7.28 7.27 7.26 7.24 7.23 7.21 6.88 6.87 6.86 6.85 6.85 6.84 6.82 6.82 6.81 6.80 6.79 6.79 6.78 6.77 4.09 4.07 3.93 3.91 3.91 3.89 3.87 3.87 3.86 3.85 3.85 3.84 3.83 3.83 3.82 3.82 3.81 3.76 3.75 2.41 2.40 2.00 1.80 1.80 1.79 1.78 1.78 1.77 1.76 1.28
OMe
O
S
N
H
O
+
OMe
O
S
N
H
O
750
700
650
600
550
500
450
400
350
300
250
200
150
100
50
0
−50
10.5 9.5 8.5 7.5 6.5 5.5 4.5 3.5 2.5 1.5 0.5 −0.5 −1.5
f1 (ppm)

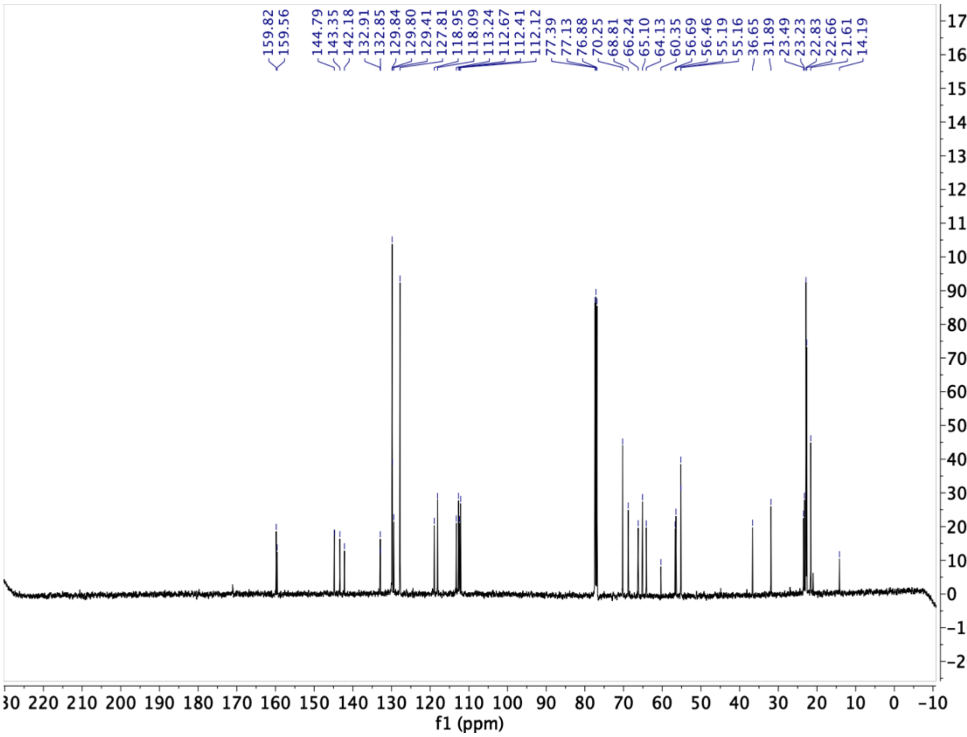
159.82 159.56 144.79 143.35 142.18 132.91 132.85 129.84 129.80 129.41 127.81 118.95 118.09 113.24 112.67 112.41 112.12 77.39 77.13 76.88 70.25 68.81 66.24 65.10 64.13 60.35 56.69 56.46 55.19 55.16 36.65 31.89 23.49 23.23 22.83 22.66 21.61 14.19
1700
1600
1500
1400
1300
1200
1100
1000
900
800
700
600
500
400
300
200
100
0
−100
−200
30 220 210 200 190 180 170 160 150 140 130 120 110 100 90 80 70 60 50 40 30 20 10 0 −10
f1 (ppm)

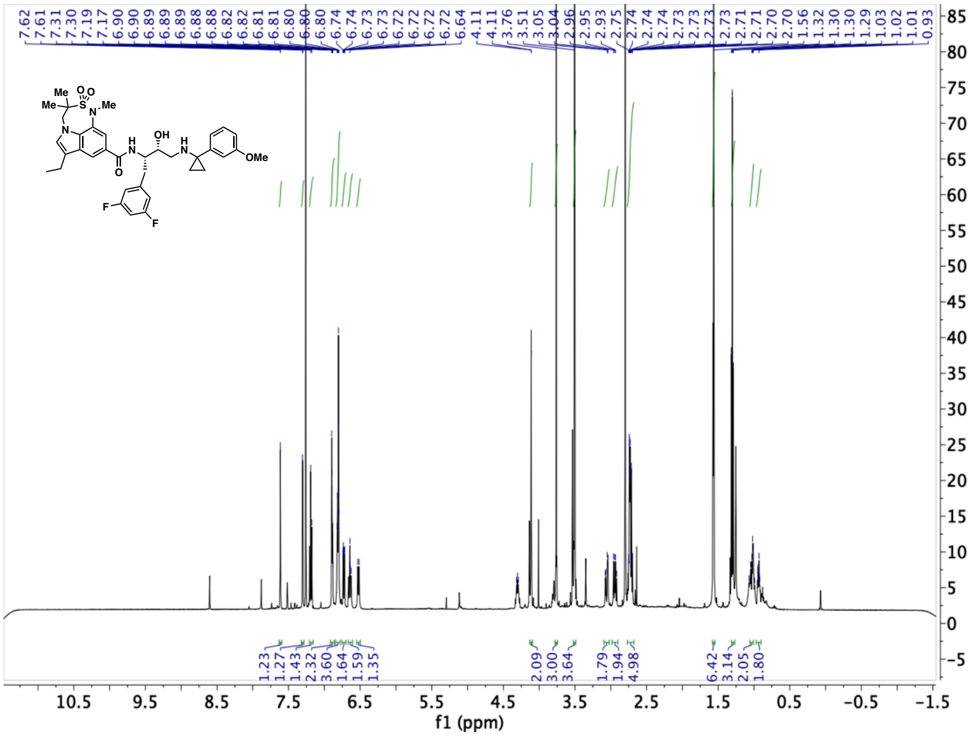
7.62
7.61
7.31
7.30
7.19
7.17
6.90
6.89
6.89
6.89
6.88
6.88
6.82
6.82
6.81
6.81
6.80
6.80
6.80
6.74
6.74
6.73
6.73
6.72
6.72
6.72
6.72
6.64
4.11
4.11
3.76
3.51
3.05
3.04
2.96
2.95
2.93
2.75
2.74
2.74
2.74
2.74
2.73
2.73
2.73
2.71
2.71
2.71
2.70
1.56
1.32
1.30
1.30
1.29
1.03
1.02
1.01
0.93
Me
Me
S
O
O
N
Me
N
H
N
OH
H
N
OMe
O
F
F
1.23
1.27
1.43
2.32
3.60
1.64
1.59
1.35
2.09
3.00
3.64
1.79
1.94
4.98
6.42
3.14
2.05
1.80
85
80
75
70
65
60
55
50
45
40
35
30
25
20
15
10
5
0
-5
10.5
9.5
8.5
7.5
6.5
5.5
4.5
3.5
2.5
1.5
0.5
-0.5
-1.5
f1 (ppm)

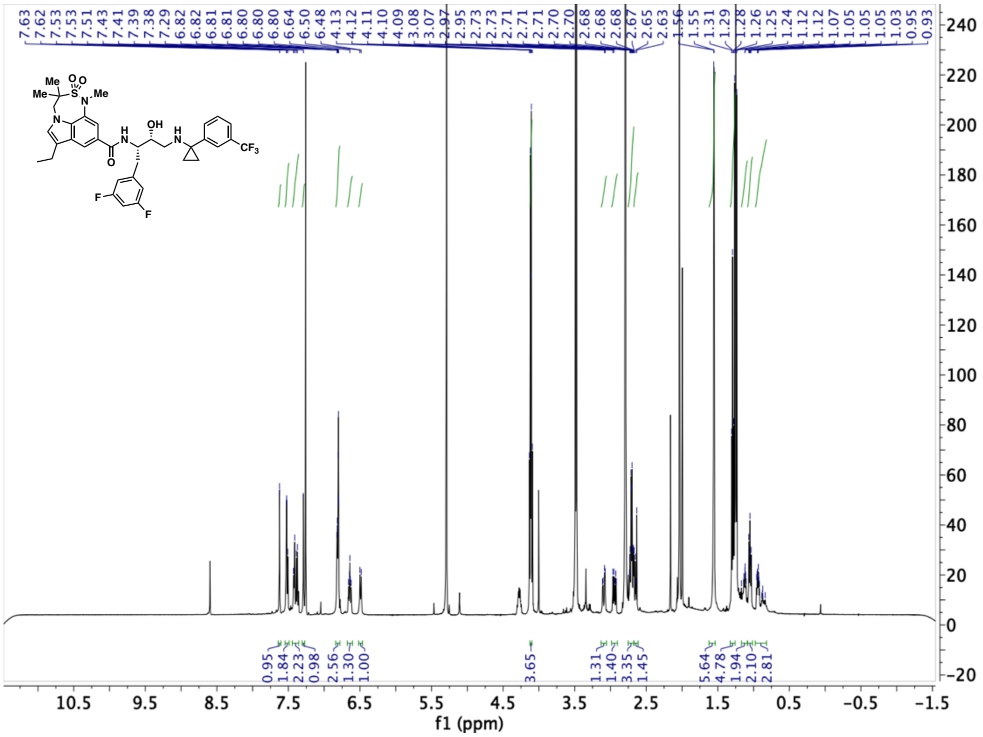
7.63
7.62
7.53
7.51
7.43
7.41
7.39
7.38
7.29
6.82
6.81
6.81
6.80
6.80
6.64
6.50
6.48
4.13
4.12
4.11
4.10
4.09
3.08
3.07
2.95
2.73
2.71
2.71
2.70
2.68
2.68
2.68
2.67
2.65
2.63
1.55
1.31
1.29
1.28
1.26
1.25
1.24
1.12
1.12
1.07
1.05
1.05
1.05
1.03
0.95
0.93
Me
Me
S
O
O
N
Me
N
H
N
OH
H
N
CF3
O
F
F
0.95
1.84
2.23
0.98
2.56
1.30
1.00
3.65
1.31
1.40
3.35
1.45
5.64
4.78
1.94
2.10
2.81
240
220
200
180
160
140
120
100
80
60
40
20
0
-20
10.5
9.5
8.5
7.5
6.5
5.5
4.5
3.5
2.5
1.5
0.5
-0.5
-1.5
f1 (ppm)

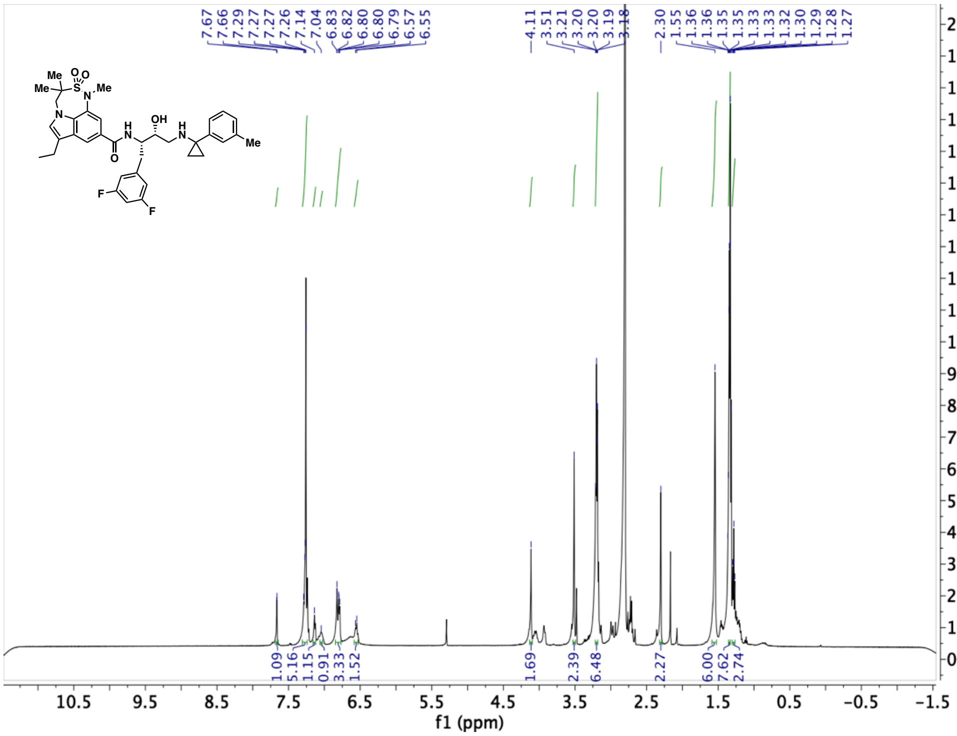
7.67
7.66
7.29
7.27
7.26
7.14
7.04
6.83
6.82
6.80
6.79
6.57
6.55
4.11
3.51
3.21
3.20
3.20
3.19
3.18
2.30
1.55
1.36
1.36
1.35
1.35
1.33
1.33
1.32
1.30
1.29
1.28
1.27
Me
Me
O
O
S
N
Me
N
H
N
OH
H
N
Me
F
F
1.09
5.16
1.15
0.91
3.33
1.52
1.69
2.39
6.48
2.27
6.00
7.62
2.74
10.5
9.5
8.5
7.5
6.5
5.5
4.5
3.5
2.5
1.5
0.5
−0.5
−1.5
f1 (ppm)
200
190
180
170
160
150
140
130
120
110
100
90
80
70
60
50
40
30
20
10
0

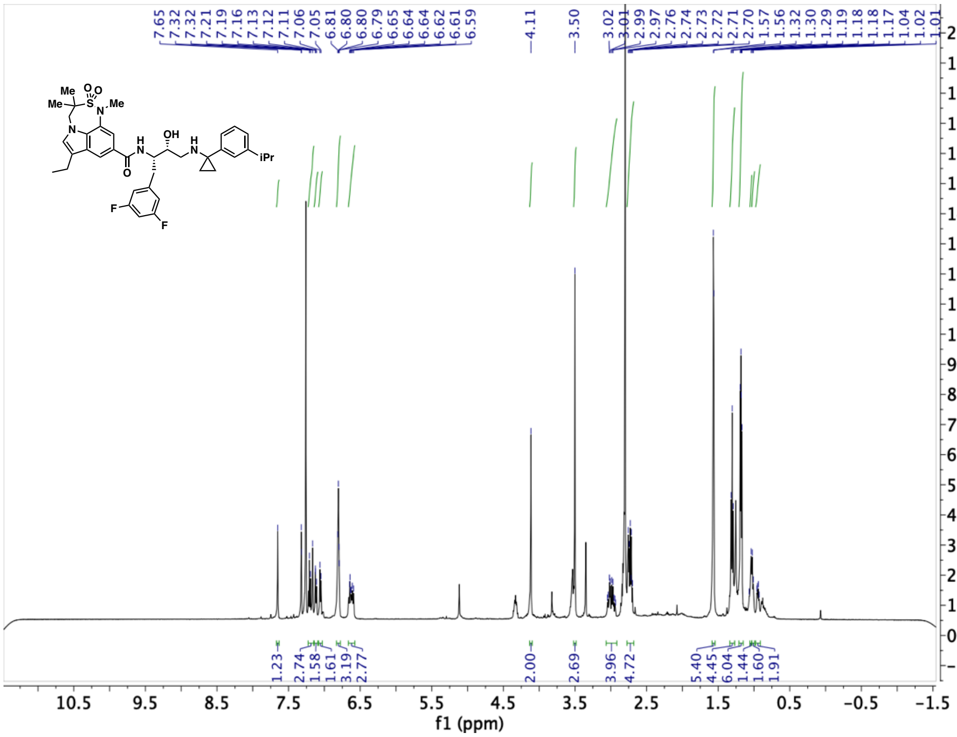
7.65
7.32
7.21
7.19
7.16
7.13
7.12
7.11
7.06
7.05
6.81
6.80
6.79
6.65
6.64
6.62
6.61
6.59
4.11
3.50
3.02
3.01
2.99
2.97
2.76
2.74
2.73
2.72
2.71
2.70
1.57
1.56
1.32
1.30
1.29
1.19
1.18
1.17
1.04
1.02
1.01
Me
Me
O
O
S
N
Me
N
H
N
OH
H
N
iPr
F
F
1.23
2.74
1.58
1.61
3.19
2.77
2.00
2.69
3.96
4.72
5.40
4.45
6.04
1.44
1.60
1.91
10.5
9.5
8.5
7.5
6.5
5.5
4.5
3.5
2.5
1.5
0.5
−0.5
−1.5
f1 (ppm)
200
190
180
170
160
150
140
130
120
110
100
90
80
70
60
50
40
30
20
10
0
−10

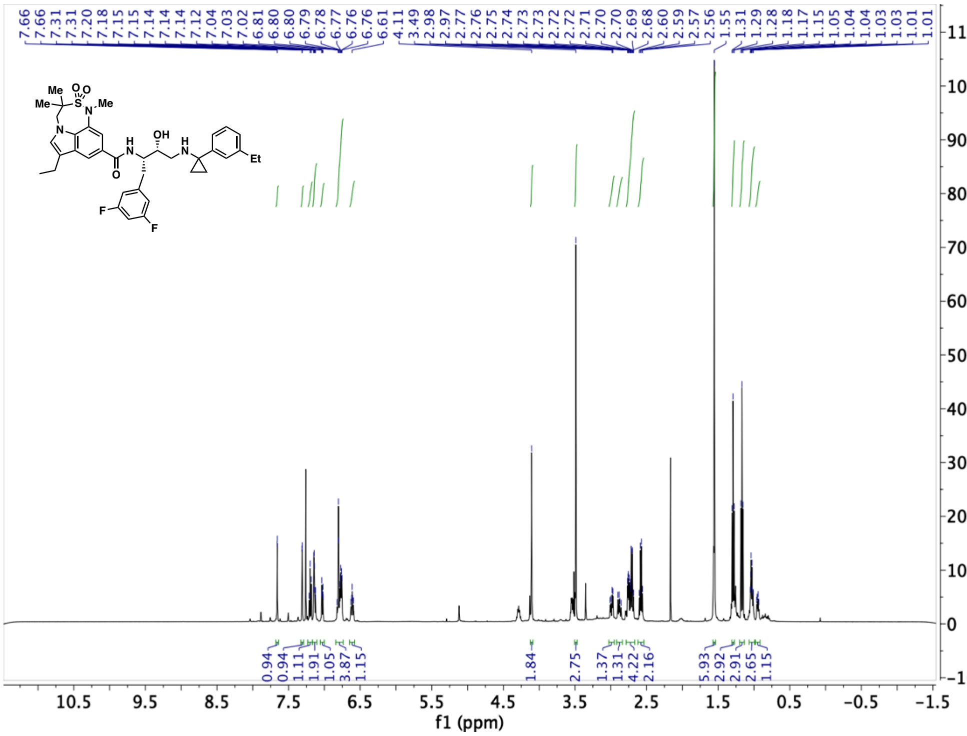
7.66
7.66
7.31
7.31
7.20
7.18
7.15
7.15
7.14
7.14
7.12
7.04
7.03
7.02
6.81
6.80
6.80
6.79
6.78
6.77
6.77
6.76
6.76
6.61
4.11
3.49
2.98
2.97
2.77
2.76
2.75
2.74
2.73
2.73
2.72
2.72
2.71
2.70
2.70
2.69
2.68
2.60
2.59
2.57
2.56
1.55
1.31
1.31
1.29
1.28
1.18
1.17
1.15
1.05
1.04
1.04
1.03
1.01
1.01
Me
Me
O
O
S
N
Me
N
H
N
OH
H
N
Et
O
F
F
0.94
0.94
1.11
1.91
1.05
3.87
1.15
1.84
2.75
1.37
1.31
4.22
2.16
5.93
2.92
2.91
2.65
1.15
1100
1000
900
800
700
600
500
400
300
200
100
0
-100
10.5
9.5
8.5
7.5
6.5
5.5
4.5
3.5
2.5
1.5
0.5
-0.5
-1.5
f1 (ppm)

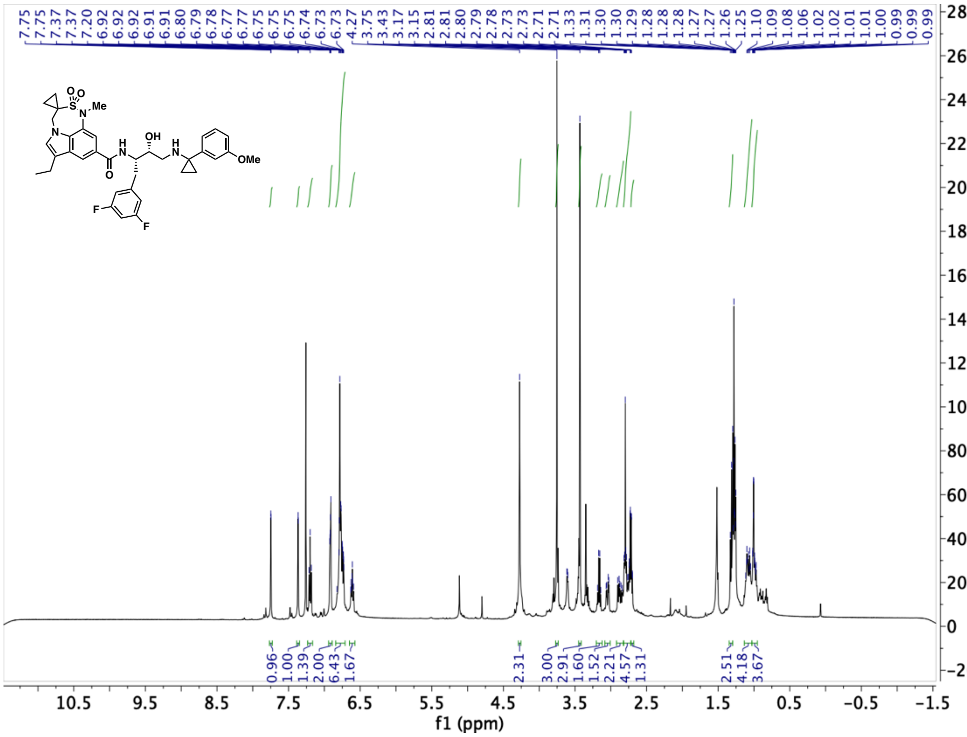
7.75
7.75
7.37
7.37
7.20
6.92
6.92
6.91
6.91
6.80
6.79
6.78
6.77
6.77
6.75
6.75
6.74
6.73
6.73
4.27
3.75
3.43
3.17
3.15
2.81
2.80
2.79
2.78
2.73
2.71
2.71
1.33
1.31
1.30
1.29
1.28
1.28
1.27
1.26
1.25
1.10
1.09
1.08
1.06
1.02
1.01
1.01
1.00
0.99
0.99
0.99
O
O
S
N
Me
N
H
N
OH
H
N
OMe
O
F
F
0.96
1.00
1.39
2.00
6.43
1.67
2.31
3.00
2.91
1.60
1.52
2.21
4.57
1.31
2.51
4.18
3.67
280
260
240
220
200
180
160
140
120
100
80
60
40
20
0
-20
10.5
9.5
8.5
7.5
6.5
5.5
4.5
3.5
2.5
1.5
0.5
-0.5
-1.5
f1 (ppm)

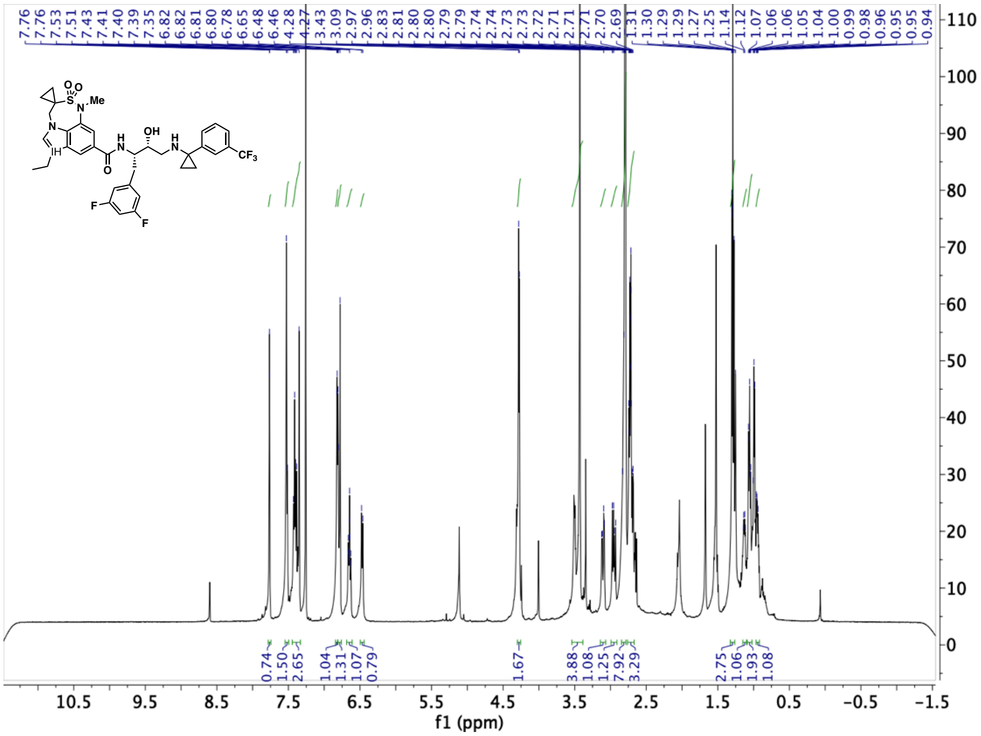
7.76
7.76
7.53
7.51
7.43
7.41
7.40
7.39
7.35
6.82
6.82
6.81
6.80
6.78
6.65
6.48
6.46
4.28
4.27
3.43
3.09
2.97
2.96
2.83
2.81
2.80
2.80
2.79
2.74
2.74
2.73
2.73
2.72
2.71
2.71
2.71
2.70
2.69
1.31
1.30
1.29
1.29
1.27
1.25
1.14
1.12
1.07
1.06
1.06
1.05
1.04
1.00
0.99
0.98
0.96
0.95
0.95
0.94
O
O
S
N
Me
N
N
IH
O
H
N
OH
H
N
CF3
F
F
0.74
1.50
2.65
1.04
1.31
1.07
0.79
1.67
3.88
1.08
1.25
7.92
3.29
2.75
1.06
1.93
1.08
110
100
90
80
70
60
50
40
30
20
10
0
10.5
9.5
8.5
7.5
6.5
5.5
4.5
3.5
2.5
1.5
0.5
−0.5
−1.5
f1 (ppm)

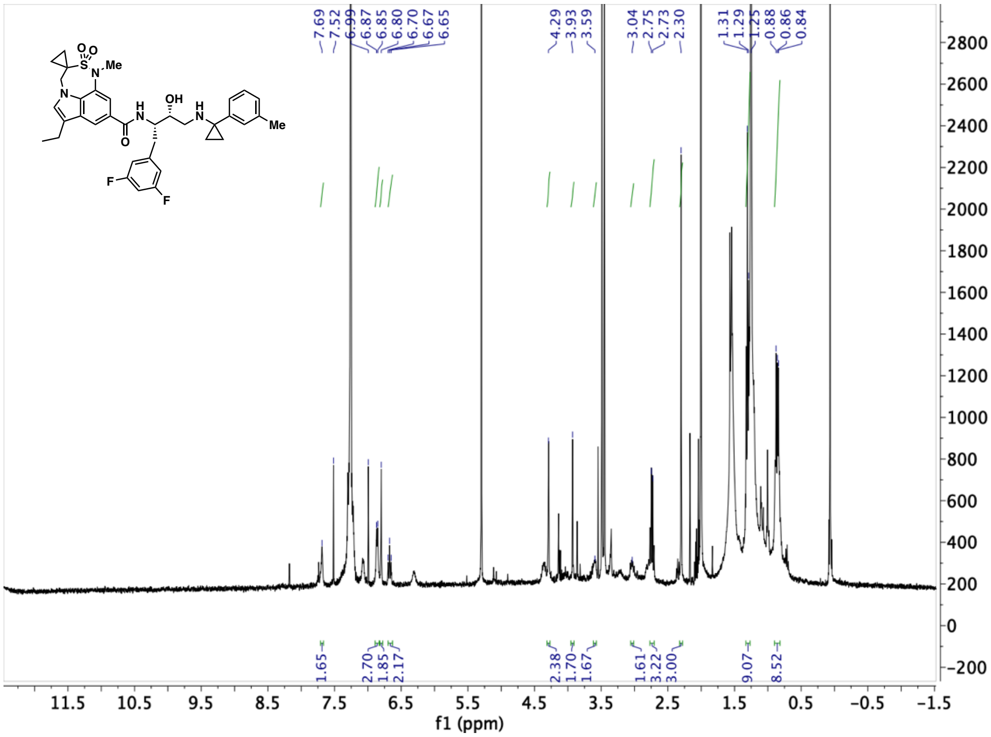
7.69
7.52
6.99
6.87
6.85
6.80
6.70
6.67
6.65
4.29
3.93
3.59
3.04
2.75
2.73
2.30
1.31
1.29
1.25
0.88
0.86
0.84
O
O
S
N
Me
N
H
N
OH
H
N
O
Me
F
F
1.65
2.70
1.85
2.17
2.38
1.70
1.67
1.61
3.22
3.00
9.07
8.52
2800
2600
2400
2200
2000
1800
1600
1400
1200
1000
800
600
400
200
0
−200
11.5
10.5
9.5
8.5
7.5
6.5
5.5
4.5
3.5
2.5
1.5
0.5
−0.5
−1.5
f1 (ppm)

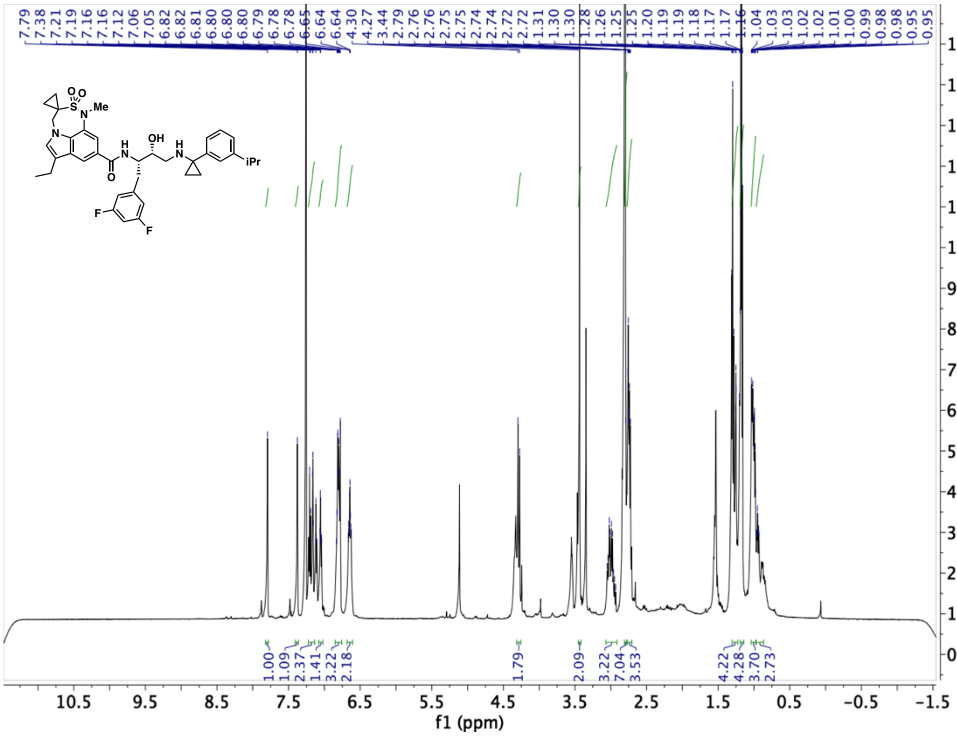
7.79
7.38
7.21
7.19
7.16
7.16
7.12
7.06
7.05
6.82
6.82
6.81
6.80
6.80
6.79
6.78
6.78
6.65
6.64
6.64
4.30
4.27
3.44
2.79
2.76
2.76
2.75
2.75
2.74
2.72
2.72
1.31
1.30
1.28
1.26
1.25
1.25
1.20
1.19
1.19
1.18
1.17
1.17
1.17
1.16
1.04
1.03
1.03
1.02
1.01
1.00
0.99
0.98
0.95
0.95
S
O
O
N
Me
N
H
OH
N
H
iPr
O
F
F
1.00
1.09
2.37
1.41
3.22
2.18
1.79
2.09
3.22
7.04
3.53
4.22
4.28
3.70
2.73
150
140
130
120
110
100
90
80
70
60
50
40
30
20
10
0
10.5
9.5
8.5
7.5
6.5
5.5
4.5
3.5
2.5
1.5
0.5
−0.5
−1.5
f1 (ppm)

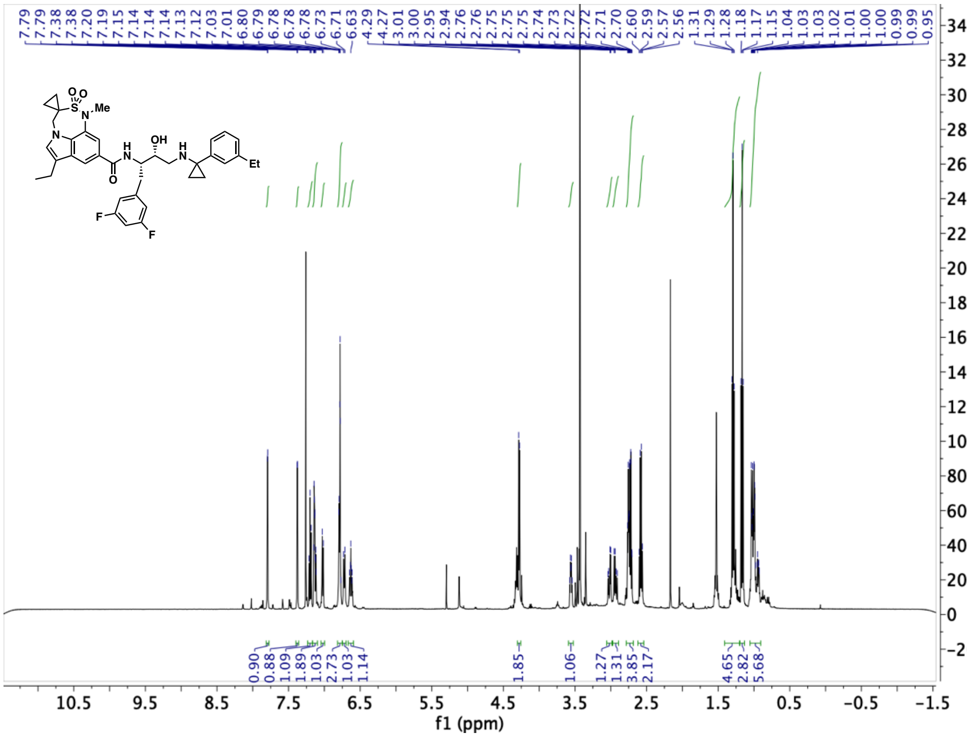
7.79
7.79
7.38
7.38
7.20
7.19
7.15
7.14
7.14
7.13
7.12
7.03
7.01
6.80
6.79
6.78
6.78
6.73
6.71
6.63
4.29
4.27
3.01
3.00
2.95
2.94
2.76
2.76
2.75
2.75
2.74
2.73
2.73
2.72
2.71
2.70
2.60
2.59
2.57
2.56
1.31
1.29
1.28
1.18
1.17
1.15
1.04
1.03
1.03
1.02
1.01
1.01
1.00
0.99
0.99
0.95
S
O
O
N
Me
N
H
OH
N
H
Et
O
F
F
0.90
0.88
1.09
1.89
1.03
2.73
1.03
1.14
1.85
1.06
1.27
1.31
3.85
2.17
4.65
2.82
5.68
340
320
300
280
260
240
220
200
180
160
140
120
100
80
60
40
20
0
−20
10.5
9.5
8.5
7.5
6.5
5.5
4.5
3.5
2.5
1.5
0.5
−0.5
−1.5
f1 (ppm)

REFERENCES

(1) Selkoe, D. J. Alzheimer's Disease: Genes, Proteins, and Therapy. *Physiol. Rev.* **2001**, *81* (2), 741–766. https://doi.org/10.1152/physrev.2001.81.2.741.

(2) 2012 Alzheimer's Disease Facts and Figures. *Alzheimers Dement.* **2012**, *8* (2), 131–168. https://doi.org/10.1016/j.jalz.2012.02.001.

(3) Alzheimer's Statistics. *Alzheimers.net*.

(4) Anand, P.; Singh, B. A Review on Cholinesterase Inhibitors for Alzheimer's Disease. *Arch. Pharm. Res.* **2013**, *36* (4), 375–399. https://doi.org/10.1007/s12272-013-0036-3.

(5) Hansen, R. A.; Gartlehner, G.; Webb, A. P.; Morgan, L. C.; Moore, C. G.; Jonas, D. E. Efficacy and Safety of Donepezil, Galantamine, and Rivastigmine for the Treatment of Alzheimer's Disease: A Systematic Review and Meta-Analysis. *Clin. Interv. Aging* **2008**, *3* (2), 211–225.

(6) Olivares, D.; K. Deshpande, V.; Shi, Y.; K. Lahiri, D.; H. Greig, N.; T. Rogers, J.; Huang, X. N-Methyl D-Aspartate (NMDA) Receptor Antagonists and Memantine Treatment for Alzheimer's Disease, Vascular Dementia and Parkinson's Disease. *Curr. Alzheimer Res.* **2012**, *9* (6), 746–758. https://doi.org/10.2174/156720512801322564.

(7) Hyde, C.; Peters, J.; Bond, M.; Rogers, G.; Hoyle, M.; Anderson, R.; Jeffreys, M.; Davis, S.; Thokala, P.; Moxham, T. Evolution of the Evidence on the Effectiveness and Cost-Effectiveness of Acetylcholinesterase Inhibitors and Memantine for Alzheimer's Disease: Systematic Review and Economic Model†. *Age Ageing* **2013**, *42* (1), 14–20. https://doi.org/10.1093/ageing/afs165.

(8) Selkoe, D. J. Translating Cell Biology into Therapeutic Advances in Alzheimer's Disease. *Nature* **1999**, *399* (6738), A23–A31. https://doi.org/10.1038/399a023.

(9) Citron, M. Alzheimer's Disease: Strategies for Disease Modification. *Nat. Rev. Drug Discov.* **2010**, *9* (5), 387–398. https://doi.org/10.1038/nrd2896.

(10) Billings, L. M.; Oddo, S.; Green, K. N.; McGaugh, J. L.; LaFerla, F. M. Intraneuronal Aβ Causes the Onset of Early Alzheimer's Disease-Related Cognitive Deficits in Transgenic Mice. *Neuron* **2005**, *45* (5), 675–688. https://doi.org/10.1016/j.neuron.2005.01.040.

(11) Selkoe, D. J. Cell Biology of the Amyloid Beta-Protein Precursor and the Mechanism of Alzheimer's Disease. *Annu. Rev. Cell Biol.* **1994**, *10* (1), 373–403. https://doi.org/10.1146/annurev.cb.10.110194.002105.

(12) Selkoe, D. J. Alzheimer's Disease Is a Synaptic Failure. *Science* **2002**, *298* (5594), 789–791. https://doi.org/10.1126/science.1074069.

(13) Ohno, M.; Cole, S. L.; Yasvoina, M.; Zhao, J.; Citron, M.; Berry, R.; Disterhoft, J. F.; Vassar, R. BACE1 Gene Deletion Prevents Neuron Loss and Memory Deficits in 5XFAD APP/PS1 Transgenic Mice. *Neurobiol. Dis.* **2007**, *26* (1), 134–145. https://doi.org/10.1016/j.nbd.2006.12.008.

(14) Kang, J.; Lemaire, H.-G.; Unterbeck, A.; Salbaum, J. M.; Masters, C. L.; Grzeschik, K.-H.; Multhaup, G.; Beyreuther, K.; Müller-Hill, B. The Precursor of Alzheimer's Disease Amyloid A4 Protein Resembles a Cell-Surface Receptor. *Nature* **1987**, *325* (6106), 733–736. https://doi.org/10.1038/325733a0.

(15) Weidemann, A.; König, G.; Bunke, D.; Fischer, P.; Salbaum, J. M.; Masters, C. L.; Beyreuther, K. Identification, Biogenesis, and Localization of Precursors of Alzheimer's Disease A4 Amyloid Protein. *Cell* **1989**, *57* (1), 115–126. https://doi.org/10.1016/0092-8674(89)90177-3.

(16) Seubert, P.; Oltersdorf, T.; Lee, M. G.; Barbour, R.; Blomquist, C.; Davis, D. L.; Bryant, K.; Fritz, L. C.; Galasko, D.; Thal, L. J.; et al. Secretion of β-Amyloid Precursor Protein Cleaved at the Amino Terminus of the β-Amyloid Peptide. *Nature* **1993**, *361* (6409), 260–263. https://doi.org/10.1038/361260a0.

(17) Haass, C. The Presenilins in Alzheimer's Disease--Proteolysis Holds the Key. *Science* **1999**, *286* (5441), 916–919. https://doi.org/10.1126/science.286.5441.916.

(18) Citron, M.; Vigo-Pelfrey, C.; Teplow, D. B.; Miller, C.; Schenk, D.; Johnston, J.; Winblad, B.; Venizelos, N.; Lannfelt, L.; Selkoe, D. J. Excessive Production of Amyloid Beta-Protein by Peripheral Cells of Symptomatic and Presymptomatic Patients Carrying the Swedish Familial Alzheimer Disease Mutation. *Proc. Natl. Acad. Sci.* **1994**, *91* (25), 11993–11997. https://doi.org/10.1073/pnas.91.25.11993.

(19) Kumar-Singh, S.; Jonghe, C. D.; Cruts, M.; Kleinert, R.; Wang, R.; Mercken, M.; Strooper, B. D.; Vanderstichele, H.; Löfgren, A.; Vanderhoeven, I.; et al. Γ42-Secretase Site Mutation Points to an Essential Role. 10.

(20) Ancolio, K.; Dumanchin, C.; Barelli, H.; Warter, J. M.; Brice, A.; Campion, D.; Frebourg, T.; Checler, F. Unusual Phenotypic Alteration of Amyloid Precursor Protein (APP) Maturation by a New Val-715 -> Met APP-770 Mutation Responsible for Probable Early-Onset Alzheimer's Disease. *Proc. Natl. Acad. Sci.* **1999**, *96* (7), 4119–4124. https://doi.org/10.1073/pnas.96.7.4119.

(21) Murrell, J.; Farlow, M.; Ghetti, B.; Benson, M. A Mutation in the Amyloid Precursor Protein Associated with Hereditary Alzheimer's Disease. *Science* **1991**, *254* (5028), 97–99. https://doi.org/10.1126/science.1925564.

(22) Kwok, J. B. J.; Li, Q.-X.; Hallupp, M.; Whyte, S.; Ames, D.; Beyreuther, K.; Masters, C. L.; Schofield, P. R. Novel Leu723Pro Amyloid Precursor Protein Mutation Increases Amyloid B42(43) Peptide Levels and Induces Apoptosis. *Ann. Neurol.* **2000**, *47* (2), 249–253. https://doi.org/10.1002/1531-8249(200002)47:2<249::AID-ANA18>3.0.CO;2-8.

(23) Van Broeckhoven, C.; Haan, J.; Bakker, E.; Hardy, J.; Van Hul, W.; Wehnert, A.; Vegter-Van der Vlis, M.; Roos, R. Amyloid Beta Protein Precursor Gene and Hereditary Cerebral Hemorrhage with Amyloidosis (Dutch). *Science* **1990**, *248* (4959), 1120–1122. https://doi.org/10.1126/science.1971458.

(24) Hardy, J. The Amyloid Hypothesis of Alzheimer's Disease: Progress and Problems on the Road to Therapeutics. *Science* **2002**, *297* (5580), 353–356. https://doi.org/10.1126/science.1072994.

(25) Buxbaum, J. D.; Liu, K.-N.; Luo, Y.; Slack, J. L.; Stocking, K. L.; Peschon, J. J.; Johnson, R. S.; Castner, B. J.; Cerretti, D. P.; Black, R. A. The Alzheimer Amyloid Protein Precursor. 4.

(26) Lammich, S.; Kojro, E.; Postina, R.; Gilbert, S.; Pfeiffer, R.; Jasionowski, M.; Haass, C.; Fahrenholz, F. Constitutive and Regulated -Secretase Cleavage of Alzheimer's Amyloid Precursor Protein by a Disintegrin Metalloprotease. *Proc. Natl. Acad. Sci.* **1999**, *96* (7), 3922–3927. https://doi.org/10.1073/pnas.96.7.3922.

(27) Wolfe, M. S.; Xia, W.; Ostaszewski, B. L.; Diehl, T. S.; Kimberly, W. T.; Selkoe, D. J. Two Transmembrane Aspartates in Presenilin-1 Required for Presenilin Endoproteolysis and g-Secretase Activity. **1999**, *398*, 5.

(28) Haass, C. Take Five—BACE and the γ-Secretase Quartet Conduct Alzheimer's Amyloid β-Peptide Generation. *EMBO J.* **2004**, *23* (3), 483–488. https://doi.org/10.1038/sj.emboj.7600061.

(29) Esler, W. P.; Kimberly, W. T.; Ostaszewski, B. L.; Diehl, T. S.; Moore, C. L.; Tsai, J.-Y.; Rahmati, T.; Xia, W.; Selkoe, D. J.; Wolfe, M. S. Transition-State Analogue Inhibitors of γ-Secretase Bind Directly to Presenilin-1. *Nat. Cell Biol.* **2000**, *2* (7), 428–434. https://doi.org/10.1038/35017062.

(30) Saftig, P.; Peters, C.; von Figura, K.; Craessaerts, K.; Van Leuven, F.; De Strooper, B. Amyloidogenic Processing of Human Amyloid Precursor Protein in Hippocampal Neurons Devoid of Cathepsin D. *J. Biol. Chem.* **1996**, *271* (44), 27241–27244. https://doi.org/10.1074/jbc.271.44.27241.

(31) Yan, R.; Bienkowski, M. J.; Shuck, M. E.; Miao, H.; Tory, M. C.; Pauley, A. M.; Brashler, J. R.; Stratman, N. C.; Mathews, W. R.; Buhl, A. E.; et al. Membrane-Anchored Aspartyl Protease with Alzheimer's Disease b-Secretase Activity. **1999**, *402*, 5.

(32) Bennett, B. D.; Babu-Khan, S.; Loeloff, R.; Louis, J.-C.; Curran, E.; Citron, M.; Vassar, R. Expression Analysis of BACE2 in Brain and Peripheral Tissues. *J. Biol. Chem.* **2000**, *275* (27), 20647–20651. https://doi.org/10.1074/jbc.M002688200.

(33) Huber, A. B.; Brösamle, C.; Mechler, H.; Huber, G. Metalloprotease MP100: A Synaptic Protease in Rat Brain. *Brain Res.* **1999**, *837* (1–2), 193–202. https://doi.org/10.1016/S0006-8993(99)01693-5.

(34) Hussain, I.; Powell, D.; Howlett, D. R.; Tew, D. G.; Meek, T. D.; Chapman, C.; Gloger, I. S.; Murphy, K. E.; Southan, C. D.; Ryan, D. M.; et al. Identification of a Novel Aspartic Protease (Asp 2) as β-Secretase. *Mol. Cell. Neurosci.* **1999**, *14* (6), 419–427. https://doi.org/10.1006/mcne.1999.0811.

(35) Vassar, R. Beta-Secretase Cleavage of Alzheimer's Amyloid Precursor Protein by the Transmembrane Aspartic Protease BACE. *Science* **1999**, *286* (5440), 735–741. https://doi.org/10.1126/science.286.5440.735.

(36) Sinha, S.; Anderson, J. P.; Barbour, R.; Basi, G. S.; Caccavello, R.; Davis, D.; Doan, M.; Dovey, H. F.; Frigon, N.; Hong, J.; et al. Purification and Cloning of Amyloid Precursor Protein β-Secretase from Human Brain. *Nature* **1999**, *402* (6761), 537–540. https://doi.org/10.1038/990114.

(37) Lin, X.; Koelsch, G.; Wu, S.; Downs, D.; Dashti, A.; Tang, J. Human Aspartic Protease Memapsin 2 Cleaves the Beta -Secretase Site of Beta -Amyloid Precursor Protein. *Proc. Natl. Acad. Sci.* **2000**, *97* (4), 1456–1460. https://doi.org/10.1073/pnas.97.4.1456.

(38) Benjannet, S.; Elagoz, A.; Wickham, L.; Mamarbachi, M.; Munzer, J. S.; Basak, A.; Lazure, C.; Cromlish, J. A.; Sisodia, S.; Checler, F.; et al. Post-Translational Processing of β-Secretase (β-Amyloid-Converting Enzyme) and Its Ectodomain Shedding: THE PRO- AND TRANSMEMBRANE/CYTOSOLIC DOMAINS AFFECT ITS CELLULAR ACTIVITY AND AMYLOID-β PRODUCTION. *J. Biol. Chem.* **2001**, *276* (14), 10879–10887. https://doi.org/10.1074/jbc.M009899200.

(39) Shi, X.-P.; Chen, E.; Yin, K.-C.; Na, S.; Garsky, V. M.; Lai, M.-T.; Li, Y.-M.; Platchek, M.; Register, R. B.; Sardana, M. K.; et al. The Pro Domain of β-Secretase Does Not Confer Strict Zymogen-like Properties but Does Assist Proper Folding of the Protease Domain. *J. Biol. Chem.* **2001**, *276* (13), 10366–10373. https://doi.org/10.1074/jbc.M009200200.

(40) Ermolieff, J.; Loy, J. A.; Koelsch, G.; Tang, J. Proteolytic Activation of Recombinant Pro-Memapsin 2 (Pro-β-Secretase) Studied with New Fluorogenic Substrates †. *Biochemistry* **2000**, *39* (40), 12450–12456. https://doi.org/10.1021/bi001494f.

(41) Huse, J. T.; Pijak, D. S.; Leslie, G. J.; Lee, V. M.-Y.; Doms, R. W. Maturation and Endosomal Targeting of β-Site Amyloid Precursor Protein-Cleaving Enzyme: THE ALZHEIMER'S DISEASE β-SECRETASE. *J. Biol. Chem.* **2000**, *275* (43), 33729–33737. https://doi.org/10.1074/jbc.M004175200.

(42) Fischer, F.; Molinari, M.; Bodendorf, U.; Paganetti, P. The Disulphide Bonds in the Catalytic Domain of BACE Are Critical but Not Essential for Amyloid Precursor Protein Processing Activity. *J. Neurochem.* **2002**, *80* (6), 1079–1088. https://doi.org/10.1046/j.0022-3042.2002.00806.x.

(43) Hong, L. Structure of the Protease Domain of Memapsin 2 (Beta -Secretase) Complexed with Inhibitor. *Science* **2000**, *290* (5489), 150–153. https://doi.org/10.1126/science.290.5489.150.

(44) Roberds, S. L. BACE Knockout Mice Are Healthy despite Lacking the Primary Beta-Secretase Activity in Brain: Implications for Alzheimer's Disease Therapeutics. *Hum. Mol. Genet.* **2001**, *10* (12), 1317–1324. https://doi.org/10.1093/hmg/10.12.1317.

(45) Luo, Y.; Bolon, B.; Kahn, S.; Bennett, B. D.; Babu-Khan, S.; Denis, P.; Fan, W.; Kha, H.; Zhang, J.; Gong, Y.; et al. Mice Deficient in BACE1, the Alzheimer's β-Secretase, Have Normal Phenotype and Abolished β-Amyloid Generation. *Nat. Neurosci.* **2001**, *4* (3), 231–232. https://doi.org/10.1038/85059.

(46) Nishitomi, K.; Sakaguchi, G.; Horikoshi, Y.; Gray, A. J.; Maeda, M.; Hirata-Fukae, C.; Becker, A. G.; Hosono, M.; Sakaguchi, I.; Minami, S. S.; et al. BACE1 Inhibition Reduces Endogenous Abeta and Alters APP Processing in Wild-Type Mice. *J. Neurochem.* **2006**, *99* (6), 1555–1563. https://doi.org/10.1111/j.1471-4159.2006.04178.x.

(47) Hu, X.; Zhou, X.; He, W.; Yang, J.; Xiong, W.; Wong, P.; Wilson, C. G.; Yan, R. BACE1 Deficiency Causes Altered Neuronal Activity and Neurodegeneration. *J. Neurosci.* **2010**, *30* (26), 8819–8829. https://doi.org/10.1523/JNEUROSCI.1334-10.2010.

(48) Hu, X.; Hicks, C. W.; He, W.; Wong, P.; Macklin, W. B.; Trapp, B. D.; Yan, R. Bace1 Modulates Myelination in the Central and Peripheral Nervous System. *Nat. Neurosci.* **2006**, *9* (12), 1520–1525. https://doi.org/10.1038/nn1797.

(49) Kobayashi, D.; Zeller, M.; Cole, T.; Buttini, M.; McConlogue, L.; Sinha, S.; Freedman, S.; Morris, R. G. M.; Chen, K. S. BACE1 Gene Deletion: Impact on Behavioral Function in a Model of Alzheimer's Disease. *Neurobiol. Aging* **2008**, *29* (6), 861–873. https://doi.org/10.1016/j.neurobiolaging.2007.01.002.

(50) Hitt, B.; Riordan, S. M.; Kukreja, L.; Eimer, W. A.; Rajapaksha, T. W.; Vassar, R. β-Site Amyloid Precursor Protein (APP)-Cleaving Enzyme 1 (BACE1)-Deficient Mice Exhibit a Close Homolog of L1 (CHL1) Loss-of-Function Phenotype Involving Axon Guidance Defects. *J. Biol. Chem.* **2012**, *287* (46), 38408–38425. https://doi.org/10.1074/jbc.M112.415505.

(51) Laird, F. M. BACE1, a Major Determinant of Selective Vulnerability of the Brain to Amyloid- Amyloidogenesis, Is Essential for Cognitive, Emotional, and Synaptic Functions. *J. Neurosci.* **2005**, *25* (50), 11693–11709. https://doi.org/10.1523/JNEUROSCI.2766-05.2005.

(52) Savonenko, A. V.; Melnikova, T.; Laird, F. M.; Stewart, K.-A.; Price, D. L.; Wong, P. C. Alteration of BACE1-Dependent NRG1/ErbB4 Signaling and Schizophrenia-like Phenotypes in BACE1-Null Mice. *Proc. Natl. Acad. Sci.* **2008**, *105* (14), 5585–5590. https://doi.org/10.1073/pnas.0710373105.

(53) *Aspartic Acid Proteases as Therapeutic Targets*; Ghosh, A. K., Ed.; Methods and principles in medicinal chemistry; Wiley-VCH: Weinheim, 2010.

(54) Bennett, B. D.; Babu-Khan, S.; Loeloff, R.; Louis, J.-C.; Curran, E.; Citron, M.; Vassar, R. Expression Analysis of BACE2 in Brain and Peripheral Tissues. *J. Biol. Chem.* **2000**, *275* (27), 20647–20651. https://doi.org/10.1074/jbc.M002688200.

(55) Turner, R. T.; Koelsch, G.; Hong, L.; Castenheira, P.; Ghosh, A.; Tang, J. Subsite Specificity of Memapsin 2 (β-Secretase): Implications for Inhibitor Design †. *Biochemistry* **2001**, *40* (34), 10001–10006. https://doi.org/10.1021/bi015546s.

(56) Hong, L.; Tang, J. Flap Position of Free Memapsin 2 (β-Secretase), a Model for Flap Opening in Aspartic Protease Catalysis † , ‡. *Biochemistry* **2004**, *43* (16), 4689–4695. https://doi.org/10.1021/bi0498252.

(57) Hong, L.; Turner, R. T.; Koelsch, G.; Shin, D.; Ghosh, A. K.; Tang, J. Crystal Structure of Memapsin 2 (β-Secretase) in Complex with an Inhibitor OM00-3 †. *Biochemistry* **2002**, *41* (36), 10963–10967. https://doi.org/10.1021/bi026232n.

(58) Chang, W.-P.; Koelsch, G.; Wong, S.; Downs, D.; Da, H.; Weerasena, V.; Gordon, B.; Devasamudram, T.; Bilcer, G.; Ghosh, A. K.; et al. In Vivo Inhibition of Aβ Production by Memapsin 2 (β-Secretase) Inhibitors: Inhibition of Aβ Production in Vivo. *J. Neurochem.* **2004**, *89* (6), 1409–1416. https://doi.org/10.1111/j.1471-4159.2004.02452.x.

(59) Meredith, J. E.; Thompson, L. A.; Toyn, J. H.; Marcin, L.; Barten, D. M.; Marcinkeviciene, J.; Kopcho, L.; Kim, Y.; Lin, A.; Guss, V.; et al. P-Glycoprotein Efflux and Other Factors Limit Brain Amyloid Reduction by -Site Amyloid Precursor Protein-Cleaving Enzyme 1 Inhibitors in Mice. *J. Pharmacol. Exp. Ther.* **2008**, *326* (2), 502–513. https://doi.org/10.1124/jpet.108.138974.

(60) Sinha, S.; Lieberburg, I. Cellular Mechanisms of Beta -Amyloid Production and Secretion. *Proc. Natl. Acad. Sci.* **1999**, *96* (20), 11049–11053. https://doi.org/10.1073/pnas.96.20.11049.

(61) Ghosh, A. K.; Shin, D.; Koelsch, G.; Lin, X.; Ermolieff, J.; Tang, J. Design of Potent Inhibitors for Human Brain Memapsin 2 (β-Secretase). *J. Am. Chem. Soc.* **2000**, *122* (14), 3522–3523. https://doi.org/10.1021/ja000300g.

(62) Ghosh, A. K.; Bilcer, G.; Harwood, C.; Kawahama, R.; Shin, D.; Hussain, K. A.; Hong, L.; Loy, J. A.; Nguyen, C.; Koelsch, G.; et al. Structure-Based Design: Potent Inhibitors of Human Brain Memapsin 2 (β-Secretase). *J. Med. Chem.* **2001**, *44* (18), 2865–2868. https://doi.org/10.1021/jm0101803.

(63) Ghosh, A. K.; Osswald, H. L. BACE1 (β-Secretase) Inhibitors for the Treatment of Alzheimer's Disease. *Chem Soc Rev* **2014**, *43* (19), 6765–6813. https://doi.org/10.1039/C3CS60460H.

(64) Cummings, J. L.; Morstorf, T.; Zhong, K. Alzheimer's Disease Drug-Development Pipeline: Few Candidates, Frequent Failures. *Alzheimers Res. Ther.* **2014**, *6* (4), 37. https://doi.org/10.1186/alzrt269.

(65) Ghosh, A. K.; Kumaragurubaran, N.; Hong, L.; Lei, H.; Hussain, K. A.; Liu, C.-F.; Devasamudram, T.; Weerasena, V.; Turner, R.; Koelsch, G.; et al. Design, Synthesis and X-Ray Structure of Protein−Ligand Complexes: Important Insight into Selectivity of Memapsin 2 (β-Secretase) Inhibitors. *J. Am. Chem. Soc.* **2006**, *128* (16), 5310–5311. https://doi.org/10.1021/ja058636j.

(66) Ghosh, A. K.; Kumaragurubaran, N.; Hong, L.; Kulkarni, S. S.; Xu, X.; Chang, W.; Weerasena, V.; Turner, R.; Koelsch, G.; Bilcer, G.; et al. Design, Synthesis, and X-Ray Structure of Potent Memapsin 2 (β-Secretase) Inhibitors with Isophthalamide Derivatives as the P $_2$ - P $_3$ -Ligands. *J. Med. Chem.* **2007**, *50* (10), 2399–2407. https://doi.org/10.1021/jm061338s.

(67) Stachel, S. J.; Coburn, C. A.; Steele, T. G.; Jones, K. G.; Loutzenhiser, E. F.; Gregro, A. R.; Rajapakse, H. A.; Lai, M.-T.; Crouthamel, M.-C.; Xu, M.; et al. Structure-Based Design of Potent and Selective Cell-Permeable Inhibitors of Human β-Secretase (BACE-1). *J. Med. Chem.* **2004**, *47* (26), 6447–6450. https://doi.org/10.1021/jm049379g.

(68) Chang, W.-P.; Huang, X.; Downs, D.; Cirrito, J. R.; Koelsch, G.; Holtzman, D. M.; Ghosh, A. K.; Tang, J. β-Secretase Inhibitor GRL-8234 Rescues Age-Related Cognitive Decline in APP Transgenic Mice. *FASEB J.* **2011**, *25* (2), 775–784. https://doi.org/10.1096/fj.10-167213.

(69) Ghosh, A. K.; Kumaragurubaran, N.; Hong, L.; Kulkarni, S.; Xu, X.; Miller, H. B.; Srinivasa Reddy, D.; Weerasena, V.; Turner, R.; Chang, W.; et al. Potent Memapsin 2 (β-Secretase) Inhibitors: Design, Synthesis, Protein-Ligand X-Ray Structure, and in Vivo Evaluation. *Bioorg. Med. Chem. Lett.* **2008**, *18* (3), 1031–1036. https://doi.org/10.1016/j.bmcl.2007.12.028.

(70) Beswick, P.; Charrier, N.; Clarke, B.; Demont, E.; Dingwall, C.; Dunsdon, R.; Faller, A.; Gleave, R.; Hawkins, J.; Hussain, I.; et al. BACE-1 Inhibitors Part 3: Identification of Hydroxy Ethylamines (HEAs) with Nanomolar Potency in Cells. *Bioorg. Med. Chem. Lett.* **2008**, *18* (3), 1022–1026. https://doi.org/10.1016/j.bmcl.2007.12.020.

(71) Charrier, N.; Clarke, B.; Cutler, L.; Demont, E.; Dingwall, C.; Dunsdon, R.; Hawkins, J.; Howes, C.; Hubbard, J.; Hussain, I.; et al. Second Generation of BACE-1 Inhibitors Part 3: Towards Non Hydroxyethylamine Transition State Mimetics. *Bioorg. Med. Chem. Lett.* **2009**, *19* (13), 3674–3678. https://doi.org/10.1016/j.bmcl.2009.03.149.

(72) Coburn, C. A.; Stachel, S. J.; Jones, K. G.; Steele, T. G.; Rush, D. M.; DiMuzio, J.; Pietrak, B. L.; Lai, M.-T.; Huang, Q.; Lineberger, J.; et al. BACE-1 Inhibition by a Series of ψ[CH2NH] Reduced Amide Isosteres. *Bioorg. Med. Chem. Lett.* **2006**, *16* (14), 3635–3638. https://doi.org/10.1016/j.bmcl.2006.04.076.

(73) Ghosh, A. K.; Venkateswara Rao, K.; Yadav, N. D.; Anderson, D. D.; Gavande, N.; Huang, X.; Terzyan, S.; Tang, J. Structure-Based Design of Highly Selective β-Secretase Inhibitors: Synthesis, Biological Evaluation, and Protein–Ligand X-Ray Crystal Structure. *J. Med. Chem.* **2012**, *55* (21), 9195–9207. https://doi.org/10.1021/jm3008823.

(74) Machauer, R.; Laumen, K.; Veenstra, S.; Rondeau, J.-M.; Tintelnot-Blomley, M.; Betschart, C.; Jaton, A.-L.; Desrayaud, S.; Staufenbiel, M.; Rabe, S.; et al. Macrocyclic Peptidomimetic β-Secretase (BACE-1) Inhibitors with Activity in Vivo. *Bioorg. Med. Chem. Lett.* **2009**, *19* (5), 1366–1370. https://doi.org/10.1016/j.bmcl.2009.01.055.

(75) Cole, D. C.; Manas, E. S.; Stock, J. R.; Condon, J. S.; Jennings, L. D.; Aulabaugh, A.; Chopra, R.; Cowling, R.; Ellingboe, J. W.; Fan, K. Y.; et al. Acylguanidines as Small-Molecule β-Secretase Inhibitors. *J. Med. Chem.* **2006**, *49* (21), 6158–6161. https://doi.org/10.1021/jm0607451.

(76) Thomas, A. A.; Hunt, K. W.; Volgraf, M.; Watts, R. J.; Liu, X.; Vigers, G.; Smith, D.; Sammond, D.; Tang, T. P.; Rhodes, S. P.; et al. Discovery of 7-Tetrahydropyran-2-Yl Chromans: β-Site Amyloid Precursor Protein Cleaving Enzyme 1 (BACE1) Inhibitors That Reduce Amyloid β-Protein (Aβ) in the Central Nervous System. *J. Med. Chem.* **2014**, *57* (3), 878–902. https://doi.org/10.1021/jm401635n.

(77) Congreve, M.; Aharony, D.; Albert, J.; Callaghan, O.; Campbell, J.; Carr, R. A. E.; Chessari, G.; Cowan, S.; Edwards, P. D.; Frederickson, M.; et al. Application of Fragment Screening by X-Ray Crystallography to the Discovery of Aminopyridines as Inhibitors of β-Secretase [§]. *J. Med. Chem.* **2007**, *50* (6), 1124–1132. https://doi.org/10.1021/jm061197u.

(78) Malamas, M. S.; Barnes, K.; Hui, Y.; Johnson, M.; Lovering, F.; Condon, J.; Fobare, W.; Solvibile, W.; Turner, J.; Hu, Y.; et al. Novel Pyrrolyl 2-Aminopyridines as Potent and Selective Human β-Secretase (BACE1) Inhibitors. *Bioorg. Med. Chem. Lett.* **2010**, *20* (7), 2068–2073. https://doi.org/10.1016/j.bmcl.2010.02.075.

(79) Hills, I. D.; Katharine Holloway, M.; de León, P.; Nomland, A.; Zhu, H.; Rajapakse, H.; Allison, T. J.; Munshi, S. K.; Colussi, D.; Pietrak, B. L.; et al. A Conformational Constraint Improves a β-Secretase Inhibitor but for an Unexpected Reason. *Bioorg. Med. Chem. Lett.* **2009**, *19* (17), 4993–4995. https://doi.org/10.1016/j.bmcl.2009.07.071.

(80) Swahn, B.-M.; Holenz, J.; Kihlström, J.; Kolmodin, K.; Lindström, J.; Plobeck, N.; Rotticci, D.; Sehgelmeble, F.; Sundström, M.; Berg, S. von; et al. Aminoimidazoles as BACE-1 Inhibitors: The Challenge to Achieve in Vivo Brain Efficacy. *Bioorg. Med. Chem. Lett.* **2012**, *22* (5), 1854–1859. https://doi.org/10.1016/j.bmcl.2012.01.079.

(81) Malamas, M. S.; Erdei, J.; Gunawan, I.; Turner, J.; Hu, Y.; Wagner, E.; Fan, K.; Chopra, R.; Olland, A.; Bard, J.; et al. Design and Synthesis of 5,5′-Disubstituted Aminohydantoins as Potent and Selective Human β-Secretase (BACE1) Inhibitors. *J. Med. Chem.* **2010**, *53* (3), 1146–1158. https://doi.org/10.1021/jm901414e.

(82) Caldwell, J. P.; Mazzola, R. D.; Durkin, J.; Chen, J.; Chen, X.; Favreau, L.; Kennedy, M.; Kuvelkar, R.; Lee, J.; McHugh, N.; et al. Discovery of Potent Iminoheterocycle BACE1 Inhibitors. *Bioorg. Med. Chem. Lett.* **2014**, *24* (23), 5455–5459. https://doi.org/10.1016/j.bmcl.2014.10.006.

(83) Woltering, T. J.; Wostl, W.; Hilpert, H.; Rogers-Evans, M.; Pinard, E.; Mayweg, A.; Göbel, M.; Banner, D. W.; Benz, J.; Travagli, M.; et al. BACE1 Inhibitors: A Head Group Scan on a Series of Amides. *Bioorg. Med. Chem. Lett.* **2013**, *23* (14), 4239–4243. https://doi.org/10.1016/j.bmcl.2013.05.003.

(84) Baxter, E. W.; Conway, K. A.; Kennis, L.; Bischoff, F.; Mercken, M. H.; De Winter, H. L.; Reynolds, C. H.; Tounge, B. A.; Luo, C.; Scott, M. K.; et al. 2-Amino-3,4-Dihydroquinazolines as Inhibitors of BACE-1 (β-Site APP Cleaving Enzyme): Use of Structure Based Design to Convert a Micromolar Hit into a Nanomolar Lead. *J. Med. Chem.* **2007**, *50* (18), 4261–4264. https://doi.org/10.1021/jm0705408.

(85) Ghosh, A. K.; Pandey, S.; Gangarajula, S.; Kulkarni, S.; Xu, X.; Rao, K. V.; Huang, X.; Tang, J. Structure-Based Design, Synthesis, and Biological Evaluation of Dihydroquinazoline-Derived Potent β-Secretase Inhibitors. *Bioorg. Med. Chem. Lett.* **2012**, *22* (17), 5460–5465. https://doi.org/10.1016/j.bmcl.2012.07.043.

(86) Cheng, Y.; Judd, T. C.; Bartberger, M. D.; Brown, J.; Chen, K.; Fremeau, R. T.; Hickman, D.; Hitchcock, S. A.; Jordan, B.; Li, V.; et al. From Fragment Screening to In Vivo Efficacy: Optimization of a Series of 2-Aminoquinolines as Potent Inhibitors of Beta-Site Amyloid Precursor Protein Cleaving Enzyme 1 (BACE1). *J. Med. Chem.* **2011**, *54* (16), 5836–5857. https://doi.org/10.1021/jm200544q.

(87) Stachel, S. J.; Steele, T. G.; Petrocchi, A.; Haugabook, S. J.; McGaughey, G.; Katharine Holloway, M.; Allison, T.; Munshi, S.; Zuck, P.; Colussi, D.; et al. Discovery of Pyrrolidine-Based β-Secretase Inhibitors: Lead Advancement through Conformational Design for Maintenance of Ligand Binding Efficiency. *Bioorg. Med. Chem. Lett.* **2012**, *22* (1), 240–244. https://doi.org/10.1016/j.bmcl.2011.11.024.

(88) Huang, Y.; Strobel, E. D.; Ho, C. Y.; Reynolds, C. H.; Conway, K. A.; Piesvaux, J. A.; Brenneman, D. E.; Yohrling, G. J.; Moore Arnold, H.; Rosenthal, D.; et al. Macrocyclic BACE Inhibitors: Optimization of a Micromolar Hit to Nanomolar Leads. *Bioorg. Med. Chem. Lett.* **2010**, *20* (10), 3158–3160. https://doi.org/10.1016/j.bmcl.2010.03.097.

(89) Boy, K. M.; Guernon, J. M.; Wu, Y.-J.; Zhang, Y.; Shi, J.; Zhai, W.; Zhu, S.; Gerritz, S. W.; Toyn, J. H.; Meredith, J. E.; et al. Macrocyclic Prolinyl Acyl Guanidines as Inhibitors of β-Secretase (BACE). *Bioorg. Med. Chem. Lett.* **2015**, *25* (22), 5040–5047. https://doi.org/10.1016/j.bmcl.2015.10.031.

(90) A Safety Study of LY2811376 Single Doses in Healthy Subjects - Full Text View - ClinicalTrials.gov https://clinicaltrials.gov/ct2/show/NCT00838084 (accessed Jun 3, 2019).

(91) May, P. C.; Dean, R. A.; Lowe, S. L.; Martenyi, F.; Sheehan, S. M.; Boggs, L. N.; Monk, S. A.; Mathes, B. M.; Mergott, D. J.; Watson, B. M.; et al. Robust Central Reduction of Amyloid- in Humans with an Orally Available, Non-Peptidic -Secretase Inhibitor. *J. Neurosci.* **2011**, *31* (46), 16507–16516. https://doi.org/10.1523/JNEUROSCI.3647-11.2011.

(92) LY2886721 | ALZFORUM https://www.alzforum.org/therapeutics/ly2886721 (accessed Jun 3, 2019).

(93) A Safety Study of LY2886721 Multiple Doses in Healthy Subjects - Full Text View - ClinicalTrials.gov https://clinicaltrials.gov/ct2/show/NCT01227252 (accessed Jun 4, 2019).

(94) Ghosh, A. K.; Cárdenas, E. L.; Osswald, H. L. The Design, Development, and Evaluation of BACE1 Inhibitors for the Treatment of Alzheimer's Disease. In *Alzheimer's Disease II*; Wolfe, M. S., Ed.; Topics in Medicinal Chemistry; Springer International Publishing: Cham, 2017; pp 27–85. https://doi.org/10.1007/7355_2016_16.

(95) Study of LY2886721 in Mild Cognitive Impairment Due to Alzheimer's Disease or Mild Alzheimer's Disease - Full Text View - ClinicalTrials.gov https://clinicaltrials.gov/ct2/show/NCT01561430 (accessed Jun 3, 2019).

(96) Jeppsson, F.; Eketjäll, S.; Janson, J.; Karlström, S.; Gustavsson, S.; Olsson, L.-L.; Radesäter, A.-C.; Ploeger, B.; Cebers, G.; Kolmodin, K.; et al. Discovery of AZD3839, a Potent and Selective BACE1 Inhibitor Clinical Candidate for the Treatment of Alzheimer Disease. *J. Biol. Chem.* **2012**, *287* (49), 41245–41257. https://doi.org/10.1074/jbc.M112.409110.

(97) Quartino, A.; Huledal, G.; Sparve, E.; Lüttgen, M.; Bueters, T.; Karlsson, P.; Olsson, T.; Paraskos, J.; Maltby, J.; Claeson-Bohnstedt, K.; et al. Population Pharmacokinetic and Pharmacodynamic Analysis of Plasma $A\beta_{40}$ and $A\beta_{42}$ Following Single Oral Doses of the BACE1 Inhibitor AZD3839 to Healthy Volunteers: Clinical Pharmacology in Drug Development. *Clin. Pharmacol. Drug Dev.* **2014**, *3* (5), 396–405. https://doi.org/10.1002/cpdd.130.

(98) Jacobsen, H.; Ozmen, L.; Caruso, A.; Narquizian, R.; Hilpert, H.; Jacobsen, B.; Terwel, D.; Tanghe, A.; Bohrmann, B. Combined Treatment with a BACE Inhibitor and Anti-A Antibody Gantenerumab Enhances Amyloid Reduction in APPLondon Mice. *J. Neurosci.* **2014**, *34* (35), 11621–11630. https://doi.org/10.1523/JNEUROSCI.1405-14.2014.

(99) A Study on Safety, Pharmacokinetics and Pharmacodynamics of RO5508887 in Healthy Volunteers - Full Text View - ClinicalTrials.gov https://clinicaltrials.gov/ct2/show/NCT01461967 (accessed Jun 3, 2019).

(100) A Pharmacodynamic and Pharmacokinetic Study of RO5508887 in Healthy Volunteers - Full Text View - ClinicalTrials.gov https://clinicaltrials.gov/ct2/show/NCT01592331 (accessed Jun 3, 2019).

(101) A Single-Center Study of RO5508887 in Healthy Volunteers - Full Text View - ClinicalTrials.gov https://clinicaltrials.gov/ct2/show/NCT01664143 (accessed Jun 3, 2019).

(102) Forman, M.; Palcza, J.; Tseng, J.; Leempoels, J.; Ramael, S.; Han, D.; Jhee, S.; Ereshefsky, L.; Tanen, M.; Laterza, O.; et al. The Novel BACE Inhibitor MK-8931 Dramatically Lowers Cerebrospinal Fluid Aβ Peptides in Healthy Subjects Following Single- and Multiple-Dose Administration. *Alzheimers Dement.* **2012**, *8* (4), P704. https://doi.org/10.1016/j.jalz.2012.05.1900.

(103) A Study of the Safety, Tolerability, and Pharmacodynamics of MK-8931 in Participants With Alzheimer's Disease (MK-8931-010 AM1 [P07820 AM1]) - Full Text View - ClinicalTrials.gov https://clinicaltrials.gov/ct2/show/NCT01496170 (accessed Jun 3, 2019).

(104) A Two-Part, Single-Dose Study of the Pharmacokinetics of MK-8931 in Subjects With Renal Insufficiency (MK-8931-009 [P08535]) - Full Text View - ClinicalTrials.gov https://clinicaltrials.gov/ct2/show/NCT01537757 (accessed Jun 3, 2019).

(105) An Efficacy and Safety Trial of Verubecestat (MK-8931) in Mild to Moderate Alzheimer's Disease (P07738) - Full Text View - ClinicalTrials.gov https://clinicaltrials.gov/ct2/show/NCT01739348 (accessed Jun 3, 2019).

(106) A Two-part Single and Multiple Dose Study to Assess the Safety , Pharmacokinetics and Effects of AZD3293 in Healthy Japanese Young and Elderly Volunteers - Full Text View - ClinicalTrials.gov https://clinicaltrials.gov/ct2/show/NCT02005211 (accessed Jun 3, 2019).

(107) A Single Dose Study to Assess the Safety, Effects, and Blood and Urine Drug Levels of AZD3293 in Healthy Subjects - Full Text View - ClinicalTrials.gov https://clinicaltrials.gov/ct2/show/NCT01739647 (accessed Jun 3, 2019).

(108) A Two-part Multiple Dose Study to Assess the Safety and Effects of AZD3293 in Healthy Elderly and Alzheimer's Patients - Full Text View - ClinicalTrials.gov https://clinicaltrials.gov/ct2/show/NCT01795339 (accessed Jun 3, 2019).

(109) A Phase I Study in Healthy Volunteers to Assess the Effect of Cytochrome3A4 (CYP3A4) Inhibitors (Diltiazem and Itraconazole) on the Pharmacokinetics (PK) of AZD3293 and the Effects of AZD3293 on the Pharmacokinetics of Midazolam, a Cytochrome 3A4 and Cytochrome 3A5 (CYP3A4/CYP3A5) Substrate - Full Text View - ClinicalTrials.gov https://clinicaltrials.gov/ct2/show/NCT02010970 (accessed Jun 3, 2019).

(110) AZD3293 Thorough QT Study in Healthy Male Volunteers - Full Text View - ClinicalTrials.gov https://clinicaltrials.gov/ct2/show/NCT02040987 (accessed Jun 3, 2019).

(111) Assessment of Safety, Tolerability and Blood Concentrations of Single Doses of AZD3839 in Healthy Volunteers - Full Text View - ClinicalTrials.gov https://clinicaltrials.gov/ct2/show/NCT01348737 (accessed Jun 3, 2019).

(112) Devi, L.; Tang, J.; Ohno, M. Beneficial Effects of the β-Secretase Inhibitor GRL-8234 in 5XFAD Alzheimer's Transgenic Mice Lessen during Disease Progression. *Curr. Alzheimer Res.* **2015**, *12* (1), 13–21.

(113) Ghosh, A.; Bilcer, G.; Hong, L.; Koelsch, G.; Tang, J. Memapsin 2 (Beta-Secretase) Inhibitor Drug, between Fantasy and Reality. *Curr. Alzheimer Res.* **2007**, *4* (4), 418–422. https://doi.org/10.2174/156720507781788864.

(114) Citron, M. β-Secretase Inhibition for the Treatment of Alzheimer's Disease – Promise and Challenge. *Trends Pharmacol. Sci.* **2004**, *25* (2), 92–97. https://doi.org/10.1016/j.tips.2003.12.004.

(115) Maillard, M. C.; Hom, R. K.; Benson, T. E.; Moon, J. B.; Mamo, S.; Bienkowski, M.; Tomasselli, A. G.; Woods, D. D.; Prince, D. B.; Paddock, D. J.; et al. Design, Synthesis, and Crystal Structure of Hydroxyethyl Secondary Amine-Based Peptidomimetic Inhibitors of Human β-Secretase †. *J. Med. Chem.* **2007**, *50* (4), 776–781. https://doi.org/10.1021/jm061242y.

(116) Hom, R. K.; Gailunas, A. F.; Mamo, S.; Fang, L. Y.; Tung, J. S.; Walker, D. E.; Davis, D.; Thorsett, E. D.; Jewett, N. E.; Moon, J. B.; et al. Design and Synthesis of Hydroxyethylene-Based Peptidomimetic Inhibitors of Human β-Secretase. *J. Med. Chem.* **2004**, *47* (1), 158–164. https://doi.org/10.1021/jm0304008.

(117) Ghosh, A. K.; Osswald, H. L.; Prato, G. Recent Progress in the Development of HIV-1 Protease Inhibitors for the Treatment of HIV/AIDS. *J. Med. Chem.* **2016**, *59* (11), 5172–5208. https://doi.org/10.1021/acs.jmedchem.5b01697.

(118) Ghosh, A. K.; Bilcer, G.; Schiltz, G. Syntheses of FDA Approved HIV Protease Inhibitors. *Synthesis* **2001**, *2001* (15), 2203–2229. https://doi.org/10.1055/s-2001-18434.

(119) Ghosh, A. K.; Fidanze, S. Transition-State Mimetics for HIV Protease Inhibitors: Stereocontrolled Synthesis of Hydroxyethylene and Hydroxyethylamine Isosteres by Ester-Derived Titanium Enolate Syn and Anti-Aldol Reactions. *J. Org. Chem.* **1998**, *63* (18), 6146–6152. https://doi.org/10.1021/jo980159i.

(120) Ghosh, A. K.; Cárdenas, E. L.; Brindisi, M. Highly Stereoselective Asymmetric Aldol Routes to Tert-Butyl-2-(3,5-Difluorophenyl)-1-Oxiran-2-Yl)Ethyl)Carbamates: Building Blocks for Novel Protease Inhibitors. *Tetrahedron Lett.* **2017**, *58* (43), 4062–4065. https://doi.org/10.1016/j.tetlet.2017.09.025.

(121) Ghosh, A. K.; Onishi, M. Synthesis of Enantiomerically Pure Anti-Aldols: A Highly Stereoselective Ester-Derived Titanium Enolate Aldol Reaction. *J. Am. Chem. Soc.* **1996**, *118* (10), 2527–2528. https://doi.org/10.1021/ja9539148.

(122) Gadakh, S. K.; Santhosh Reddy, R.; Sudalai, A. Enantioselective Synthesis of HIV Protease Inhibitor Amprenavir via Co-Catalyzed HKR of 2-(1-Azido-2-Phenylethyl)Oxirane. *Tetrahedron Asymmetry* **2012**, *23* (11), 898–903. https://doi.org/10.1016/j.tetasy.2012.06.003.

(123) Evans, D. A.; Bartroli, J.; Shih, T. L. Enantioselective Aldol Condensations. 2. Erythro-Selective Chiral Aldol Condensations via Boron Enolates. *J. Am. Chem. Soc.* **1981**, *103* (8), 2127–2129. https://doi.org/10.1021/ja00398a058.

(124) Ghosh, A. K.; Osswald, H. L.; Glauninger, K.; Agniswamy, J.; Wang, Y.-F.; Hayashi, H.; Aoki, M.; Weber, I. T.; Mitsuya, H. Probing Lipophilic Adamantyl Group as the P1-Ligand for HIV-1 Protease Inhibitors: Design, Synthesis, Protein X-Ray Structural Studies, and Biological Evaluation. *J. Med. Chem.* **2016**, *59* (14), 6826–6837. https://doi.org/10.1021/acs.jmedchem.6b00639.

(125) Caron, M.; Carlier, P. R.; Sharpless, K. B. Regioselective Azide Opening of 2,3-Epoxy Alcohols by [Ti(O-i-Pr)2(N3)2]: Synthesis of .Alpha.-Amino Acids. *J. Org. Chem.* **1988**, *53* (21), 5185–5187. https://doi.org/10.1021/jo00256a063.

(126) Brown, H. C.; McFarlin, R. F. The Reaction of Lithium Aluminum Hybride with Alcohols. Lithium Tri-t-Butoxyaluminohydride as a New Selective Reducing Agent [1,2]. *J. Am. Chem. Soc.* **1958**, *80* (20), 5372–5376. https://doi.org/10.1021/ja01553a013.

(127) Lebel, H.; Marcoux, J.-F.; Molinaro, C.; Charette, A. B. Stereoselective Cyclopropanation Reactions. *Chem. Rev.* **2003**, *103* (4), 977–1050. https://doi.org/10.1021/cr010007e.

(128) Motherwell, W. B.; Nutley, C. J. The Role of Zinc Carbenoids in Organic Synthesis. *Contemp. Org. Synth.* **1994**, *1* (4), 219. https://doi.org/10.1039/co9940100219.

(129) Corey, E. J.; Chaykovsky, Michael. **Dimethylsulfoxonium Methylide**. *J. Am. Chem. Soc.* **1962**, *84* (5), 867–868. https://doi.org/10.1021/ja00864a040.

(130) Johnson, A. W.; LaCount, R. B. The Chemistry of Ylids. VI. Dimethylsulfonium Fluorenylide—A Synthesis of Epoxides [1]. *J. Am. Chem. Soc.* **1961**, *83* (2), 417–423. https://doi.org/10.1021/ja01463a040.

(131) McGarrigle, E. M.; Myers, E. L.; Illa, O.; Shaw, M. A.; Riches, S. L.; Aggarwal, V. K. Chalcogenides as Organocatalysts. *Chem. Rev.* **2007**, *107* (12), 5841–5883. https://doi.org/10.1021/cr068402y.

(132) Kulinkovich, O. G.; Sviridov, S. V.; Vasilevski, D. A. Titanium(IV) Isopropoxide-Catalyzed Formation of 1-Substituted Cyclopropanols in the Reaction of Ethylmagnesium Bromide with Methyl Alkanecarboxylates. *Synthesis* **1991**, *1991* (03), 234–234. https://doi.org/10.1055/s-1991-26431.

(133) Bertus, P.; Szymoniak, J. Titanium-Mediated Synthesis of Primary Cyclopropylamines from Nitriles and Grignard Reagents. *Synlett* **2007**, *2007* (9), 1346–1356. https://doi.org/10.1055/s-2007-980342.

(134) Tagad, H. D.; Hamada, Y.; Nguyen, J.-T.; Hidaka, K.; Hamada, T.; Sohma, Y.; Kimura, T.; Kiso, Y. Structure-Guided Design and Synthesis of P1′ Position 1-Phenylcycloalkylamine-Derived Pentapeptidic BACE1 Inhibitors. *Bioorg. Med. Chem.* **2011**, *19* (17), 5238–5246. https://doi.org/10.1016/j.bmc.2011.07.002.

(135) Robak, M. T.; Herbage, M. A.; Ellman, J. A. Synthesis and Applications of *Tert* -Butanesulfinamide. *Chem. Rev.* **2010**, *110* (6), 3600–3740. https://doi.org/10.1021/cr900382t.

(136) Barrow, J. C.; Ngo, P. L.; Pellicore, J. M.; Selnick, H. G.; Nantermet, P. G. A Facile Three-Step Synthesis of 1,2-Amino Alcohols Using the Ellman Homochiral Tert-Butylsulfinamide. *Tetrahedron Lett.* **2001**, *42* (11), 2051–2054. https://doi.org/10.1016/S0040-4039(01)00122-8.

(137) Tang, T. P.; Volkman, S. K.; Ellman, J. A. Asymmetric Synthesis of Protected 1,2-Amino Alcohols Using *Tert* -Butanesulfinyl Aldimines and Ketimines. *J. Org. Chem.* **2001**, *66* (26), 8772–8778. https://doi.org/10.1021/jo0156868.

(138) Delgado, O.; Monteagudo, A.; Van Gool, M.; Trabanco, A. A.; Fustero, S. A Practical Entry to β-Aryl-β-Alkyl Amino Alcohols: Application to the Synthesis of a Potent BACE1 Inhibitor. *Org. Biomol. Chem.* **2012**, *10* (33), 6758. https://doi.org/10.1039/c2ob25845e.

(139) Rombouts, F. J. R.; Tresadern, G.; Delgado, O.; Martínez-Lamenca, C.; Van Gool, M.; García-Molina, A.; Alonso de Diego, S. A.; Oehlrich, D.; Prokopcova, H.; Alonso, J. M.; et al. 1,4-Oxazine β-Secretase 1 (BACE1) Inhibitors: From Hit Generation to Orally Bioavailable Brain Penetrant Leads. *J. Med. Chem.* **2015**, *58* (20), 8216–8235. https://doi.org/10.1021/acs.jmedchem.5b01101.

(140) Ghosh, A. K.; Brindisi, M.; Yen, Y.-C.; Cárdenas, E. L.; Ella-Menye, J.-R.; Kumaragurubaran, N.; Huang, X.; Tang, J.; Mesecar, A. D. Design, Synthesis, and X-Ray Structural Studies of BACE-1 Inhibitors Containing Substituted 2-Oxopiperazines as P1′-P2′ Ligands. *Bioorg. Med. Chem. Lett.* **2017**, *27* (11), 2432–2438. https://doi.org/10.1016/j.bmcl.2017.04.011.

(141) Charrier, N.; Demont, E.; Dunsdon, R.; Maile, G.; Naylor, A.; O'Brien, A.; Redshaw, S.; Theobald, P.; Vesey, D.; Walter, D. Synthesis of Indoles: Efficient Functionalisation of the 7-Position. *Synthesis* **2006**, *2006* (20), 3467–3477. https://doi.org/10.1055/s-2006-950223.

(142) Ghosh, A. K.; Venkateswara Rao, K.; Yadav, N. D.; Anderson, D. D.; Gavande, N.; Huang, X.; Terzyan, S.; Tang, J. Structure-Based Design of Highly Selective β-Secretase Inhibitors: Synthesis, Biological Evaluation, and Protein–Ligand X-Ray Crystal Structure. *J. Med. Chem.* **2012**, *55* (21), 9195–9207. https://doi.org/10.1021/jm3008823.

(143) Banner, D. W.; Gsell, B.; Benz, J.; Bertschinger, J.; Burger, D.; Brack, S.; Cuppuleri, S.; Debulpaep, M.; Gast, A.; Grabulovski, D.; et al. Mapping the Conformational Space Accessible to BACE2 Using Surface Mutants and Cocrystals with Fab Fragments, Fynomers and Xaperones. *Acta Crystallogr. D Biol. Crystallogr.* **2013**, *69* (6), 1124–1137. https://doi.org/10.1107/S0907444913006574

VITA

Emilio Leal Cárdenas was born in Fresno, California on August 30th, 1991. He was raised in the rural farming community of Fowler, California which is located in the heart of the San Joaquin Valley. He attended Fowler High School where he graduated in 2009. Emilio elected to remain close to home for his undergraduate studies and attended California State University, Fresno in the Fall of 2009. During his time at California State University, Fresno he worked under the supervision of Professor Santanu Maitra where he explored the modulation of Apolipoprotein E which was implicated as a target for Alzheimer’s Disease. In spring of 2014, He graduated from California State University, Fresno with a Bachelor of Science in Chemistry with honors. In Fall of 2014, he started his graduate studies at Purdue University in West Lafayette, Indiana and started research under the supervision of Professor Arun K. Ghosh. During his time at Purdue University, his research focused on the design, synthesis, and biological evaluation of BACE1 inhibitors as a potential treatment for Alzheimer’s disease. After completion of his degree at Purdue University, Emilio has plans to start a post-doctoral position in the laboratory of Professor Amanda L. Garner at the University of Michigan. In the future, he hopes to secure a position as a professor and run his own academic laboratory.

PUBLICATIONS

1) Ghosh, A. K.*; Brindisi, M.; Yen, Y.; Lendy, E. K.; Kovela, S.; **Cárdenas E. L.**; Reddy, B. S.; Rao, K. V.; Downs, D.; Huang, X.; Tang, J.; Mesecar, A. D. "Highly selective and potent human β-secretase 2 (BACE2) inhibitors against type 2 diabetes: design, synthesis, x-ray structure, and structure-activity relationship studies" *ChemMedChem*, 2019, 14, 545-560*,* DOI: 10.1002/cmdc.201800725.

2) Ghosh, A. K.*; **Cárdenas E. L.**; Brindisi, M. "Highly Stereoselective Asymmetric Aldol Route to tert-Butyl-2-(3,5-difluorophenyl)-1-oxyran-2yl)ethyl)carbamates: Building Blocks for Novel Protease Inhibitors" *Tetrahedron Letters*, 2017, 58, 4062-4065, DOI: 10.1016/j.tetlet.2017.09.025.

3) Ghosh, A. K.*; Brindisi, M.; Yen, Y.; **Cárdenas E. L.**; Ella-Menya, J.; Kumaragurubaran, N.; Huang, X.; Tang, J.; Mesecar, A. D. "Design, synthesis, and x-ray structural studies of BACE-1 inhibitors 2-oxopiperazine as P1'-P2' ligands" *Bioorganic & Medicinal Chemistry Letters*, 2017, 27(11) 2432-3438, DOI: 10.1016/j.bmcl.2017.04.011

4) Ghosh, A. K.*; **Cárdenas E. L.**; Osswald, H. L. "The design, development, and evaluation of BACE1 inhibitors for the treatment of Alzheimer's disease" *Topics of Medicinal Chemistry*, 2017, 24, 27-85, DOI: 10.1007/7355_2016_16.

5) Ghosh, A. K.*; Lv, K.; Ma, N.; **Cárdenas E. L.**; Effenberger, K. A.; Jurica, J. S. "Design, synthesis, and in vitro splicing inhibition of desmethyl and carba-derivatives of herboxidiene" *Organic & Biomolecular Chemistry*, 2016, 14, 5263-5271.DOI: 10.1039/C6OB00725B.

6) Ghosh, A. K.*; Reddy, B. S.; Yen, Y.; **Cárdenas E. L.**; Rao, K. V.; Downs, D.; Huang, X.; Tang, J.; Mescar A. D. "Design of potent and highly selective inhibitors for human β-secretase (memapsin 1), a target for type 2 diabetes" *Chemical Science*, 2016, 7, 3117-3122, DOI: 10.1039/C5SC03718B.

Tetrahedron Letters 58 (2017) 4062–4065

Contents lists available at ScienceDirect

Tetrahedron Letters

journal homepage: www.elsevier.com/locate/tetlet

Highly stereoselective asymmetric aldol routes to *tert*-butyl-2-(3,5-difluorophenyl)-1-oxiran-2-yl)ethyl)carbamates: Building blocks for novel protease inhibitors

Arun K. Ghosh *, Emilio L. Cárdenas, Margherita Brindisi

Department of Chemistry and Department of Medicinal Chemistry, Purdue University, 560 Oval Drive, West Lafayette, IN 47907, United States

A R T I C L E I N F O

Article history:
Received 14 August 2017
Revised 6 September 2017
Accepted 13 September 2017
Available online 14 September 2017

Keywords:
Aldol reaction
Asymmetric
Protease inhibitor
Fluoroisostere
Stereoselective

ABSTRACT

Enantioselective syntheses of *tert*-butyl ((*S*)-2-(3,5-difluorophenyl)-1-((*S*)-oxiran-2-yl)ethyl)carbamate and ((*S*)-2-(3,5-difluorophenyl)-1-((*R*)-oxiran-2-yl)ethyl)carbamate are described. We utilized asymmetric *syn*- and *anti*-aldol reactions to set both stereogenic centers. We investigated ester-derived Ti-enolate aldol reactions as well as Evans' diastereoselective *syn*-aldol reaction for these syntheses. We have converted optically active ((*S*)-2-(3,5-difluorophenyl)-1-((*S*)-oxiran-2-yl)ethyl)carbamate to a potent β-secretase inhibitor.

© 2017 Elsevier Ltd. All rights reserved.

The design of aspartic acid protease inhibitors continues to be an important area for drug development and discovery against a variety of human diseases.[1] These include renin inhibitors for hypertension, HIV protease inhibitors for HIV/AIDS and β- and γ-secretase inhibitors for Alzheimer's disease.[1–3] The β-secretase inhibitors are particularly receiving much attention due to their potential for the treatment of Alzheimer's disease (AD).[4] BACE1 is a membrane anchored aspartic acid protease, responsible for the initial cleavage of amyloid precursor protein to neurotoxic amyloid-Aβ-peptides in the brain. The amyloid-β-peptide is the main component of amyloid plaques, the neuropathological hallmark of AD.[5,6] Since the discovery of BACE1 in 1999, extensive research efforts led to the evolution of a variety of small-molecule peptidomimetic and non-peptide BACE1 inhibitors with therapeutic potentials.[7,8] Over the years, many potent and selective peptidomimetic BACE1 inhibitors have been designed based upon incorporation of traditional hydroxyethylene and hydroxyethylamine transition-state isosteres at the cleavage site of BACE1.[4,9,10] The majority of early BACE1 inhibitors containing phenylalanine and leucine side chains as the P1 ligand showed low nanomolar BACE1 K_i values and they also exhibited good reduction of cellular Aβ production.[4,7,8] At present, there are at least three small molecule BACE1 inhibitors that have advanced to clinical trials.[11,12]

A clinically effective BACE1 inhibitor, however, needs to have the ability to cross the blood-brain barrier (BBB) and the neuronal membrane.[13] In this context, traditional transition-state isosteres were made more lipophilic by inserting fluorines in an effort to improve membrane permeability, metabolic stability, and enzyme-inhibitor interactions.[4,7,8] As exemplified in Fig. 1, peptidomimetic inhibitors **1** (BACE1 $IC_{50} = 5$ nM; Cell $IC_{50} = 3$ nM) and **2** (BACE1 $IC_{50} = 30$ nM; Cell $IC_{50} = 3$ μM) incorporated hydroethylamine and hydroxyethylene dipeptide isosteres, respectively, with a 3,5-difluorophenylmethyl group as the P1 ligand.[14,15] These difluoro-dipeptide isosteres have been utilized in the design and synthesis of many other potent and selective BACE1 inhibitors with BBB permeability.[4,7,8]

In general, BACE1 inhibitors containing hydroxyethylamine isosteres show potent BACE1 inhibitory activity and cellular activity. The synthesis of inhibitors involves the opening of an aminoalkyl epoxide with an appropriate amine followed by the functionalization of the *N*-terminus with suitable P2 ligands.[2,4] As shown in Fig. 2, BACE1 inhibitors containing a 3,5-difluorophenylmethyl side chain as the P1 ligand in a general inhibitor **3**, can be synthesized from *tert*-butyl-((*S*)-1-(*S*)-oxiran-2yl)-2-phenylethyl carbamate **4**. Enantioselective synthesis of such epoxide is typically carried out with optically active 3,5-difluorophenyl alanine **5**.[16,17] In our continuing interest in the design and synthesis of novel BACE1 inhibitors containing fluorines at the P1-ligand, we have investigated the synthesis of difluoroepoxide **4** utilizing an asymmetric *syn*-aldol as the key step.[18,19] In principle, aldol product such as **6** would

---

* Corresponding author.
E-mail address: akghosh@purdue.edu (A.K. Ghosh).

https://doi.org/10.1016/j.tetlet.2017.09.025
0040-4039/© 2017 Elsevier Ltd. All rights reserved.

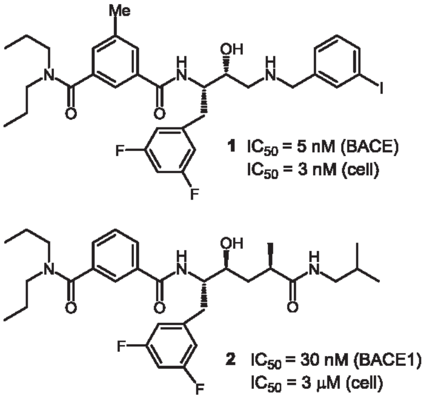
Me
OH
1 IC_{50} = 5 nM (BACE)
IC_{50} = 3 nM (cell)
2 IC_{50} = 30 nM (BACE1)
IC_{50} = 3 μM (cell)

Fig. 1. Structures of BACE-1 inhibitors **1** and **2**.

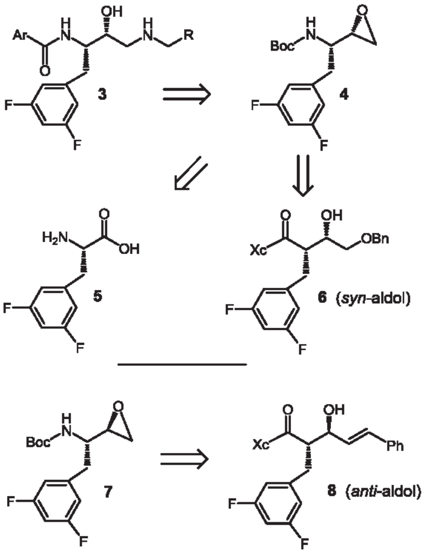
3
4
5
6 (*syn*-aldol)
7
8 (*anti*-aldol)
Boc
Xc
OBn
Ph

Fig. 2. Structures of epoxides **4** and **7** and their respective aldol precursors.

provide access to epoxide by removal of chiral auxiliary (X$_C$) followed by Curtius rearrangement of the resulting acid to install the amine functionality.[20,21] Furthermore, *anti*-aldol product such as **8**, obtained from a diastereoselective *anti*-aldol reaction,[22] could provide access to diastereomeric oxirane derivative **7** for the synthesis of BACE1 inhibitors with hydroxyethylene isosteres. Herein, we report a highly diastereoselective synthesis of (2*R*, 3*S*)-1,2-epoxy-3-(Boc-amino)-4-(3,5-difluorophenylmethyl) -butane **4** and (2*R*, 3*R*)-1,2-epoxy-3-(Boc-amino)-4-(3,5-difluorophenylmethyl)butane **7** (Fig. 2) utilizing an asymmetric aldol reaction as the key step. The overall route is amenable to quantities of difluoroepoxide cores **4** and **7** in high optical purity.

We first investigated ester-derived titanium-enolate based aldol reactions to afford both *syn*- and *anti*-aldol products for the stereoselective synthesis of aminoalkyl oxiranes **4** and **7**. These reactions have been utilized in the synthesis of a number of dipeptide isosteres.[19,20,23] The synthesis of oxirane **4** using *syn*-aldol reaction is shown in Scheme 1. 3,5-Difluorohydrocinnamic acid **9** was prepared in multigram scale as described in the literature.[24,25] Reaction of this acid with commercially available *N*-tosyl-1-aminoindan-2-ol **10** with DCC in the presence of DMAP in CH_2Cl_2 at 23 °C for 18 h afforded ester **11** in 76% yield. Treatment of ester **11** with 1 M $TiCl_4$ in the presence of diisopropylethylamine (DIPEA) in CH_2Cl_2 at 0 °C to 23 °C for 2 h provided the corresponding Ti-enolate. Reaction of this Ti-enolate with (benzyloxy)acetaldehyde precomplexed with $TiCl_4$ in CH_2Cl_2 (1 M CH_2Cl_2) at −78 °C for 2 h provided the *syn*-aldol product **12** in 60% yield. The ^{1}H NMR analysis revealed the presence of a single diastereomer. Saponification of aldol product **12** with aqueous lithium hydroperoxide at 0 °C to 23 °C for 12 h provided the corresponding acid which was subjected to Curtius rearrangement[20,26] with diphenylphosphorazidate in the presence of triethylamine in dry benzene at 90 °C for 12 h to afford oxazolidinone derivative **13** in 70% yield over 2-steps. Oxazolidinone was converted to Boc-derivative **14** in a two-step sequence. Hydrolysis of **13** with

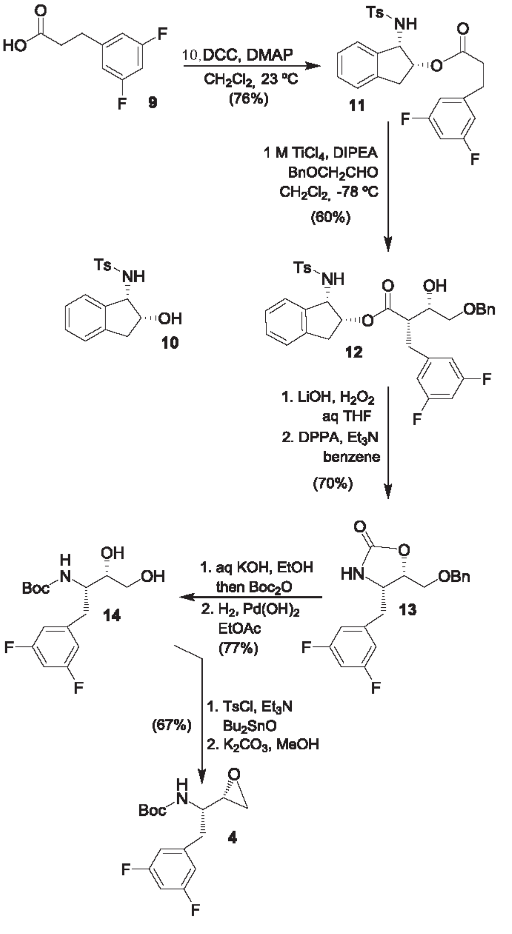
9
10, DCC, DMAP
CH_2Cl_2, 23 °C
(76%)
11
1 M $TiCl_4$, DIPEA
$BnOCH_2CHO$
CH_2Cl_2, -78 °C
(60%)
10
12
1. LiOH, H_2O_2
aq THF
2. DPPA, Et_3N
benzene
(70%)
13
1. aq KOH, EtOH
then Boc_2O
2. H_2, $Pd(OH)_2$
EtOAc
(77%)
14
1. TsCl, Et_3N
Bu_2SnO
2. K_2CO_3, MeOH
(67%)
4

Scheme 1. Synthesis of 3,5-difluorobenzyl epoxide **4**.

aqueous KOH provided the corresponding aminoalcohol which was reacted with di-*tert*-butyl dicarbonate in a mixture (1:1) of CH_2Cl_2 and water at 23 °C for 4 h to afford the Boc-derivative. Catalytic hydrogenation of benzyl ether over Pearlman's catalyst using a hydrogen-filled balloon in ethyl acetate removed the benzyl group and diol **14** was obtained in 77% yield over 2-steps. The diol **14** was converted to epoxide **4** by a regioselective monotosylation of the primary alcohol with *p*-toluenesulfonylchloride and triethylamine in the presence of a catalytic amount (25 mol%) of dibutyltin oxide at 23 °C for 4 h to provide the corresponding tosylate. Exposure of this tosylate to K_2CO_3 in MeOH at 0 °C to 23 °C for 1 h afforded (*S*)-2-(3,5-difluorophenyl)-1(*S*)-oxiranyl ethyl carbamate **4** in 67% yield over two-steps. The overall route is straightforward and provided fluorine substituted chiral epoxide for the synthesis of BACE1 inhibitors.

For the synthesis of 3,5-difluorobenzyl oxirane **7**, we carried diastereoselective *anti*-aldol reaction of ester **11** with cinnamaldehyde as shown in Scheme 2. Ester **11** was converted to Ti-enolate with 1 M $TiCl_4$ in CH_2Cl_2 in the presence of DIPEA as described above. This enolate was reacted with *trans*-cinnamaldehyde precomplexed with 1.3 equivalents of $TiCl_4$ at −78 °C for 3 h to provide *anti*-aldol product **15** as a single isomer (by ^{1}H NMR and ^{13}C NMR analysis). Saponification of ester **15** with aqueous lithium hydroperoxide followed by Curtius rearrangement of the resulting acid as described above resulted in oxazolidinone derivative **16** in 96% yield over 2-steps. Ozonolytic cleavage of the double bond in compound **16** was achieved by passing ozone through a mixture (4:1) of CH_2Cl_2 and MeOH at −78 °C followed by reduction with $NaBH_4$ providing alcohol **17** in 90% yield. Exposure of alcohol **17** to aqueous KOH followed by reaction of the resulting aminoalcohol with $(Boc)_2O$ in CH_2Cl_2 afforded Boc-derivative **18** in 67% yield. Diol derivative **18** was converted to (*S*,*R*)-3,5-difluorophenyl oxirane **7** by selective tosylation followed by treatment of the resulting tosylate with K_2CO_3 in MeOH as described for compound **14** in Scheme 1 to provide oxirane **7** in 67% yield over 2-steps.

The synthesis of (*S*)-2-(3,5-difluorophenyl)-1-(*S*)-(oxiran-2-yl) ethyl carbamate **4** using Evans' *syn*-aldol reaction is shown in Scheme 3. Difluorohydrocinnamic acid **9** was transformed into a mixed anhydride with pivaloyl chloride and triethylamine at −78 °C. The resulting mixed anhydride was reacted with lithio derivative of chiral oxazolidinone **19** to furnish carboximide **20**.[27,28] Treatment of this chiral carboximide derivative with dibutylboron trifluoromethanesulfonate (Bu_2BOTf) in the presence of *N*,*N*-diisopropylethylamine at −78 °C provided the boron enolate. Reaction of this boron enolate with benzyloxyacetaldehyde furnished aldol product **21** in 46% yield after standard work up and silica gel chromatography. The ^{1}H and ^{13}C NMR analysis showed the presence of a single diastereomer. In an effort to improve the overall efficiency of this asymmetric aldol route, we further explored the Evan's asymmetric aldol reaction of chiral carboximide **20** with relatively inexpensive cinnamaldehyde. As shown in Scheme 3, formation of boron enolate with Bu_2BOTf and aldol reaction with cinnamaldehyde proceeded very well providing *syn*-aldol product **22** in near quantitative yield. Aldol product **22** was obtained as a single diastereomer by ^{1}H and ^{13}C NMR analysis. This is a significant improvement over aldol reaction with benzyloxyacetaldehyde for aldol product **21**. Exposure of aldol product **21** to lithium hydroperoxide in aqueous THF at 0 °C to 23 °C for 10 h to provide the corresponding carboxylic acid. This

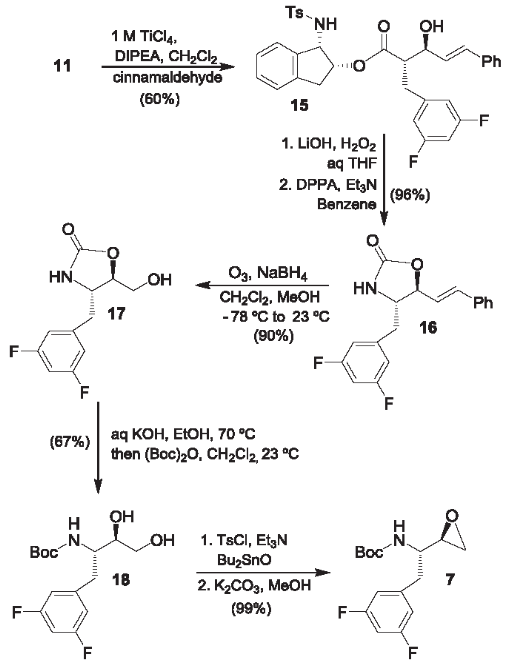
11
1 M TiCl4, DIPEA, CH2Cl2
cinnamaldehyde
(60%)
Ts
NH
O
OH
Ph
15
F
F
1. LiOH, H2O2 aq THF
2. DPPA, Et3N Benzene
(96%)
O
HN
O
Ph
16
O3, NaBH4
CH2Cl2, MeOH
-78 °C to 23 °C
(90%)
OH
17
(67%)
aq KOH, EtOH, 70 °C then (Boc)2O, CH2Cl2, 23 °C
H
Boc
N
OH
18
1. TsCl, Et3N Bu2SnO
2. K2CO3, MeOH
(99%)
7

Scheme 2. Synthesis of 3,5-difluorobenzyl epoxide **7**.

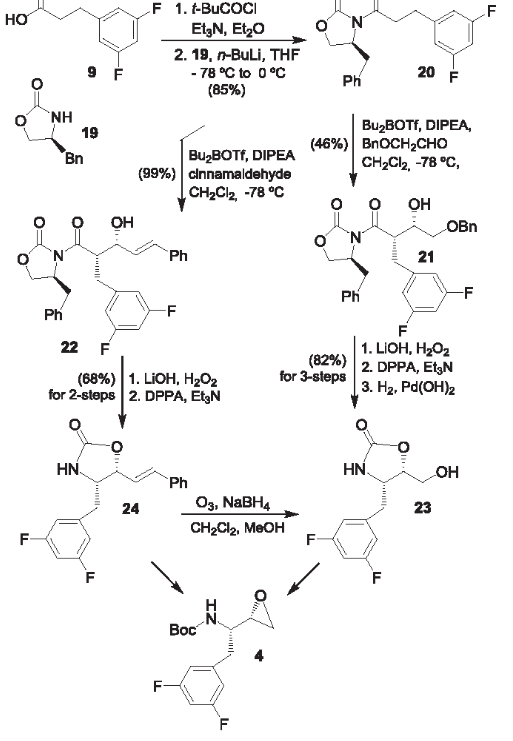
HO
9
F
1. t-BuCOCl Et3N, Et2O
2. 19, n-BuLi, THF -78 °C to 0 °C
(85%)
O
N
Ph
20
NH
19
Bn
(99%)
Bu2BOTf, DIPEA cinnamaldehyde CH2Cl2, -78 °C
(46%)
Bu2BOTf, DIPEA, BnOCH2CHO CH2Cl2, -78 °C,
OH
OBn
21
22
(68%) for 2-steps
1. LiOH, H2O2
2. DPPA, Et3N
(82%) for 3-steps
1. LiOH, H2O2
2. DPPA, Et3N
3. H2, Pd(OH)2
HN
24
O3, NaBH4
CH2Cl2, MeOH
23
H
Boc
N
4

Scheme 3. Synthesis of 3,5-difluorobenzyl epoxide **4**.

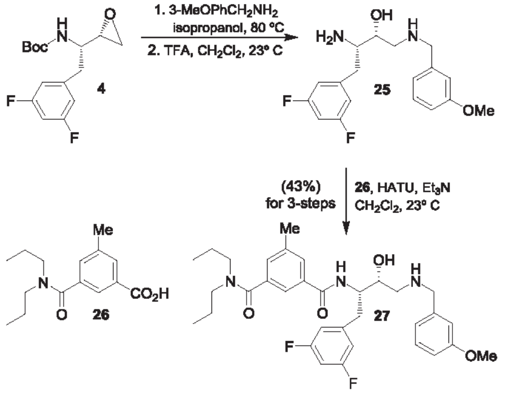

Scheme 4. Synthesis of BACE1 inhibitor **27**.

acid was subjected to Curtius rearrangement[20,21] with diphenyl phosphorazidate in the presence of triethylamine in toluene at 90 °C for 16 h to provide the corresponding oxazolidinone derivative. Catalytic hydrogenation of benzyl ether over Pearlman's catalyst provided alcohol **23** in 82% yield over 3-steps. This was converted to epoxide **4** as described above.

Aldol product **22** was also converted to epoxide **4**. The removal of the chiral auxiliary by exposure to lithium hydroperoxide followed by Curtius rearrangement of the resulting acid with DPPA as described above furnished oxazolidinone derivative **24** in 68% yield after silica gel chromatography. Ozonolysis of olefin in a mixture (4:1) of CH$_2$Cl$_2$ and methanol at −78 °C followed by a reductive workup with NaBH$_4$ furnished alcohol **23** in 90% yield. Alcohol **23** was readily converted to Boc-derivative **14** by exposure to aqueous KOH in ethanol followed by protection of the resulting crude amine as Boc derivative **14** as described previously.

We demonstrated the utility of difluorophenylethyl oxirane derivative **4** in the synthesis of known BACE1 inhibitor **27**.[14] As shown in Scheme 4, reaction of oxirane **4** with 3-methoxy-benzylamine in isopropanol at 80 °C for 12 h provided the corresponding aminoalcohol. Deprotection of the Boc-group by exposure to trifluoroacetic acid (TFA) in CH$_2$Cl$_2$ at 23 °C for 2 h afforded aminoalcohol **25**. Coupling of the primary amine with known[14] isophthalic acid derivative **26** in the presence of HATU and triethylamine in CH$_2$Cl$_2$ at 23 °C for 16 h furnished inhibitor **27** in 43% yield over three steps.

In conclusion, we accomplished convenient syntheses of aminoalkyl oxiranes **4** and **7** containing 3,5-difluorobenzyl side chain using an asymmetric aldol reaction as the key step. The stereochemistry of both stereogenic centers was set by highly diastereoselective *syn*- and *anti*-aldol reactions. The removal of the chiral auxiliary followed by Curtius rearrangement of the resulting acid installed the amine functionality. This was readily converted to epoxides **4** and **7** efficiently. These epoxides are important building blocks for the synthesis of a variety of BACE1 inhibitors incorporating hydroxyethylamine and hydroxyethylene isosteres. The overall route is quite efficient, scalable and provides facile access to diverse inhibitors. We have converted epoxide **4** to BACE1 inhibitor **27**. Further application of these epoxides in the synthesis of novel protease inhibitors is in progress in our laboratory.

Acknowledgments

Financial support by the National Institutes of Health (GM53386) is gratefully acknowledged. We would also like to thank the Purdue University Center for Cancer Research, which supports the shared NMR and mass spectrometry facilities.

A. Supplementary data

Supplementary data associated with this article can be found, in the online version, at http://dx.doi.org/10.1016/j.tetlet.2017.09.025.

References

1. Ghosh AK, ed. *Aspartic acid protease as therapeutic targets*. Weinheim, Germany: Wiley-VCH; 2010.
2. Ghosh AK, Osswald HL, Prato G. *J Med Chem*. 2016;59:5172–5208.
3. Ghosh AK, Cárdenas EL, Osswald HL. *Top. Med. Chem*. 2016. ASAP;
Ghosh AK, Tang J. *ChemMedChem*. 2015;10:1463–1466.
4. Ghosh AK, Osswald HL. *Chem Soc Rev*. 2014;43:6765–6813.
5. Hardy J, Selkoe DJ. *Science*. 2002;297:353–356.
6. Selkoe DJ, Schenk D. *Annu Rev Pharamacol*. 2003;43:545–584.
7. Citron M. *Trends Pharma Sci*. 2004;25:92–97.
8. Iserloh U, Cummins JN. In: Ghosh AK, ed. *Peptidomimetic BACE1 inhibitors for treatment of Alzheimer's disease: design and evolution in aspartic acid proteases as therapeutic targets*. Wiley-VCH; 2010:441–479.
9. Cole CD, Bursavich M. Nonpeptide BACE1 inhibitors: design and synthesis. In: Ghosh AK, ed. *Aspartic acid proteases as therapeutic targets*. Wiley-VCH; 2010:481–509.
10. Ghosh AK, Brindisi M, Tang J. *J Neurochem*. 2012;120:71–83.
11. Vassar R, Kovacs DM, Yan R, Wong PC. *J Neurosci*. 2009;29:12787–12794.
12. Vassar R. *Alzheimer's Res Ther*. 2014;6:89.
13. Ghosh AK, Bilcer G, Hong L, Koelsch G, Tang J. *Curr Alzheimer Res*. 2007;4:418–422.
14. Maillard MC, Hom RK, Benson TE, et al. *J Med Chem*. 2007;50:776–781.
15. Hom RK, Gailunas AF, Mamo S, et al. *J Med Chem*. 2004;47:158–164.
16. Greenlee WJ. *Med Res Rev*. 1990;10:173–236.
17. Ghosh AK, Bilcer G, Schiltz G. *Synthesis*. 2001;15:2203–2229.
18. Evans DA, Takacs JM, McGee LR, Ennis MD, Mathre DJ, Bartroli J. *Pure Appl Chem*. 1981;53:1109–1127.
19. Ghosh AK, Dawson Z. *Synthesis*. 2009;17:2992–3002.
20. Ghosh AK, Fidanze S. *J Org Chem*. 1998;63:6146–6152.
21. am Ende DJ, DeVries KM, Clifford PJ, Brenek SJ. *Org Proc Res Dev*. 1998;2:382–392.
22. Ghosh AK, Onishi M. *J Am Chem Soc*. 1996;118:2527–2528.
23. Akaji K, Teruya K, Aimoto S. *J Org Chem*. 2003;68:4755–4763.
24. Shi Z et al. *Bioorg Med Chem Lett*. 2005;13:4200–4208.
25. Jin YZ et al. *Green Chem*. 2002;4:498–500.
26. Ghosh AK, Kumaragurubaran N, Hong L, et al. *J Med Chem*. 2007;50:2399–2407.
27. Evans DA, Bartroli J, Shih TL. *J Am Chem Soc*. 1981;103:2127–2129.
28. Gage JR, Evans DA. *Org Synth*. 1990;68:83–91.